UNIVERSITÀ DEGLI STUDI DI PADOVA

Centro Interdipartimentale di Studi e Attività Spaziali (CISAS)

DOTTORATO DI RICERCA IN SCIENZE, TECNOLOGIE E MISURE SPAZIALI

XXI Ciclo

Sede Amministrativa: Università degli Studi di Padova

Indirizzo: Astronautica e scienze da satellite

Curriculum: Navigazione satellitare

Determinazione Orbitale Precisa di satelliti in orbita LEO per la Radio Occultazione attraverso sistemi GNSS

Precise Orbit Determination (POD) of LEO Satellites for Radio Occultation with GNSS

Dottorando: Paolo Zoccarato .....

Supervisore: Ch.mo Prof. Stefano Casotto .....
(Dipartimento di Astronomia, Università degli Studi di Padova)

Coordinatore del corso: Ch.mo Prof. Giampiero Naletto .....

Direttore della scuola: Ch.mo Prof. Cesare Barbieri .....

February 1, 2010

A Francesca, ai miei genitori.

Desidero sinceramente ringraziare il Prof. Stefano Casotto, mio supervisore durante questa tesi di Dottorato, per i preziosi consigli, gli insegnamenti e la sua grande esperienza messa a disposizione in questi anni di intenso studio e lavoro.

Un grazie anche ad ASI per l'importante occasione offertami di partecipare ad un progetto vasto e stimolante come è stato ed è ROSA ROSSA.

Grazie al gruppo di ricerca di ROSA ROSSA per la piacevole e quasi goliardica collaborazione che più volte ha portato a utili incontri per l'Italia.

Thanks to EUMETSAT, for providing GRAS data and the ready support.

Infine grazie a tutte le persone che ho conosciuto e ho avuto il piacere di incontrare quotidianamente in quei luoghi di gioia e dolore che sono il Dipartimento di Astronomia e il CISAS (e naturalmente una in particolare per il suo supporto estremo...)

Summary

The Global Positioning System (GPS) is a satellite navigation system producing high precision observations used for positioning and time services. The radio broadcast signal is basically is a carrier wave modulated by a pseudo-random binary code. The receiver creates a synchronized replica of the transmitter received signal, so that, by overlapping the two waves, the time interval between the emission and the reception (including the receiver clock error) becomes known. The time interval multiplied by the speed of light c gives the pseudo-distance between the GPS satellite and the receiver. With four pseudorange observations it becomes possible to determine the user position and the error of his receiver clock. The situation is complicated by the presence of several errors on the measurements due to various effects, as like ionospheric or troposheric refraction, relativistic effects, multipath etc.

To satisfy increasingly stringent requirements dependent on high precision and accuracy of the positioning solution, GPS is employed in different disciplines, like Earth sciences, land, sea and air navigation and military applications. In particular, the GPS system has the capability of providing continuous tracking of low Earth orbiting satellites, allowing Precise Orbit Determination (POD) applications. Many space-based scientific applications need to know the precise satellite orbit to use in an efficient manner the data acquired by the instruments on board. One of the most challenging application of POD is the *Radio Occultation* (RO) technique. When a radio signal passes through the atmosphere its phase is perturbed in a manner related to the refractivity along the ray path. Measurements of the phase perturbations can reveal the refractivity, from which one can then derive such quantities as atmospheric density, pressure, temperature, moisture, geopotential heights and winds. This technique was pioneered by JPL and Stanford University in the early 1960s for study of planetary atmospheres and ionospheres, when Mariners 3 and 4, viewed from Earth, passed behind Mars. In this case, a LEO satellite uses the Global Positioning System (GPS) to probe the Earth's atmosphere. This technique is suited for monitoring global atmospheric temperatures, pressures and moisture distributions with high accuracy and spatial resolution and for studying the ionosphere.

The Italian Space Agency (ASI - Agenzia Spaziale Italiana) founded a pool of Italian Universities and Research Centers for the implementation of the overall (and state-of-the-art) RO processing chain which is called ROSA ROSSA (ROSA-Research and Operational Satellite and Software Activities). The ROSA ROSSA project deals with the agreement between the ASI and the ISRO (Indian Space Research Organization) to make fly the Italian instrument ROSA (Radio Occultation Sounder of the Atmosphere), on board the Indian Satellite Oceansat-2. ROSA is an advanced GNSS receiver designed to track GNSS signals in the lower atmosphere during near radio occultation events. In particular, this thesis concerns the realization of a new innovative software for POD and RO purposes, called SWOrD(SoftWare for Oceansat-2 oRbit Determination). SWOrDis a software subsystem of the ROSA ROSSA project that fully supports the orbit determination, orbit prediction and phase excess data generation activities. SWOrDis designed to meet the requirement of high accuracy in the relative velocity between the two occulting S/C, and the low latency between the time-tag of the last RO observation and the time of assimilation of RO processed products into numerical weather prediction (NWP) codes. SWOrDis being developed according to an object-oriented (OOP), database-driven, multilanguage (C++ and Fortran95) approach that enhances flexibility, portability, and extensibility of the software system. These features define a product that is susceptible to applications with similar requirements in other Earth satellite missions. Although its development is still in progress, SWOrDis

presently functional.

SWOrDaccepts pseudorange and phase observations from an orbiting receiver and several ground stations to perform the orbit determination task for the low Earth satellite. SWOrDimplements a fully dynamic approach to orbit determination as well as a reduced-dynamic and a kinematic approach based on the use of zero- or double-differences of both pseudorange and carrier phase observations. Data are preprocessed on the basis of a reference orbit obtained from a precise point positioning solution of the LEO satellite. SWOrDalso predicts the LEO orbit over 24 hours for the purpose of identifying future RO events.

The architectural design of this software is based on simple concepts, the main of which is that all data are processed while being constantly kept in RAM. I/O operations are thus limited to initial data input and final data output. Another characteristic of SWOrDis that all quantities that can be computed only once during processing are not recomputed at each iteration. This includes all dynamical and kinematical quantities that depend on the observation time tag directly, not through the position of bodies or parameters being estimated. A third feature of SWOrDis that the observational and support data are inserted into database structures that are designed to allow fast identification and access through the use of multiply indexed relational tables via the Boost Multi-Index C++ library, which enables the construction of containers maintaining one or more indices with different sorting and access semantics. The input data to SWOrDare managed through XML files validated with W3C XML schemas (XSD). The XML reader classes are automatically generated from the schema by the Code Synthesis utility and directly populate interface classes. Preliminary data validation and configuration are performed at this time by the XML reader classes as well. SWOrDmakes use of interoperability between C++ and Fortran in order to take advantage of the numerical computation performance of the Fortran language and allow the use of legacy software modules. SWOrDincludes the open-source GPSTk Core Library to take advance of several implemented feature, i.e. the RINEX and SP3 file reading and the DayTime object for time instant representation. SWOrDsource code is also documented in the format suitable for the documentation generator tool Doxygen.

The SWOrDdata container–the core of the software system–consists of a series of singleton classes that implement an in-core database with multiple search indices that allow fast (hashing table) and ordered data access. This database is implemented by using the Boost Multiindex library. The BoostMulti-index Containers Library provides a class template named multi index container which enables the construction of containers maintaining one or more indices with different sorting and access semantics. User-defined multiple iterators (one for each indexing typology defined) permit to access data and to scroll through them contiguously.

The *orbit determination procedures* are *statistical techniques* that allow to estimate the orbital parameters of a spacecraft or a celestial body during its motion in the Solar System (here in particular specialized for the motion around the Earth). The aim of these procedures is to find a workaround that overcome the limited knowledge of the *true state* (position, velocity and several other parameters) of the considered body in the contest of a *simplified modeling* of the orbital motion. In particular, a *least squares approach* is used to minimize the differences between observations and a model of them, computed through a set of parameters, the *state vector* that form the dynamic and kinematic models and propagated in time through a set of differential equations (equations of motion). This requires a parametrization of the problem and depends on the physics of the problem itself. There are essentially two ways to update the state vector: if a new estimate is obtained after each observation, we talk about *sequential or recursive estimation*; if, instead, all the measurements are collected and then processed to obtain an estimate of the state vector at a specified initial epoch (batch epoch), we talk about *batch estimation*. Generally speaking, a sequential estimator (filter) is more sensitive to the quality of the individual measures than a batch filter. Besides, a sequential algorithm converges faster (if properly tuned) to the right solution than a batch algorithm. The latter may require several iterations before converging.

A statistical orbit determination process has to deal with four types of approximations:

1. measurement errors;

2. approximations in the dynamic, kinematic and observation models;

3. inaccuracies in the estimation process;

4. numerical approximations.

In order to obtain an orbit estimation as accurate as possible, there are several aspects to consider to handle each of the four approximations.

1. A sufficiently large number of observations must be collected over the time span of interest.

2. Generally, the measurements are nonlinear functions of the state vector parameters and, consequently, also the differential equations that describe the motion. This implies that multiple solutions can be found, but only one being optimal.

3. Once an optimal estimate of the orbital parameters is determined, a set of ephemerides of the satellite can be obtained by simply integrating the equations of motion by using the parameters just determined. The accuracy of the obtained ephemerides, or orbit, is strictly related to the precision and accuracy of the models and to the measurements error.

4. Any parameter that affects the orbital motion of the satellite can be estimated in the process of orbit estimation, not only the orbital parameters (e.g. the ground station positions, the Earth orientation parameters, the atmospheric delays and the gravity field coefficients).

The problem of orbit determination essentially consists in deriving orbital parameters from a set of observations. For an artificial satellite, in particular, this problem refers to the reduction of its tracking measurements, affected by both random and systematic errors, through an approximate analytical force model to obtain the best estimate of the orbital ephemerides describing the spacecraft motion in any time.

In most cases, the tracking system adopted to provide data for a precise orbit determination of LEO satellites is a GPS receiver. Differently from the conventional tracking systems, GPS presents numerous advantages: apart from a relative low cost implementation, it allows a three-dimensional position information from range measurements, to work in any atmospheric conditions and a continuous tracking of a LEO satellite, where a precise trajectory may be reconstructed only through elaborate orbit models.

Much work was performed in the last decade to develop and evaluate different orbit determination strategies for LEOs using GPS. The approach depends on requirements like precision, latency and availability. The orbital altitudes of the satellites range between about 300 km and 2000 km, leading to different perturbation characteristics. The orbit determination strategies may be divided into two main groups: the *kinematic strategies* and the *dynamic* and *reduced-dynamic strategies*.

Kinematic POD procedures estimate the satellite position for each observation epoch based on the GPS observations only, not needing any information concerning the gravity field and other parameters of the dynamical orbit models. The orbit solution is referenced to the phase center of the on-board GPS antenna instead of the satellite's center of mass. Kinematic solutions are more sensitive to geometrical factors, such as the direction of the GPS satellites and the GPS orbit accuracy, and they require the resolution of phase ambiguities. Nowadays, the accuracy of kinematic orbit determination may reach a few millimeters [82, Svehla & Rothacher, 2001].

On the other hand, the dynamic orbit determination requires precise models of the forces acting on the satellite. This approach implies that satellite positions are computed arc-by arc rather than point-by-point. The equations of motion are solved using the technique of numerical integration. The dynamic POD has been applied to many successful satellite missions and has become the mostly used POD approach. Dynamic model errors are the limiting factor for this technique, such as the geopotential model errors and atmospheric drag model errors.

In order to compute the satellite orbit as accurate as possible, the orbit determination process is very often a compromise between a kinematic approach and a dynamic approach, resulting in a so-called reduced-dynamic orbit determination.

The GPS data processing procedures for the LEO are common to both groups. These procedures may be distinguished by their *differencing* level namely the *zero-difference* (ZD), *double-difference*

(DD) or *triple-difference* (TD) level of the original observations. All strategies make direct or indirect use of the GPS ground network, the IGS network. Direct use is made if the observations of the ground stations are used together with the LEO GPS data for the processing (DD and TD). Indirect use is made if the observations of the ground stations are not used for the LEO GPS data processing (ZD), in which case the ground based observations are required to estimate GPS clock corrections. In any case ground station data are required to compute precise GPS satellite orbits.

The different procedures for the LEO GPS data processing are illustrated by Figure **??**. All procedures require GPS orbits, Earth rotation information and LEO GPS data as input for the processing. The GPS orbits and Earth rotation parameters are taken either from the IGS (or one of its analysis centers) or they may be estimated together with the LEO orbit. On the right hand side Figure **??** shows the TD and DD approaches requiring GPS data of an array of terrestrial receivers as well as the coordinates and troposphere information of these stations. The two ZD approaches on the left hand side do not need these data, but precise GPS clock corrections at a high sampling rate (30 seconds) are required. In the two approaches in the center of the figure, the well-known ZD and the DD procedures, the ambiguities have to be estimated as real values making the procedures complex and time-consuming.

To reduce the computational complexity of orbit determination problem, its solution has been divided in two subsequent steps: first a preliminary orbit determination and then a differential correction of the orbit.

Currently, the SWOrDPOD process is based on ionosphere-free combinations of phase double differences. However, future developments will include the use of ionosphere-free zero difference observables. SWOrDvalidation tests have been performed using three days of CHAMP data, from 20 July 2004 to 22 July 2004, which are part of the ROSA ROSSA validation dataset, and one day of GRAS data, 13 October 2007, made available by EUMETSAT.

The phase excess is the final datum that SWOrDproduces starting from RO GPS measurements and its own LEO precise orbit determination. The following data generators of the ROSA ROSSA chain extract Doppler excess from the phase excess to accomplish their climatological and meteorological studies. In the following we describe the processing algorithm we are using to extract phase excess. The term phase excess indicates the difference between the phase measured by a GPS receiver on a LEO satellite (appropriately corrected for the time tag error) and the geometric distance between the centers of phase of the LEO and the GPS antennas.

Sommario

Il Global Positioning System (GPS) è un sistema di nagazione satellitare in grado di produrre osservazioni di elevata precisione utilizzate sia per il posizionamento, sia come base di riferimento temporale. Il segnale radio trasmesso è costituito da una portante modulata da una sequenza di codici pseudo-casuali; il ricevitore crea una replica sincronizzata dei segnali che gli arrivano e per confronto si riesce a conoscere l'intervallo di tempo trascorso tra l'istante di emissione e quello di ricezione, a meno dell'errore dell'orologio, il quale dovrebbe essere sincronizzato con il tempo atomico GPS, ma è soggetto ad uno scarto che varia col trascorrere del tempo. Moltiplicando l'intervallo di tempo suddetto per la velocità della luce c, quest'ultimo diventa una lunghezza, che rappresenta la pseudo-distanza tra satellite e ricevitore. Con almeno quattro osservazioni di pseudo-distanza, si è in grado di determinare la posizione dell'utente e l'errore del suo orologio. Nella realtà la situazione è complicata dal fatto che sulle misure gravano errori dovuti a diversi fenomeni, come l'azione della ionosfera e della troposfera, gli effetti relativistici, ecc.

Per soddisfare obiettivi sempre più stringenti dipendenti dall'elevata precisione e accuratezza della soluzione di posizionamento, il GPS viene impiegato in numerose discipline, come le Scienze della Terra, la navigazione aerea, marittima e terrestre e per scopi militari. Una caratteristica fondamentale del sistema GPS è la sua capacità di effettuare l'inseguimento continuo di satelliti in orbita bassa (LEO), favorendo diverse applicazioni di determinazione orbitale precisa (POD), come la tecnica della Radio Occultazione. Essa si basa sul principio fisico che avviene quando un segnale radio attraversa l'atmosfera, ovvero la perturbazione della fase del segnale stesso in maniera dipendente dalla rifrattività lungo il cammino. Di conseguenza, dalle misure delle perturbazioni di fase si possono estrarre informazioni sulla rifrattività del mezzo attraversato e con queste si possono derivare profili ad elevata risoluzione spaziale di pressione, densità e temperatura dell'atmosfera e la distribuzione chimica dei composti in essa contenuti. La tecnica della Radio Occultazione è stata impiegata per la prima volta al JPL e all'Università di Stanford attorno al 1960 per lo studio delle atmosfere e delle ionosfere planetarie, quando i Mariner 3 e 4 visti dalla Terra sono passati dietro Marte.

L'Agenzia Spaziale italiana (ASI) ha fondato un gruppo formato dalle Università italiane e Centri di Ricerca per la realizzazione di una catena completa (ed all'avanguardia) di trattamento dati di RO chiamata Rosa ROSSA (ROSA-Research and Operational Satellite and Software Activities). Il progetto Rosa ROSSA si inserisce nell'accordo tra l'ASI e l'ISRO (Indian Space Research Organization) di far volare lo strumento italiano ROSA (Radio Occultation Sounder of the Atmosphere), a borso del Satellite indiano Oceansat-2. Rosa è un ricevitore GNSS avanzato progettato per localizzare segnali GNSS nell'atmosfera più bassa durante gli eventi di radio occultazione. In particolare, questa tesi si inserisce nella realizzazione di un software innovativo e nuovo per scopi di POD e RO, chiamato SWOrD(SoftWare for Oceansat-2 oRbit Determination). SWOrDè un sottosistema di software del progetto Rosa ROSSA (ROSA Research and Operational Satellite and Software Activities) che pienamente sostiene la determinazione e predizione orbitale la e la generazione dei dati di eccesso di fase. SWOrDè progettato per soddisfare il requisito dell'alta accuratezza nella velocità relativa fra il due satelliti che occultano, e una bassa latenza di tempo nel processare i dati. SWOrDè sviluppato secondo un approccio orientato agli oggetti (OOP), basato su database e multilinguaggio (C++ e Fortran95) che migliora la flessibilità, portabilità, ed estendibilità del sistema software. Queste caratteristiche definiscono un prodotto che bene si adatta per altre missioni di satellitari con simili requisiti. Anche

se il suo sviluppo è ancora in avanzamento, SWOrDè al momento funzionale.

SWOrDaccetta pseudorange ed osservazioni di fase da un ricevitore orbitale e da alcune stazioni di terra col fine di effettuare la determinazione orbitale del satellite LEO. Esso implementa un approccio completamente dinamico alla determinazione orbitale, così come un approccio a dinamica-ridotta e uno cinematico, fondato sull'uso di zero o doppie differenze sia dei pseudorange, sia delle osservazioni di fase. I dati sono pre-processati sulla base di un'orbita di riferimento ottenuta da una soluzione di posizionamento puntuale precisa del satellite LEO. Inoltre il software predice l'orbita del satellite LEO su un arco di 24 ore con lo scopo di identificare eventi di RO futuri.

Il disegno architettonico di questo software è basato su semplici concetti, il principale dei quali è che tutti i dati sono elaborati mentre vengono tenuti in memoria continuamente. Le operazioni di I/O sono limitate quindi all'inserimento iniziale dei dati e alla scrittura finale dei risultati. Un'altra caratteristica di SWOrDè che tutte le quantità che possono essere calcolate solamente una volta durante il processamento dati, non sono ricalcolate ad ogni iterazione. Questo include tutte le quantità dinamiche e cinematiche che dipendono direttamente dall'istante di osservazione e non quelle dipendenti dalla posizione di corpi o dalla stima di parametri. Una terza caratteristica di SWOrDconsiste nel fatto che i dati ausiliari sono inseriti in database progettati per permettere l'identificazione veloce e l'accesso attraverso l'uso di tabelle relazionali a indici multipli attraverso la libreria C++ Boost Multi-Index, che consentono la creazione di contenitori che mantengono uno o più indici con diversi metodi di accesso e ordinamento dei dati. I dati in input a SWOrDsono maneggiati attraverso file XML validati tramite lo schema XML W3C. Le classi di lettura XML sono generate automaticamente dallo schema grazie al programma Code Synthesis. La validazione dei dati preliminari e la configurazione sono compiute, a questo punto, dalle classi di lettura XML. SWOrDsi avvale dell'interoperabilità tra C++ e Fortran per trarre vantaggio delle migliori prestazioni di calcolo numerico del Fortran e permette l'impiego di legacy software. SWOrDutilizza la libreria open-source GPSTk, la quale possiede alcune funzioni già implementate, come la lettura dei file RINEX e SP3 e l'oggetto DayTime per la rappresentazione degli istanti temporali. Il codice sorgente di SWOrDè inoltre documentato nel formato adatto per il programma di generazione di documentazione Doxygen.

Attualmente, il processo di POD di SWOrD è basato su combinazioni ionosphere free delle doppie differenze di fase. Comunque, prossimi sviluppi includeranno l'uso di osservabili ionosphere-free non differenziati. Test di convalidazione di SWOrDsono state compiute usando tre giorni di dati di CHAMP, dal 20 al 22 luglio 2004, i quali fanno parte del dataset di ROSA ROSSA per la convalidazione, ed un giorno di dati GRAS, il 13 ottobre 2007, resi disponibili da EUMETSAT.

L'eccesso di fase è il dato finale che SWOrDproduce a partire dalla misure GPS di RO e dalla propsia determinazione orbitale del satellite LEO. L'eccesso di fase indica la differenza tra la fase misurata da un ricevitore GPS su un satellite LEO (corretta per l'errore di dell'oscillatore del ricevitore) e la distanza geometrica tra i centri di fase del LEO e le antenne GPS. I generatori di dati successivi a SWOrDnella catena di processamento ROSA ROSSA estragono l'eccesso Doppler dall'eccesso di fase per portare a termine i loro studi climatologici e meteorologici.

Frequently Used Acronyms

AFRL	Air Force Research Laboratories
AS	Anti-Spoofing
ASI	Agenzia Spaziale Italiana
C/A-code	Coarse-Acquisition, Clear-Access or Civil-Access code
CHAMP	CHAllenging Minisatellite Payload
CNES	Centre Nationale d'Etudes Spatiale
CONAE	Comision National de Actividades Espaciales
DCB	Differential Code Bias
DLR	Deutsches Zentrums für Luft und Raumfahrt
DOP	Dilution Of Precision
DORIS	Doppler Orbitography and Radio-positioning Integrated by Satellite
DOY	Day of Year
EOP	Earth Orientation Parameter
ERP	Earth Rotation Parameter
EUMETSAT	EUropean organization for the exploitation of METeorological SATellite
GFZ	GeoForschungsZentrum
GIOVE	Galileo In-Orbit Validation Element
GLONASS	GLObal NAvigation Satellite System
GNSS	Global Navigation Satellite System
GOCE	Gravity field and steady-state Ocean Circulation Explorer
GPS	Global Positioning System
GRACE	Gravity Recovery And Climate Experiment
GRAS	GNSS Receiver for Atmospheric Sounding
ICESat	Ice, Cloud and land Elevation Satellite
IGS	International GPS Service
IRNSS	Indian Regional Navigational Satellite System
ISRO	Indian Space Research Organization
JPL	Jet Propulsion Laboratory
LC	Linear Combination
LEO	Low Earth Orbiter
LIDAR	Laser Imaging Detection And Ranging
MEO	Medium Earth Orbit
MetOp	Meteorological Operational
NASA	National Aeronautics and Space Administration
NAVSTAR	NAVigation Satellite Timing And Ranging
ONERA	Office National d'Etudes et de Recherches Aérospatiales
P-code	Precise or Protected code
POD	Precise Orbit Determination
RINEX	Receiver-INdependent EXchange Format

RMS	Root Mean Square
RO	Radio Occultation
ROSA	Radio Occultation Sounder of the Atmosphere
ROSSA	ROSA-Research and Operational Satellite and Software Activities
SA	Selective Availability
SLR	Satellite Laser Ranging
SWOrD	SoftWare for Orbit Determination
TAS-I	Thales Alenia Space–Italy
TOPEX	TOPography EXperiment

Contents

List of Figures

List of Tables

Chapter 1

General information about GPS system

1.1. Introduction

In this chapter it is presented a general view of the Global Positioning System (GPS), a satellite navigation system producing high precision observations used for positioning and time services. In particular, the GPS system has the capability of providing continuous tracking of low Earth orbiting satellites, allowing Precise Orbit Determination (POD) applications. The main space missions consisting of a LEO satellite equipped with a GPS receivers are listed and for each one is given a short description.

Finally it is treated the GPS Radio Occultation (RO) technique, from which profiles of atmospheric pressure, density and temperature can be derived. In particular, it is illustrated the ASI (Agenzia Spaziale Italiana) project ROSA ROSSA (ROSA Research and Operational Satellite and Software Activities), that concerns the implementation of the ground segment for the data analysis of the GNSS (Global Navigation Satellite System) receiver for radio occultation ROSA (Radio Occultation Sounder of the Atmosphere) built by TAS-I (Thales Alenia Space–Italy) and mounted on board the Indian satellite Oceansat-22. Within the ROSA ROSSA project, in which this thesis is involved, it is under development the subsystem software SWOrD, that fully supports the orbit determination, orbit prediction and phase excess data generation activities.

1.2. The Global Navigation Satellite Systems - GNSSs

Satellite navigation systems, generically referred to as *Global Navigation Satellite Systems (GNSSs)*, are constellations of Earth satellites that autonomously provide very precise positioning on both static and moving receivers with global and continuous coverage. Each GNSS essentially consists of two main segments:

- a space segment, a constellation of Earth satellites transmitting radio-frequency signals;
- a ground segment, a network of electronic receivers that can determine their location (longitude, latitude and altitude) within a few meters detecting the navigation signals transmitted; receivers with a fixed position can also be used to calculate the precise time reference for scientific experiments.

To satisfy increasingly stringent requirements dependent on high precision and accuracy of the positioning solution, GNSSs are employed in different disciplines, like Earth sciences, land, sea and air navigation and military applications.

Actually the United States NAVSTAR (NAVigation by Satellite Timing And Ranging) GPS (Global Positioning System) is the only fully operational GNSS. The Russian GLobal NAvigation Satellite System (GLONASS) is a GNSS in restoring phase. In 2005 Europe launched the first test satellite of Galileo positioning system, GIOVE-A (Galileo In-Orbit Validation Element-A), which is a next generation GNSS, scheduled to start the operational phase in 2013. China has planned a new global

navigation satellite system called Compass (also known as Beidou-2), that will be active approximately in 2015. Finally, IRNSS (Indian Regional Navigational Satellite System) is a next generation GNSS, scheduled to be operational around 2015.

1.2.1. The Global Positioning System - GPS

The main observation data used for elaboration in this work are the microwave signals received by the satellite navigation system called NAVSTAR GPS, developed by the U.S. Department of Defense since 1973. The GPS system is not only used for position or time determination but also for various Earth Sciences high-precision applications. The GPS system architecture can be divided in three segments: the *space* segment, which includes the orbiting satellites; the *control* segment, which consists of a master control station, monitor stations and ground control stations and it is responsible for the monitoring and operations of the space segment; the *user* segment, comprising the user's GPS hardware (receivers and antennas) and GPS data processing software.

The GPS satellite constellation is designed to have four to eight satellites in view (above 15° elevation angle) anytime and anywhere to an user on the ground. For this purpose the space segment nominally consists of 24 Mean Earth Orbit (MEO) satellites (21 operational satellites plus three active spares for replenishment), with an altitude of about 20200 km above the Earth's surface and a distribution over six orbital planes separated by 60° on the equator. The GPS satellites have nearly circular orbits inclined by 55° with respect to the equatorial plane and an orbital period of half a sidereal day (11^h58^m), therefore over the same geographical location the entire satellite geometry repeats every sidereal day (23^h56^m).

On board GPS satellites there are very precise atomic clocks or oscillators[1] generating the fundamental frequency f_0 =10.23 MHz, used to produce the two L-band microwave signals (L_1 and L_2) transmitted and received by the GPS satellites: this duality is necessary to eliminate the major source of error, the ionospheric refraction. In particular, the two carrier frequencies f_1 (1575.42 MHz, wavelength about λ =19 cm, $f_1 = 154 \cdot f_0$) and f_2 (1227.6 MHz, wavelength about λ =24 cm, $f_2 = 120 \cdot f_0$) are modulated with the pseudo-random noise (PRN) ranging codes and the navigation message containing information about the satellite status, the satellite clock and the satellite ephemerides. The C/A-code (Coarse-Acquisition, Clear-Access, or Civil-Access) is modulated on the L_1 carrier only, has a period of 1 millisecond and it is available for civilian use. The P-code (Precise or Protected) is modulated on both L_1 and L_2 carriers, has a period of 7 days and it has been reserved for U. S. military and other authorized users.

The accuracy that civilian users can achieve using a GPS receiver is limited either by Selective Availability (SA) or by Anti-Spoofing (AS). Selective Availability (SA), consisting of a deliberate deterioration (*dither*) of the satellite clock frequency and a manipulation of the navigation message orbit data, was deactivated on May 2, 2000, 4:00 UTC. This change of policy has increased the point positioning accuracy, allowing a better estimate of the satellite clock corrections and improving the zero-difference applications that require the satellite clock information for processing. On the other hand, Anti-Spoofing (AS) is a protection against corrupted transmissions of satellite data by encrypting the P-code to form the Y-code[2]. Although AS is fully active, nowadays methods are known to eliminate part of the deteriorating effects.

The most important GPS observables are pseudorange and carrier phase measurements which can be acquired on both frequencies (f_1 and f_2): the first has an accuracy of a few decimeters, while the

[1] Two Rubidium (Rb) clocks and two Cesium (Cs) clocks were used in the GPS Block II/IIA satellites. These clocks are the first ones produced in any quantity for space operation, and have experienced lower-than-expected life, even though no GPS II/IIA satellite has been lost due to clock failure. Two Rb clocks and one Cs clock were originally planned for each satellite in the GPS Block IIR program. The selected Rb clocks resulted from second source development performed at EG&G during Block II/IIA procurement. However, after several years of unsuccessful attempts by the IIR Cs clock contractor to space-qualify a production unit, a three Rb clock configuration was selected for the IIR program to maintain schedule. Testing of the first two GPS Block IIR satellites on-orbit and results from a dedicated Rb clock life-test ongoing at the Naval Research Laboratory (NRL) indicate that the Rb clock is performing nicely (much better than specification), and indications of mission success are excellent. A clock configuration consisting of three Cs clocks and one Rb clock has been chosen for the GPS Block IIF spacecraft.

[2] The Y-code is used in place of the P-code whenever the Anti-Spoofing mode of operation is activated.

second is accurate to a few millimeters. The pseudorange observation derives from the difference in time between the receiver's local clock and an atomic clock on board a GPS satellite, multiplied by the speed of light to convert it into units of range. Phase measurements are ambiguous because the initial integer number of cycles between satellite and receiver is unknown: in order to relate the phase measurement with the geometric range, this integer number of wavelengths has to be estimated in the data processing. For a detailed description of the whole GPS satellite system and fundamental processing aspects we refer to [46, Hofmann-Wellenhof et al., 2001], [80, Springer, 2000], [77, Schaer, 1999].

The Full Operational Capability (FOC)[3] of GPS was declared on July 17, 1995, when the system reached all the program's requirements to be operational. However, additional advances in technology and the growing demand from military, civil, commercial and scientific users led to the effort to modernize the GPS constellation. In 1999 the USA announced the GPS modernization concept, referred to as GPS III. This next generation of satellites will offer significant improvements in accuracy, navigation capabilities, interoperability, jam resistance and it will provide new services to military and civilian users. The project will involve new ground stations, new satellites and four additional navigation signals. In particular, new civilian signals will be called L1C, L2C, L5 (1176.45 MHz) and the new military code will be M-Code. The first launch of a GPS III satellite is expected in 2014. See http://www.navcen.uscg.gov/gps/ for further information on the current GPS status.

1.3. LEO satellites with GPS receivers

Low Earth Orbit (LEO) satellites operate with orbiting altitudes in the range of 100 - 2000 km above the Earth's surface, much lower than traditional communications satellites, which brings them into frequent radio contact with ground stations with smaller propagation delays. The orbital period varies between less than 90 minutes and 2 hours. In a Low Earth Orbit the most important non-gravitational force acting on the satellite is the atmospheric drag decreasing rapidly with increasing height. It depends on the atmospheric density which is governed by altitude, solar activity, daytime, season and geographical longitude and latitude.

Satellite	Altitude (km)	Inclination (°)	Launch date
TOPEX/Poseidon	1336	66	10 August 1992
MicroLab-1/GPS/MET	730	60	9 April 1995
ØRSTED	640/850	96.5	23 February 1999
CHAMP	470-300	87	15 July 2000
SAC-C	705	98	23 November 2000
Jason-1	1336	66	7 December 2001
GRACE	450	89	17 March 2002
ICESat	600	94	12 January 2003
GRAS-MetOp	817	98.7	19 October 2006
GOCE	255	96.5	17 March 2009
Oceansat-2	720	98.3	23 September 2009

Table 1.1. The most important LEO satellites equipped with GPS receivers.

Numerous satellites are in Low Earth Orbits for different purposes: for mobile telephone communications, like Iridium constellation, or for scientific studies related, for example, to the Earth's gravity field, like GRACE (Gravity Recovery And Climate Experiment) and GOCE (Gravity field and steady-state Ocean Circulation Explorer) missions, or magnetic field, like Ørsted mission. A large number of LEO satellites are suited to be equipped with a tracking system based on GPS signals. The era of GPS receivers used for spaceborne applications began in the early 1980's. Initially they were launched into orbit only for demonstration of the concept of satellite tracking with GPS. The first receivers tracked only the pseudorange (Landsat 5, [Heuberger, 1984, Heuberger, 1984]). The

[3] See http://www.navcen.uscg.gov/gps/geninfo/global.htm.

first mission using pseudorange and carrier phase measurements of GPS for orbit determination is the radar altimeter mission TOPEX/Poseidon (TOPography EXperiment) launched in 1992. In Table 1.1 the most important LEO satellites carrying on board a GPS receiver are listed in order for launch date and below we will describe each mission briefly.

1.3.1. TOPEX/Poseidon

TOPEX/Poseidon [32, Fu et al., 1994] was a joint project operated by NASA (National Aeronautics and Space Administration, USA) and CNES (Centre Nationale d'Etudes Spatiale, France). It was launched in 1992 and it ceased operations in 2006. The satellite was put in a circular orbit inclined by 66 ° on the equator with an altitude of 1336 km. The main purpose of the mission has been the study of Earth's oceans, providing the first continuous and global coverage of ocean surface topography using a radar altimeter. TOPEX/Poseidon[4] allowed estimates of the global average sea level with an unprecedented accuracy of approximately 4.3 cm along the same path every 10 days.

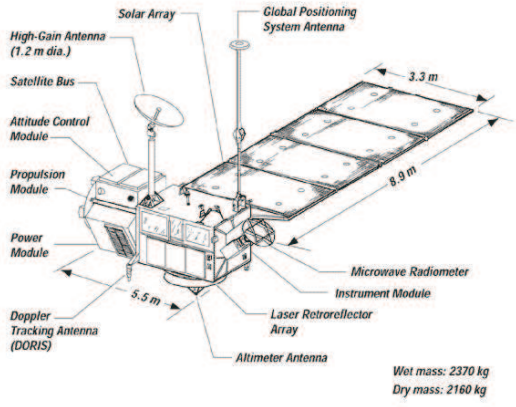

(a) TOPEX/Poseidon satellite structure.

(b) Artistic picture of TOPEX/Poseidon.

Figure 1.1. TOPEX/Poseidon satellite (both images are available at http://topex-www.jpl.nasa.gov).

To determine the distance between the satellite and the ocean surface, the satellite had on board two altimeters, sharing the same antenna, but only one altimeter was operating at any time (see Figure 1.1). To correct errors in the altimeter measurements, a microwave radiometer was used to calculate the total water vapour content in the atmosphere. In addition to these instruments, the satellite was equipped with a laser retro-reflector array for SLR measurements, a DORIS (Doppler Orbitography and Radio-positioning Integrated by Satellite) receiver and a GPS receiver. These three independent devices was used for orbit determination of the TOPEX/Poseidon satellite. The GPS could track up to six satellites simultaneously, but unfortunately, due to the receiver construction, it tracked both frequencies only during periods when AS was turned off [2, Bertiger et al.,1994].

1.3.2. MicroLab-1 - GPS/MET

The MicroLab-1 satellite was launched in 1995 and collected data until 1997, orbiting with an inclination of 60 ° and an altitude of about 730 km. The satellite carried on board the GPS/MET (GPS/METeorology) receiver which studied for the first time the occultation technique of GPS navigation satellite signals by the atmosphere to derive meteorological information. For more details on the technique we refer to [60, Melbourne et al., 1994]. The GPS/MET used an aft-looking antenna (see 1.2), therefore only half of the GPS satellites above the horizon of MicroLab-1 was tracked providing

[4]

TOPEX : The NASA built Nadir pointing Radar Altimeter using C band (5.3 GHz) and K_u band (13.6 GHz) for measuring height above sea surface.

Poseidon : The CNES built solid state Nadir pointing Radar Altimeter using K_u band (13.65 GHz).

100-150 globally distributed occultations per day. The GPS receiver was a space qualified TurboRogue capable of tracking up to 8 GPS satellites simultaneously at both frequencies transmitted by GPS. The success of the GPS/MET sensor has further validated the concept of using space-based sensors to improve worldwide weather prediction.

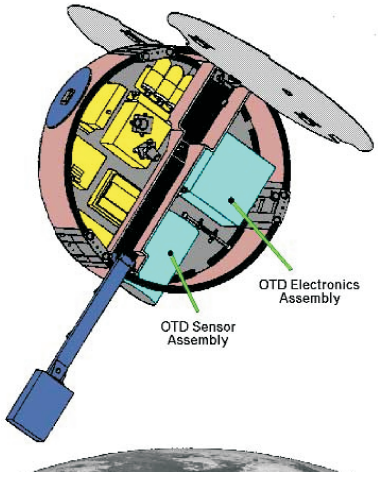

Figure 1.2. MicroLab-1 satellite (available at http://earthobservatory.nasa.gov).

1.3.3. ØRSTED

ØRSTED satellite, launched in 1999, is named after Hans Christian Ørsted (1777-1851), a Danish physicist and professor at the University of Copenhagen that found the relationship between an electric current and magnetism. The orbit, inclined 96.5° with respect to the Earth's equator, is sun-synchronous and allows to map almost the entire globe as the Earth rotates. Ørsted satellite, originally intended to last for 14 months, is still operational and continues to collect accurate measurements of the Earth's magnetic field, in particular to determine its temporal variations.

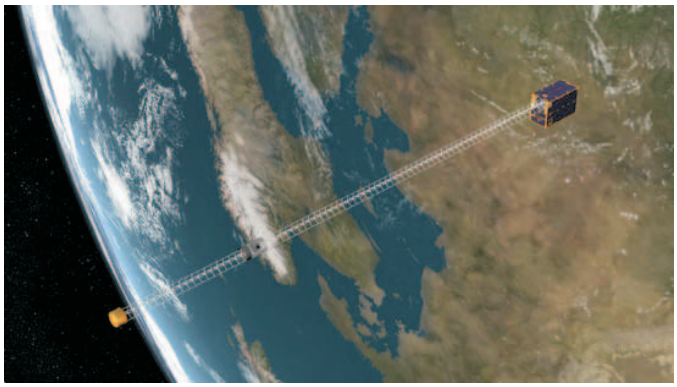

Figure 1.3. Artistic picture of Ørsted satellite (available at http://www.dmi.dk/dmi/oersted).

Based on data from the Ørsted satellite, researchers from Danish Space Research Institute concluded that the Earth's magnetic poles are moving and that the speed with which they are moving has been increasing for the past few years. This apparent acceleration indicates, that the poles of the Earth might be in the process of switching around, which could have serious consequences for land-based biological life. Three sensors are situated at the end of an 8 meter boom so disturbance from the satellite's electrical systems is minimal (see Figure 1.3):

- Flux-gate Magnetometer (CSC), used to measure the three vector components of the geomagnetic field;
- Overhauser Magnetometer (OVH), used to measure the strength of the geomagnetic field, but not the direction;

- Star Imager (SIM), used to examine images of the sky and compare them with a star catalogue in order to determine the CSC-magnetometer orientation and the satellite attitude.

The other three instruments are located in the main body of the satellite:

- Charged Particle Detectors (CPD), used to detect electrons in the energy range from 30 keV to 1 MeV and protons and alpha particles from 200 keV to 100 MeV;
- TurboRogue GPS Receiver, used to accurately determine the satellite's position and provide atmospheric occultation data, like atmospheric pressure, temperature and humidity;
- Trimble TANS GPS Receiver, also used to determine the satellite's position.

The GPS receiver on-board ØRSTED is working well but the measurements are not sufficient in quantity and quality to be used for reliable POD.

1.3.4. CHAMP

CHAMP (CHAllenging Minisatellite Payload) ([73, Reigber et al., 1998]) is a German mission under the leadership of the GFZ (GeoForschungsZentrum)in Potsdam, Germany, and with the partnership of NASA (National Agency Space Administration), CNES and AFRL (Air Force Research Laboratories, USA). The satellite was launched in 2000 from Plesetzk, Russia, onto an almost circular, near polar orbit, with an average altitude of 450 km. Although the design lifetime of the satellite system was 5 years, CHAMP is currently collecting data used for many scientific applications, such as GPS radio occultation.

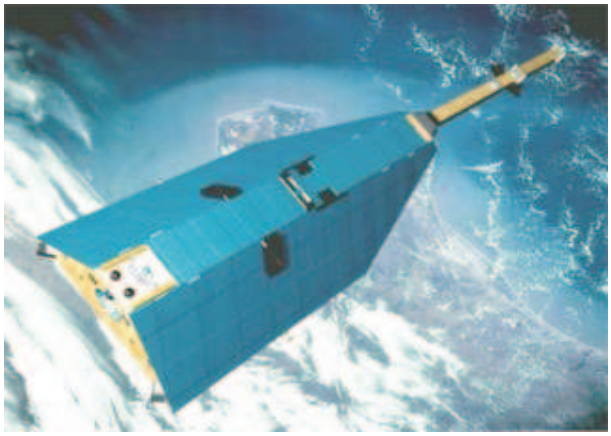

Figure 1.4. Artistic picture of CHAMP satellite (available at http://www.colorado.edu).

The primary objectives of CHAMP are the mapping of the global static Earth's gravity field, the recovering of the global magnetic field and the profiling of the ionosphere and the troposphere. The main instruments to achieve the mission goals are:

- a dual-frequency GPS receiver (provided by NASA/JPL), to determine the satellite orbit;
- a three-axis accelerometer (provided by CNES), to measure the non-gravitational accelerations acting on the satellite which are mainly due to atmospheric drag, solar radiation pressure, Earth albedo radiation and attitude maneuvers. Using these measurements allows to generate a dynamic orbit of the LEO without modeling the non-gravitational forces which is very helpful for gravity field recovery. A cold gas propulsion system has been employed in order to control the attitude and to perform orbit change maneuvers; the attitude of the spacecraft is not stable over a long time period due to the design of the satellite. The attitude is corrected by thruster pulses of the cold gas propulsion system, which may happen between 70 and 200 times per day;
- a laser retro-reflector array for SLR (Satellite Laser Ranging) measurements. The SLR technique is a completely independent technique to determine precise orbits for the LEO. SLR observations

are accurate ($\sim$ 1 cm), unambiguous and free of atmospheric propagation effects due to water vapour. This is why the SLR technique is very useful for calibrating the orbit resulting from the GPS tracking;

- a fluxgate magnetometer, to measure the vector components of the Earth's magnetic field;

A detailed description of the instruments used for POD (GPS receiver, laser retro-reflector array, accelerometer instrument and attitude sensor) may be found in [43, Grunwaldt & Meehan, 2003]. Figure 1.4 shows an artistic picture of the satellite.

1.3.5. SAC-C

The Earth observation satellite SAC-C was launched in 2000 [76, SAC-C web site]. It is a joint mission between the Argentine CONAE (Comisión National de Actividades Espaciales, National Commission on Space Activities), which has the main responsibility, and NASA. Moreover there are the contributions from Brazil, Denmark, France and Italy. SAC-C is orbiting at an altitude of 702 km and the sun-synchronous orbit has an inclination of 98 ° with respect to the equator. The SAC-C scientific objectives are to provide multispectral images of the Earth in order to monitor the environmental conditions, to conduct studies on the structure and dynamics of both the atmosphere and the ionosphere using GPS based techniques, to map the Earth's magnetic field and to measure the influence of high energy space radiation on the advanced electronic components (see Figure 1.5).

Figure 1.5. SAC-C satellite structure (available at http://www.gsfc.nasa.gov/gsfc).

The SAC-C mission comprises 11 different instruments. The instrument of interest for POD is the BlackJack GPS receiver provided by JPL. In addition, the satellite is equipped with a Lagrange GPS/GLONASS demonstration receiver, which is part of the INES (Italian Navigation Experiment) and should demonstrate the capability of a secondary attitude determination sensor. The BlackJack GPS receiver has four antennas looking towards the up, down, fore and aft directions. Therefore, the GPS signals may be used for POD (up), for radio occultations (fore and aft), and for GPS altimetry (down) making use of the GPS signals reflected by the Earth's oceans.

1.3.6. Jason-1

The Jason-1[5] satellite altimeter [**?**, Jason-1 web site], the follow-on to the TOPEX/Poseidon mission, is a joint project between NASA and CNES with the purpose to measure the ocean surface topography. It was launched in 2001 and is orbiting at an altitude of 1336 km in an almost circular orbit with an inclination of 66 °. During the first months Jason-1 shared an almost identical orbit to TOPEX which allowing for cross calibration. At the end of this period TOPEX was moved to a new orbit midway

[5]The program is named after the Greek mythological hero Jason who led the Argonauts on the search for the Golden Fleece.

between each Jason ground track. Like TOPEX, Jason-1 has a repeat cycle of 10 days and is equipped with the same but revised instruments:

- Poseidon 2 Nadir pointing Radar Altimeter using C band and Ku band for measuring height above sea surface;
- JMR (Jason Microwave Radiometer) measures water vapour along altimeter path to correct for pulse delay;
- DORIS (Doppler Orbitography and Radiopositioning Integrated by Satellite) dual-frequency system receiver for orbit determination to within 10 cm or less and ionospheric correction data for Poseidon 2;
- BlackJack GPS receiver, that provides precise orbit ephemeris data for POD; the GPS antenna is placed at the side of the satellite body and is tilted with respect to the axes of the satellite (see Figure 1.6); the GPS data are available since 2002;
- Laser retro-reflector array, that works with ground stations to track the satellite and calibrate and verify altimeter measurements.

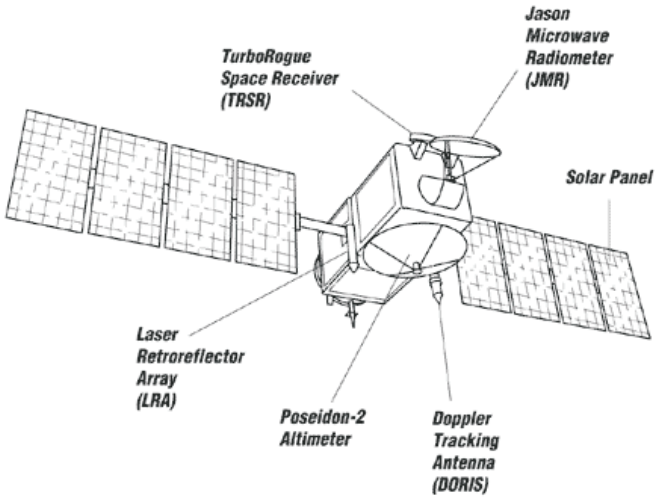

Figure 1.6. Jason-1 satellite structure (available at http://topex-www.jpl.nasa.gov).

Jason-1 has provided measurements of the surface height of oceans to an accuracy of 3.3 centimeters continues to collect scientific data. In 2009 the Jason-1 satellite has been put on the opposite side of Earth from the Jason-2 satellite, which is operated by the U.S. and French weather agencies. This combination provides twice the number of measurements of the ocean's surface.

1.3.7. GRACE

GRACE (Gravity Recovery And Climate Experiment) [41, GRACE web site], launched in 2002, may be viewed as the following mission of CHAMP. It is a joint project between NASA and DLR (Deutschen Zentrums für Luft- und Raumfahrt) and consists of two earth satellites (see Figure 1.7), following each other along the same orbital trajectory, with a relative distance of 220 km±50 km. The inclination of the orbit is 89 ° and the orbit altitude was initially 500 km. The main purpose of GRACE is the determination of the Earth's gravity field and its temporal variations. A K-Band Ranging (KBR) system is the fundamental instrument of GRACE because it allows to measure the range and range-rate between the two spacecrafts with a precision of respectively 10 μm and 1 μm/s with a 5 s data interval. This dual-band microwave link provides a new and independent observation type for mapping the gravity field of the Earth.

Both the satellites are equipped with a codeless dual frequency GPS receiver that provides data for the POD of GRACE and for ionospheric profiling. Differently from CHAMP, the GPS POD antenna is not aft-looking, but it is placed in the middle of the satellite body. Moreover each satellite carries on board a laser retro-reflector array used together with the GPS for the POD, an accelerometer to measure all non-gravitational accelerations and a cold gas thruster.

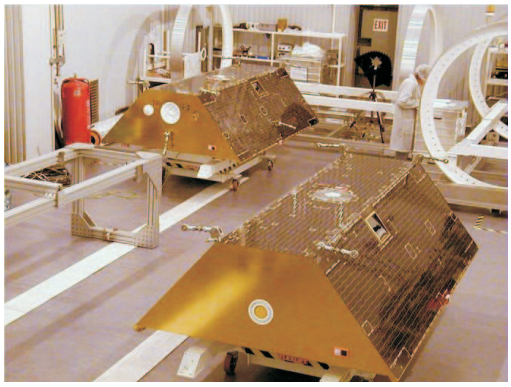

(a) GRACE A and GRACE B satellites (photo reported by Tapley, 12-14 April 2005, 15th Sea Space Remote Sensing Conference, The University of Texas, Center for Space Research, Austin, Texas).

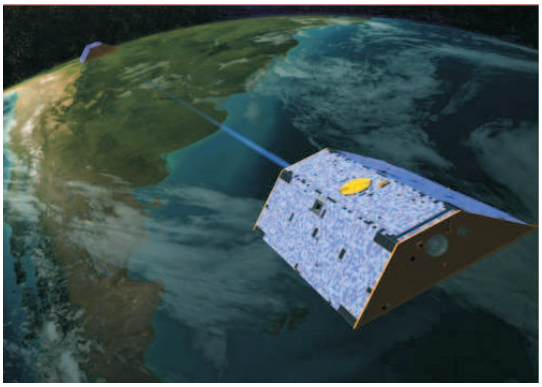

(b) Artistic picture of GRACE in space.

Figure 1.7. Artistic picture of the GRACE satellites (available at http://www.csr.utexas.edu/grace/).

1.3.8. ICESat

The ICESat (Ice, Cloud, and land Elevation Satellite) mission is designed for measuring the mass balance of ice sheets, cloud and aerosol heights, optical densities, vegetation and land topography. The satellite (Figure 1.8 [48, ICESat web site]) was launched in 2003 into a near-circular, near-polar orbit with an altitude of 600 km height and an inclination of 94°. The main purpose of ICESat is to provide elevation data needed to determine ice sheet mass balance as well as cloud property information, especially for stratospheric clouds common over polar areas. Further objectives include measurement of cloud and aerosol height profiles, land elevation and vegetation cover and sea ice thickness.

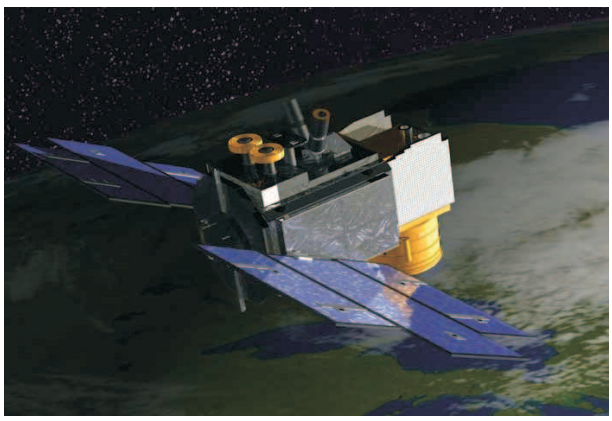

Figure 1.8. Artistic picture of ICESat satellite (available at http://icesat.gsfc.nasa.gov).

The only scientific instruments are the GLAS (Geoscience Laser Altimeter System), a space-based LIDAR (Laser Imaging Detection And Ranging) developed at the Goddard Space Flight Center, and the GPS receiver. GLAS combines a precision surface LIDAR with a sensitive dual-wavelength cloud and aerosol LIDAR. The GLAS lasers emit infrared and visible laser pulses at 1064 and 532 nm wavelengths: the infrared pulse is used for surface altimetry, while the green pulse is used for atmosphere measurements. The pulse repetition rate is 40 pulses/sec. Like ICESat orbits, GLAS produces a series

of approximately 70 m diameter laser spots that are separated by nearly 170 m along the spacecraft's ground track.

During the commissioning phase of the mission, the ICESat was placed into an orbit which allowed the ground track to repeat every 8 days. During August and September 2004, the satellite was maneuvered into a 91-day repeating ground track for the main portion of the mission.

ICESat was designed to operate for three to five years. Testing indicated that each GLAS laser should last for two years, requiring GLAS to carry three lasers in order to fulfill the nominal mission length. An investigation indicated that a corrosive degradation of the pump diodes, due to an improper material usage in manufacture, had possibly reduced the reliability of the lasers. Consequentially, the total operational life for the GLAS instrument was expected to be as little as less than a year as a result. After the two months of full operation, the operational plan for GLAS was changed. GLAS now operates for one-month periods out of every three to six months in order to extend the time series of measurements, particularly for the ice sheets.

1.3.9. MetOp-GRAS

The MetOp (Meteorological Operational) satellite programme is a European series of three satellites operated by ESA and EUMETSAT (EUropean organization for the exploitation of METeorological SATellites), providing weather data services that will be used to monitor climate and improve weather forecasts. The first satellite MetOp-A was launched in 2006 (see Figure 1.9), while the other two MetOp satellites will be launched, nominally each 5 years, to ensure the delivery of continuous, high-quality global meteorological data until at least 2020. MetOp-A is in polar orbit at an altitude of about 817 km and inclined 98.7° with respect to the equator.

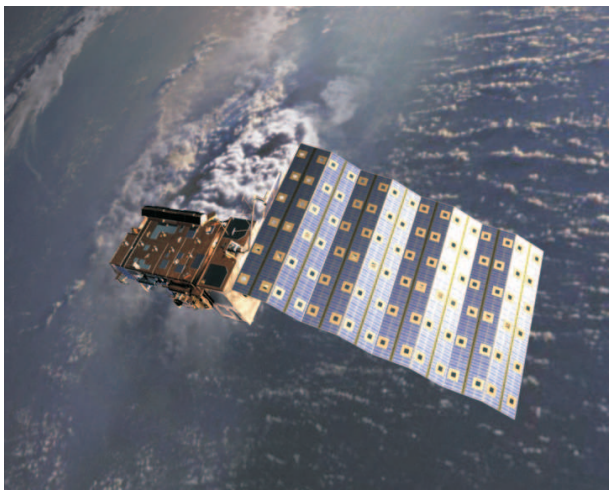

Figure 1.9. Artistic picture of MetOp satellite (available at http://www.esa.int/esaLP).

MetOp satellites payload includes GRAS (GNSS Receiver for Atmospheric Sounding), which is a new European Global Navigation Satellite System receiver that operates as an atmospheric sounder. It was launched in 2006 and will provide unprecedented observations of atmospheric temperature and humidity to improve weather forecasting and climate change monitoring. GRAS uses radio occultation to measure vertical profiles of atmospheric temperature and humidity by tracking signals received from a constellation of GPS navigation satellites while they are setting or rising behind the Earth's atmosphere. GRAS navigation data are only used for POD of the MetOp spacecraft. However, the GRAS navigation measurements can be used to monitor the electron content above the spacecraft.

1.3.10. GOCE

GOCE (Gravity field and steady-state Ocean Circulation Explorer) is a satellite mission of the ESA Living Planet Programme, launched in 2009 (see Figure 1.10). GOCE is flying at the very low altitude of about 255 km in a sun-synchronous orbit inclined 96.5° with respect to the Earth's equator. The main purpose of GOCE is to map the static part of Earth's gravity field with an unprecedented

precision of 1 mGal = 10^5 m/s^2 and to model the geoid heights with an accuracy of 1-2 cm, achieving these results at a spatial resolution of 100 km.

The main scientific instrument on board GOCE is a three-axis EGG (Electrostatic Gravity Gradiometer), for the first time employed in a satellite mission. The EGG consists of three pairs of accelerometers able to measure gravity gradients in three spatial orthogonal directions. The payload of GOCE is also composed by a 12-channel GPS receiver, working on both L1 and L2 frequencies, with a sampling rate of 1 Hz. The gradiometer and the GPS receiver are dedicated to gravity field recovery, where the GPS observations are mainly useful to recover the low degree and order terms of the geopotential, while the gradiometer allows to obtain the high degree and order terms of the gravity field. Moreover GOCE is carrying on board a laser retro-reflector array, used for SLR measurements, providing mainly an independent validation of the GPS POD, star cameras for the attitude control and an ion thruster for the realization of a drag-free control of the satellite in along-track direction.

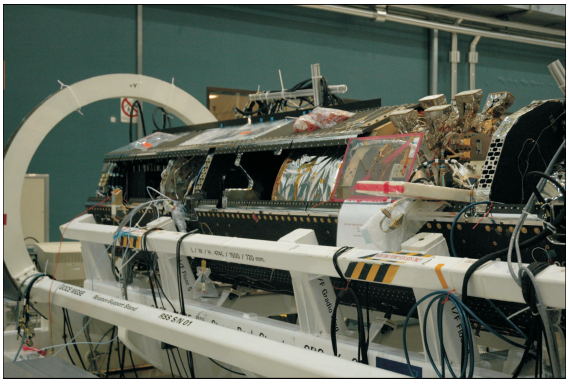

(a) GOCE before going to Russia for the last space test (Turin, TASI class 10000 clean room, photo personally taken).

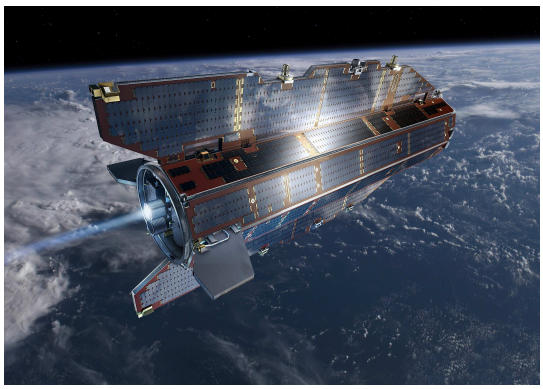

(b) Artistic picture of GOCE in space (available at http://www.esa.int/esaLP/).

Figure 1.10. GOCE satellite.

1.3.11. Oceansat-2

Launched in 2009, Oceansat-2 is a remote sensing satellite operated by ISRO (Indian Space Research Organization) and dedicated to ocean research (see Figure 1.11). The satellite will provide continuity to Oceansat-1 mission, which was launched in 1999. Oceansat-2 is orbiting the Earth at an altitude of about 720 km and inclined 98.3° with respect to the equator.

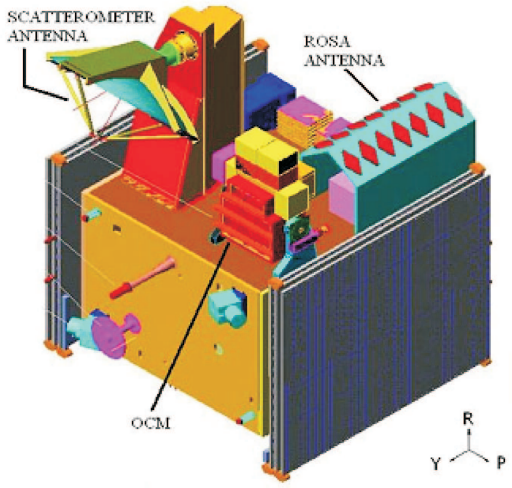

Figure 1.11. Oceansat-2 satellite (available at http://www.asi.it/Rosa/RosaIT/OCEANSAT-II.htm).

Oceansat-2 is equipped with three scientific instruments, of which two are Indian and one is from the Italian Space Agency:

- OCM (Ocean Color Monitor), that can provide observations in eight spectral bands in the range between 402 and 885 nm (VIS-NIR);
- SCAT (Scanning Scatterometer), operating in Ku-band (13.515 GHz) to measure sea surface wind velocity;
- ROSA (Radio Occultation Sounder for Atmosphere), a GPS occultation receiver provided by ASI to obtain profiles of the lower atmosphere and the ionosphere; for more details about ROSA we refer to Section 1.5.

Oceansat-2 is in orbit with 6 smaller satellites, technological demonstrators provided by different European universities.

1.4. Radio Occultation for Earth Weather Science

When a radio signal passes through the atmosphere its phase is perturbed in a manner related to the refractivity along the ray path (see Figure 1.12). Measurements of the phase perturbations can reveal the refractivity, from which one can then derive such quantities as atmospheric density, pressure, temperature, moisture, geopotential heights and winds. In this paragraph we describe a particular remote-sensing application that is well suited for micro-satellites in Low earth Orbit: the *Radio Occultation technique*. This technique, completely described in [60, Melbourne et al., 1994] and here only reported an extract, was pioneered by JPL and Stanford University in the early 1960s for study of planetary atmospheres and ionospheres, when Mariners 3 and 4, viewed from Earth, passed behind Mars. In this case, a LEO satellite uses the Global Positioning System (GPS) to probe the Earth's atmosphere. This technique is suited for monitoring global atmospheric temperatures, pressures and moisture distributions with high accuracy and spatial resolution and for studying the ionosphere.

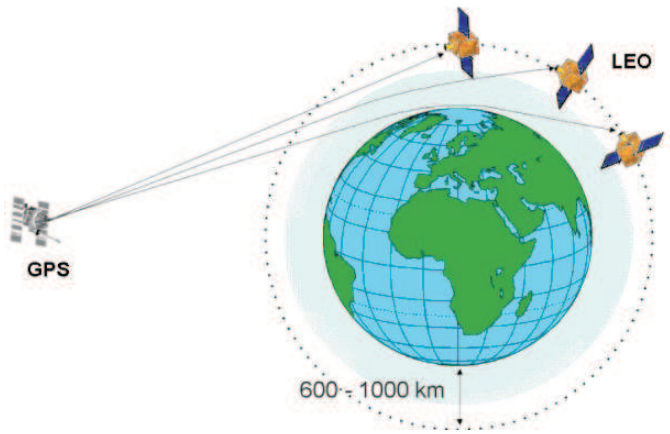

Figure 1.12. Geometry of an RO measurement (available at http://geodaf.mt.asi.it/html_old/GPSAtmo/space.html).

The GPS receiver on board a micro-satellite in a LEO tracks the high precision L-band navigation signals from the constellation of GPS satellites. The GPS satellites broadcast on two coherent radio frequency carriers that are separated in frequency by 350 MHz. The fundamental measurements made by the receiver are the phase and signal strength of each carrier, which are sampled at a rate up to 50 Hz.

When the LEO receiver tracks a GPS satellite that is observed to rise or set through the Earth's atmosphere (that is, a satellite being occulted by the Earth), the arrival time of the received radio signal is retarded because of the refractive bending and slowing of the signal as it traverses the atmosphere. By measuring the change in carrier phase over the entire occultation event, about 1 minute in duration for the neutral atmosphere, we can determine the atmospheric refractive index as a function of altitude. Pressure and temperature profiles can then be derived through a downward integration using the gas law, the known linear relationship between refractivity and density of dry air, and the assumption of hydrostatic equilibrium (see Figure 1.13).

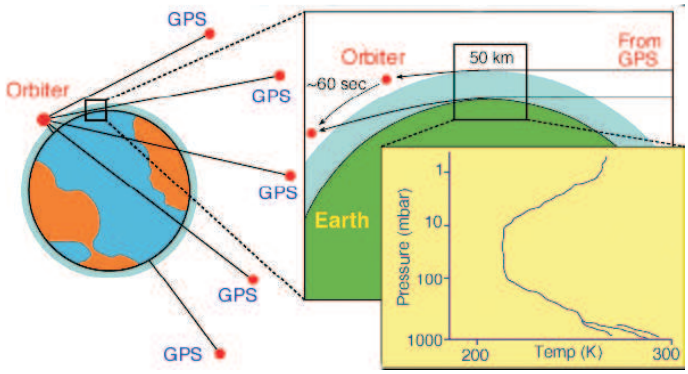

Figure 1.13. Atmospheric pressure and temperature profiling by GPS occultation [60, Melbourne et al., 1994].

Below the tropopause, the presence of water vapour limits the accuracy of temperature recovery because of uncertainty in the distribution and relative abundance of the water vapour in the troposphere. The refractivity of a mole of water vapour for microwaves is about 17 times that of dry air. On the other hand, it is possible to exploit this high sensitivity to recover water vapour profiles in the troposphere by using meteorological models and other sensor information for temperature and pressure to separate the dry air and water vapour signatures on the tracking data. With this approach, the LEO can also chart much-needed water vapour distributions in the lower troposphere, particularly over tropical oceanic areas.

From the time series of the difference in phase on the two L-band carriers that are measured by the LEO receiver, the change in the integrated ionospheric electron content along the line between the GPS and LEO satellites can be precisely determined (to less than 0.1% of the total). With this technique, tomographic studies of ionospheric electron distributions can also be undertaken with the combined LEO space platforms and GPS ground tracking network. Because the GPS RO technique is free of instrumental biases, it can also serve as a calibration system. An operational RO system that provides long-term coverage will furnish an absolute standard for calibrating other global change monitoring instruments to ensure long-term stability in their atmospheric measurement series.

This technique also requires (for satellite ephemeris control and elimination of oscillator errors) a globally distributed ground network of GPS receivers that are concurrently tracking all observable GPS satellites. The data streams from the ground network and the LEO are synchronously combined (by interpolation) at a central facility and processed in parallel to form high accuracy positions and velocities of all the satellites including the LEO, and generate highly precise differential phase residuals of the retarded signal arriving at the LEO from the occulted GPS satellite. All instrumental biases are eliminated because the concurrent and synchronous observation set enables us to remove the effect of instrumental (transmitter and receiver) phase delay and oscillator errors in the measurements and because signal processing circuitry in the receiver is digital.

A single LEO observing both rising and setting satellites would provide about 500 globally distributed temperature profiles daily with sub-kelvin accuracies over altitudes of 8-45 km. The vertical resolutions would be comparable to those from the best limb sounders (4 km). The technique is essentially all-weather and unaffected by clouds and particles. RO measurements provide the potential of measuring refractivity profiles in regions where ground-based sensors cannot easily be located, such as deep sea waters. Furthermore, constellations of RO satellite receivers can be used to provide a very large number of measurements with a global distribution.

1.5. The ROSA ROSSA project

The ROSA ROSSA project deals with the agreement between the Italian Space Agency (ASI - Agenzia Spaziale Italiana) and the Indian Space Research Organization (ISRO) to make fly the Italian instrument ROSA (Radio Occultation Sounder of the Atmosphere), a GNSS receiver for Radio Occultation, on board the Indian Satellite Oceansat-2. ROSA is an advanced GNSS receiver designed to track GNSS signals in the lower atmosphere during near radio occultation events.

India successfully launched its 16th remote-sensing satellite Oceansat-2 and six European nano-satellites in 1,200 seconds with the help of Polar Satellite Launch Vehicle (PSLV) from Sriharikota on 23 September 2009. The launch was carried out as per schedule at 11.51 am and ended at 12.06 pm. The 44.4-meter tall, 230-tonne Indian rocket PSLV freed itself from the launch pad at the spaceport and lifted itself up, lugging the 960-kg Oceansat-2 and the six nano-satellites all together weighting 20 kg.

In the framework of this opportunity, the Italian Space Agency (ASI) founded a pool of Italian Universities and Research Centers for the implementation of the overall (and state-of-the-art) RO processing chain which is called ROSA ROSSA (ROSA-Research and Operational Satellite and Software Activities). The ROSA ROSSA will be integrated in the operative ROSA Ground Segment by an Italian Software enterprise (INNOVA, located in Matera, Italy), and the ROSA ground segment will operate in Italy (at the ASI Space Geodesy Center, near Matera) and in India (at the Indian National Remote Sensing Agency, near Hyderabad) starting from the 2009 Autumn season. In this first release (the ROSA ROSSA "Base" Version), software modules are based on well consolidated algorithms, while the RO state-of-the-art algorithms will be implemented in the final ROSA ROSSA release (namely the "Extended" version) expected for May, 2010 [69, Perona et al., 2009], [70, Perona et al., 2009]. This "Extended" version will be developed and, for the first time, it will run on a distributed hardware and software infrastructure exploiting a GRID computing strategy.

In particular, my thesis concerns with the realization of a new innovative software for POD and RO purposes, called SWOrD(SoftWare for Oceansat-2 oRbit Determination). SWOrDis a software subsystem of the ROSA ROSSA (ROSA Research and Operational Satellite and Software Activities) project that fully supports the orbit determination, orbit prediction and phase excess data generation activities.

After a preliminary quality check carried out by the QC1A Data Generator, the ROSA ROSSA processing chain is performed through the following software modules (see Figure 1.14).

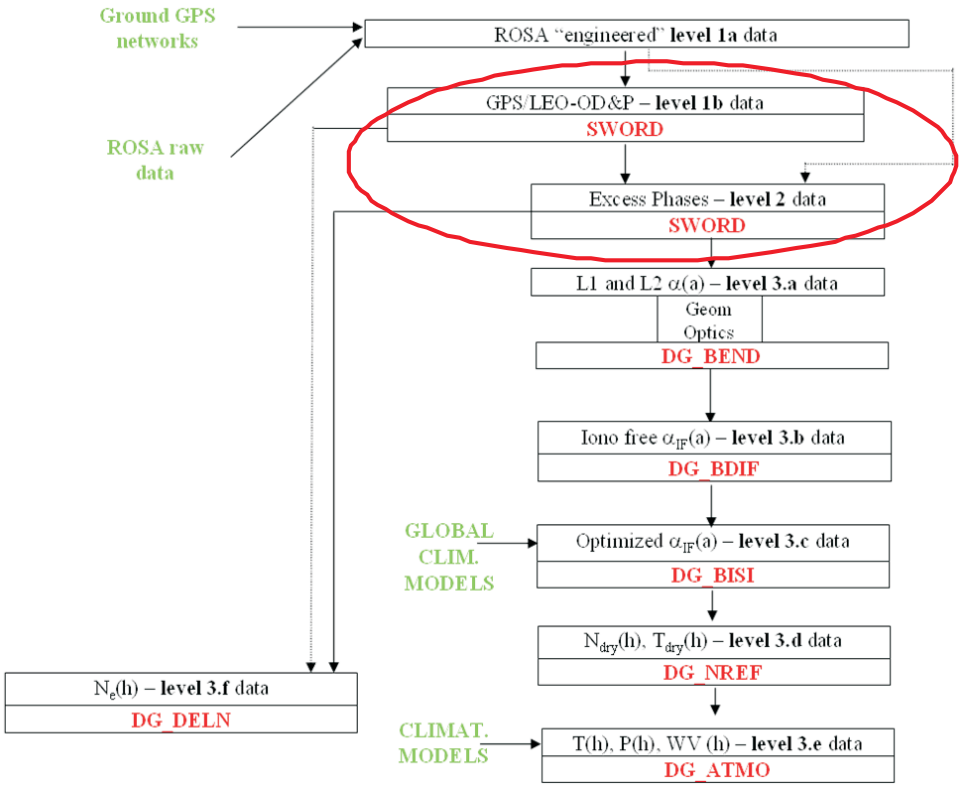

Figure 1.14. ROSA ROSSA data processing chain and data flow (from the ROSA ROSSA documentation).

SWOrD SWOrD(SoftWare for Oceansat-2 Orbit Determination) is the software package that fully supports the LEO orbit determination (Level 1b data) and the Level 2 data generation; in the ROSA ROSSA "Base" version GPS orbits are taken by IGS, while in the "Extended" version they

will be determined by the final SWOrDversion. LEO orbit data (Level 1b data) are computed using daily ROSA NAV_F observations and support data and are given in output as daily (or 6 hours, in the "Extended" Version) sp3 files. Then, after the occultation events splitting, SWOrDcomputes single event excess phase profiles on both GPS signal carriers L1 and L2 (Level 2 data) using occultation observations (OCC_CD and OCC_E input data files). Level 2 data are formatted into ASCII files. For each day of observations, SWOrDproduces also a table which describes the location of all the occultation events in an ECEF (Earth Centered Earth Fixed) reference frame. This table is based on estimated orbits (or predicted orbits, in the "Extended" ROSA ROSSA release).

DG_BEND DG_BEND (DG_BENDing) provides raw bending and impact parameter profiles computed on L1 and L2 GPS excess phase data (filtered using different cut-off frequencies). In the first ROSA ROSSA release the standard Geometric Optics approach has been adopted (see [1]) while algorithms based on Fourier operator (see [7]) are expected to be implemented in the "Extended" ROSA ROSSA release. For each value of the filtered bending and corresponding impact parameter, the geometrical location of the real tangent point is given. All data are time tagged and all this information is stored on an ASCII file (Level 3.a data).

DG_BDIF DG_BDIF (DG_BenDing Iono Free) provides a bending and impact parameter profile on which ionospheric effects have been compensated for. The standard linear combination is applied to L1 and L2 bending and impact parameter profiles (see [8]). The computed profile is given in output to this DG as an ASCII formatted file (Level 3.b data).

DG_BISI DG_BISI (DG_Bending Iono-free Stratospherical Initialized) provides bending angle and impact parameter profiles initialized in the stratosphere, using the corresponding climatological values (or ECMWF data in the "Extended" Version). This DG performs a statistically optimal approach for smoothing the bending angles derived from RO measurements above 40 km, as described in [9]. The actual version of the optimization technique combines the observed bending angle profile with a smooth background estimate derived from climatology in a statistical optimal way, to obtain the most probable bending angle profile. The method assigns more weight to the background if the standard deviation of the observations is greater than the standard deviation of the background and viceversa. As a consequence, decreasing the altitude, the contribution of the observed bending angles to the final profile increases. Output data are stored on an ASCII file (Level 3.c data).

DG_NREF DG_NREF (DG_N REFractivity) computes the refractivity, the dry air temperature and the pressure "quasi-vertical" profiles from iono-free and initialized bending and impact parameter profiles, by applying the classical inverse Abel integral (see [1]). Geodetic latitude, longitude and height corresponding to the location of each point of the profile are given on a global domain above the EGM96 Geoid model. An ASCII file is available in output (Level 3.d data).

DG_ATMO DG_ATMO (DG_ATMOspheric profiles) allows the evaluation of water vapour and temperature profiles using Global Climatological Models (in the ROSA ROSSA "Base" Version) or Numerical Weather Prediction data (in the "Extended" Version) following a 1DVAR approach. The error covariance matrices for the background field are based on the inter-level correlations as shown in [10] and the error matrix covariance is specified following the one used by the GRAS-SAF algorithm. An ASCII file is available in output (Level 3.e data).

DG_DELN DG_DELN (DG_Density ELectroN) computes the electron density profile in ionosphere. It receives in input Level 2 data files and produces vertical electron density profiles following the onion peeling approach (see [1]). Locations of each profile point (latitude, longitude and altitude) are also stored. For each event an ASCII file is produced as an output (Level 3.f data).

Chapter 2

GPS Measurement Models

2.1. Introduction

This chapter is devoted to the introduction of the measurement equations used by SWOrD. Specifically, observation equations will be introduced for the pseudorange measurements, for the carrier phase measurements, some of their linear combinations (LC), and for their single and double differences. he GPS observables are measurements of time (using PRN code sequences) or phase differences between received signals and related receiver generated signals. The ranges between the receivers and the transmitters are computed from these measurements using the *one way concept*, where two clocks are used, one in the transmitter and one in the receiver. A GPS receiver measures the incoming GPS signal with respect to its internal time scale. Therefore the measurements may need to be realigned with GPS time because the long term behavior of the receiver clock can cause misalignment of time-tags w.r.t. the reference time scale, the GPS time. This is particularly true if the receiver is steered by a poor-quality clock, like a cheap quartz. This correction has to be considered because the most natural choice for the time associated to a measure is the reception time. Therefore the *time tags of the measurements have to be shifted by the receiver clock error* and the code and phase *observables measured have to be correct by the receiver and transmitter clock errors*. Since the ranges are biased by clock errors, they are denoted as *psudoranges*. To remove clock and other observable errors it has become a common practice to use various linear combinations of the code and phase observables (double and triple differences, wide- and narrow-line combination, geometry-free and ionospheric-free combination and many others), even if also undifferenced observables can be used with the opportune corrections. In high-precision surveying it is necessary to use the phase observable. For this reason in this chapter will be initially provided several definitions about question related to *time* and its *measurement*.

2.2. Time measurement

Time[1] is currently one of the few fundamental quantities[2]. Thus, similar to definition of other fundamental quantities (like space and mass), time is defined via measurement[3].

The measurement of time is so critical to the functioning of modern societies that it is coordinated at an international level. The basis for scientific time is a continuous count of seconds based on atomic clocks around the world, known as the *International Atomic Time* (TAI)[4]. This is the yardstick for other time scales, including Coordinated Universal Time (UTC)[5], which is the basis for civil time.

Measurement, by its nature, is inexact and the magnitude of that "inexactness" is the error. Error is inherent in measurement, and incorporates such things as the *precision* and the *accuracy* of the measuring tools, their proper adjustment, and competent application. The analysis of the magnitude of probable error is appropriate in examining the suitability of methods or equipment used to obtain, portray and utilize an acceptable result.

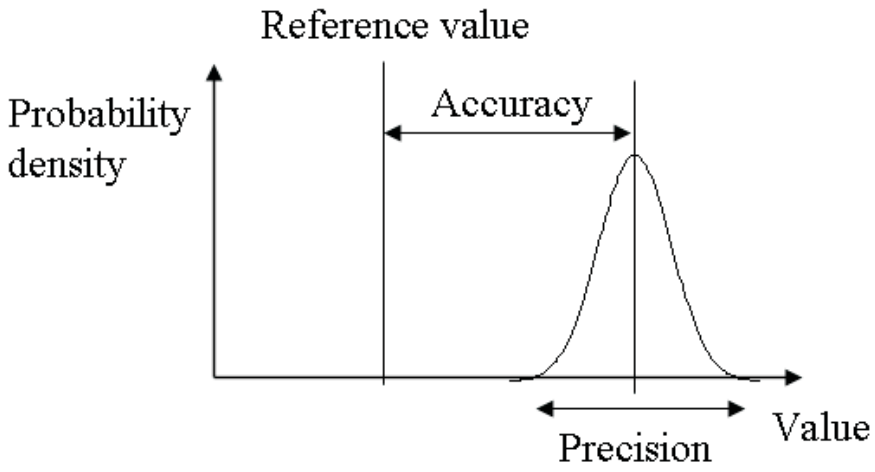

Figure 2.1. Statistical proprieties for accuracy and precision.

Definition 1 (Accuracy) *Accuracy is the degree of conformity of a measured or calculated quantity to its actual (true) value.*

[1]Two distinct views exist on the meaning of time. One view is that time is part of the fundamental structure of the universe, a dimension in which events occur in sequence. This is the realist view, to which Isaac Newton [1] subscribed, in which time itself is something that can be measured. A contrasting view is that time is part of the fundamental intellectual structure (together with space and number) within which we sequence events, quantify the duration of events and the intervals between them, and compare the motions of objects. In this view, time does not refer to any kind of entity that "flows", that objects "move through", or that is a "container" for events. This view is in the tradition of Gottfried Leibniz and Immanuel Kant, in which time, rather than being an objective thing to be measured, is part of the mental measuring system.

[2]Fundamental quantities cannot be defined via other quantities because there is nothing more fundamental than what is presently known.

[3]The SI base unit for time is the SI second. From the second, larger units such as the minute, hour and day are defined, though they are "non-SI" units because they do not use the decimal system, and also because of the occasional need for a leap-second. They are, however, officially accepted for use with the International System. There are no fixed ratios between seconds and months or years as months and years have significant variations in length. The official SI definition of the second is as follows:

> "The second is the duration of 9,192,631,770 periods of the radiation corresponding to the transition between the two hyperfine levels of the ground state of the caesium 133 atom."

[4]International Atomic Time (TAI, from the French name Temps Atomique International) is a high-precision atomic time standard that tracks proper time on Earth's geoid. It is the principal realisation of Terrestrial Time, and the basis for Coordinated Universal Time which is used for civil timekeeping all over the Earth's surface.

[5]Coordinated Universal Time (UTC) is a high-precision atomic time standard. UTC has uniform seconds defined by International Atomic Time (TAI), with leap seconds announced at irregular intervals to compensate for the earth's slowing rotation, and other discrepancies. The leap seconds allow UTC to closely track Universal Time (UT), which is a time standard based on the earth's angular rotation, rather than a uniform passage of seconds.

Definition 2 (Precision) *Precision, also called reproducibility or repeatability, is the degree to which further measurements or calculations will show the same or similar results.*

The results of calculations or a measurement can be accurate but not precise, precise but not accurate, neither or both. A result is called valid if it is both accurate and precise. The related terms in surveying are error (random variability in research) and bias (non-random or directed effects caused by a factor or factors unrelated by the independent variable). In other words accuracy is the degree of veracity while precision is the degree of reproducibility. The accuracy and precision of a measurement process is usually established by repeatedly measuring some traceable reference standard. Such standards are defined in the International System of Units and maintained by national standards organizations.

Precision is usually characterised in terms of the *standard deviation of the measurements*, sometimes called the *measurement process's standard error*. The interval defined by the standard deviation is the 68.3% ("one sigma") confidence interval of the measurements. If enough measurements have been made to accurately estimate the standard deviation of the process, and if the measurement process produces normally distributed errors, then it is likely that 68.3% of the time, the true value of the measured property will lie within one standard deviation, 95.4% of the time it will lie within two standard deviations, and 99.7% of the time it will lie within three standard deviations of the measured value. This also applies when measurements are repeated and averaged. In that case, the term standard error is properly applied: the precision of the average is equal to the known standard deviation of the process divided by the square root of the number of measurements averaged. Further, the central limit theorem shows that the probability distribution of the averaged measurements will be closer to a normal distribution than that of individual measurements. Precision is sometimes stratified into:

- repeatability: the variation arising when all efforts are made to keep conditions constant by using the same instrument and operator, and repeating during a short time period;
- reproducibility: the variation arising using the same measurement process among different instruments and operators, and over longer time periods.

With regard to accuracy we can distinguish:

- the difference between the mean of the measurements and the reference value, the bias. Establishing and correcting for bias is necessary for calibration;
- the combined effect of that and precision.

We recall some terms usually employed in time metrology, mostly taken from the US *National Institute of Standards and Technology* (NIST) web site[6].

Definition 3 (Nominal frequency) *If T is the period of a repetitive event, then the rate of occurrence of the repetitive event is the frequency $f = 1/T$.*

Devices that produce a known frequency are called *frequency standards*. These devices must be calibrated so that they remain within the tolerance required by the user's application. *Frequency calibrations* measure the performance of frequency standards. The frequency standard being calibrated is called the *device under test* (DUT). In most cases, the DUT is a quartz, rubidium, or cesium oscillator. In order to perform the calibration, the DUT must be compared to a *standard* or *reference*. The standard should outperform the DUT by a specified ratio in order for the calibration to be valid. This ratio is called the *test uncertainty ratio* (TUR). A TUR of 10:1 is preferred, but not always possible. Once the calibration is completed, the metrologist should be able to state how close the DUT's output is to its *nominal frequency* f_0, also called *nameplate frequency*. The calibration measures the difference between the actual frequency and the nameplate frequency. This difference is called the *frequency offset*. There is a high probability that the frequency offset will stay within a

[6] http://www.nist.gov/, http://tf.nist.gov/timefreq/general/glossary.htm. Another very useful source of information is the Bureau International des Poids et Mesures (BIPM) located near Paris, France. The task of the BIPM is to ensure worldwide uniformity of measurements and their traceability to the International System of Units (SI). http://www.bipm.fr.

certain range of values, called the *frequency uncertainty*. Once the DUT meets specifications, it has been successfully calibrated[7].

We define the two main specifications of a frequency calibration, *frequency offset* and *stability* and show how they are measured. Keep in mind during this discussion that frequency offset is often referred to simply as *accuracy* (or *frequency accuracy*), and that stability is nearly the same thing as *frequency uncertainty*. Measuring the frequency offset of a DUT requires comparing it to a reference. This is normally done by making a phase comparison between the frequency produced by the DUT and the frequency produced by the reference. Once we know the amount of phase deviation and the measurement period, we can estimate the frequency offset of the DUT. The measurement period is the length of time over which phase comparisons are made.

Definition 4 (Frequency offset) *Frequency offset is estimated as follows*

$$f_{offset} = \frac{-\Delta t}{T}, \tag{2.2.1}$$

where Δt is the amount of phase deviation, and T is the measurement period.

Table 2.1 lists the approximate offset values for some standard units of phase deviation and some standard measurement periods.

Measurement Period	Phase Deviation	Frequency offset
1 s	1 ms	1.00×10^{-3}
1 s	1 µs	1.00×10^{-6}
1 s	1 ns	1.00×10^{-9}
1 hour	1 ms	2.78×10^{-7}
1 hour	1 µs	2.78×10^{-10}
1 hour	1 ns	2.78×10^{-13}
1 day	1 ms	1.16×10^{-8}
1 day	1 µs	1.16×10^{-11}
1 day	1 ns	1.16×10^{-14}

Table 2.1. Frequency offset values for given amounts of phase deviation.

The frequency offset values in Table 2.1 can be converted to units of frequency (Hz) if the nameplate frequency is known. To illustrate this, consider an oscillator with a nameplate frequency of 5 MHz that is high in frequency by 1.16×10^{-11}. To find the frequency offset in hertz, multiply the nameplate frequency by the dimensionless offset value

$$\left(5 \times 10^{6}\right)\left(+1.16 \times 10^{-11}\right) = 5.80 \times 10^{-5} = +0.000058 \text{ Hz}. \tag{2.2.2}$$

The nameplate frequency is 5 MHz, or 5000000 Hz. Therefore, the actual frequency being produced by the frequency standard is 5000000 Hz + 0.000058 Hz. Frequency offset is the quantity of greatest interest to a calibration laboratory because it tells us how close a DUT is to its nameplate frequency. You will probably notice that the term *frequency accuracy* (or just accuracy) often appears on oscillator specification sheets instead of the term frequency offset. Frequency accuracy and frequency offset are equivalent terms that refer to the result of a measurement at a given time. Frequency offset is a measure of how closely an oscillator produces its nameplate frequency, or how well an oscillator is adjusted. It doesn't tell us about the quality of an oscillator.

Definition 5 (Frequency uncertainty) *Frequency uncertainty indicates the limits (upper and lower) of the frequency offset. ISO defines uncertainty as a:*

[7] If an oscillator is calibrated and then turned off, the calibration could be invalid when the oscillator is turned back on. We can use transfer standards to deliver a frequency reference from the national standard to the calibration laboratory. Transfer standards are devices that receive and process radio signals that provide frequency traceable

> *"Parameter, associated with the result of a measurement, that characterizes the dispersion of values that could reasonably be attributed to the measurand".*

In other words, the frequency uncertainty shows us the possible range of values (or limits) for the frequency offset. It is now standard practice to use a 2σ uncertainty test. This means that there is a 95.4% probability that the frequency offset will stay within the stated range during the measurement period. The range of values is obtained by both adding the frequency uncertainty to and subtracting it from the average (or mean) frequency offset. Therefore, frequency uncertainty is sometimes stated with a "plus or minus" sign ($\pm 1 \times 10^{-12}$) to show the upper and lower limits of the offset. If the "±" symbol is omitted, it is still implied. The largest contributor to the frequency uncertainty is usually the *stability* of the device under test.

Stability indicates how well an oscillator can produce the same frequency over a given period of time. It doesn't indicate whether the frequency is "right" or "wrong", only whether it stays the same. Also, the stability doesn't necessarily change when the frequency offset changes. You can adjust an oscillator and move its frequency either further away from or closer to its nameplate frequency without changing its stability at all.

Definition 6 (Stability) *Stability is defined as the statistical estimate of the frequency fluctuations of a signal over a given time interval. Short-term stability usually refers to fluctuations over intervals less than* 100 [s]*. Long-term stability can refer to measurement intervals greater than* 100 [s]*, but usually refers to periods longer than 1 day.*

A typical oscillator specification sheet might list stability estimates for intervals of 1, 10, 100, and 1000 s. Stability estimates can be made in the frequency domain or time domain, and statistical tools exist to easily convert from one domain to the other. Time domain estimates are more widely used, since *time interval counters* (TIC) are often used to measure frequency. To estimate stability in the time domain, we must start with a set of frequency offset measurements y_i that consists of individual measurements, y_1, y_2, y_3, and so on. Once this data set is obtained, we need to determine the dispersion or scatter of the y_i as a measure of oscillator noise. The larger the dispersion, or scatter, of the y_i , the greater the instability of the output signal of the oscillator. Normally, classical statistics such as *standard deviation* (or *variance*, the square of the standard deviation) are used to measure dispersion. Variance is a measure of the numerical spread of a data set with respect to the average or mean value of the data set. However, variance works only with stationary data, where the results must be timeindependent. This assumes the noise is white, meaning that its power is evenly distributed across the frequency band of the measurement. Oscillator data is usually nonstationary, since it contains time-dependent noise contributed by the frequency offset. For stationary data, the mean and variance will converge to particular values as the number of measurements increases. With nonstationary data, the mean and variance never converge to any particular values. Instead, we have a moving mean that changes each time we add a new measurement. For these reasons, a non classical statistic is used to estimate stability in the time domain. This statistic is often called the *Allan variance*, but since it is actually the square root of the variance, its proper name is the *Allan deviation*. By recommendation of the Institute of Electrical and Electronics Engineers (IEEE), the Allan deviation is used by manufacturers of frequency standards as a standard specification for stability. The equation for the Allan deviation is

$$\sigma_y(\tau) = \sqrt{\frac{1}{2(M-1)} \sum_{i=1}^{M-1} (\bar{y}_{i+1} - \bar{y}_i)^2}, \tag{2.2.3}$$

where M is the number of values in the y_i series, and the data are equally spaced in segments τ seconds long. Note that while classical deviation subtracts the mean from each measurement before squaring their summation, the Allan deviation subtracts the previous data point. Since stability is a measure of frequency fluctuations and not of frequency offset, successive data points are differenced to remove the time-dependent noise contributed by the frequency offset.

Be sure not to confuse stability with frequency offset when you read a specifications sheet. For example, a DUT with a frequency offset of 1×10^{-8} might still reach a stability of 1×10^{-12} in 1000 [s]. This means that the output frequency of the DUT is stable, even though it is not particularly close

to its nameplate frequency. To help clarify this point, Figure 2.2 is a graphical representation of the relationship between frequency offset (accuracy) and stability.

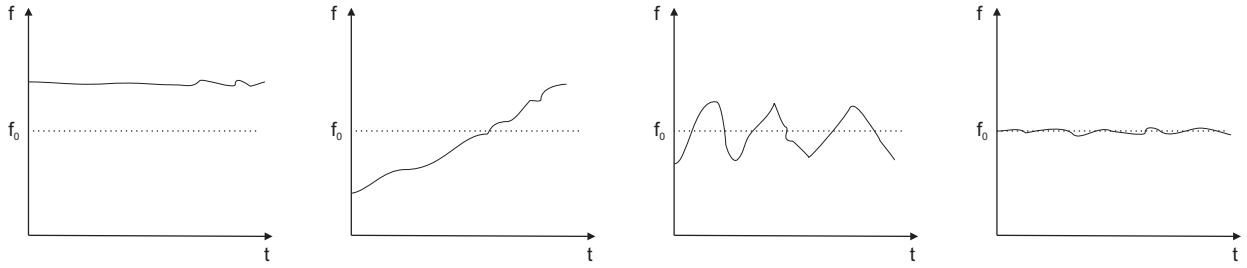

(a) Stable but not accurate.

(b) Not stable and not accurate.

(c) Accurate but not stable.

(d) Accurate and stable.

Figure 2.2. Statistical proprieties for accuracy and stability.

Frequency standards are normally calibrated by comparing them to a traceable reference frequency[8]. Under normal circumstances, the phase changes in an orderly, predictable fashion. However, external factors such as power outages, component failures, or human errors can cause a sudden phase change, or phase step. A calibration system measures the total amount of phase shift (caused either by the frequency offset of the DUT or a phase step) over a given measurement period (see Figure 2.3).

Table 2.2 summarizes the characteristics of the different types of oscillators[9].

Here follows some definitions about terms in Table 2.2 not yet explained.

Definition 7 (Primary standard) *Cesium oscillators are primary frequency standards because the SI second is based on the resonance frequency of the cesium atom (^{133}Cs), which is* 9192631770 Hz.

[8]Several types of calibration systems can be used to compare phase. For example, the *time interval method* uses a device called a '*time interval counter* (TIC) to measure the time interval between two signals. A TIC has inputs for two electrical signals. One signal starts the counter and the other signal stops it. If the two signals have the same frequency, the time interval will not change. If the two signals have different frequencies, the time interval will change, although usually very slowly. By looking at the rate of change, you can calibrate the device. It takes two time interval measurements to produce useful information. By subtracting the first measurement from the second, we can tell whether time was gained or lost. TIC's differ in specification and design details, but they all contain several basic parts known as the *time base*, the *main gate*, and the *counting assembly*. The time base provides evenly spaced pulses used to measure time interval. The time base is usually an internal quartz oscillator that can often be phase locked to an external reference. It must be stable because time base errors will directly affect the measurements. The main gate controls the time at which the count begins and ends. Pulses passing through the gate are routed to the counting assembly where they are displayed on the TIC's front panel or read by computer. The counter can then be reset (or armed) to begin another measurement. The stop and start inputs are usually provided with level controls that set the amplitude limit (or trigger level) at which the counter responds to input signals. The TIC begins measuring a time interval when the start signal reaches its trigger level and stops measuring when the stop signal reaches its trigger level. The time interval between the start and stop signals is measured by counting cycles from the time base. The measurements produced by a TIC are in time units: milliseconds, microseconds, nanoseconds, and so on. These measurements assign a value to the phase difference between the reference and DUT. The most important specification of a TIC is resolution, which is the degree to which a measurement can be determined. In traditional TIC designs, the resolution is limited to the period of the TIC's time base frequency. This is because traditional TIC designs count whole time base cycles to measure time interval and cannot resolve time intervals smaller than the period of one cycle. To improve this situation, some TIC designers have multiplied the time base frequency to get more cycles and thus more resolution. However, a more common way to increase resolution is to detect parts of a time base cycle through interpolation and not be limited by the number of whole cycles. Interpolation has made 1 [ns] TICs commonplace, and even 20 [ps] TICs are available. Low frequency start and stop signals must be used (typically 1 [Hz]). Since oscillators typically produce frequencies such as 1, 5, and 10 [MHz] the solution is to use a frequency divider to convert them to a lower frequency. A frequency divider could be a stand-alone instrument, a small circuit, or just a single chip. Most divider circuits divide by multiples of 10, so it is common to find circuits that divide by one thousand, one million, and so on. For example, dividing a 1 [MHz] signal by 10^6 produces a 1 [Hz] signal. Using low frequency signals reduces the problem of counter overflows and underflows and helps prevent errors that could be made if the start and stop signals are too close together. The time interval method is probably the most common method in use today. It has many advantages, including low cost, simple design, and excellent performance when measuring long term frequency offset or stability.

[9]Frequency standards all have an internal device that produces a periodic, repetitive event. This device is called the resonator. Of course, the resonator must be driven by an energy source. Taken together, the energy source and the resonator form an oscillator.

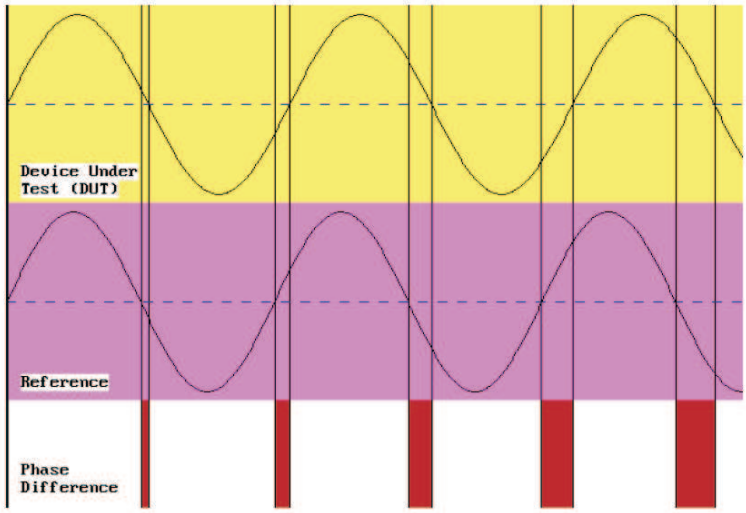

Figure 2.3. Two signals with a changing phase relationship. The top sine wave represents a signal from the DUT, and the bottom sine wave represents a signal from the reference. Vertical lines have been drawn through the points where each sine wave crosses zero. The bottom of the figure shows "bars" that indicate the size of the phase difference between the two signals. If the phase relationship between the signals is changing, the phase difference will either increase or decrease to indicate that the DUT has a frequency offset (high or low) with respect to the reference.

Oscillator Type	**Quartz (TCXO)**	**Quartz (MCXO)**	**Quartz (OCXO)**	**Rubidium**	**Cesium**	**Hydrogen Maser**
Primary Standard	No	No	No	No	Yes	No
Intrinsic Standard	No	No	No	Yes	Yes	Yes
Resonance Frequency	Mechanical (varies)	Mechanical (varies)	Mechanical (varies)	6.834682608 GHz	9.19263177 GHz	1.42040575 GHz
Leading Cause of Failure	None	None	None	Rubidium Lamp (15 years or more)	Cesium Beam Tube (3 to 25 years)	Hydrogen Depletion (7 years or more)
Stability, $\sigma_y(\tau)$, $\tau = 1\ s$	1×10^{-9}	1×10^{-10}	1×10^{-12}	5×10^{-11} to 5×10^{-12}	5×10^{-11} to 5×10^{-12}	1×10^{-12}
Noise Floor, $\sigma_y(\tau)$	1×10^{-9} ($\tau = 1$ to $10^2\ s$)	1×10^{-10} ($\tau = 1$ to $10^2\ s$)	1×10^{-12} ($\tau = 1$ to $10^2\ s$)	1×10^{-12} ($\tau = 10^3$ to $10^5\ s$)	1×10^{-14} ($\tau = 10^5$ to $10^7\ s$)	1×10^{-15} ($\tau = 10^3$ to $10^5\ s$)
Aging/year	5×10^{-7}	5×10^{-8}	5×10^{-9}	2×10^{-10}	None	$\sim 1 \times 10^{-13}$
Frequency Offset after warm up	1×10^{-6}	1×10^{-7} to 1×10^{-8}	1×10^{-8} to 1×10^{-10}	5×10^{-10} to 1×10^{-12}	5×10^{-12} to 1×10^{-14}	1×10^{-12} to 1×10^{-13}
Warm-Up Time	$< 10\ s$ to 1×10^{-6}	$< 10\ s$ to 1×10^{-8}	< 5 min to 1×10^{-8}	< 5 min to 1×10^{-10}	30 min to 1×10^{-12}	24 hours to 1×10^{-12}
Cost (2008)	$100	$1000	$2000	$3000 to $8000	$30000 to $80000	$200000 to $300000

Table 2.2. Summary of oscillator types.

Definition 8 (Intrinsic Standards) *All atomic oscillators are intrinsic standards, since their frequency is inherently derived from a fundamental natural phenomenon. Atomic oscillators contain an internal quartz oscillator that is locked to a resonance frequency generated by the atom of interest. Most of the factors that degrade the long-term performance of a quartz oscillator disappear, since the atomic resonance frequency is much less sensitive to environmental conditions than the quartz resonance frequency. As a result, the long-term stability and uncertainty of an atomic oscillator are much better than those of a quartz oscillator, but the short-term stability is unchanged.*

Definition 9 (Aging) *Aging is defined as "a systematic change in frequency with time due to internal changes in the oscillator". Aging is usually observed as a nearly linear change over time in the resonance frequency. Aging can be positive or negative, and occasionally, a reversal in aging direction is observed. Often, the resonance frequency decreases, which might indicate that the crystal is getting larger. Aging has many possible causes including: contamination of the crystal due to deposits of foreign material, changes in the oscillator circuitry, or changes in the quartz material or crystal structure. The vibrating motion of the crystal can also contribute to aging.*

2.2.1. Relations between time basic quantities

At this point it is possible to formalize the relations that exists between the basic quantities *time*, *frequency* and *phase*of a sinusoidal signal generated by an oscillator.

Definition 10 *The frequency f of a signal is the time derivative of the phase ϕ of the signal.*

$$f(t) = \frac{d\phi(t)}{dt}. \tag{2.2.4}$$

Definition 11 *The phase of the signal is the time integral of the signal frequency.*

$$\phi(t) = \int_{t_0}^{t} f(\tau)d\tau + \phi(t_0), \tag{2.2.5}$$

where $\phi(t_0)$ is the initial phase *of the signal at epoch t_0.*

The signal phase is measured in units of cycles, the frequency in units of Hertz [Hz][10].

Definition 12 *The phase of a signal can be converted to time t_i by subtracting the initial phase $\phi(t_0)$ and dividing by the* nominal oscillator frequency *f_0.*

$$t_i(t) = \frac{\phi(t) - \phi(t_0)}{f_0} = \frac{\phi(t)}{f_0} - t_i(t_0). \tag{2.2.6}$$

In the last equation it has been defined

$$\frac{\phi(t_0)}{f_0} \doteq t_i(t_0). \tag{2.2.7}$$

Substituting the Equation 2.2.5 into Equation 2.2.6, the time is related to the oscillator frequency by

$$\begin{aligned} t_i(t) &= \frac{1}{f_0}\left(\int_{t_0}^{t} f(\tau)d\tau + \phi(t_0)\right) - \frac{\phi(t_0)}{f_0} \\ &= \frac{1}{f_0}\int_{t_0}^{t} f(\tau)d\tau + \frac{\phi(t_0)}{f_0} - \frac{\phi(t_0)}{f_0} \\ &= \frac{1}{f_0}\int_{t_0}^{t} f(\tau)d\tau. \end{aligned} \tag{2.2.8}$$

[10] The phase can also be represented in units of radians multiplied by 2π, then $\omega(t) = 2\pi f(t)$ is known as *angular frequency* $\omega(t)$ (*pulsazione*, in Italian)

If the oscillator frequency is constant and equal to its nominal frequency, Equation (2.2.8) becomes

$$t_i(t) = t - t_0. \tag{2.2.9}$$

Considering a *real* oscillator, the *actual frequency* can be separated into the *nominal frequency* and the *frequency deviation* (or *frequency error*), yielding

$$t_i(t) = \frac{1}{f_0} \int_{t_0}^{t} (f_0 + df(\tau))\, d\tau. \tag{2.2.10}$$

Introducing the definition *time deviation* as

$$dt_i(t) = \int_{t_0}^{t} \frac{\delta f(\tau)}{f_0} d\tau, \tag{2.2.11}$$

the final relation between the *time measured* from the phase of an oscillator-generated signal and the *true time* t becomes

$$t_i(t) = t + dt_i(t). \tag{2.2.12}$$

This convention is used by...

2.2.2. The Stochastic Clock Model

Any clock may be considered a device composed by two functional parts: the first part is an *oscillating device* for determining the length of the second or some other desired time interval, that is usually referred to as the *clock's frequency standard*, which oscillates at some rate determined by the laws of physics (i.e., the pendulum[11], the quartz-crystal[12] or a quantum transition between two energy levels in an atom[13]); the second part is a *counter* (sometimes called an integrator, adder, or accumulator) that keeps track of the number of seconds or clock cycles that have occurred. It keeps track of hours, minutes, and seconds. After being set initially, the clock can then provide its estimate of the correct time by adding up the number of clock cycles. In principle, if a clock were set perfectly and if its frequency or rate remained perfect, it would keep the correct time indefinitely. In practice, this is impossible for several reasons:

- the clock cannot be set perfectly;
- random and systematic variations are intrinsic to any oscillator, and when these random variations are averaged, the result is often not well-behaved;

[11] A pendulum's theoretical frequency is given by

$$\nu = \frac{\sqrt{g/\ell}}{2\pi}, \tag{2.2.13}$$

where g is the gravitational acceleration at the location of the pendulum and ℓ is the length of the pendulum bob's support wire. Specifically, an ideal pendulum that swings through its lowest point once per second (one full cycle every two seconds, 0.5 Hz) will have a length $\ell = 99.3621$ centimeters if it is at sea level and at 45 latitude. By its nature, a pendulum clock will depend upon several parameters, including both its location and its environment since, for example, most materials expand with increasing temperature. An increase in temperature would cause the support wire to get longer and the pendulum clock to slow down.

[12] Currently, the typical wristwatch has as its frequency standard a quartz-crystal tuning fork with an oscillation frequency of 32.768 Hz. This number of oscillations is convenient for the associated digital electronic circuit, because if this number is divided by 2^{15}, which is easy for a digital chip divider, the result is one cycle or pulse per second.

[13] Atomic clocks generally provide a much more accurate frequency than can be generated by any physical device such as a pendulum or quartz crystal oscillator. An atomic clock uses as its reference the oscillation of an electromagnetic signal associated with a quantum transition between two energy levels in an atom. This bundle of electromagnetic energy is called a photon and its energy, E, is equal to the difference in energy between these two levels. The photon may be either given off or absorbed by the atom. For a given quantum transition, the photons emitted or absorbed have a unique frequency proportional to the energy difference with little variability around this value. The relationship between this energy difference and the electromagnetic vibration frequency of the photons is given by $E = h\nu$, where h is Planck's constant and ν is the Greek letter denoting the frequency of the photon's electromagnetic wave. The trick in atomic clock metrology is harnessing the frequency of these photons while producing minimum perturbations on the natural atomic resonance.

- time is a function of position and motion (relativistic effects);
- environmental changes cause the clock's frequency to vary from ideal.

The quality of a clock depends on how well it is *set*, how *accurate* and *stable* its frequency is, and the degree of *immunity* the clock has to environmental changes. Typically the intrinsic nature of atomic clocks usually yields a more accurate estimate of correct frequency for the determination of the second. The choice of which clock is most appropriate for a given application should be considered from a systems point of view. Four useful measures for describing the quality of a clock are: *frequency accuracy*, *frequency stability*, *time accuracy*, and *time stability*. These measures are not all independent. A *clock's frequency (or rate) accuracy* is how well it can realize the defined length of the second. A commonly-used measure is the change in the error of a clock's time divided by the elapsed time, t, over which the change occurred. This is often called the *fractional or normalized frequency departure*, $y(t)$, and is a time-dependent, dimensionless number[14]. Of course, the smaller the number, the better the clock. *Frequency stability*, on the other hand, indicates the change in frequency from one period of time to the next. A clock can have a significant frequency error and still be very stable; in other words, the frequency or rate error stays about the same. For example, a clock may have a rate inaccuracy of gaining one second a day, but if that rate remains the same, it would have perfect frequency stability[15]. *Time accuracy*, by definition, means how well a clock agrees with UTC. There are often cases where what is needed is consistency of time at several locations in a system. What may be important is the time accuracy of each of the clocks with respect to the system[16]. Time stability is usually correlated with frequency stability, but it is often useful as a measure of changes with respect to some uniform flow of time in time-measurement systems and/or time-distribution or time-dissemination systems. For instance, consider the clock mentioned before, which gains one second a day and does this day after day. While its time accuracy may be degrading a second a day from its initial setting, it would have perfect frequency stability, and consequently perfect time predictability. If the time or frequency errors of a clock can be estimated, then compensating corrections can be made.

Like shown in [85, Tavella & Zucca, 2005], the clock errors can be modeled by means of stochastic processes obeying to *Stochastic Differential Equations*[17] (SDE). The clock noises involved in the SDE

[14] The goal of the Harrison chronometers was to have $y(t)$ less than three seconds per day, $3/86400 = 3.5 \times 10^{-5}$. The best primary frequency standards in the world today have $y(t)$ values less than 1×10^{-14}.

[15] Two very important kinds of atomic clocks, a hydrogen-maser and a cesium-beam, are good examples of clocks having different stabilities and accuracies. A hydrogen-maser clock typically has better frequency stability than a cesium-beam clock from second to second or from hour to hour, but often not from month to month and longer. On the other hand, the typical cesium-beam clock is more accurate than the hydrogen-maser clock. Quartz-oscillator based clocks can be very stable for short times, but they drift in frequency and don't have the frequency accuracy of atomic clocks.

[16] This is exactly the case for the U.S. Department of Defense's (DoD's) Global Positioning System (GPS) whose time differs from UTC. Specifically, the GPS time broadcast by each of the satellites needs to be synchronous with all of the other satellites in the constellation to within a small number of nanoseconds in order for the system to work properly. This is accomplished for GPS by the presence of atomic clocks on board the satellites.

[17] Given t a generic discrete instant, $t = 0, 1, 2, \ldots$ ($t \in \mathbb{N}_0$), and x_t the value assumed by a deterministic and discrete variable x in t, the temporal evolution of x_t is done by a difference equation of the first order

$$x_{t+1} = H(x_t, t), \tag{2.2.14}$$

where $H : \mathbb{R} \times \mathbb{N}_0 \to \mathbb{R}$. Equation (2.2.14) establish the evolutionary mechanism from a given epoch t to the following $t+1$ and determine the variable value x_{t+1} at any epoch from the variable value at the previous epoch t. If the initial value x_0 is known, the whole future history is completely describable. It is possible to establish an evolutionary mechanism where x_{t+1} is determined by a part of the passed history, obtaining in this way a deterministic equation of order n

$$x_{t+1} = H\left(x_t, x_{t-1}, x_{t-2}, \ldots, x_{t-(n-1)}, t\right), \tag{2.2.15}$$

where $H : \mathbb{R}^n \times \mathbb{N}_0 \to \mathbb{R}$. It has no sense if all the history affects x_t because it would not be an evolutionary mechanism: it would not describe the evolutionary mechanism but the evolution itself. Very often the variable x_t is not a deterministic one but an aleatory one. A very simple way to formalize this randomness is to overlap a deterministic mechanism and an aleatory one

$$x_{t+1} = H(x_t, t) + Y_t, \tag{2.2.16}$$

where Y_t is an aleatory variable (va) with $E(Y_t) = 0 \quad \forall t \in \mathbb{N}$ Equation (2.2.16) is called *Stochastic Difference Equation*. A Stochastic Difference Equation describes the evolution of a variable with a succession of aleatory numbers (that is va) called *discrete parameter stochastic process* (or stochastic succession).

are generally introduced through a covariance matrix that contains diffusion coefficients, which are the variances of the Wiener processes driving the fundamental noises. In the time and frequency community, conversely, the clock noises are in general characterized by means of variances evaluated on successive differences of frequency values. The most common definition of variance used in this context is the *Allan variance*. The three-state clock model appears as

$$\begin{cases} dX_1(t) = (X_2(t) + \mu_1)\, dt + \sigma_1 dW_1(t) \\ dX_2(t) = (X_3(t) + \mu_2)\, dt + \sigma_2 dW_2(t) \\ dX_3(t) = \mu_3 dt + \sigma_3 dW_3(t) \end{cases} , \quad t \geq 0 \tag{2.2.17}$$

with initial conditions

$$\begin{cases} X_1(0) = c_1 \\ X_2(0) = c_2 \\ X_3(0) = c_3 \end{cases} , \tag{2.2.18}$$

where $\{W_i(t), \quad t \geq 0\}$, $i = 1, 2, 3$ are three independent, one-dimensional standard Wiener processes (standard Brownian motion), each one defined as a Gaussian process with stationary independent increments such that $W(t) - W(s)$ $\mathcal{N}(0, t-s)$ and $W(0) = 0$. This implies $W(t)$ $\mathcal{N}(0, t)$. The expression $\mathcal{N}(0, t)$ indicates that variable has a Gaussian distribution with zero mean and variance t; therefore, both the increments and the Wiener processes have Gaussian distribution as indicated. The Wiener process is often referred to as the integral of white noise $\xi(t)$ and is formally written as $dW(t) = \xi(t)dt$.

2.3. GPS Observables

Throughout this and the following chapters, a superscript identifies the satellite (generally p and q) and a subscript identifies the receiver (generally k and m) when used with code or phase symbols. The L_1 and L_2 carriers are indicated by the subscripts 1 and 2, respectively. Terms whose numerical values depend on the pseudorange or the carrier phase are identified with the subscripts P and φ, respectively.

The following definitions and considerations have been inspired by [55, Leick, 1995], [47, Hugentobler, 2006], [99, Zin,2001], [95, Xu, 2003] and [46, Hofmann et al., 2001].

2.3.1. Code pseudorange

The code pseudorange is a measure of the distance between the transmitter (on GPS satellites) and the receiver's antennas, referring to the epochs of emission and reception of the code. The transmission time of the signal is measured by correlating identical pseudorandom noise (PRN) code generated by the satellite with those generated internally by the receiver. The code-tracking loop within the receiver shifts the internal replica of the PRN code in time, until maximum correlation occurs. The receiver codes are derived from the receiver's own clock and the codes of the satellite transmission are generated by the satellite system of clocks. Unavoidable timing errors in both the satellite and the receiver clock will cause the measured pseudorange to differ from the geometric distance corresponding to the epochs of emission and reception. Code pseudorange is applicable to P- and/or C/A-codes.

Zero differences code pseudorange observable

Let us denote by t_k the nominal time of the receiver clock k *at the instant of reception* of a signal and by t^p the nominal time of the satellite clock p *at emission*. As explained in section 2.2.1, the nominal times are related to the true times $t_{r,k}$ and t^p_r (such as GPS time) via the clock error terms, dt_k and dt^p by

$$t_k = t_{r,k} + dt_k \tag{2.3.1}$$

$$t^p = t^p_r + dt^p. \tag{2.3.2}$$

and then

$$t_{r,k} = t_k - dt_k \tag{2.3.3}$$
$$t_r^p = t^p - dt^p, \tag{2.3.4}$$

Since this data type measures directly the time interval ΔT between the time t_k at which the signal arrives ate the receiver and the time t^p at which the signal left the satellite, the pseudorange measurement between the satellite p and the receiver k at the carrier frequency L_i $(i = 1, 2)$, $P^p_{k,L_i}(t_k)$, is expressed in units of length (multiplying it for the speed of light c) by

$$P^p_{k,L_i}(t_k) = c\Delta T = c\left(t_k - t^p\right) = c\left(t_{r,k} - t_r^p\right) - c\left(dt_k - dt^p\right), \tag{2.3.5}$$

where the last equality has been obtained introducing Equations (2.3.2) and (2.3.1) [47, Hugentobler, 2006]. The range equivalent form of this equation is

$$P^p_{k,L_i}(t_k) = \left|\mathbf{R}^p\left(t^p + dt^p\right) - \mathbf{R}_k\left(t_k + dt_k\right)\right| + \Delta r_{corr} - c\left(dt_k - dt^p\right), \tag{2.3.6}$$

where $\mathbf{R}^p\left(t^p + dt^p\right)$ and $\mathbf{R}_k\left(t_k + dt_k\right)$ are the inertial transmitter and receiver positions, respectively at instants $t^p + dt^p$ and $t_k + dt_k$, while Δr_{corr} is an error term that accounts for *atmospheric* and *electronic* delays [99, Zin,2001]. Expressing the time of transmission in terms of time of reception, the pseudorange equation becomes

$$P^p_{k,L_i}(t_k) = \left|\mathbf{R}^p\left(t_k - \Delta T + dt^p\right) - \mathbf{R}_k\left(t_k + dt_k\right)\right| + \Delta r_{corr} - c\left(dt_k - dt^p\right). \tag{2.3.7}$$

Expanding the position vectors $\mathbf{R}^p$ and $\mathbf{R}_k$ at first order around t_k in Equation (2.3.8), the following equation is obtained

$$P^p_{k,L_i}(t_k) = \left|\mathbf{R}^p(t_k) + \dot{\mathbf{R}}^p(t_k)\left(-\Delta T + dt^p\right) - \mathbf{R}_k(t_k) + \dot{\mathbf{R}}_k(t_k)\, dt_k\right| + \Delta r_{corr} - c\left(dt_k - dt^p\right). \tag{2.3.8}$$

Recalling that the absolute value for small values of ΔR is

$$|\mathbf{R} + \Delta\mathbf{R}| = R + \hat{\mathbf{R}} \cdot \Delta\mathbf{R} + \frac{|\Delta\mathbf{R}|^2}{2R} + O\left(|\Delta\mathbf{R}|^3\right) \tag{2.3.9}$$

and defining the vector that points from the receiver to the satellite as $\mathbf{r}_k^p = \mathbf{R}^p - \mathbf{R}_k$, at first order the pseudorange equation is

$$c\Delta t = r_k^p(t_k) + \Delta r_{corr} + \hat{\mathbf{r}}_k^p(t_k) \cdot \left[\dot{\mathbf{R}}^p(t_k)\, dt^p - \hat{\mathbf{R}}_k(t_k)\, dt_k - \dot{\mathbf{R}}^p(t_k)\,\Delta T\right] - c\left(dt_k - dt^p\right). \tag{2.3.10}$$

Solving for ΔT gives

$$\begin{aligned}\Delta T = \frac{1}{c + \hat{\mathbf{r}}_k^p(t_k) \cdot \dot{\mathbf{R}}^p(t_k)} \Big[&r_k^p(t_k) + \Delta r_{corr} + \left(c + \hat{\mathbf{r}}(t_k) \cdot \dot{\mathbf{R}}^p(t_k)\right) dt^p \\ &- \left(c + \hat{\mathbf{r}}(t_k) \cdot \dot{\mathbf{R}}_k(t_k)\right) dt_k\Big],\end{aligned} \tag{2.3.11}$$

where all the quantities are expressed at reception times t_u. Substituting Equation (2.3.12) in (2.3.5) it becomes

$$\begin{aligned}P^p_{k,L_i}(t_k) = \frac{c}{c + \hat{\mathbf{r}}_k^p(t_k) \cdot \dot{\mathbf{R}}^p(t_k)} \Big[&r_k^p(t_k) + \Delta r_{corr} + \left(c + \hat{\mathbf{r}}(t_k) \cdot \dot{\mathbf{R}}^p(t_k)\right) dt^p \\ &- \left(c + \hat{\mathbf{r}}(t_k) \cdot \dot{\mathbf{R}}_k(t_k)\right) dt_k\Big],\end{aligned} \tag{2.3.12}$$

and expanding the factor outside brackets to the first order the pseudorange measurement model is expressed by

$$\begin{aligned} P^p_{k,L_i}(t_k) &= \left(1 - \frac{\hat{\mathbf{r}}^p_k(t_k) \cdot \dot{\mathbf{R}}^p(t_k)}{c}\right)\left(r^p_k(t_k) + \Delta r_{corr}\right) - \left(c - \hat{\mathbf{r}}^p_k(t_k) \cdot \dot{\mathbf{r}}^p_k(t_k)\right) dt_k + c dt_p \\ &\simeq \left(1 - \frac{\hat{\mathbf{r}}^p_k(t_k) \cdot \dot{\mathbf{R}}^p(t_k)}{c}\right) r^p_k(t_k) - c\left(1 - \frac{\dot{\rho}^p_k(t_k)}{c}\right) dt_k + c dt^p + \Delta r_{corr}, \end{aligned} \tag{2.3.13}$$

where the last approximation has been achieved considering that

$$\left(\hat{\mathbf{r}}^p_k \cdot \dot{\mathbf{R}}^p c\right) \Delta r_{corr} \leq 1 \text{ mm and} \tag{2.3.14}$$

$$\hat{\mathbf{r}}^p_k(t_k) \cdot \dot{\mathbf{r}}^p_k(t_k) = \dot{\rho}^p_k(t_k). \tag{2.3.15}$$

All the components of the term Δr_{corr} are explicitly exposed in Equation (2.5.68), becoming

$$\begin{aligned} P^p_{k,L_i}(t_k) = \rho^p_k(t_{r,k}) - c\left(1 - \frac{\dot{\rho}^p_k(t_k)}{c}\right) dt_k + c\, dt^p + \delta I^p_{k,L_i,P}(t_k) + \delta T^p_k(t_k) \\ + \delta E_{k,L_i,P}(t_k) + \delta E^p_{L_i,P}(t_k) + \delta M^p_{k,L_i,P}(t_k) + \epsilon^p_{k,L_i,P}(t_k), \end{aligned} \tag{2.3.16}$$

with

$$\left(1 - \frac{\hat{\mathbf{r}}^p_k(t_k) \cdot \dot{\mathbf{R}}^p(t_k)}{c}\right) r^p_k(t_k) = \rho^p_k(t_{r,k}), \tag{2.3.17}$$

and where

- $\rho^p_k(t_{r,k})$ is the distance traveled by the signal between the instants of signal emission and reception, or *topocentric distance*,
- dt_k is the receiver k clock bias,
- dt^p is the GPS satellite p clock bias,
- $\delta I^p_{k,L_i,P}(t_k)$ is the delay due to the ionosphere (always positive) between the receiver k and the GPS satellite p for the carrier frequency L_i, $i = 1, 2$,
- $\delta T^p_k(t_k)$ is the delay due to the troposphere (always positive) between the receiver k and the GPS satellite p,
- $\delta E_{k,L_i,P}(t_k)$ is the receiver k hardware code delay,
- $\delta E^p_{L_i,P}(t_k)$ is the GPS satellite p hardware code delay,
- $\delta M^p_{k,L_i,P}(t_k)$ is the code multipath and
- $\epsilon^p_{k,L_i,P}(t_k)$ is the random measurement noise.

The subscript P identifies all terms whose numerical values are specific to code pseudoranges. The measurement units of all terms in Equation (2.5.68) are meters.

2.3.2. Carrier phase pseudorange

The carrier phase observable consists in the difference between carrier phase received from the GPS satellite (as sensed by the receiver's antenna) and the phase of the receiver oscillator. This measurement does not take into account the number of whole carrier wavelengths between the transmitter and the receiver, before the first instant of reception. The variation in time of the carrier phase observable is related to changes of the topocentric distance [55, Leick, 1995].

Zero differences carrier phase observable

The carrier phase observables $\varphi^p_{k,L_i}(t_k)$ for receiver k and GPS satellite p at carrier frequency L_i $(i = 1, 2)$ is

$$\begin{aligned}\varphi^p_{k,L_i}(t_k) = \varphi_{k,L_i}(t_k) - \varphi^p_{L_i}(t_k) + N^p_{k,L_i,\varphi} + \delta I^p_{k,L_i,\varphi}(t_k) + \frac{f_i}{c}\delta T^p_k(t_k) \\ + \delta E_{k,L_i,\varphi}(t_k) + \delta E^p_{L_i,\varphi}(t_k) + \delta M^p_{k,L_i,\varphi}(t_k) + \epsilon^p_{k,L_i,\varphi}(t_k),\end{aligned} \tag{2.3.18}$$

where

- $\varphi_{k,L_i}(t_k)$ is the receiver k phase at the nominal reception time t_k,
- $\varphi^p_{L_i}(t_k)$ is the satellite p phase at the nominal reception time t_k,
- $N^p_{k,L_i,\varphi}$ is the initial integer ambiguity and
- f_i is the nominal carrier frequency of L_i, $i = 1, 2$.

The terms with the subscript φ are expressed in units of cycles. The tropospheric delay is convert to cycles using the factor f_i/c. The ionospheric term has a *negative value* because the ionosphere advances the carrier phase[18] (see section 2.4.2), that is

$$\delta I^p_{k,L_i,P}(t) = -\frac{f_i}{c}\delta I^p_{k,L_i,\varphi}(t). \tag{2.3.26}$$

The idea at the base of carrier phase observable is the equivalence of the received carrier phase and the emitted phase at the satellite τ^p_k seconds earlier, that is

$$\varphi^p_{L_i}(t_k) = \varphi^p_{TX,L_i}(t_k - \tau^p_k), \tag{2.3.27}$$

[18] Consider a single electromagnetic wave propagation in a medium with wavelength λ and frequency f. The velocity of its phase

$$v_{ph} = \frac{\omega}{|\mathbf{k}|} \tag{2.3.19}$$

is denoted as *phase velocity*, where $\omega = 2\pi/f$ is the wave pulsation and $\mathbf{k}$ is the phase vector. For a uniform plane wave in a lossless medium $|\mathbf{k}| = \omega\sqrt{\mu\epsilon} = 2\pi/\lambda$, where ϵ is the permittivity and μ is the permeability, and then the velocity phase is

$$v_{ph} = \frac{1}{\sqrt{\mu\epsilon}} = c = \lambda f. \tag{2.3.20}$$

In a low loss medium, for the conductivity $\gamma \to 0$ ($\gamma \ll \omega\epsilon$), the phase velocity tends to the light velocty ($v_{ph} \to c$), that is $v_{ph} \simeq c$. For GPS, the carrier waves L_1 and L_2 are propagating with this velocity. A single plane wave, with pulsation ω, repeat itself periodically in time; therefore it is not able to transmit any information from one point to another one. This is why it not possible to interpret the phase velocity as the propagation velocity of a synchronization signal between two clocks. To transmit information it is necessary a nonzero spectral width, that is a modulated wave; to determine the propagation velocity of information transmitted through an electromagnetic wave it necessary to consider a non-monochromatic field. For a group of waves with slightly different frequencies the propagation of the resultant energy is defined by the *group velocity* []

$$v_{gr} = \frac{df}{d\lambda}\lambda^2. \tag{2.3.21}$$

This velocity has to be considered for GPS code measurements. A relation between phase and group velocity is expressed by the Rayleigh equation

$$v_{gr} = v_{ph} - \lambda\frac{dv_{ph}}{d\lambda}. \tag{2.3.22}$$

Phase and group velocity are equal in nondispersive media and correspond to the speed of light in vacuum. The wave propagation in a medium depends on the refractive index. Generally, the phase and group propagation velocity are obtained from

$$v_{ph} = c/n_{ph}, \tag{2.3.23}$$
$$v_{gr} = c/n_{gr}. \tag{2.3.24}$$

Then, the modified Rayleigh equation is

$$n_{gr} = n_{ph} - \lambda\frac{dn_{ph}}{d\lambda} = n_{ph} + f\frac{dn_{ph}}{df}. \tag{2.3.25}$$

where τ_k^p is the vacuum travel time. The phase for nominal time t_k and true time $t_{r,k}$ are related to the clock errors as follows

$$\varphi_{k,L_i}(t_{r,k}) = \varphi_{k,L_i}(t_k) + f_i\, dt_k \tag{2.3.28}$$
$$\varphi^p_{TX,L_i}(t_{r,k} - \tau_k^p) = \varphi^p_{TX,L_i}(t_k - \tau_k^p) + f_i\, dt_k \tag{2.3.29}$$

Solving 2.3.28 for $\varphi_{k,L_i}(t_k)$ and combining 2.3.29 with 2.3.27 gives

$$\varphi_{k,L_i}(t_k) = \varphi_{k,L_i}(t_{r,k}) - f_i\, dt_k \tag{2.3.30}$$
$$\varphi^p_{L_i}(t_k) \equiv \varphi^p_{TX,L_i}(t_k - \tau_k^p) = \varphi^p_{TX,L_i}(t_{r,k} - \tau_k^p) - f_i\, dt_k. \tag{2.3.31}$$

Modeling the satellite frequency using the simple model

$$\dot\varphi^p_{TX,L_i}(t_{r,k}) = f + a^p + b^p t, \tag{2.3.32}$$

where a^p and b^p are the satellite frequency offset and drift at emission time, $\varphi^p_{TX,L_i}(t_{r,k} - \tau_k^p)$ can be expanded as

$$\begin{aligned}\varphi^p_{TX,L_i}(t_{r,k} - \tau_k^p) &= \varphi^p_{TX,L_i}(t_{r,k}) - \int_\tau \dot\varphi^p_{TX,L_i}(t_k)dt \\ &= \varphi^p_{TX,L_i}(t_{r,k}) - [f + a^p + \frac{1}{2}b^p\tau_k^p]\tau_k^p\end{aligned} \tag{2.3.33}$$

and therefore

$$\begin{aligned}&\varphi_{k,L_i}(t_{r,k}) - \varphi^p_{TX,L_i}(t_{r,k} - \tau_k^p) - f_i\, dt_k + f_i\, dt^p + N^p_{k,L_i,\varphi} = \\ &\varphi_{k,L_i}(t_{r,k}) - \varphi^p_{TX,L_i}(t_{r,k}) - f_i\, dt_k + f_i\, dt^p + (f + a^p + \frac{1}{2}b^p\tau_k^p)\tau_k^p + N^p_{k,L_i,\varphi} = \\ &- f_i\, dt_k + f_i\, dt^p + (f + a^p+)\tau_k^p + N^p_{k,L_i,\varphi}.\end{aligned} \tag{2.3.34}$$

The last equality is obtained by ignoring the terms $\varphi_{k,L_i}(t_{r,k})$ and $\varphi^p_{TX,L_i}(t_{r,k})$ because they cannot be separated from the clock errors $f_i\, dt_k$ and $f_i\, dt^p$ and by neglecting the frequency drift term $b^p\tau_k^p$ because the time travel τ_k^p is short (about 70 ms).

Finally, relating the signal travel time to the topocentric range as

$$\tau_k^p = \frac{\rho_k^p(t_k) + \dot\rho_k^p(t_k)dt_k}{c}, \tag{2.3.35}$$

and substituting 2.3.34 and 2.3.35 into gives

$$\begin{aligned}\varphi^p_{k,L_i}(t_k) = \frac{f_i}{c}\rho_k^p(t_k) - f_i\left[1 - \frac{\dot\rho_k^p(t_k)}{c}\right]dt_k + f_i\, dt^p + N^p_{k,L_i,\varphi} + \frac{a^p}{c}\rho_k^p(t_k) + \delta I^p_{k,L_i,\varphi}(t_k) \\ + \frac{f_i}{c}\delta T_k^p(t_k) + \delta E_{k,L_i,\varphi}(t_k) + \delta E^p_{L_i,\varphi}(t_k) + \delta M^p_{k,L_i,\varphi}(t_k) + \epsilon^p_{k,L_i,\varphi}(t_k).\end{aligned} \tag{2.3.36}$$

Equation 2.3.36 is the fully developed expression for the undifferenced carrier phase observation. Apart the general scaling factor f_i/c the expressions of the code pseudorange and of the carrier phase pseudorange differ only because of the GPS satellite frequency offset term a^p. The small a^p term is often not listed explicitly or it is simply added to count for the change in received phase due to the satellite frequency offset. Following that line of thought, there is no need to introduce terms like $\varphi_{k,L_i}(t_{r,k})$ or $\varphi^p_{TX,L_i}(t_{r,k})$ found in 2.3.34

Single differences carrier phase observable with two receivers

Given two receivers k and m observing the same satellite p at the same nominal receiver epoch, the *single difference* carrier phase observable between the two receivers is defined as

$$\begin{aligned}\varphi^p_{km,L_i}(t_k) &\equiv \varphi^p_{k,L_i}(t_k) - \varphi^p_{m,L_i}(t_k)\\ &= \frac{f_i}{c}\left[\rho^p_k(t_k) - \rho^p_m(t_k)\right] + \frac{a^p}{c}\left[\rho^p_k(t_k) - \rho^p_m(t_k)\right]\\ &\quad + \frac{f_i}{c}\left[\dot\rho^p_k(t_k)dt_k - \dot\rho^p_m(t_k)dt_m\right] + N^p_{km,L_i,\varphi} - f_i(dt_k - dt_m)\\ &\quad + \delta I^p_{km,L_i,\varphi}(t_k) + \frac{f_i}{c}\delta T^p_{km}(t_k) + \delta E_{km,L_i,\varphi}(t_k) + \delta M^p_{km,L_i,\varphi}(t_k) + \epsilon^p_{km,L_i,\varphi}(t_k),\end{aligned} \tag{2.3.37}$$

where

$$N^p_{km,L_i,\varphi} = N^p_{k,L_i,\varphi} - N^p_{m,L_i,\varphi}, \tag{2.3.38}$$
$$\delta I^p_{km,L_i,\varphi}(t_k) = \delta I^p_{k,L_i,\varphi}(t_k) - \delta I^p_{m,L_i,\varphi}(t_k), \tag{2.3.39}$$
$$\delta T^p_{km}(t_k) = \delta T^p_k(t_k) - \delta T^p_m(t_k), \tag{2.3.40}$$
$$\delta E_{km,L_i,\varphi}(t_k) = \delta E_{k,L_i,\varphi}(t_k) - \delta E_{m,L_i,\varphi}(t_k), \tag{2.3.41}$$
$$\delta M^p_{km,L_i,\varphi}(t_k) = \delta M^p_{k,L_i,\varphi}(t_k) - \delta M^p_{m,L_i,\varphi}(t_k), \tag{2.3.42}$$
$$\epsilon^p_{km,L_i,\varphi}(t_k) = \epsilon^p_{k,L_i,\varphi}(t_k) - \epsilon^p_{m,L_i,\varphi}(t_k). \tag{2.3.43}$$

Even though the nominal reception time is the same, the emission time differ slightly because of different distances between the satellite and the two receivers k and m.

Single differences carrier phase observable with two transmitters

Given two transmitters p and q observed the same receiver k at the same nominal receiver epoch, the *single difference* carrier phase observable between the two transmitters is defined as

$$\begin{aligned}\varphi^{pq}_{k,L_i}(t_k) &\equiv \varphi^p_{k,L_i}(t_k) - \varphi^q_{k,L_i}(t_k)\\ &= \frac{f_i}{c}\left[\rho^p_k(t_k) - \rho^q_k(t_k)\right] + \frac{a^p}{c}\rho^p_k(t_k) - \frac{a^q}{c}\rho^q_k(t_k)\\ &\quad + \frac{f_i dt_k}{c}\left[\dot\rho^p_k(t_k) - \dot\rho^q_k(t_k)\right] + N^{pq}_{k,L_i,\varphi}\\ &\quad + \delta I^{pq}_{k,L_i,\varphi}(t_k) + \frac{f_i}{c}\delta T^{pq}_k(t_k) + \delta E^{pq}_{L_i,\varphi}(t_k) + \delta M^{pq}_{k,L_i,\varphi}(t_k) + \epsilon^{pq}_{k,L_i,\varphi}(t_k),\end{aligned} \tag{2.3.44}$$

where

$$N^{pq}_{k,L_i,\varphi} = N^p_{k,L_i,\varphi} - N^q_{k,L_i,\varphi}, \tag{2.3.45}$$
$$\delta I^{pq}_{k,L_i,\varphi}(t_k) = \delta I^p_{k,L_i,\varphi}(t_k) - \delta I^q_{k,L_i,\varphi}(t_k), \tag{2.3.46}$$
$$\delta T^{pq}_k(t_k) = \delta T^p_k(t_k) - \delta T^q_k(t_k), \tag{2.3.47}$$
$$\delta E^{pq}_{L_i,\varphi}(t_k) = \delta E^p_{L_i,\varphi}(t_k) - \delta E^q_{L_i,\varphi}(t_k), \tag{2.3.48}$$
$$\delta M^{pq}_{k,L_i,\varphi}(t_k) = \delta M^p_{k,L_i,\varphi}(t_k) - \delta M^q_{k,L_i,\varphi}(t_k), \tag{2.3.49}$$
$$\epsilon^{pq}_{k,L_i,\varphi}(t_k) = \epsilon^p_{k,L_i,\varphi}(t_k) - \epsilon^q_{k,L_i,\varphi}(t_k). \tag{2.3.50}$$

Even though the nominal reception time is the same, the emission time differ slightly because of different distances between the receiver k and the two satellites p and q.

Double differences carrier phase observable

If two receivers k and m observe two satellite p and q at the same nominal time, the *double difference* carrier phase observable is

$$\begin{aligned}\varphi^{pq}_{km,L_i}(t_k) &\equiv \varphi^{p}_{km,L_i}(t_k) - \varphi^{q}_{km,L_i}(t_k)\\ &= \frac{f_i}{c}\left[\rho^p_k(t_k) - \rho^p_m(t_k)\right] - \frac{f_i}{c}\left[\rho^q_k(t_k) - \rho^q_m(t_k)\right]\\ &\quad + \frac{a^p}{c}\left[\rho^p_k(t_k) - \rho^p_m(t_k)\right] - \frac{a^q}{c}\left[\rho^q_k(t_k) - \rho^q_m(t_k)\right]\\ &\quad + \frac{f_i}{c}\left[\dot\rho^p_k(t_k)dt_k - \dot\rho^p_m(t_k)dt_m\right] - \frac{f_i}{c}\left[\dot\rho^q_k(t_k)dt_k - \dot\rho^q_m(t_k)dt_m\right]\\ &\quad + N^{pq}_{km,L_i,\varphi} + \delta I^{pq}_{km,L_i,\varphi}(t_k) + \frac{f_i}{c}\delta T^{pq}_{km}(t_k) + \delta M^{pq}_{km,L_i,\varphi}(t_k) + \epsilon^{pq}_{km,L_i,\varphi}(t_k),\end{aligned} \tag{2.3.51}$$

where

$$N^{pq}_{km,L_i,\varphi} = N^{p}_{km,L_i,\varphi} - N^{q}_{km,L_i,\varphi}, \tag{2.3.52}$$

$$\delta I^{pq}_{km,L_i,\varphi}(t_k) = \delta I^{p}_{km,L_i,\varphi}(t_k) - \delta I^{q}_{km,L_i,\varphi}(t_k), \tag{2.3.53}$$

$$\delta T^{pq}_{km}(t_k) = \delta T^{p}_{k}(t_k) - \delta T^{p}_{m}(t_k), \tag{2.3.54}$$

$$\delta M^{pq}_{km,L_i,\varphi}(t_k) = \delta M^{p}_{km,L_i,\varphi}(t_k) - \delta M^{q}_{km,L_i,\varphi}(t_k), \tag{2.3.55}$$

$$\epsilon^{pq}_{km,L_i,\varphi}(t_k) = \epsilon^{p}_{km,L_i,\varphi}(t_k) - \epsilon^{q}_{km,L_i,\varphi}(t_k). \tag{2.3.56}$$

Double difference cancels the large receiver clock errors dt_k and dt_m.

Delta ranges carrier phase observable

The difference in time of carrier phase observables involving one station and one satellite are called *delta range observables*

$$\varphi^{p}_{k,L_i}(t_2,t_1) \equiv \varphi^{p}_{k,L_i}(t_2) - \varphi^{p}_{k,L_i}(t_1). \tag{2.3.57}$$

These delta ranges are a function of the change in topocentric distance between the station and the satellite provided there is no cycle sleep between the epochs t_1 and t_2. They do not depend on the initial ambiguity because of the differentiation over time.

Triple differences carrier phase observable

The *triple difference* is the difference of two double differences between two successive epochs

$$\begin{aligned}\varphi^{pq}_{km,L_i}(t_2,t_1) &\equiv \varphi^{pq}_{km,L_i}(t_2) - \varphi^{pq}_{km,L_i}(t_1)\\ &= \left[\varphi^{p}_{km,L_i}(t_2) - \varphi^{q}_{km,L_i}(t_2)\right] - \left[\varphi^{p}_{km,L_i}(t_1) - \varphi^{q}_{km,L_i}(t_1)\right]\\ &= \varphi^{p}_{km,L_i}(t_2,t_1) - \varphi^{q}_{km,L_i}(t_2,t_1)\\ &= \left[\varphi^{p}_{k,L_i}(t_2) - \varphi^{p}_{m,L_i}(t_2)\right] - \left[\varphi^{p}_{k,L_i}(t_1) - \varphi^{p}_{m,L_i}(t_1)\right]\\ &\quad - \left[\varphi^{q}_{k,L_i}(t_2) - \varphi^{q}_{m,L_i}(t_2)\right] - \left[\varphi^{q}_{k,L_i}(t_1) - \varphi^{q}_{m,L_i}(t_1)\right]\\ &= \left[\varphi^{pq}_{k,L_i}(t_2) - \varphi^{pq}_{m,L_i}(t_2)\right] - \left[\varphi^{pq}_{k,L_i}(t_1) - \varphi^{pq}_{m,L_i}(t_1)\right]\\ &= \varphi^{pq}_{k,L_i}(t_2,t_1) - \varphi^{pq}_{m,L_i}(t_2,t_1)\end{aligned} \tag{2.3.58}$$

where

$$\begin{aligned}\varphi^{pq}_{k,L_i}(t_k) &\equiv \varphi^{p}_{k,L_i}(t_k) - \varphi^{q}_{k,L_i}(t_k)\\ &= \frac{f_i}{c}\left[\rho^p_k(t_k) - \rho^q_k(t_k)\right] + \frac{a^p}{c}\rho^p_k(t_k) - \frac{a^p}{c}\rho^q_k(t_k)\\ &\quad + \frac{f_i}{c}\left[\dot\rho^p_k(t_k)dt_k - \dot\rho^q_k(t_k)dt_m\right] + N^{pq}_{k,L_i,\varphi} + f_i(dt^p - dt^q)\\ &\quad + \delta I^{pq}_{k,L_i,\varphi}(t_k) + \frac{f_i}{c}\delta T^{pq}_{k}(t_k) + \delta E^{\varphi}_{L_i,pq}(t_k) + \delta M^{pq}_{k,L_i,\varphi}(t_k) + \epsilon^{pq}_{k,L_i,\varphi}(t_k)\end{aligned} \tag{2.3.59}$$

and

$$\varphi^{pq}_{k,L_i}(t_2,t_1) \equiv \varphi^{pq}_{k,L_i}(t_2) - \varphi^{pq}_{k,L_i}(t_1), \tag{2.3.60}$$

with

$$N^{pq}_{k,L_i,\varphi} = N^{p}_{k,L_i,\varphi} - N^{q}_{k,L_i,\varphi}, \tag{2.3.61}$$
$$\delta I^{pq}_{k,L_i,\varphi}(t_k) = \delta I^{p}_{k,L_i,\varphi}(t_k) - \delta I^{q}_{k,L_i,\varphi}(t_k), \tag{2.3.62}$$
$$\delta T^{pq}_{k}(t_k) = \delta T^{p}_{k}(t_k) - \delta T^{q}_{k}(t_k), \tag{2.3.63}$$
$$\delta E^{\varphi}_{L_i,pq}(t_k) = \delta E^{\varphi}_{L_i,p}(t_k) - \delta E^{\varphi}_{L_i,q}(t_k), \tag{2.3.64}$$
$$\delta M^{pq}_{k,L_i,\varphi}(t_k) = \delta M^{p}_{k,L_i,\varphi}(t_k) - \delta M^{q}_{k,L_i,\varphi}(t_k), \tag{2.3.65}$$
$$\epsilon^{pq}_{k,L_i,\varphi}(t_k) = \epsilon^{p}_{k,L_i,\varphi}(t_k) - \epsilon^{q}_{k,L_i,\varphi}(t_k). \tag{2.3.66}$$

2.4. Environmental Corrections

2.4.1. Tropospheric Corrrection

The tropospheric disturbance $\delta T^p_k(t_k)$ is due to the electromagnetic signal interaction with the non-ionized atmosphere. It affects the carrier propagation causing a phase delay or, equivalently, an increase in the radio path length. It also causes a bending of the path due to the phenomenon of refraction. Since the troposphere is a non-dispersive medium, it affects both the phase and the group propagation the same way, so that the phase and group delay are identical, that is

$$T^p_{k,\varphi}(t_k) = T^p_{k,P}(t_k) = T^p_k(t_k, E), \tag{2.4.1}$$

where E is the elevation.

The tropospheric delay can be modeled as the sum of a dry (hydrostatic) component D and a wet (water vapour) component W as a function of elevation E as

$$T^p_k(t_k, E) = D^p_k(t_k, E) + W^p_k(t_k, E), \tag{2.4.2}$$

which can be computed according to several different models, including the Hopfield, modified Hopfield, and Saastamoinen models. In all cases, use is made of mapping functions (e.g., the Niell mapping functions, or the Marini mapping functions) to extend the validity of the zenith model to any elevation E.

2.4.2. Ionospheric Correction

The ionosphere is a dispersive mean for GPS radio signal that extends on several belts from around 50 km to 1000 km above the Earth. The ionospheric disturbance (also known as ionospheric range error) is due to the electromagnetic signal interaction with the ionized atmosphere. Since the ionosphere is a dispersive medium, it affects differently the phase and the group propagation, but is such a way that the phase and group delay are equal in magnitude, but of opposite sign, as expressed in (2.3.26). In fact, one speaks of "phase advance" and "group delay" in connection with the ionospheric disturbance on radio signals. The effect is that the carrier phase measurement is reduced, while pseudorange measurement is increased by the presence of the ionosphere. The following notation identifies the units and the signs

$$\delta I^p_{k,L_i,P}(t_k) = -\delta I^p_{k,L_i,F}(t_k) = -\lambda_i \delta I^p_{k,L_i,\varphi}(t_k). \tag{2.4.3}$$

It is well known that an excellent approximation to the ionospheric range correction is proportional to the total electron content (TEC) on the transmission path and inversely proportional to the square of the frequency,

$$\delta I^p_{k,L_i,P}(t_k) = \frac{40.3(TEC)^p_k}{f^2}. \tag{2.4.4}$$

As a consequence, the ionospheric disturbances at two different frequencies will be in the inverse proportion as the square of their frequencies.

$$\frac{\delta I^p_{k,L_1,P}(t_k)}{\delta I^p_{k,L_2,P}(t_k)} = \frac{\delta I^p_{k,L_1,F}(t_k)}{\delta I^F_{k,L_2,L}(t_k)} = \frac{f_2^2}{f_1^2}, \tag{2.4.5}$$

where F express the carrier phase in unit of length, while the carrier phases expressed in unit of cycle will be in the inverse proportion as their frequencies

$$\frac{\delta I^p_{k,L_1,\varphi}(t_k)}{\delta I^p_{k,L_2,\varphi}(t_k)} = \frac{f_2}{f_1}. \tag{2.4.6}$$

2.5. Linear Combinations

Data combination are methods of combining GPS data measured with the same receiver. A general phase-phase linear combination can be formed by

$$\varphi = n_1\varphi_1 + n_2\varphi_2, \tag{2.5.1}$$

where n_1, n_2 are arbitrary constants called *phase coefficients*. The combined signal has frequency f and wavelength λ such as

$$f = n_1 f_1 + n_2 f_2, \tag{2.5.2}$$
$$\lambda = c/f, \tag{2.5.3}$$
$$c = f_1\lambda_1 = f_2\lambda_2 = f\lambda \tag{2.5.4}$$

Given F the carrier phase observable expressed in meters, that is $F = \lambda\varphi$ is the measurement distance with ambiguity, and given frm Equation (2.5.4) that

$$\lambda = \frac{f_1\lambda_1}{f} = \frac{f_2\lambda_2}{f}, \tag{2.5.5}$$

F can be processed alternatively as

$$\begin{aligned} F = \lambda\varphi &= \lambda\left(n_1\varphi_1 + n_2\varphi_2\right) \\ &= \frac{1}{f}\left(f_1\lambda_1 n_1\varphi_1 + f_2\lambda_2 n_2\varphi_2\right) \\ &= m_1\lambda_1\varphi_1 + m_2\lambda_2\varphi_2 = m_1F_1 + m_2F_2, \end{aligned} \tag{2.5.6}$$

where

$$m_i = \frac{n_i f_i}{f} = \frac{n_i\lambda}{\lambda_i}, \quad \text{for } i = 1, 2 \tag{2.5.7}$$

are the *code coefficients*. Inversely, phase coefficients can be obtain from code coefficients by

$$n_i = \frac{m_i f}{f_i} = \frac{m_i\lambda_i}{\lambda}, \quad \text{for } i = 1, 2. \tag{2.5.8}$$

Denoting the standard deviation of phase observable F_i as σ_i, for $i = 1, 2$, the newly formed observation has a standard deviation of

$$\sigma^2 = m_1^2\sigma_1^2 + m_2^2\sigma_2^2, \tag{2.5.9}$$

that is the data combination will degrade the quality of the original data.

A general code-code combination can be formed by

$$P = m_1P_1 + m_2P_2. \tag{2.5.10}$$

Denoting the standard deviation of observable P_i as σ_{ci}^2, for $i = 1, 2$, the newly formed code observation P has a standard deviation of

$$\sigma_c^2 = m_1^2\sigma_{c1}^2 + m_2^2\sigma_{c2}^2. \tag{2.5.11}$$

2.5.1. Differential Code Bias

GPS receivers have responded to restrictions on the GPS signal structure in different ways. The impact of their decisions means that different GPS observable combinations are available depending on which receiver is used. GPS receivers provide C/A code, subsequently addressed as C1, plus a subset of the following code observable types: P1, P2 and X2, equivalent to C1+(P2-P1). Therefore, dual frequency receivers can be distinguished between five classes, summarized in Table 2.3.

Receiver Type	Pseudorange observables	Characteristics	Epoch
P code correlating	P1, P2	Unencrypted P code	1980's
C/A code correlating	C1	Encryption of P code (Y code)	1990's
Hybrid L2 cross correlation	C1, X2	Encryption of P code (Y code)	Nowadays
1^{st} generation Y code	C1, P1, P2	Z-tracking	Nowadays
2^{st} generation Y code	C1, P2	Y code only on L2	Nowadays

Table 2.3. Five typical receiver types and their data characteristics. The cross-correlation type produce degraded accuracy.

It has long been known that there are GPS satellite-dependent biases, B_{C1}, B_{P1}, B_{P2}, with respect to the pseudorange observables, C/A, P1 and P2. These biases can, for example, adversely affect carrier phase ambiguity resolution [47, Hugentobler, 2006]. These biases are not accessible (in an absolute sense). It is common to consider the following differences of code biases

$$B_{P1-P2} = B_{P1} - B_{P2}, \tag{2.5.12}$$
$$B_{P1-C1} = B_{P1} - B_{C1}, \tag{2.5.13}$$

where B_{P1-P2} and B_{P1-C1} are called Differential Code Biases (DCBs). By convention, IGS precise satellite clock corrections contain an ionosphere-free linear combination of the P1 and P2 observables, with which the corrections have to be consistent. This implies that each clock correction contains the ionosphere-free linear combination of (unknown) B_{P1} and B_{P1} biases. Code tracking data from both the C1/X2 and the C1/P2 receiver class must be corrected in order to achieve full consistency with P1/P2 data, or precise satellite clock information. On the basis of B_{P1-P2} and B_{P1-C1} DCB values for the GPS/GLONASS satellite constellation, corrections may be derived for the last three receiver types of the five classes initially introduced (see Table 2.4).

Observable	P1, P2	C1, X2	C1, P2
L1	$+\frac{f_2^2}{f_1^2-f_2^2}B_{P1-P2}$	$+\frac{f_2^2}{f_1^2-f_2^2}B_{P1-P2}+B_{P1-C1}$	$+\frac{f_2^2}{f_1^2-f_2^2}B_{P1-P2}+B_{P1-C1}$
L2	$+\frac{f_1^2}{f_1^2-f_2^2}B_{P1-P2}$	$+\frac{f_1^2}{f_1^2-f_2^2}B_{P1-P2}+B_{P1-C1}$	$+\frac{f_1^2}{f_1^2-f_2^2}B_{P1-P2}$
L3	0	B_{P1-C1}	$+\frac{f_1^2}{f_1^2-f_2^2}B_{P1-C1}$
L4	$-B_{P1-P2}$	$-B_{P1-P2}$	$-B_{P1-P2}+B_{P1-C1}$
L5	$-\frac{f_1 f_2}{f_1^2-f_2^2}B_{P1-P2}$	$-\frac{f_1 f_2}{f_1^2-f_2^2}B_{P1-P2}+B_{P1-C1}$	$-\frac{f_1 f_2}{f_1^2-f_2^2}B_{P1-P2}+\frac{f_1}{f_1-f_2}B_{P1-C1}$
L6	0	$-B_{P1-C1}$	$-\frac{f_1}{f_1-f_2}B_{P1-C1}$

Table 2.4. Code bias correction for every observable in dependence of the receiver type.

2.5.2. Ionosphere-Free Linear Combination

The ionosphere-free linear combinations $\varphi^p_{k,L_3}(t_k)$ of the undifferenced phase measurements, obtained by setting $n_1 = \frac{f_1^2}{f_1^2 - f_2^2}$ and $n_2 = -\frac{f_1 f_2}{f_1^2 - f_2^2}$ in Equation (2.5.1), is given by

$$\begin{aligned}\varphi^p_{k,L_3}(t_k) &\doteq n_1\varphi^p_{k,L_1}(t_k) + n_2\varphi^p_{k,L_2}(t_k) = \left(f_1\varphi^p_{k,L_1}(t_k) - f_2\varphi^p_{k,L_2}(t_k)\right)\frac{f_1}{f_1^2 - f_2^2} \\ &= \frac{f_1}{c}\rho^p_k(t_k) - f_1\left[1 - \frac{\dot\rho^p_k(t_k)}{c}\right]dt_k + f_1\,dt^p + B^p_{k,L_3,\varphi} + \frac{a^p}{c}\rho^p_k(t_k) \\ &\quad + \frac{f_1}{c}\delta T^p_k(t_k) + \delta E_{k,L_3,\varphi}(t_k) + \delta E^p_{L_3,\varphi}(t_k) + \delta M^p_{k,L_3,\varphi}(t_k) + \epsilon^p_{k,L_3,\varphi}(t_k),\end{aligned} \tag{2.5.14}$$

with

$$B^p_{k,L_3,\varphi} = \left(f_1 N^p_{k,L_1,\varphi} - f_2 N^p_{k,L_2,\varphi}\right)\frac{f_1}{f_1^2 - f_2^2}, \tag{2.5.15}$$

$$\delta E_{k,L_3,\varphi}(t_k) = \left(f_1\delta E_{k,L_1,\varphi}(t_k) - f_2\delta E_{k,L_2,\varphi}(t_k)\right)\frac{f_1}{f_1^2 - f_2^2}, \tag{2.5.16}$$

$$\delta E^p_{L_3,\varphi}(t_k) = \left(f_1\delta E^p_{L_1,\varphi}(t_k) - f_2\delta E^p_{L_2,\varphi}(t_k)\right)\frac{f_1}{f_1^2 - f_2^2}, \tag{2.5.17}$$

$$\delta M^p_{k,L_3,\varphi}(t_k) = \left(f_1\delta M^p_{k,L_1,\varphi}(t_k) - f_2\delta M^p_{k,L_2,\varphi}(t_k)\right)\frac{f_1}{f_1^2 - f_2^2}, \tag{2.5.18}$$

$$\epsilon^p_{k,L_3,\varphi}(t_k) = \left(f_1\epsilon^p_{k,L_1,\varphi}(t_k) - f_2\epsilon^p_{k,L_2,\varphi}(t_k)\right)\frac{f_1}{f_1^2 - f_2^2}. \tag{2.5.19}$$

As the name implies, the ionospheric-free linear combination is unaffected by ionospheric disturbances. From Equations (2.5.2) and (2.5.3) it is easy to obtain the ionosphere-free combination frequency and wavelength

$$f_3 = n_1 f_1 + n_2 f_2 = \frac{f_1^3 - f_1 f_2^2}{f_1^2 - f_2^2} = f_1, \tag{2.5.20}$$

$$\lambda_3 = \frac{c}{f_3} = \lambda_1, \tag{2.5.21}$$

and then, from Equation (2.5.7), the *code coefficients* m_1 and m_2 by

$$m_1 = \frac{n_1\lambda_3}{\lambda_1} = \frac{n_1\lambda_1}{\lambda_1} = n_1 = \frac{f_1^2}{f_1^2 - f_2^2} \tag{2.5.22}$$

$$m_2 = \frac{n_2\lambda_3}{\lambda_2} = \frac{n_2\lambda_1}{\lambda_2} = \frac{f_1 f_2\lambda_1}{\left(f_1^2 - f_2^2\right)\lambda_2} = \frac{f_1 f_2^2}{\left(f_1^2 - f_2^2\right) f_1} = \frac{f_2^2}{f_1^2 - f_2^2}. \tag{2.5.23}$$

Equation (2.5.20) shows that the ionospheric-free combination frequency is the same as that of L_1. From Equation (2.5.6), the ionosphere-free linear combinations $F^p_{k,L_3}(t_k)$ of the undifferenced phase measurements expressed in meters is given by

$$\begin{aligned}F^p_{k,L_3}(t_k) &\doteq m_1 F^p_{k,L_1}(t_k) + m_2 F^p_{k,L_2}(t_k) = \left(f_1^2 F^p_{k,L_1}(t_k) - f_2^2 F^p_{k,L_2}(t_k)\right)\frac{1}{f_1^2 - f_2^2} \\ &= \rho^p_k(t_{r,k}) - c\left[1 - \frac{\dot\rho^p_k(t_k)}{c}\right]dt_k + c\,dt^p + B^p_{k,L_3,P} + \delta T^p_k(t_k) \\ &\quad + \delta E_{k,L_3,P}(t_k) + \delta E^p_{L_3,P}(t_k) + \delta M^p_{k,L_3,P}(t_k) + \epsilon^p_{k,L_3,P}(t_k),\end{aligned} \tag{2.5.24}$$

while, from Equation (2.5.10), the ionosphere-free linear combinations $P^p_{k,L_3}(t_k)$ of the undifferenced pseudorange is given by

$$\begin{aligned}P^p_{k,L_3}(t_k) &\doteq m_1 P^p_{k,L_1}(t_k) + m_2 P^p_{k,L_2}(t_k) = \left(f_1^2 P^p_{k,L_1}(t_k) - f_2^2 P^p_{k,L_2}(t_k)\right)\frac{1}{f_1^2 - f_2^2} \\ &= \rho^p_k(t_{r,k}) - c\left[1 - \frac{\dot\rho^p_k(t_k)}{c}\right]dt_k + c\,dt^p + \delta T^p_k(t_k) \\ &\quad + \delta E_{k,L_3,P}(t_k) + \delta E^p_{L_3,P}(t_k) + \delta M^p_{k,L_3,P}(t_k) + \epsilon^p_{k,L_3,P}(t_k),\end{aligned} \tag{2.5.25}$$

where

$$B^p_{k,L_3,P} = \left(f_1^2 N^p_{k,L_1,P} - f_2^2 N^p_{k,L_2,P}\right) \frac{1}{f_1^2 - f_2^2}, \tag{2.5.26}$$

$$\delta E_{k,L_3,P}(t_k) = \left(f_1^2 \delta E_{k,L_1,P}(t_k) - f_2^2 \delta E_{k,L_2,P}(t_k)\right) \frac{1}{f_1^2 - f_2^2}, \tag{2.5.27}$$

$$\delta E^p_{L_3,P}(t_k) = \left(f_1^2 \delta E^p_{L_1,P}(t_k) - f_2^2 \delta E^p_{L_2,P}(t_k)\right) \frac{1}{f_1^2 - f_2^2}, \tag{2.5.28}$$

$$\delta M^p_{k,L_3,P}(t_k) = \left(f_1^2 \delta M^p_{k,L_1,P}(t_k) - f_2^2 \delta M^p_{k,L_2,P}(t_k)\right) \frac{1}{f_1^2 - f_2^2}, \tag{2.5.29}$$

$$\epsilon^p_{k,L_3,P}(t_k) = \left(f_1^2 \epsilon^p_{k,L_1,P}(t_k) - f_2^2 \epsilon^p_{k,L_2,P}(t_k)\right) \frac{1}{f_1^2 - f_2^2}, \tag{2.5.30}$$

and

$$N^p_{k,L_i,P} = \lambda_i N^p_{k,L_i,\varphi}, \tag{2.5.31}$$

$$B^p_{k,L_i,P} = \lambda_i B^p_{k,L_i,\varphi}. \tag{2.5.32}$$

Equations (2.5.15) and (2.5.26) show that the combined ambiguity is not an integer anymore.

2.5.3. Geometry-Free Linear Combination

The geometry-free combination is the kernel in a combination used to reduce ionospheric effects and it can be formed, setting $m_1 = 1$ and $m_2 = -1$ in Equation (2.5.10), by

$$\begin{aligned} P^p_{k,L_4}(t_k) &\doteq m_1 P^p_{k,L_1}(t_k) + m_2 P^p_{k,L_2}(t_k) = P^p_{k,L_1}(t_k) - P^p_{k,L_2}(t_k) \\ &= \delta I^p_{k,L_4,P}(t_k) + \delta E_{k,L_4,P}(t_k) + \delta E^p_{L_4,P}(t_k) + \delta M^p_{k,L_4,P}(t_k) + \epsilon^p_{k,L_4,P}(t_k), \end{aligned} \tag{2.5.33}$$

while the geometry-free combination of the carrier phase observable expressed in meters can be formed by

$$\begin{aligned} F^p_{k,L_4}(t_k) &\doteq m_1 F^p_{k,L_1}(t_k) + m_2 F^p_{k,L_2}(t_k) = F^p_{k,L_1}(t_k) - F^p_{k,L_2}(t_k) \\ &= \delta I^p_{k,L_4,P}(t_k) + N^p_{k,L_4,P} + \delta E_{k,L_4,P}(t_k) + \delta E^p_{L_4,P}(t_k) + \delta M^p_{k,L_4,P}(t_k) + \epsilon^p_{k,L_4,P}(t_k), \end{aligned} \tag{2.5.34}$$

where

$$\begin{aligned} \delta I^p_{k,L_4,P}(t_k) &= \delta I^p_{k,L_1,P}(t_k) - \delta I^p_{k,L_2,P}(t_k) \\ &= \left(1 - \frac{f_1^2}{f_2^2}\right) \delta I^p_{k,L_1,P}(t_k), \end{aligned} \tag{2.5.35}$$

$$N^p_{k,L_4,P} = N^p_{k,L_1,P} - N^p_{k,L_2,P}, \tag{2.5.36}$$

$$\delta E_{k,L_4,P}(t_k) = \delta E_{k,L_1,P}(t_k) - \delta E_{k,L_2,P}(t_k), \tag{2.5.37}$$

$$\delta E^p_{L_4,P}(t_k) = \delta E^p_{L_1,P}(t_k) - \delta E^p_{L_2,P}(t_k), \tag{2.5.38}$$

$$\delta M^p_{k,L_4,P}(t_k) = \delta M^p_{k,L_1,P}(t_k) - \delta M^p_{k,L_2,P}(t_k), \tag{2.5.39}$$

$$\epsilon^p_{k,L_4,P}(t_k) = \epsilon^p_{k,L_1,P}(t_k) - \epsilon^p_{k,L_2,P}(t_k). \tag{2.5.40}$$

The geometry-free combinations cancel out all other terms in the observation equation except the ionospheric term and the ambiguity parameters. From Equations (2.5.2) and (2.5.7) it is possible to obtain n_1 and n_2 by solving the homogenous linear system

$$\begin{cases} n_1 f_1 & +n_2 f_2 & -f_4 & = 0 \\ n_1 f_1 & & -f_4 & = 0 \\ & n_2 f_2 & +f_4 & = 0 \end{cases} \tag{2.5.41}$$

for n_1, n_2, f_4. The vector equation is equivalent to a matrix equation of the form

$$\mathbf{A}\mathbf{x} = \mathbf{0}, \tag{2.5.42}$$

with

$$\mathbf{A} = \begin{bmatrix} f_1 & f_2 & -1 \\ f_1 & 0 & -1 \\ 0 & f_2 & 1 \end{bmatrix}, \tag{2.5.43}$$

$$\mathbf{x} = \begin{bmatrix} n_1 \\ n_2 \\ f \end{bmatrix}, \tag{2.5.44}$$

where $\mathbf{A}$ is the *coefficient matrix*. By the Rouché-Capelli theorem the solution is unique and it is $n_1 = 0$, $n_2 = 0$, $f_4 = 0$, that is the geometry-free combination has zero frequency and then infinite wavelength, $\lambda_4 = \infty$. For this reason it is not possible to obtain n_i from the m_i values using Equation (2.5.8), so that one can assume $n_1 = 1$, $n_2 = -\frac{f_1}{f_2}$ (this choice still leads to $f_4 = f_1 - \frac{f_1 f_2}{f_2} = 0$). The geometry-free combination of the carrier phase observable is expressed by

$$\begin{aligned} \varphi^p_{k,L_4}(t_k) &\doteq n_1\varphi^p_{k,L_1}(t_k) + n_2\varphi^p_{k,L_2}(t_k) = \varphi^p_{k,L_1}(t_k) - \frac{f_1}{f_2}\varphi^p_{k,L_2}(t_k) \\ &= \delta I^p_{k,L_4,\varphi}(t_k) + N^p_{k,L_4,P} + \delta E_{k,L_4,P}(t_k) + \delta E^p_{L_4,P}(t_k) + \delta M^p_{k,L_4,P}(t_k) + \epsilon^p_{k,L_4,P}(t_k), \end{aligned} \tag{2.5.45}$$

where

$$\begin{aligned} \delta I^p_{k,L_4,\varphi}(t_k) &= \delta I^p_{k,L_1,\varphi}(t_k) - \frac{f_1}{f_2}\delta I^p_{k,L_2,\varphi}(t_k) \\ &= \left(1 - \frac{f_1^2}{f_2^2}\right)\delta I^p_{k,L_1,\varphi}(t_k), \end{aligned} \tag{2.5.46}$$

$$N^p_{k,L_4,\varphi} = N^p_{k,L_1,\varphi} - \frac{f_1}{f_2}N^p_{k,L_2,\varphi}, \tag{2.5.47}$$

$$\delta E_{k,L_4,\varphi}(t_k) = \delta E_{k,L_1,\varphi}(t_k) - \frac{f_1}{f_2}\delta E_{k,L_2,\varphi}(t_k), \tag{2.5.48}$$

$$\delta E^p_{L_4,\varphi}(t_k) = \delta E^p_{L_1,\varphi}(t_k) - \frac{f_1}{f_2}\delta E^p_{L_2,\varphi}(t_k), \tag{2.5.49}$$

$$\delta M^p_{k,L_4,\varphi}(t_k) = \delta M^p_{k,L_1,\varphi}(t_k) - \frac{f_1}{f_2}\delta M^p_{k,L_2,\varphi}(t_k), \tag{2.5.50}$$

$$\epsilon^p_{k,L_4,\varphi}(t_k) = \epsilon^p_{k,L_1,\varphi}(t_k) - \frac{f_1}{f_2}\epsilon^p_{k,L_2,\varphi}(t_k). \tag{2.5.51}$$

2.5.4. The Wide-Lane Linear Combination

The wide-lane combination of the carrier phase observable is defined assuming $n_1 = 1$ and $n_2 = -1$ by

$$\varphi^p_{k,wl}(t_k) \doteq n_1\varphi^p_{k,L_1}(t_k) + n_2\varphi^p_{k,L_2}(t_k) = \varphi^p_{k,L_1}(t_k) - \varphi^p_{k,L_2}(t_k). \tag{2.5.52}$$

The wide-lane frequency and wavelength are

$$f_{wl} = f_1 - f_2 = 347.82 \quad \text{MHz}, \tag{2.5.53}$$

$$\lambda_{wl} = \frac{c}{f_1 - f_2} = 0.861918400322006 \quad \text{m}. \tag{2.5.54}$$

The wide-lane carrier phase expressed in units of length, considering that $m_1 = \frac{f_1}{f_1 - f_2}$ and $m_2 = -\frac{f_2}{f_1 - f_2}$, is defined by

$$F^p_{k,wl}(t_k) = m_1 F^p_{k,L_1}(t_k) + m_2 F^p_{k,L_2}(t_k) = \frac{f_1}{f_1 - f_2}F^p_{k,L_1}(t_k) - \frac{f_2}{f_1 - f_2}F^p_{k,L_2}(t_k), \tag{2.5.55}$$

and for the wide-lane pseudorange likewise

$$P^p_{k,wl}(t_k) \doteq m_1 P^p_{k,L_1}(t_k) + m_2 P^p_{k,L_2}(t_k) = \frac{f_1}{f_1 - f_2}P^p_{k,L_1}(t_k) - \frac{f_2}{f_1 - f_2}P^p_{k,L_2}(t_k). \tag{2.5.56}$$

The wide-lane combination L_{wl}, for $L = \varphi, F, P$, is also called L_5.

2.5.5. The Narrow-Lane Linear Combination

The narrow-lane combination of the carrier phase observable is defined assuming $n_1 = 1$ and $n_2 = 1$ by

$$\varphi^p_{k,nl}(t_k) \doteq n_1\varphi^p_{k,L_1}(t_k) + n_2\varphi^p_{k,L_2}(t_k) = \varphi^p_{k,L_1}(t_k) + \varphi^p_{k,L_2}(t_k). \tag{2.5.57}$$

The narrow-lane frequency and wavelength are

$$f_{nl} = f_1 + f_2 = 2803.02 \quad \text{MHz}, \tag{2.5.58}$$

$$\lambda_{nl} = \frac{c}{f_1 + f_2} = 0.106953378142147 \quad \text{m}. \tag{2.5.59}$$

The narrow-lane carrier phase expressed in units of length, considering that $m_1 = \frac{f_1}{f_1+f_2}$ and $m_2 = \frac{f_2}{f_1+f_2}$, is defined by

$$F^p_{k,nl}(t_k) \doteq m_1F^p_{k,L_1}(t_k) + m_2F^p_{k,L_2}(t_k) = \frac{f_1}{f_1 + f_2}F^p_{k,L_1}(t_k) + \frac{f_2}{f_1 + f_2}F^p_{k,L_2}(t_k), \tag{2.5.60}$$

and for the narrow-lane pseudorange likewise

$$P^p_{k,nl}(t_k) = m_1P^p_{k,L_1}(t_k) + m_2P^p_{k,L_2}(t_k) = \frac{f_1}{f_1 + f_2}P^p_{k,L_1}(t_k) + \frac{f_2}{f_1 + f_2}P^p_{k,L_2}(t_k). \tag{2.5.61}$$

2.5.6. The Melbourne-Wübbena Combination

The Melbourne-Wübbena linear combination is the difference between the wide-lane phase combination in units of length and the narrow-lane pseudorange combination

$$\begin{aligned} F^p_{k,MW}(t_k) &\doteq F^p_{k,wl}(t_k) - P^p_{k,nl}(t_k) \\ &= \left(\frac{f_1}{f_1 - f_2}F^p_{k,L_1}(t_k) - \frac{f_2}{f_1 - f_2}F^p_{k,L_2}(t_k)\right) \\ &- \left(\frac{f_1}{f_1 + f_2}P^p_{k,L_1}(t_k) + \frac{f_2}{f_1 + f_2}P^p_{k,L_2}(t_k)\right), \end{aligned} \tag{2.5.62}$$

in the sense that is the combination of $F^p_{k,wl}(t_k)$ and $P^p_{k,nl}(t_k)$ with $m_1 = 1$ and $m_2 = -1$. The phase coefficients are

$$n_1 = \frac{f_{MW}}{f_w l}, \tag{2.5.63}$$

$$n_2 = \frac{f_{MW}}{f_n l}, \tag{2.5.64}$$

where f_{MW} is the Melbourne-Wübbena frequency. Then, the Melbourne-Wübbena frequency and wavelength are

$$f_{MW} = n_1f_{wl} - n_2f_{nl} = \frac{f_{MW}}{f_w l}f_{wl} - \frac{f_{MW}}{f_n l}f_{nl} = 0 \quad \text{MHz}, \tag{2.5.65}$$

$$\lambda_{MW} = \frac{c}{f_{MW}} = \infty \quad \text{m}. \tag{2.5.66}$$

Since the wavelength is infinite it is not possible to obtain the phase coefficients from the code coefficients. Then, the phase coefficients are set as $n_1 = 1$ and $n_2 = \frac{\lambda_{nl}}{\lambda_{wl}}$, so that the Melbourne-Wübbena combination in units of cycles is expressed by

$$\begin{aligned} \varphi^p_{k,MW}(t_k) &\doteq \varphi^p_{k,wl}(t_k) - \frac{\lambda_{nl}}{\lambda_{wl}}G^p_{k,nl}(t_k) \\ &= \left(\varphi^p_{k,L_1}(t_k) - \varphi^p_{k,L_2}(t_k)\right) - \frac{f_1 - f_2}{f_1 + f_2}\left(G^p_{k,L_1}(t_k) + G^p_{k,L_2}(t_k)\right), \end{aligned} \tag{2.5.67}$$

where

$$\begin{aligned} G^p_{k,L_i}(t_k) &= \frac{P^p_{k,L_i}(t_k)}{\lambda_i} \\ &= \frac{f_i}{c}\rho^p_k(t_k) - f_i\left[1 - \frac{\dot\rho^p_k(t_k)}{c}\right]dt_k + f_i\,dt^p + \frac{a^p}{c}\rho^p_k(t_k) - \delta I^p_{k,L_i,\varphi}(t_k) \\ &+ \frac{f_i}{c}\delta T^p_k(t_k) + \delta E_{k,L_i,\varphi}(t_k) + \delta E^p_{L_i,\varphi}(t_k) + \delta M^p_{k,L_i,\varphi}(t_k) + \epsilon^p_{k,L_i,\varphi}(t_k). \end{aligned} \tag{2.5.68}$$

is the pseudorange expressed in units of cycles. Note that again

$$f_{MW} = n_1 f_{wl} - n_2 f_{nl} = f_{wl} - \frac{\lambda_{nl}}{\lambda_{wl}} f_{nl} = f_{wl} - \frac{f_{wl}}{f_{nl}} f_{nl} = 0 \quad \text{Hz}. \tag{2.5.69}$$

2.6. Integer Phase Ambiguity Resolution

In the following sections some methods for undifferenced and double differenced ambiguity determination will be illustrated and compared.

2.6.1. Undifferentiate Integer Phase Ambiguity Resolution

It is possible to use the Melbourne-Wübbena combination for data editing in connection with the determination of the carrier phase ambiguities. Indeed, it is possible to demonstrate that

$$N^p_{k,wl,\varphi} = \varphi^p_{k,MW}(t_k), \tag{2.6.1}$$

where $N^p_{k,wl,\varphi}$ is the *wide-lane ambiguity*. Introducing the *geometric term* and *ionospheric term*, respectively

$$a^p_k = \frac{\rho^p_k(t_k)}{c} - dt_k + dt^p \quad \text{and} \tag{2.6.2}$$

$$b^p_k = \frac{f_i^2}{c}\delta I^p_{k,L_i,P}(t_k) = \frac{40.3(TEC)^p_k}{c}, \tag{2.6.3}$$

equations (2.5.68) e (2.3.36) can be written as

$$G^p_{k,L_i}(t_k) = a^p_k f_i + \frac{b^p_k}{f_i} + \frac{\delta T^p_k(t_k)}{\lambda_{L_i}} - \frac{\dot\rho^p_k(t_k)dt_k}{\lambda_{L_p}} + \ldots + \epsilon^p_{k,L_i,P}(t_k), \tag{2.6.4}$$

$$\varphi^p_{k,L_i}(t_k) = a^p_k f_i - \frac{b^p_k}{f_i} + \frac{\delta T^p_k(t_k)}{\lambda_{L_i}} + N^p_{k,L_i,\varphi} - \frac{\dot\rho^p_k(t_k)dt_k}{\lambda_{L_p}} + \ldots + \epsilon^p_{k,L_i,P}(t_k). \tag{2.6.5}$$

Multiplying the Equation (2.6.4) by f_i, for $i = 2, 1$, and differencing the resulting equations yields the geometric term

$$a^p_k = \frac{1}{f_2^2 - f_1^2}\left(G^p_{k,L_2}(t_k)f_2 - G^p_{k,L_1}(t_k)f_1\right). \tag{2.6.6}$$

Multiplying by f_i, for $i = 1, 2$ instead, and differencing the resulting equations yields the ionospheric term

$$b^i_K = \frac{f_1 f_2}{f_2^2 - f_1^2}\left(G^p_{k,L_1}(t_k)f_2 - G^p_{k,L_2}(t_k)f_1\right). \tag{2.6.7}$$

Substituting the equations (2.6.6) and (2.6.7) into (2.6.5) leads to explicit expression for the phase ambiguities

$$N^p_{k,L_1,\varphi} = \varphi^p_{k,L_1}(t_k) + \frac{f^2_{L_2} + f^2_{L_1}}{f^2_{L_2} - f^2_{L_1}} G^p_{k,L_1}(t_k) - \frac{2f_{L_1}f_{L_2}}{f^2_{L_2} - f^2_{L_1}} G^p_{k,L_2}(t_k), \tag{2.6.8}$$

$$N^p_{k,L_2,\varphi} = \varphi^p_{k,L_2}(t_k) + \frac{2f_{L_1}f_{L_2}}{f^2_{L_2} - f^2_{L_1}} G^p_{k,L_1}(t_k) - \frac{f^2_{L_2} + f^2_{L_1}}{f^2_{L_2} - f^2_{L_1}} G^p_{k,L_2}(t_k). \tag{2.6.9}$$

By forming the difference $N^p_{k,wl,\varphi} = N^p_{k,L_1,\varphi} - N^p_{k,L_2,\varphi}$ between Equations (2.6.8) and (2.6.9) ones finally obtain

$$N^p_{k,wl,\varphi} = \varphi^p_{k,L_1}(t_k) - \varphi^p_{k,L_2}(t_k) - \frac{f_1 - f_2}{f_1 + f_2}\left(G^p_{k,L_1}(t_k) + G^p_{k,L_2}(t_k)\right), \tag{2.6.10}$$

From Equation (2.5.67) it is easy to verify that the second member of Equation (2.6.10) is the Melbourne-Wübbena combination in units of cycles, so that the Equation (2.6.1) is demonstrated.

Resolving ambiguities with dual phase data

By subtracting the wide lane phase observable from the L_1 phase observable, each one divided by its carrier frequency, the difference of the two equations gives

$$\frac{\varphi^p_{k,L_1}(t_k)}{f_1} - \frac{\varphi^p_{k,wl}(t_k)}{f_{wl}} = \frac{N^p_{k,L_1,\varphi}}{f_1} - \frac{N^p_{k,wl,\varphi}}{f_{wl}} - \frac{b^p_k}{f_1^2} + \frac{b^p_k}{f_{wl}}\left(\frac{1}{f_1} - \frac{1}{f_2}\right). \tag{2.6.11}$$

The desired ambiguity $N^p_{k,L_1,\varphi}$ follows explicitly after rearranging and multiplying the Equation (2.6.11) by f_1

$$N^p_{k,L_1,\varphi} = \varphi^p_{k,L_1}(t_k) - \frac{f_1}{f_{wl}}\left(\varphi^p_{k,wl}(t_k) - N^p_{k,wl,\varphi}\right) + \frac{b^p_k}{f_1} - \frac{b^p_k}{f_{wl}}\left(1 - \frac{f_1}{f_2}\right). \tag{2.6.12}$$

The terms reflecting the ionospheric influence may be treated as follows

$$\frac{b^p_k}{f_1} - \frac{b^p_k}{f_{wl}}\left(1 - \frac{f_1}{f_2}\right) = b^p_k \frac{f_2 + f_1}{f_1 f_2}, \tag{2.6.13}$$

leading to the expression of the phase ambiguity calculated from the wide lane ambiguity

$$N^p_{k,L_1,\varphi} = \varphi^p_{k,L_1}(t_k) - \frac{f_1}{f_{wl}}\left(\varphi^p_{k,wl}(t_k) - N^p_{k,wl,\varphi}\right) + b^p_k \frac{f_2 + f_1}{f_1 f_2}, \tag{2.6.14}$$

and, in analogous way, for $N^p_{k,L_2,\varphi}$ by exchanging the roles of L_1 and L_2. Equation (2.6.14) preserve integer nature of the term. The Equation (2.6.10) allows for the determination of the wide lane ambiguity $N^p_{k,wl,\varphi}$ for each epoch and each site. It is independent of the baseline length and of the ionospheric effect. Even if all modeled systematic effects canceled out in Equation (2.6.10), the multipath effect remains and affects phase and code differently. Multipath is almost exclusively responsible for a variation of $N^p_{k,wl,\varphi}$ by several cycles from epoch to epoch. These variations may be overcome by averaging over a longer period, that is

$$\overline{N^p_{k,wl,\varphi}} = \frac{1}{n}\sum_{i=1}^{n} N^p_{k,wl,\varphi}(t_i), \tag{2.6.15}$$

where n is the number of instant considered. Since the wide lane combination is a linear combination of GPS observables that uses integer coefficients ($n_1 = 1$ and $n_2 = -1$), the wide lane ambiguity is still an integer ambiguity that will indicated by $\| \overline{N^p_{k,wl,\varphi}} \|$

$$\| \overline{N^p_{k,wl,\varphi}} \| = nint\left(\overline{N^p_{k,wl,\varphi}}\right). \tag{2.6.16}$$

The Figure 2.4 shows an example of application of this formula: the red line is the rounded mean of the instantaneous wide lane ambiguities.

Substituting $\| \overline{N^p_{k,wl,\varphi}} \|$ into Equation (2.6.14) leads to the computation of the phase ambiguity $N^p_{k,L_1,\varphi}$

$$N^p_{k,L_1,\varphi} = \varphi^p_{k,L_1}(t_k) - \frac{f_1}{f_{wl}}\left(\varphi^p_{k,wl}(t_k) - \| \overline{N^p_{k,wl,\varphi}} \|\right) + b^p_k \frac{f_2 + f_1}{f_1 f_2}. \tag{2.6.17}$$

The ionosphere dependant term b^p_k can be eliminated by using the geometry free combination expressed in Equation2.5.34, that is

$$F^p_{k,L_4}(t_k) = \left(1 - \frac{f_1^2}{f_2^2}\right)\delta I^p_{k,L_1,P}(t_k) + N^p_{k,L_4,P} + \ldots + \epsilon^p_{k,L_4,P}(t_k), \tag{2.6.18}$$

Figure 2.4. An example of wide lane ambiguity determination for a link between the GPS receiver onboard the GRAS/Metop LEO satellite and the GPS s/v 2 on October 12 2007. It is clearly visible the trend of few cycles due to multipath. The value of the mediated wide lane ambiguity is 14.906 [L_1 cycles], while rounding to the nearest integer the mediated wide lane ambiguity is 15 [L_1 cycles].

so that b_k^p can be expressed as

$$b_k^p = \frac{f_1^2}{c}\delta I^p_{k,L_1,P}(t_k) \simeq \frac{f_1^2 f_2^2}{c\left(f_2^2 - f_1^2\right)}\left(F^p_{k,L_4}(t_k) - N^p_{k,L_4,P}\right), \tag{2.6.19}$$

so that

$$b_k^p \frac{f_2 + f_1}{f_1 f_2} = \frac{f_1 f_2}{c\left(f_2 - f_1\right)}\left(F^p_{k,L_4}(t_k) - N^p_{k,L_4,P}\right) \tag{2.6.20}$$

and then Equation (2.6.14) becomes

$$\begin{aligned} N^p_{k,L_1,\varphi} &= \varphi^p_{k,L_1}(t_k) - \frac{f_1}{f_{wl}}\left(\varphi^p_{k,wl}(t_k) - \| \overline{N^p_{k,wl,\varphi}} \|\right) + \frac{f_1 f_2}{c\left(f_2 - f_1\right)}\left(F^p_{k,L_4}(t_k) - N^p_{k,L_4,P}\right) \\ &= \varphi^p_{k,L_1}(t_k) - \frac{f_1}{f_{wl}}\left(\varphi^p_{k,wl}(t_k) - \| \overline{N^p_{k,wl,\varphi}} \|\right) + \frac{1}{f_2 - f_1}\left(f_2 F^p_{k,L_1}(t_k) - f_1 F^p_{k,L_2}(t_k) - N^p_{k,L_4,P}\right). \end{aligned} \tag{2.6.21}$$

The expression for the integer ambiguity $N^p_{k,L_2,\varphi}$ can be obtained similarly. In this way the ambiguities are corrected for any possible error, but are biased by the real geometry free ambiguity $N^p_{k,L_4,P}$.

Resolving ambiguities by combining dual frequency carrier phase and code data

In Equation (2.6.17) the ionosphere dependant term b_k^p can be eliminated by using the geometry free combination expressed in Equation (2.5.33), that is

$$P^p_{k,L_4}(t_k) = \left(1 - \frac{f_1^2}{f_2^2}\right)\delta I^p_{k,L_1,P}(t_k) + \ldots + \epsilon^p_{k,L_4,P}(t_k), \tag{2.6.22}$$

so that b_k^p can be expressed as

$$b_k^p = \frac{f_1^2}{c}\delta I^p_{k,L_1,P}(t_k) \simeq \frac{f_1^2 f_2^2}{c\left(f_2^2 - f_1^2\right)} P^p_{k,L_4}(t_k), \tag{2.6.23}$$

and then

$$b_k^p \frac{f_2 + f_1}{f_1 f_2} = \frac{f_1 f_2}{c\left(f_2 - f_1\right)} P^p_{k,L_4}(t_k). \tag{2.6.24}$$

In this way Equation (2.6.14) becomes

$$\begin{aligned} N^p_{k,L_1,\varphi} &= \varphi^p_{k,L_1}(t_k) - \frac{f_1}{f_{wl}}\left(\varphi^p_{k,wl}(t_k) - \| \overline{N^p_{k,wl,\varphi}} \|\right) + \frac{f_1 f_2}{c\,(f_2 - f_1)} P^p_{k,L_4}(t_k) \\ &= \varphi^p_{k,L_1}(t_k) - \frac{f_1}{f_{wl}}\left(\varphi^p_{k,wl}(t_k) - \| \overline{N^p_{k,wl,\varphi}} \|\right) + \frac{1}{f_2 - f_1}\left(f_2 G^p_{k,L_1}(t_k) - f_1 G^p_{k,L_2}(t_k)\right). \end{aligned} \tag{2.6.25}$$

The expression for the integer ambiguity $N^p_{k,L_2,\varphi}$ can be obtained similarly.

Another equivalent method to determine the undifferentiate integer ambiguity $N^p_{k,L_i,\varphi}$ using phase and pseudorange combinations of both carriers L_1 and L_2 is the one expressed by Equations (2.6.8) and (2.6.9).

Comparison of the undifferenced ambiguity determination methods

Figure 2.5 shows the comparison of the methods previously explained together with other simpler methods. It is clear that the ambiguity determination by combining dual frequency carrier phase and code data, Equations (2.6.25), (2.6.8) and (2.6.9), (green line with diamonds and cyan line with dots) are the best techniques, and are equivalent to adopt the combination (green line with circles)

$$\varphi^p_{k,L_1}(t_k) + G^p_{k,L_1}(t_k) - 2G^p_{k,L_3}(t_k). \tag{2.6.26}$$

In fact these methods remove completely the ionospheric contribution but introduce a lot of noise.

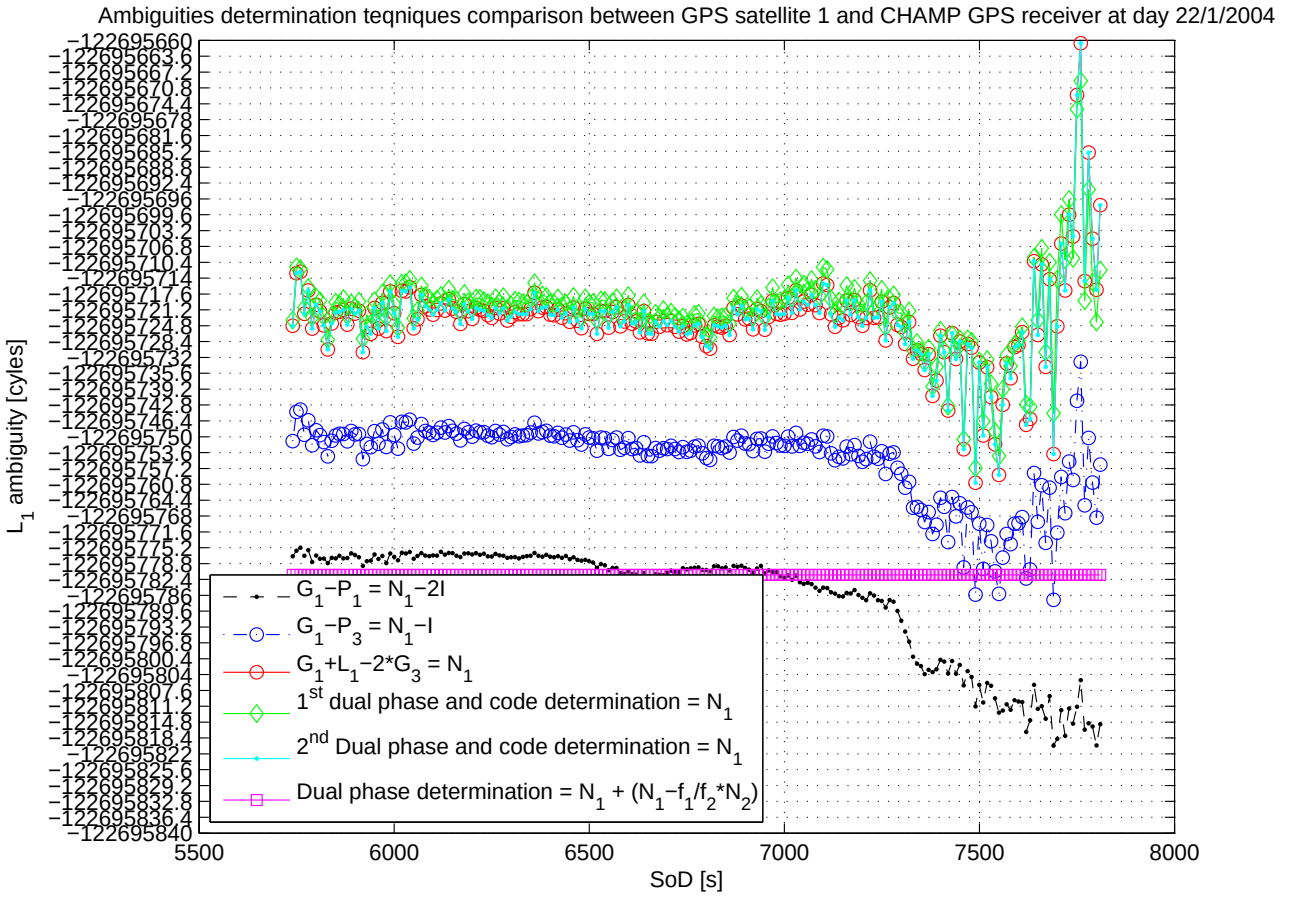

Figure 2.5. Comparison of several ambiguity determination methods for a link between the GPS receiver onboard the CHAMP LEO satellite and the GPS s/v 1 on January 22 2004.

It can be seen also that the ambiguity determination with dual phase data only, Equation (2.6.21) completely remove all kind of error but the ambiguity is biased by the geometry free ambiguity contribution.

2.6.2. Double difference ionospheric free ambiguity determination

The ambiguity determination with dual phase data becomes very precious to find out the double difference ionospheric free ambiguities. Double differentiating the Equation (2.6.17), without to correct the ionosphere term, leads to

$$\begin{aligned} N^{pq}_{km,L_i,\varphi} = {} & \varphi^{p}_{k,L_1}(t_k) - \frac{f_1}{f_{wl}}\left(\varphi^{p}_{k,wl}(t_k) - \| \overline{N^{p}_{k,wl,\varphi}} \|\right) + b^{p}_{k}\frac{f_2+f_1}{f_1 f_2} \\ & - \left(\varphi^{p}_{m,L_1}(t_k) - \frac{f_1}{f_{wl}}\left(\varphi^{p}_{m,wl}(t_k) - \| \overline{N^{p}_{m,wl,\varphi}} \|\right) + b^{p}_{m}\frac{f_2+f_1}{f_1 f_2}\right) \\ & - \left[\varphi^{q}_{k,L_1}(t_k) - \frac{f_1}{f_{wl}}\left(\varphi^{q}_{k,wl}(t_k) - \| \overline{N^{q}_{k,wl,\varphi}} \|\right) + b^{q}_{k}\frac{f_2+f_1}{f_1 f_2}\right. \\ & \left. - \left(\varphi^{q}_{m,L_1}(t_k) - \frac{f_1}{f_{wl}}\left(\varphi^{q}_{m,wl}(t_k) - \| \overline{N^{q}_{m,wl,\varphi}} \|\right) + b^{q}_{m}\frac{f_2+f_1}{f_1 f_2}\right)\right], \end{aligned} \tag{2.6.27}$$

and then computing the ionospheric free combination to

$$B^{pq}_{km,L_3,\varphi} = \left(f_1 N^{pq}_{km,L_1,\varphi} - f_2 N^{pq}_{km,L_2,\varphi}\right)\frac{f_1}{f_1^2 - f_2^2}. \tag{2.6.28}$$

The double difference ionospheric free ambiguity $B^{pq}_{km,L_3,\varphi}$ can be compared with the following computation method. The double difference inter ambiguity can be obtained as

$$N^{pq}_{AB,L_i,\varphi} = \varphi^{pq}_{AB,L_i}(t_k) - \frac{\mathbf{b}\cdot\left(\hat{\mathbf{s}}^i - \hat{\mathbf{s}}^j\right)}{\lambda} + \frac{\left(\dot{\rho}^j - \dot{\rho}^i\right)dt_{AB}}{\lambda}. \tag{2.6.29}$$

The term $-\mathbf{b}\cdot\left(\hat{\mathbf{s}}^i - \hat{\mathbf{s}}^j\right)/\lambda$ is said *geometric correction*, while the term $\left(\dot{\rho}^j - \dot{\rho}^i\right)dt_{AB}/\lambda$ is said *velocity correction*. Figures from Figure 2.6 to Figure 2.9 show an example of double difference integer ambiguity determination with receivers on the ground (respectively in Padua, receiver A, and Rovigo, B, Italy) for different couple of transmitting GPS satellites.

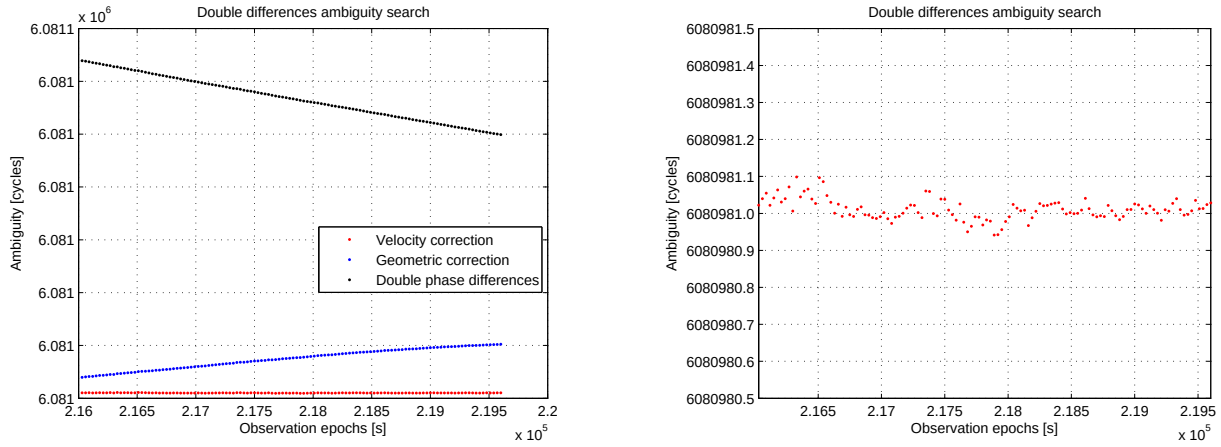

(a) Real ambiguities research.

(b) Real ambiguities around integer 6080981.

Figure 2.6. Double differences ambiguities analysis for GPS receivers A and B and GPS satellites 13 and 2.

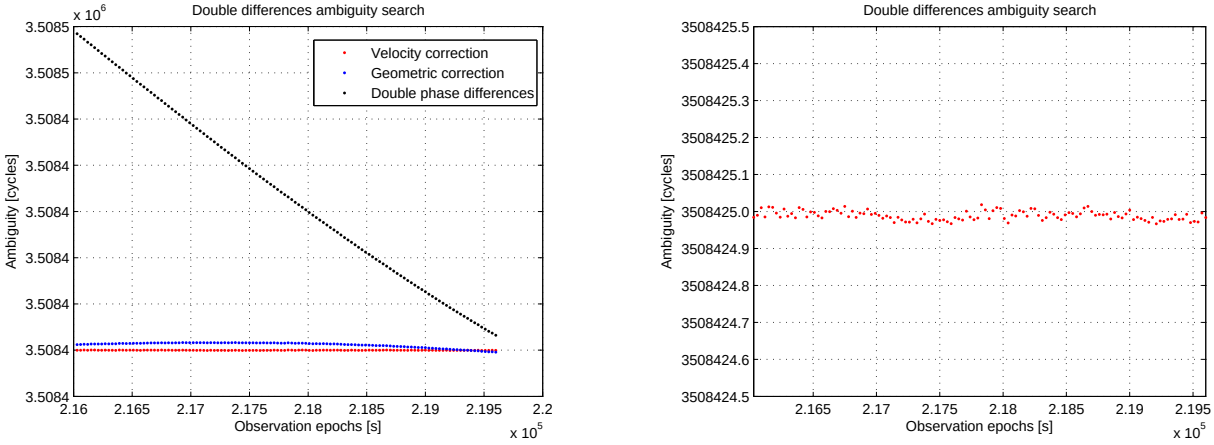

(a) Real ambiguities research. (b) Real ambiguities around integer 3508425.

Figure 2.7. Double differences ambiguities analysis for GPS receivers A and B and GPS satellites 13 and 4.

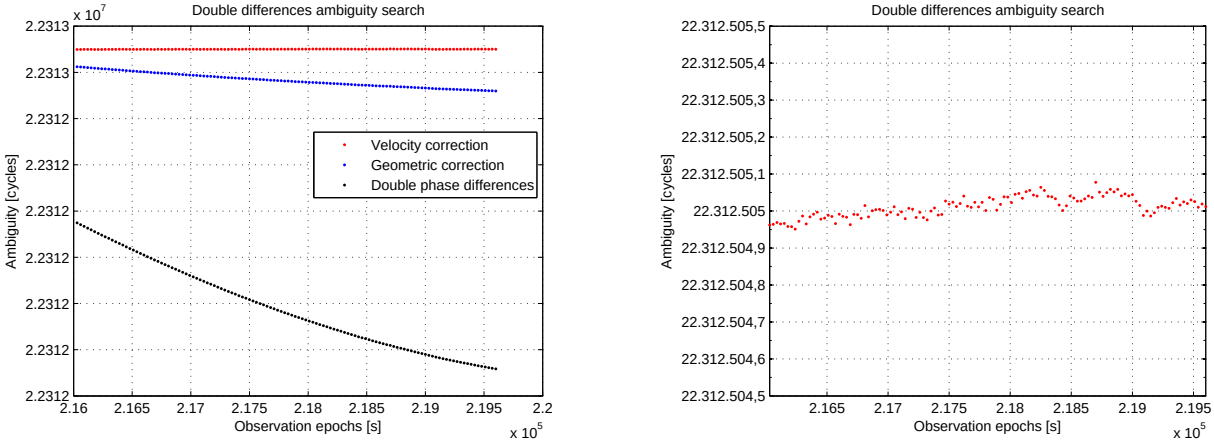

(a) Real ambiguities research. (b) Real ambiguities around integer 22312505.

Figure 2.8. Double differences ambiguities analysis for GPS receivers A and B and GPS satellites 13 and 20.

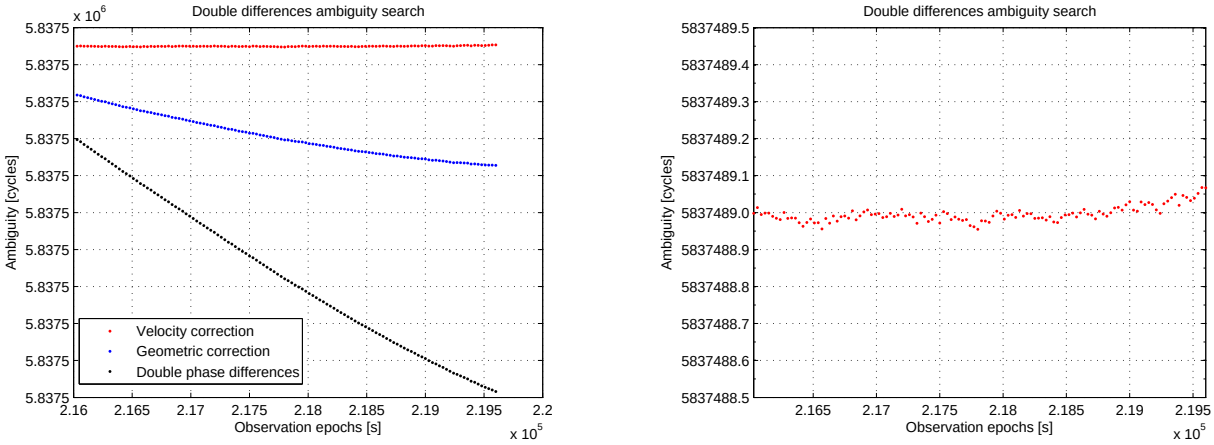

(a) Real ambiguities research. (b) Real ambiguities around integer 5837489.

Figure 2.9. Double differences ambiguities analysis for GPS receivers A and B and GPS satellites 13 and 23.

The double differences obtained with this second method can be combined with the ionospheric free

combination obtaining

$$B^{pq}_{AB,L_3,\varphi} = \left(f_1 N^{pq}_{AB,L_1,\varphi} - f_2 N^{pq}_{AB,L_2,\varphi} \right) \frac{f_1}{f_1^2 - f_2^2}. \tag{2.6.30}$$

The comparison between $B^{pq}_{km,L_3,\varphi}$ and $B^{pq}_{AB,L_3,\varphi}$ is shown in Figure 2.10, where $B^{pq}_{km,L_3,\varphi}$ is indicated as "integer ambiguity combination" and $B^{pq}_{AB,L_3,\varphi}$ as "GC-VC-TC". Both of them are compare with the ambiguity obtained subtracting the ionospheric free double difference code combination P_3 to the ionospheric free double difference phase combination L_3. The improvement is clearly visible.

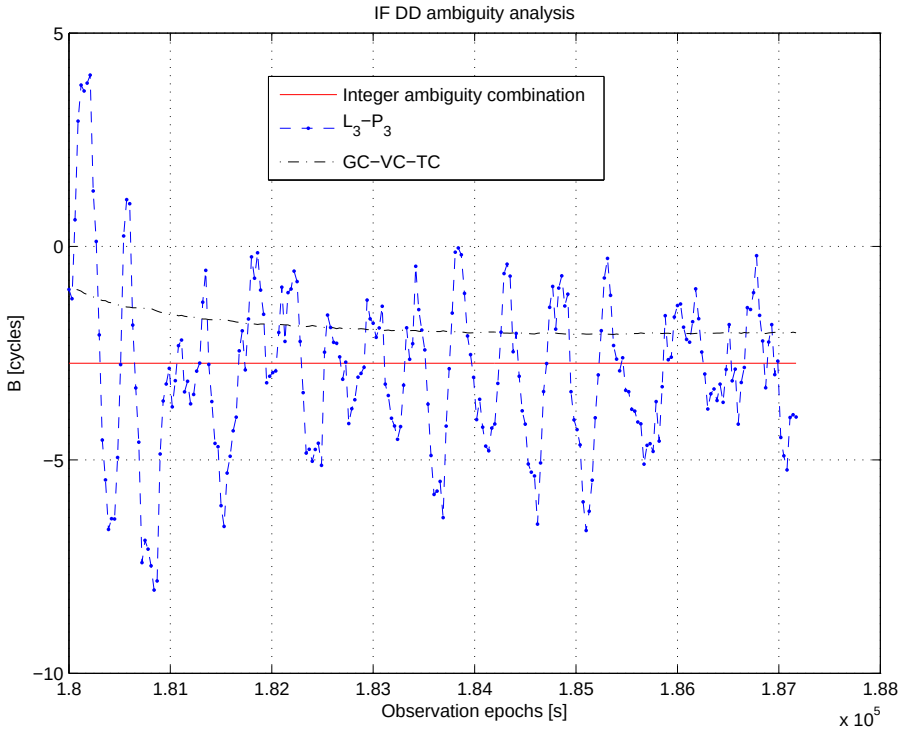

Figure 2.10. Double differences ionospheric free ambiguities comparison for GPS receivers A and B and GPS satellites 13 and 27.

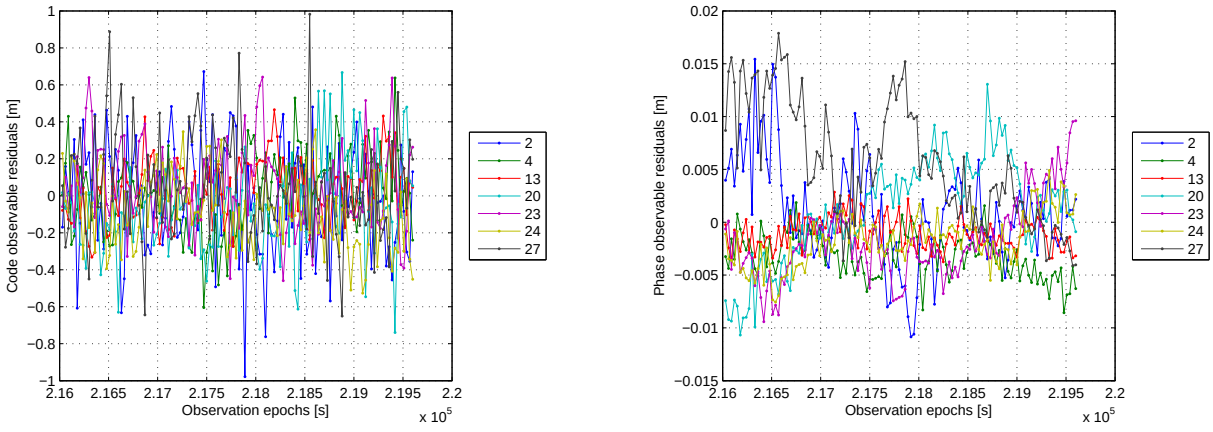

(a) Residuals of code observable.

(b) Residuals of phase observable.

Figure 2.11. Residuals for code and phase observables.

The residuals obtained using the $B^{pq}_{km,L_3,\varphi}$ ambiguities and estimating the tropospheric delay and the receivers clock error with a least square analysis (here not reported) are shown in Figure 2.11. As we can see in Figure 2.11(a) the code observable residuals are within a range of $\pm$ 1 [m], while Figure 2.11(b) shows that the phase observable residuals are within a range of $\pm$ 0.02 [m].

Chapter 3

Software Engineering

3.1. Introduction

This chapter is devoted to the definition of the architectural design of the software package SWOrD developed within the ASI project ROSA ROSSA.

SWOrD is a software code for Earth Observation satellite mission providing multi-satellite orbits determination and prediction, parameter estimation capability, RO events determination and prediction, phase excess computing during RO events.

The main characteristics of SWOrD are dictated by the high accuracy with which the relative velocity between the two occulting S/C must be known and the low latency between the time tag of the last RO observation and the time of assimilation of RO processing products into a numerical weather prediction (NWP) code. SWOrD is developed according to an object-oriented, database-driven, multi-language approach that will enhance flexibility, portability, extensibility of the software system. These characteristics define a product that will be amenable to applications with similar requirements in other Earth satellite missions of interest. SWOrD's main functionalities are Earth satellite orbit determination of LEO S/C using GPS data from both G/S's and a GNSS receiver onboard the low-Earth orbiting satellite, Earth satellite orbit prediction on the basis of the previously determined orbit elements and dynamical and space environment characterization, generation, storage and display of products and quality indices resulting from the orbit determination and orbit prediction tasks, transformation of RO observational data from level 1a to level 2. SWOrD functions as an integrated part in a complete ground segment processing center, supporting the necessary interfaces to obtain observational and ancillary information necessary to start and carry out its main functionalities, and to provide its products.

3.2. System Context

SWOrD operates in the context of the ROSA ROSSA Data Processing Center (DPC). This is shown in Figure 3.1, where it appears that SWOrD only interfaces directly with the DPC as one of a series of ROSA ROSSA Data Generators (DG) which act sequentially and are disciplined by the DPC itself. One of the requirements for the full processing chain is that each data generator, including SWOrD, will operate with minimal operator intervention. In this context, SWOrD operates with a high degree of autonomy, essentially keeping its configuration parameters in the steering file frozen. The observational data and the ancillary data necessary for the operation of SWOrD are managed and made available by the DPC.

The SWOrD structure for input files is reproduced in Figure 3.2.

The STATICDATASUPP directory contains files that don't change from a SWOrD run to the next and don't generally need to be updated. These files only need to be uploaded to the STATICDATASUPP directory once (see Table 3.1).

The directory WD_YYYYMMDD_HHMM contains the daily complement of observational and support data. The POD and RO RINEX files are in folder DATAIN. The SEMISTATIC directory contains

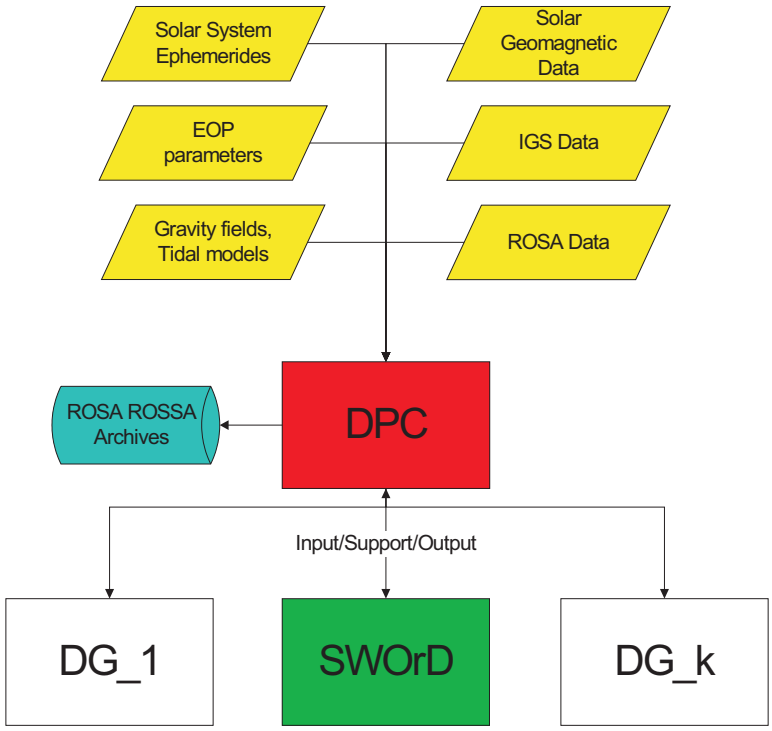

Figure 3.1. SWOrD context diagram.

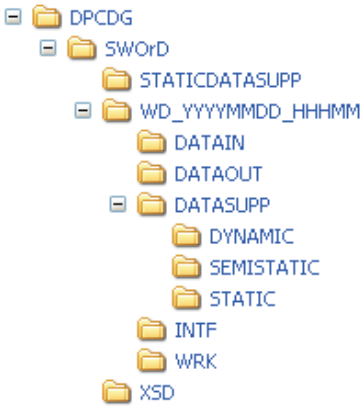

Figure 3.2. SWOrD data structure.

Description	File name	Data Source
JPL Planetary Ephemerides	de405	JPL (NASA)
JGM3 Gravity Field Model	jgm3.dat	CDDIS (GSFC NASA)
EMG96 Gravity Field Model	emg96.dat	CSR (UT Austin)
EG4 Gravity Field Model	teg4.dat	CSR (UT Austin)
Station Solutions	stats_YYYY.snx	IGS
GPS satellites attitude and physical description parameters	GPS_SV_properties.dat	CISAS

Table 3.1. SWOrD static support data.

files that need to be periodically updated maintaining data already present and integrating them with newly available data (see Table 3.2).

Description	File name	Data Source
Earth Orientation Parameters and Leap Seconds from IERS Bulletins	eop_YYYY.dat	IERS, USNO
Solar Activity and Geomagnetic Activity Indexes from National Geophysical Data Center	saga_YYYY.dat	NGDC
Receiver antenna information from IGS	igs.snx	IGS

Table 3.2. SWOrD semistatic support data.

The DYNAMIC directory contains files that change at every run because they contain a large amount of data that are not maintained locally (see Table 3.3).

Description	File name	Data Source
IGS Rapid and Final GPS products of day DDD and (DDD-1)	igrwwwwd.sp3, igswwww.sp3	IGS
IGS Rapid and Final GPS and stations clock solutions of day DDD and (DDD-1)	igrwwwwd.clk, igswwww.clk	IGS
24h ROSA attitude data of day DDD and (DDD-1)	ocns_IT_ET.att	ISRO
OCEANSAT-2 SWOrD-determined and predicted orbit in the Celestial and Terrestrial Coordinate Systems generated in the previous day solution (IT and ET here refer to the time interval covered by the previous day solution, which means the orbits determined for day (DDD-1) and the orbits predicted for day DDD.)	RSA_POD_1B_A_VB_OS2_CCS_IT_ET.sp3 RSA_POD_1B_B_VB_OS2_CTS_IT_ET.sp3	DPC

Table 3.3. SWOrD dynamic support data.

The GPS clock corrections are provided by the IGS together with GPS satellites but only with a sampling rate of five minutes. JPL provides 30-second clock corrections to the IGS (since May 1999), but many epochs are missing. For Kinematic procedure it is necessary to have clock information for the GPS satellites for each epoch the GPS satellites are observed.

3.3. SWOrD Architectural Design

The SWOrD logical model shown in Figure 3.3. This provides the reference scheme for the data-structure implementation, which is based on two main kinds of operational blocks: *interface classes* and *application classes*. A driver receives the start command from execution control, after which it commands several application classes. The first called application class triggers the reading interface classes to acquire the input data. During this process the input data are also filtered to obtain a complete set of information that will be later used by the other application classes.

The architectural design of this software, shown in Figure 3.4, is based on simple concepts, the main of which is that all data are processed while being constantly kept in RAM. I/O operations are thus limited to initial data input and final data output. Another characteristic of SWOrD is that all quantities that can be computed only once during processing are not recomputed at each iteration. This includes all dynamical and kinematical quantities that depend on the observation time tag directly, not through the position of bodies or parameters being estimated. A third feature of

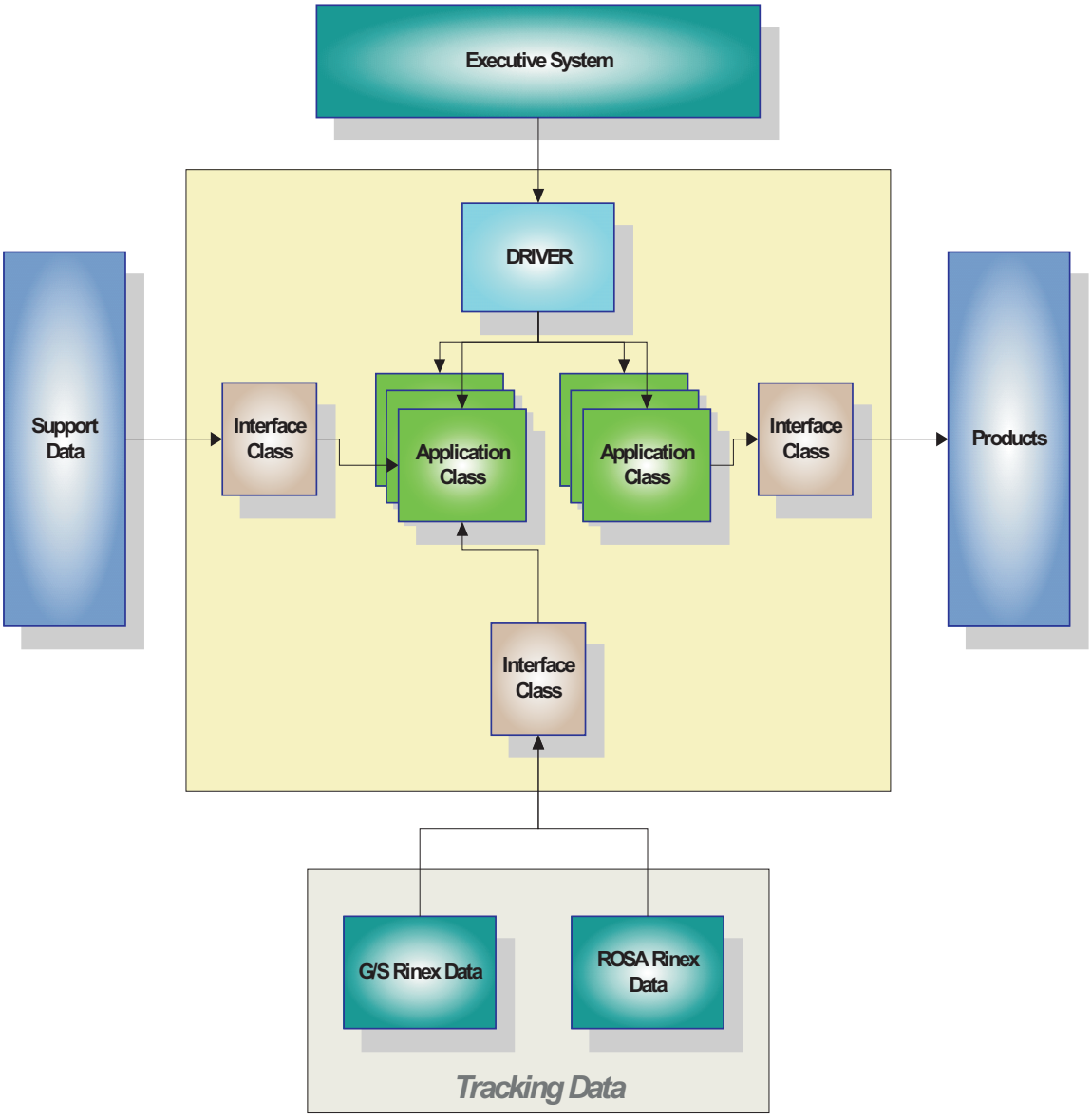

Figure 3.3. SWOrD logical decomposition.

SWOrD is that the observational and support data are inserted into database structures that are designed to allow fast identification and access through the use of multiply indexed relational tables via the *Boost Multi-Index C++ library* [13], which enables the construction of containers maintaining one or more indices with different sorting and access semantics.

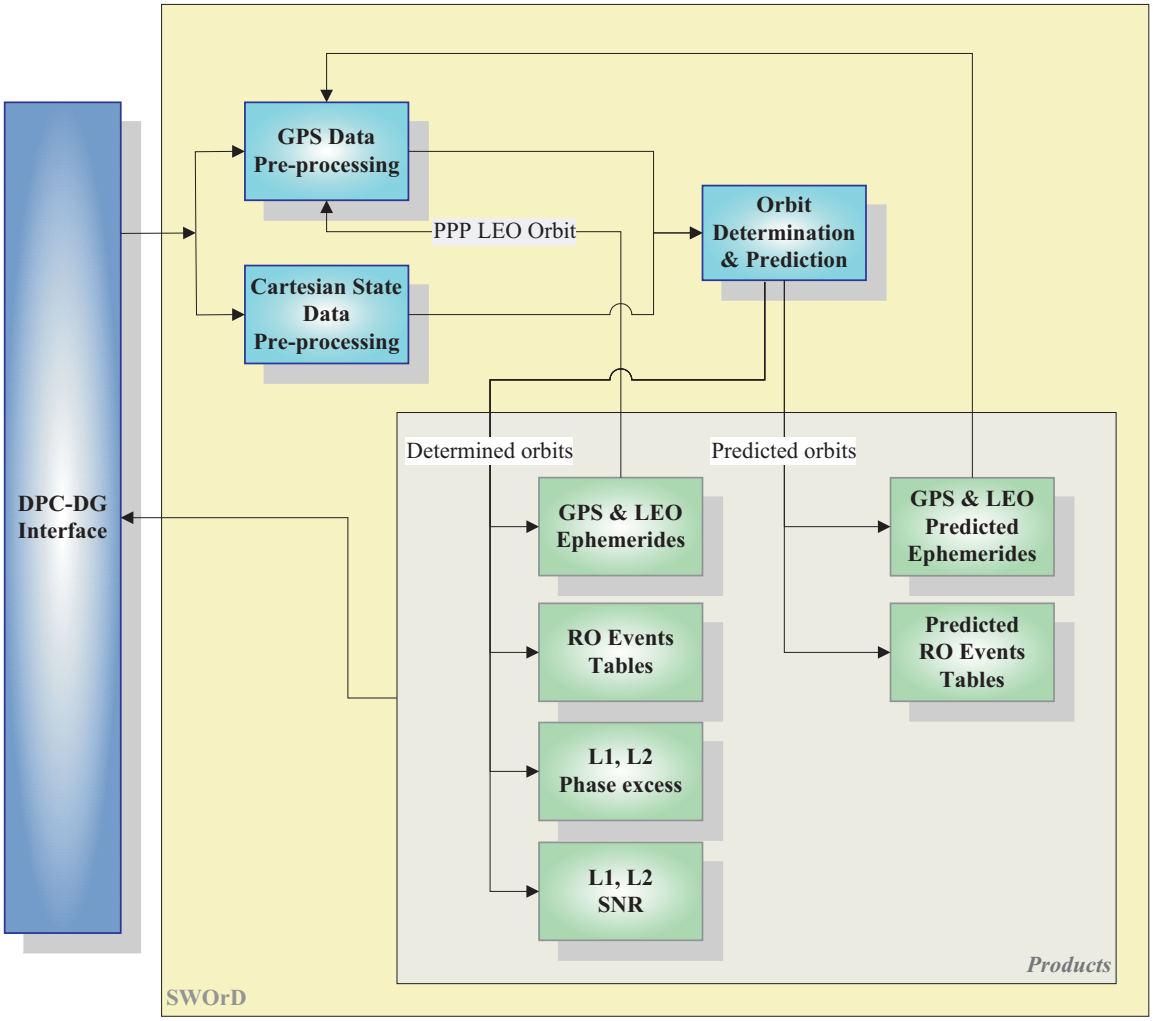

Figure 3.4. SWOrD functional architecture.

The input data to SWOrD are managed through XML files validated with *W3C XML schemas* (XSD) [94]. The XML reader classes are automatically generated from the schema by the *Code Synthesis* utility [24] and directly populate interface classes. Preliminary data validation and configuration are performed at this time by the XML reader classes as well.

SWOrD makes use of interoperability between C++ and Fortran in order to take advantage of the numerical computation performance of the Fortran language and allow the use of legacy software modules.

SWOrD includes the open-source GPSTk Core Library [39, 40] to take advance of several implemented feature, i.e. the RINEX and SP3 file reading and the DayTime object for time instant representation. SWOrD source code is also documented in the format suitable for the documentation generator tool *Doxygen* [29].

In the following paragraphs each of these characteristics will be examined.

3.3.1. Object Oriented Programming and Design Pattern

The OOP paradigm[1] has been chosen to resolve many frequent problems related to the description of properties of time, position and other entities through the utilization of the OOP mechanisms such as *inheritance*, *overloading*[2], *polymorphism*, *inlining*, *const-correctness*, *virtual classes* and *templates*[3]. The only OOP property not suited is the dynamic polymorphism (virtual class constructors), since the run time function call and dependencies resolution is time consuming while all the software developing is oriented through the *near run time* execution. Instead, templates and polymorphism has been widely used to resolve dependencies and function call resolutions at compile time. Inlining, template and polymorphism may increase the compiling time and the executable file size, but nowadays compilers implement solutions such as parallel compilation and inlining decision that greatly resolve these problems.

3.3.2. Multi-Language Interoperability

The main problem connected with interoperability concerns the correct data exchange between the languages involved. In practice, this data exchange consists in providing the correct addressing of a shared memory space. This right interpretation is strictly connected with the compilers utilized (in the present case the Fortran and C++ Linux Intel compilers).

The compiler manual asserts that Fortran programming mixed with C/C++ using Intel compilers is quite simple, because each language implements functions, subroutines and procedures quite at the same manner. The points that need special attention are reported in the following Intel manual[4] excerpt.

- Fortran and C implement functions and routines differently. For example, a C main program could call an external void function, which is actually implemented as a Fortran subroutine:

Language	Call with Return Value	Call with No Return Value
Fortran	FUNCTION	SUBROUTINE
C and C++	function	(void)function

- Generally, Fortran/C programs are mixed to allow one to use existing code written in the other language. Either Fortran or C can call the other, so the main routine can be in either language. On Linux and Mac OS X systems, if Fortran is not the main routine, the -nofor-main compiler option must be specified on the command line.

- To use the same Microsoft* visual development environment for multiple languages, you must have the same version of the visual development environment for your languages.

[1] Object Oriented Programming (OOP) is a programming paradigm that uses data structures consisting of data members and methods (the so called *objects*) and their interactions to design applications and computer programs. Programming techniques may include features such as information hiding, data abstraction, encapsulation, modularity, polymorphism, and inheritance. It was not commonly used in mainstream software application development until the early 1990s.

[2] The *overloading* is a C++ mechanism that permits to recognize and to select the right function at *compile time*. In this case, the hidden pointer *this*, introduced by the compiler, differentiates the function arguments during the *early binding*. Early binding (also called static binding) means the compiler is able to directly associate the identifier name (such as a function or variable name) with a machine address. All functions have a unique machine address, so when the compiler encounters a function call, it replaces the function call with a machine language instruction that tells the CPU to jump to the address of the function.

[3] C++ templates allow to implement a generic YourClass<T> template that has a type parameter T. T can be replaced with actual types, for example, YourClass<YourParam>, and C++ will generate the class YourClass<YourParam>. Once any changes are implemented in the template YourClass<T>, they are immediately reflected in all the classes of type YourClass<YourParam>. Templates are very useful when implementing generic constructs like vectors, stacks, lists, queues which can be used with any arbitrary type. C++ templates provide a way to re-use source code as opposed to inheritance and composition which provide a way to re-use object code. C++ provides two kinds of templates: class templates and function templates. Use function templates to write generic functions that can be used with arbitrary types. The Standard Template Library generic algorithms have been implemented as function templates, and the containers have been implemented as class templates.

[4] Original Intel compiler manual available at [50]

- Fortran adds an underscore to external names; C does not. This implies that to call from C the fortran function *my_function*, it must be invoked calling *my_function_()*.
- Fortran adds to the functions contained in a module the module name itself with the keyword *_mp_* between the function and the module names. This implies that to call from C the fortran function *my_function* contained in the module *module_name*, it must be invoked calling *module_name_mp_my_function_()*.
- Fortran changes the case of external names to lowercase; C leaves them in their original case.
- Fortran passes numeric data only by reference; C passes by value, reference and pointer.
- Fortran subroutines are equivalent to C void routines.
- Fortran requires that the length of strings be passed; C is able to calculate the length based on the presence of a trailing null. Therefore, if Fortran is passing a string to a C routine, that string needs to be terminated by a null; for example: "mystring"c or StringVar // CHAR(0).
- For the following data types, Fortran adds a hidden first argument to contain function return values: COMPLEX, REAL*16, and CHARACTER.
- On Linux* systems, the -fexceptions option enables C++ exception handling table generation, preventing Fortran routines in mixed-language applications from interfering with exception handling between C++ routines.

Once checked that the conventions about the function calls are correct, it is necessary to pay attention to the equivalence of the interpretation of Fortran and C++ data types.

Numerical Types

Table 3.4 reports the correspondence of the principal logical and numerical types between Fortran and C++.

Fortran	C
INTEGER(1)	char
INTEGER(2)	short
INTEGER(4)	int, long
INTEGER(8)	_int64
REAL(4)	float
REAL(8)	double
REAL(16)	–
CHARACTER(1)	unsigned char
COMPLEX(4)	struct complex4 { float real, imag; };
COMPLEX(8)	struct complex8 { double real, imag; };
COMPLEX(16)	–
All logical types	integer type for C

Table 3.4. Correspondence of the principal numerical types between C++ and Fortran. Extract from the Fortran compiler manual.

Pointer Types

In the Intel Fortran compiler pointers are equal to C pointers.

Array Types

It is very important to consider the differences in the indexing and memorization of the array elements between C++ and Fortran:

1. the lower bound value is different: on default, Fortran considers the first element index 1, while C and C++ 0 (it is possible to alter the Fortran behavior, setting a different lower index, but this is preferable to avoid);

2. in the arrays of two or more dimension, Fortran increments faster the most rleft index (column–major order), while C++ increment the most right one (row–major order).

Language	Array declaration	Fortran reference
Fortran	type x(i,k)	x(i,k)
C/C++	type x[k][i]	x(i-1,k-1)

User defined types

In C++ it is possible for the user to define structures through the key word struct. The passage of this data kind is immediate, after indications about the structure in question have been given.

An example is the following Fortran common block:

```
subroutine mysubr(a);
integer a
integer b(20), c(10)
common /mycommon/ b, c
...
end
```

accessed by C++ in this manner:

```
typedef struct{
    int b[20];
    int c[10];
} common_area;

int main() {
    int a;
    extern common_area mycommon_;
    ...
    mycommon_.b[3] = 10;
    ...
}
```

Usage of the STL class vector

Using the class vector, implemented in the C++ Standard Template Library, it is possible to transfer the data contained in the class instance by passing the address of the first element. This is because *vector* grants the data memory contiguity.

3.3.3. In-core Database-Driven Technology

The SWOrD data container—the core of the software system—consists of a series of singleton classes that implement an in-core database with multiple search indices that allow fast (*hashing table*) and ordered data access. This database is implemented by using the Boost Multi-index library.[5] The

[5]For further information see the URL: http://www.boost.org/doc/libs/1_39_0/libs/multi_index/doc/index.html

Figure 3.5. SWOrD in-core database UML class diagram.

Boost Multi-index Containers Library[6] provides a class template named *multi_index_container* which enables the construction of containers maintaining one or more indices with different sorting and access semantics. User-defined multiple iterators (one for each indexing typology defined) permit to access data and to scroll through them contiguously. Here follows a description of the principal classes composing the database and theirs iterators.

Antenna_Model It contains information about all the properties of an antenna placed on a satellite or a ground station. The Antenna_Model permits to store the information about the corrections to act respect to the station marker or the satellite mass center for each frequency of transmission or reception.

Iterators:

- Hashed unique by
  - frequency band
  - frequency value

Clock_Parameters It contains all clock offset, drift, aging and the complessive error for each satellite or ground station at each time instant.

Iterators:

- Ordered non unique by
  - parameter instant
- Ordered unique by
  - composite key
    - measurement device
    - parameter instant

Double_Differences It contains all GPS observable double differences computed from the input observations.

Iterators:

- Hashed unique by
  - composite key
    - tx1 rx1 observation
    - tx1 rx2 observation
    - tx2 rx2 observation
    - tx2 rx1 observation
- Ordered unique by
  - composite key
    - rx1 pointer
    - rx2 pointer
    - tx1 pointer
    - tx2 pointer

[6]The concept of multi-indexing over the same collection of elements is borrowed from relational database terminology and allows for the specification of complex data structures in the spirit of multiply indexed relational tables where simple sets and maps are not enough. A wide selection of indices is provided, modeled after analogous STL containers like *std::set*, *std::list* and hashed sets. Boost::MultiIndex features additional functionalities, like subobject searching, range querying and in-place updating of elements, which make it a convenient replacement for *std::set* and *set::multiset* even when no multi-indexing capabilities are needed. Indices provide interfaces similar to those of STL containers, making using them familiar.

        * observation time instant
    - Hashed unique by
        - composite key
            * first receiver pointer
            * second receiver pointer
            * first transmitter pointer
            * second transmitter pointer
            * observation time instant

Double_Difference_Arcs It contains all arc parameters of the computed double difference arcs obtained from the double differences formation.

Iterators:

- Ordered unique by
    - composite key
        * arc start time instant
        * first receiver pointer
        * second receiver pointer
        * first transmitter pointer
        * second transmitter pointer
- Ordered non unique by
    - arc time length

Eccentricities It contains all the antenna eccentricity vectors for phase center wrt mass center correction.

Iterators:

- Ordered unique by
    - eccentricities time interval

EOPs It contains input EOP and time scales differences and it provide values required at a given epoch by interpolation.

Iterators:

- Hashed unique by
    - MJD

Ground_Station_Networks It contains ground stations positions and velocity at a given epoch and provides the values of a required ground station and epoch.

Iterators:

- Hashed non unique by
    - name code
- Hashed unique by
    - composite key
        * name code
        * marker start time interval
- Ordered unique by
    - composite key

        * name code
        * marker start time interval

Ground_Stations It contains all information about ground stations provided by steering and SINEX files.

Iterators:

- Hashed unique by
  - name code
- Hashed non unique by
  - found SINEX
- Hashed non unique by
  - found clk file

Observations It contains all GPS observations read from RINEX files.

Iterators:

- Ordered unique
  - composite key
    * observation time instant
    * receiver pointer
    * transmitter pointer
- Ordered unique
  - composite key
    * receiver pointer
    * transmitter pointer
    * observation time instant
- Ordered unique
  - composite key
    * transmitter pointer
    * observation time instant
    * receiver pointer

Offsets It contains all the antenna offset vectors for phase center wrt mass center correction.

Iterators:

- Ordered unique by
  - offsets time interval

Satellite_Constellations It contains satellite orbits read from the IGS SP3 or the orbit reference files and provides required satellite position and velocity at a given epoch.

Iterators:

- Ordered non unique by
  - state time instant
- Ordered unique by
  - composite key
    * constellation type

        * satellite ID
        * state time instant
    - Hashed unique by
      - composite key
        * state time instant
        * satellite ID
        * constellation type

Satellites It contains all input information about satellites provided by steering, SP3 and clock files.

Iterators:

- Hashed unique by
  - composite key
    * satellite ID
    * constellation type
- Ordered unique by
  - composite key
    * constellation type
    * satellite ID
- Hashed non unique by
  - constellation type
- Hashed non unique by
  - composite key
    * found clk file
    * constellation type

Zero_Difference_Arcs It contains all arc parameters of detected arcs obtained from the read observation.

Iterators:

- Ordered unique by
  - composite key
    * receiver pointer
    * arc start time instant
    * transmitter pointer
- Ordered unique by
  - composite key
    * transmitter pointer
    * arc start time instant
    * receiver pointer

3.3.4. XML Schema Data Binding

The steering settings and the input/output files specifications (environment information) are provided to SWOrD by means of XML input files, so that SWOrD takes advantage of XML data encoding and its XML schema[7] (XSD) validation to automate both steering input correctness verification and

[7] An XML Schema describes the structure of an XML document. The XML Schema language is also referred to as XML Schema Definition (XSD). The purpose of an XML Schema is to define the legal building blocks of an XML document and, above all, XML Schemas are written in XML.

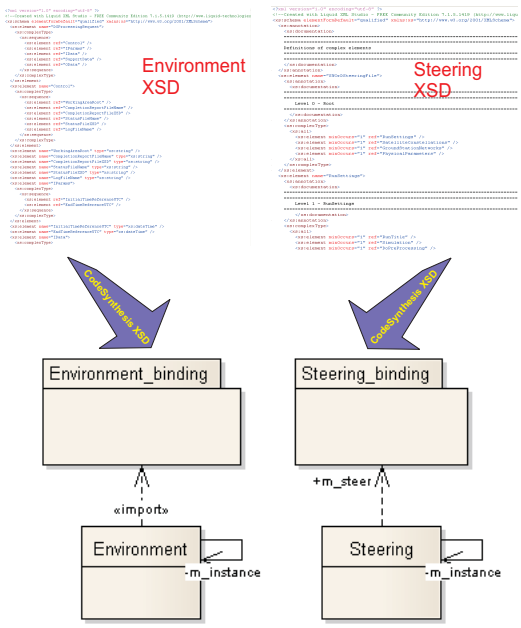

Figure 3.6. XML schema data binding.

interface class source code generation through data binding[8] from XSD. Data binding is realized by using the utility CodeSynthesis XSD, an open-source, cross-platform W3C XML Schema to C++ data binding compiler. Provided with an XML instance specification (XML Schema), it generates C++ classes that represent the given vocabulary as well as parsing and serialization code. It is then possible to access the data stored in XML using types and functions that semantically correspond to the application domain rather than dealing with the intricacies of reading and writing XML.

The advantages of this feature are enormous, mainly during the initial development phase, when changes to input steering parameters are very frequent. In fact, changes to the respective C++ classes at every change of the steering or environment XSD file became automatic. It is also very easy to access to XML data from the other software classes, since types and functions semantically correspond to the application domain.

Classes generated both for the steering and the environment files are collected by two singleton classes that easily permit XML data access all over other SWOrD classes (see Figure 3.6).

3.4. SWOrD Decomposition Description

3.4.1. Functional Decomposition

From a functional point of view SWOrD can be decomposed into three elements,

- the *data pre-processor*,
- the *orbit estimator*,
- the *excess phase generator*.

The excess pase generator will be discussed in detail in section 5, while the data pre-processor and the orbit estimator will be described here following.

[8] XML data binding refers to the process of representing the information in an XML document as an object in computer memory. This allows applications to access the data in the XML from the object rather than using the DOM or SAX to retrieve the data from a direct representation of the XML itself. An XML data binder accomplishes this by automatically creating a mapping between elements of the XML schema of the document we wish to bind and members of a class to be represented in memory. When this process is applied to convert a XML document to an object, it is called *unmarshalling*. The reverse process, to serialize an object as XML, is called *marshalling*.

Data pre-processor

The data pre-processor is responsible, besides the collection of the input data described in section 3.2 (all data are read and inserted into the in-core database, where all references and connections are automatically nested), for the handling and correction of the GNSS measurement, such as

- cycle slips detection,
- ambiguity estimation,
- time tag correction
- undifferentiated arc formation,
- double difference observation computation,
- double difference arc determination,
- tropospheric delay formulation,
- transmitter and receiver attitude correction,
- range rate influence on the receiver clock error correction.

A very simple scheme of the functioning of this component is shown in Figure 3.7.

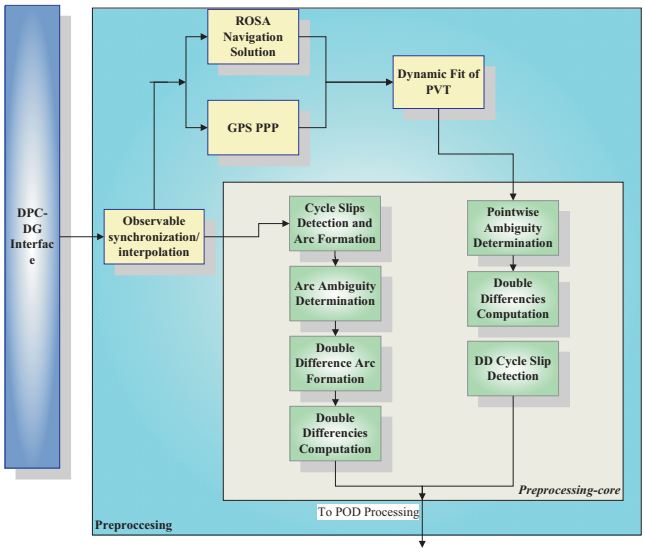

Figure 3.7. Data pre-processor functioning scheme.

Orbit estimator

The orbit estimator is fundamentally the batch filter that applies fit the force model to the pre-processed observation. Its functional scheme is shown in Figure 3.8. For further information see section 4.6.1.

3.4.2. Software decomposition

Figure 3.9 offers a general views of SWOrDclass relationships. In the following each functional package will be described.

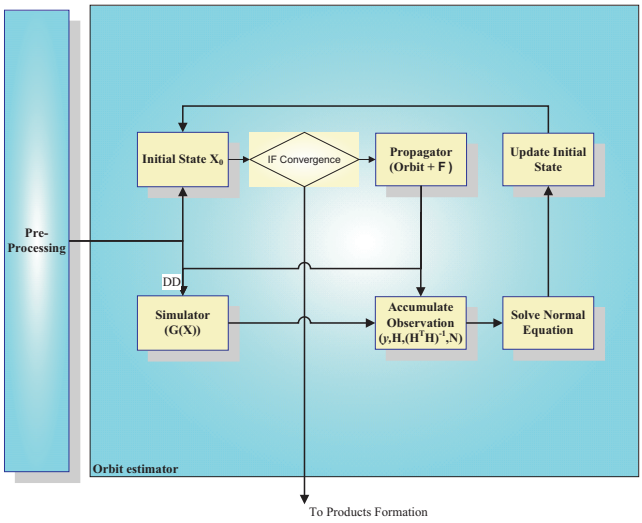

Figure 3.8. Orbit estimator functional scheme.

Time Scale and Format Conversion

The class responsible for time management is *Time_Tag* and is designed to implement time scales conversions as described in Appendix B.

The *Time_Tag* class contains a pointer to the *EOPs* class (i.e., there is an association[9] relation between them), which is responsible for storing and providing the EOPs and the time scale conversion parameters. The *EOPs* class is implemented using the singleton pattern[10] to permit a single instance and a global access to EOPs parameters in input (see the relationships in the UML class diagrams[11] Figure 3.10). *Time_Tag* objects are used extensively throughout the SWOrD classes after the the EOPs input file has been read. The *Time_Tag* class uses three *DayTime* objects, from the GPSTk library, to implement each of the TT, UTC and UT1 time scales. There are also public methods that provide TAI and GPS times starting from the memorized time scales (see Figure 3.11 to visualize the conversions between the time scales implemented by the *Time_Tag* class). Several operators are provided to permit basic arithmetic operations between *Time_Tag* objects and with C++ base data type.

[9] It is called *association* when two classes are conceptually connected each other.

[10] In software engineering, a *design pattern* is a general reusable solution to a commonly occurring problem in software design. A design pattern is not a finished design that can be transformed directly into code. It is a description or template for how to solve a problem that can be used in many different situations. Object-oriented design patterns typically show relationships and interactions between classes or objects, without specifying the final application classes or objects that are involved. The *singleton pattern* is a design pattern that is used to restrict instantiation of a class to one object. This is useful when exactly one object is needed to coordinate actions across the system. Implementation of a singleton pattern must satisfy the single instance and global access principles. It requires a mechanism to access the singleton class member without creating a class object and a mechanism to persist the value of class members among class objects. The singleton pattern is implemented by creating a class with a method that creates a new instance of the class if one does not exist. If an instance already exists, it simply returns a reference to that object. To make sure that the object cannot be instantiated in any other way, the constructor is made protected (not private), because reuse and unit test may need to access the constructor. Note the distinction between a simple static instance of a class and a singleton: although a singleton can be implemented as a static instance, it can also be lazily constructed, requiring no memory or resources until needed. Another notable difference is that static member classes cannot implement an interface, unless that interface is simply a marker. So if the class has to realize a contract expressed by an interface, it really has to be a singleton.

[11] In software engineering, a *class diagram* in the Unified Modeling Language (UML), is a type of static structure diagram that describes the structure of a system by showing the system's classes, their attributes, and the relationships between the classes.

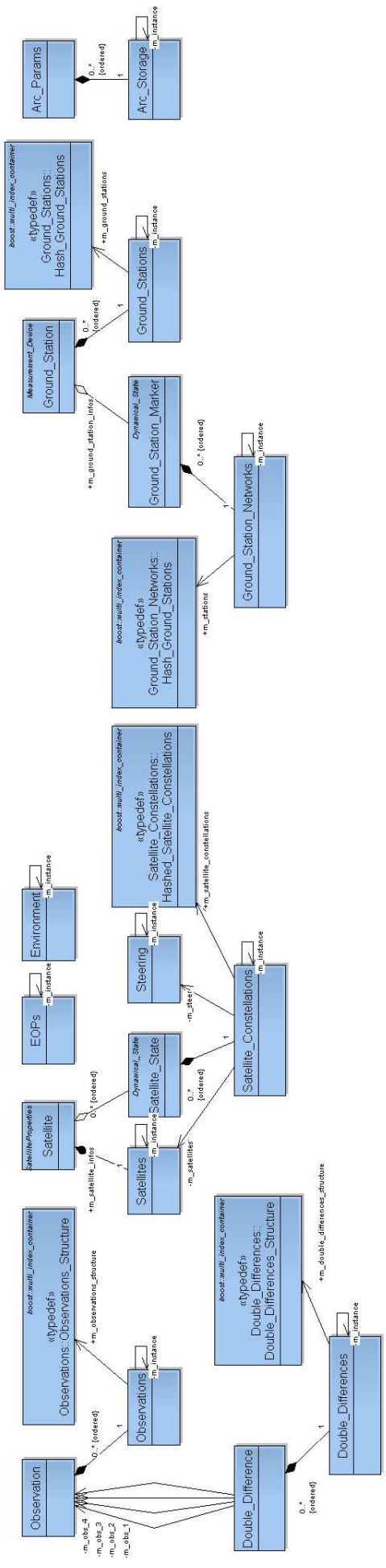

Figure 3.9. SWOrD in-core database UML class diagram.

Figure 3.10. *Time_Tag* class relations.

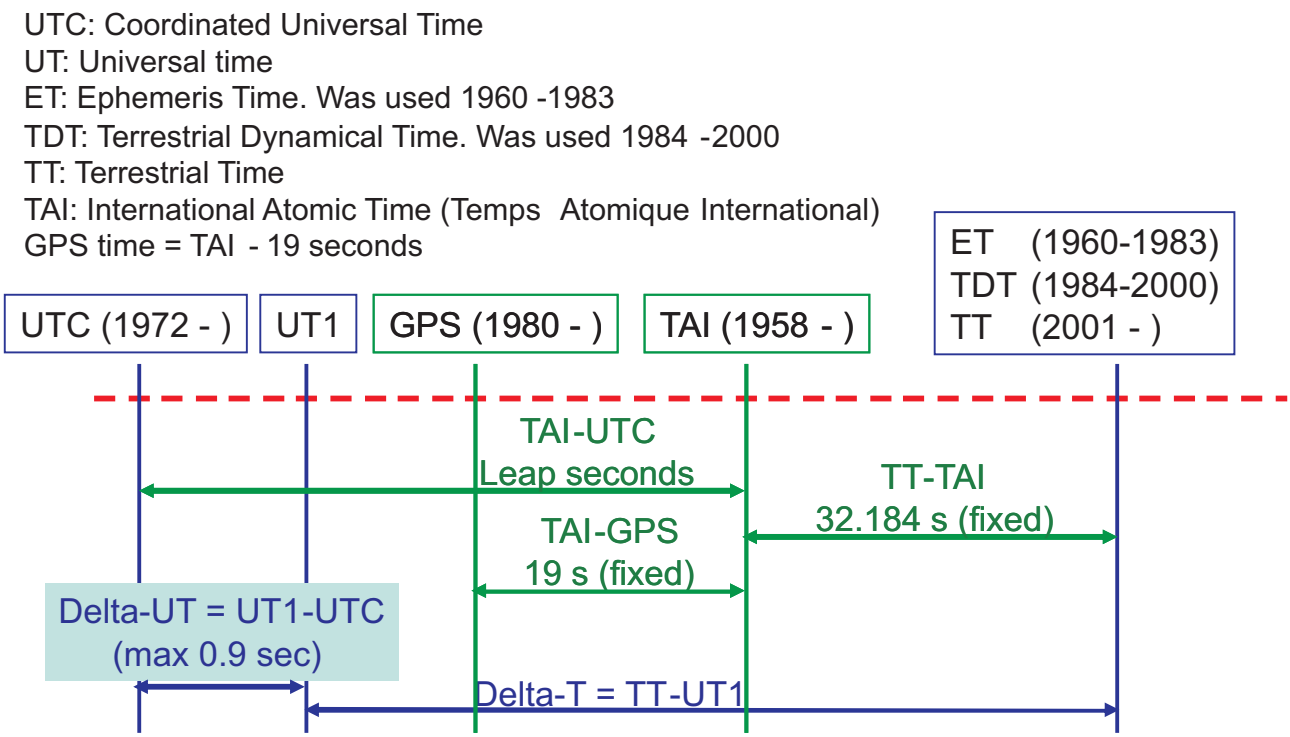

Figure 3.11. Conversions between time scales implemented by the *Time_Tag* class.

The *Clock_Time_Tag* class inherits the *Time_Tag* class to implement the *receiver time scale*. In this way, a time instant is suitable in all the time scales implemented by the *Time_Tag* class and also in the receiver time scale. The receiver time scale can be set starting from the GPS time scale, or the GPS time can be set from the receiver time (and then from GPS time all ather scales), if the clock error of the device that has produced the time tag is known. For this reason the *Clock_Time_Tag* has a pointer to the singleton storage for the clock errors, the *Clock_Parameters* class. *Clock_Parameters* is a multi-index database for *Clock_Model* objects and it is responsible for reading the GPS satellites and IGS ground stations clock error from an IGS clock (*clk*) file. *Clock_Parameters* also stores the LEO satellite(s) clock errors, that are read from the LEO navigation solution if available or produced by a Precise Point Position algorithm together with a first kinematic LEO position estimation. The *Clock_Model* stores the phase offset, drift and aging of the clock receiver at the time tag and it is used during the estimation process to maintain the clock parameters estimated.

Coordinate System Conversion

The OOP properties of *inheritance* and *template* have been exploited to realize the class *Dynamical_State*, responsible for the coordinate system conversions, as shown in Figure 3.12

The *Dynamical_State* class maintains two instances of the *Position* and *Velocity* classes to implement a Cartesian representation of position and velocity in both the J2000 and the ITRF reference frames, with public methods to obtain their intermediate coordinate system (InertialMoD, InertialToD and PseudoECEF) and other coordinate system representations (GeographicPolar, GeographicEquatorial, GeodeticPolar and GeodeticEquatorial). The *Dynamical_State* class associates to the position and velocity quantities a *Time_Tag* object that specify also the instant of the localization.

The *Position* and *Velocity* classes inherit their properties from the template class *Generic_Pos_Vel*, that, in turn, inherits the template class *Array_Estimation_Parameter_N*, a class that implements an array of N objects, where both N and the object type are user-definable through C++ templates. The *Generic_Pos_Vel* class inherits and specializes *Array_Estimation_Parameter_N*, setting $N = 3$ and the object being of type *Estimation_Units*, another template class that encapsulates values for variables to be used in the estimation process and also verifies the correctness of the measurement unit using the class *Units* of the Boost library [14]. The class *Generic_Pos_Vel* also specifies the coordinate system and the reference frame which the array values are referred to. The classes *Position* and *Velocity*

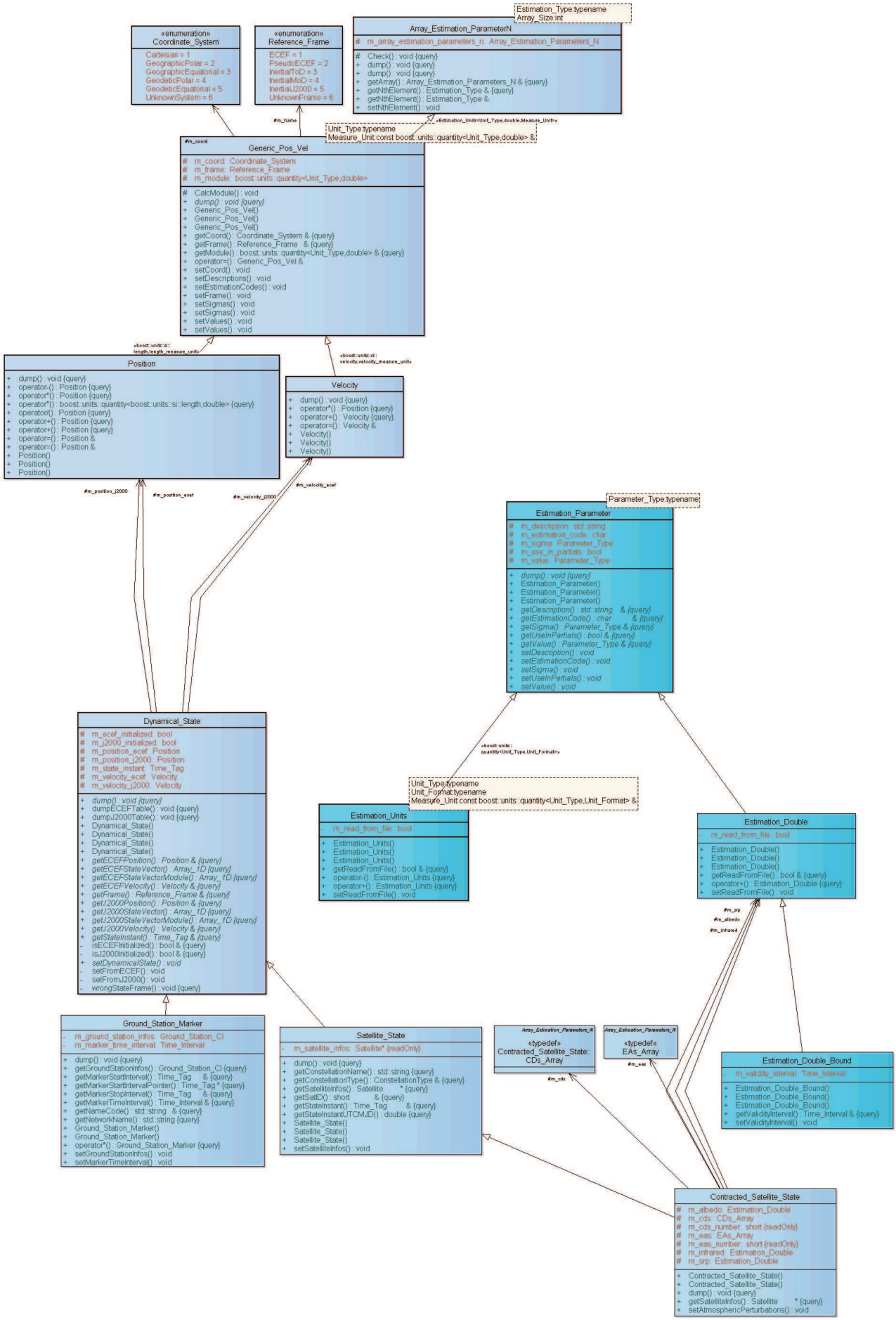

Figure 3.12. *Dinamical_State* class relations.

specialize *Generic_Pos_Vel* and specify with the template the measurement unit to be utilized. Only few class-specific operations must be specified because most of the methods, valid both for position and velocity, are already specified in *Generic_Pos_Vel* and inherited by both the classes.

The *Dynamical_State* class is inherited by the classes *Satellite_State* and *Ground_Station_Marker* that, by mean of a pointer to the *Satellite* or *Ground_Station* classes respectively, they associate to the *Dynamical_State* information a link to the properties of the satellite or ground station that have been localized.

The *Contracted_Satellite_State* class inherits the *Satellite_State* class and adds information about the solar radiation pressure coefficient, the albedo coefficient, the IR radiation coefficient, the drag coefficients and the empirical accelerations (see section 4.3 for further details).

Satellite and Ground Station Information

Information collected from input files (Steering, SP3 and Clock files) about satellites and ground stations involved in the processing are stored into two singleton classes, *Satellites* and *Ground_Stations*, which contain single *Satellite* and *Ground_Station* instances with detailed information about each single device inserted (a *strong aggregation relation* exists between *Ground_Stations* and *Ground_Station* and between *Satellites* and *Satellite*, see Figure 3.13). *Satellite* and *Ground_Station* classes inherit the same *Measurement_Device* class. This inheritance permits, when required during processing, to return a general pointer to a *Measurement_Device* object and leave to the C++ overloading to resolve whether the object is in reality a *Satellite* or a *Ground_Station* one.

The *Measurement_Device* class stores information about its antennas (offset, eccentricity, beam half amplitude) and about what kind of information has been found on input files (clock, RINEX). *Satellite* class adds information about the SV ID and its affiliation constellation, while *Ground_Station* class adds information about the Station Name Code and its affiliation ground station network.

The *Satellites* class uses the SV ID and its affiliation constellation to build the keys that permits a contemporaneous hashed and ordered indexing of inserted *Satellite* objects by means of the Boost Multi Index library (see further on). Instead, the *Ground_Station* class uses the Station Name Code to build the keys.

The *Satellite_State* and *Ground_Station_Marker* are collected by two multi-index database singleton classes, respectively the *Satellite_Constellations* and the *Ground_Station_Networks* class (see respectively Figure 3.14 and Figure 3.15). This classes read the satellite and ground station positions from IGS SP3 and SINEX data or obtain them from PPP and bach filter procedures. They also provide methods to query the position of a given satellite at any time instant belonging to the time coverage of data inserted: if the instant required is present into the database then a reference to the found state is given otherwise the state is obtained by interpolating the data present in the database using a 11th order polynomial.

Observation handling

The relations among the classes responsible for observation handling are shown in Figure 3.16.

All information about a single GNSS observation is stored into a *Observation* class. All the *Observation* object are stored into the *Observations* multi-index database class. The responsible for the observations insertion into the database is the *Observation_Insertion* class, that during the RINEX file reading and the observation insertion into the database check the observation quality, detects cycle slips and forms arc passes (see section 6.2 for further details). The quality check is based on a test over the time differences between two consecutive instant of the Melbourne-Wübbena and the geometry free combinations. If at least one of the time differences is higher than a user-fixed quantity the arc is interrupted. The arc is interrupted even if between two sequent instants of the RINEX file the satellite that is being tracked is not present anymore. When the arc is interrupted, its temporal length is checked respect to a user-defined value and it is kept if longer, discarded otherwise. The information about the arc is contained into a *Zero_Difference_Arc_Params*. All the arc objects are stored into the *Zero_Difference_Arcs* multi-index database class. After that at least one zero difference arc has been inserted into the database and every time that a new zero difference arc is inserted, the *Obser-*

Figure 3.13. *Satellites* and *Ground_Stations* classes relations.

Figure 3.14. *Satellite_Constellations* class database relations.

Figure 3.15. *Ground_Station_Networks* class database relations.

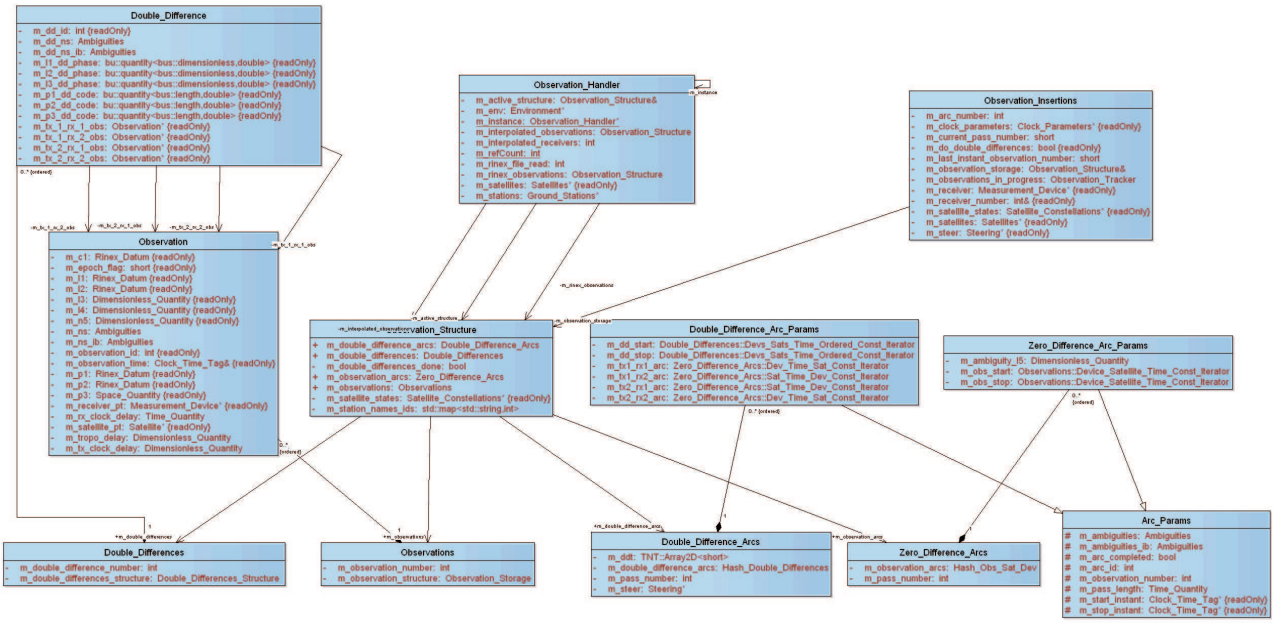

Figure 3.16. *Observations* class database relations.

vation_Insertion starts to verify if it is possible to form double differences between the observation of the arcs just inserted and those present into the database. If a double difference is formed, the it is inserted into a *Double_Difference* object and the *Observation_Insertion* starts to keep track of the double difference arc relative to the current quartine. When the arc formation is done, its information is inserted into a *Double_Difference_Arc_Params* class and, if the double difference arc length is longer than an user-defined value, the arc is inserted into the *Double_Difference_Arcs* database. Each double difference builded is stored into the *Double_Differences* multi-index database class. Every connection among these classes is realized through iterators, so that it is possible to visit both undifferenced observation and double differenced observation in a contiguous way even if it is necessary to visit the observations starting from the knowledge of the arc (see section **??** for further details).

This observation storage structure is grouped together from a *Observation_Structure* class. Since SWOrDis a software for radio occultation missions, the GNSS observation are distinguished into two observation typology: for *navigation* or for *occultation*. For each observation typology an *Observation_Structure* class is kept, that is it exists an *Observation_Structure* for navigation observation and for occultation observation. The observation structure has also the functions to interpolate or to print observations. The class responsible to chiose on which observation typology an action can be attempted is the *Observation_Handler* singleton class, which maintain and instance of an *Observation_Structure* class for each observation typology.

Chapter 4

Orbit Determination Methods

4.1. Introduction

The several *orbit determination procedures* that will be here presented are different *statistical techniques* that allow to estimate the orbital parameters of a spacecraft or a celestial body during its motion in the Solar System (here in particular specialized for the motion around the Earth). The aim of these procedures is to find a workaround that overcome the limited knowledge of the *true state* (position, velocity and several other parameters) of the considered body in the contest of a *simplified modeling* of the orbital motion. In particular, a *least squares approach* is used to minimize the differences between observations and a model of them[1], computed through a set of parameters, the *state vector* that form the dynamic and kinematic models and propagated in time through a set of differential equations (equations of motion). This requires a parametrization of the problem and depends on the physics of the problem itself. There are essentially two ways to update the state vector: if a new estimate is obtained after each observation, we talk about *sequential or recursive estimation*; if, instead, all the measurements are collected and then processed to obtain an estimate of the state vector at a specified initial epoch (batch epoch), we talk about *batch estimation*. Generally speaking, a sequential estimator (filter) is more sensitive to the quality of the individual measures than a batch filter. Besides, a sequential algorithm converges faster (if properly tuned) to the right solution than a batch algorithm. The latter may require several iterations before converging.

A statistical orbit determination process has to deal with four types of approximations:

1. measurement errors;
2. approximations in the dynamic, kinematic and observation models;
3. inaccuracies in the estimation process;
4. numerical approximations.

In order to obtain an orbit estimation as accurate as possible, there are several aspects to consider to handle each of the four approximations.

1. A sufficiently large number of observations must be collected over the time span of interest.
2. Generally, the measurements are nonlinear functions of the state vector parameters and, consequently, also the differential equations that describe the motion. This implies that multiple solutions can be found, but only one being optimal.
3. Once an optimal estimate of the orbital parameters is determined, a set of ephemerides of the satellite can be obtained by simply integrating the equations of motion by using the parameters just determined. The accuracy of the obtained ephemerides, or orbit, is strictly related to the precision and accuracy of the models and to the measurements error.

[1] The goal of the least square approach is to minimize the observation *residuals*, i.e. the difference between the true measurements and their computed values.

4. Any parameter that affects the orbital motion of the satellite can be estimated in the process of orbit estimation, not only the orbital parameters (e.g. the ground station positions, the Earth orientation parameters, the atmospheric delays and the gravity field coefficients).

The methods presented in the following can be found in [84].

4.2. Precise Orbit Determination for LEOs

The problem of orbit determination essentially consists in deriving orbital parameters from a set of observations. For an artificial satellite, in particular, this problem refers to the reduction of its tracking measurements, affected by both random and systematic errors, through an approximate analytical force model to obtain the best estimate of the orbital ephemerides describing the spacecraft motion in any time.

In most cases, the tracking system adopted to provide data for a precise orbit determination of LEO satellites is a GPS receiver. Differently from the conventional tracking systems, GPS presents numerous advantages: apart from a relative low cost implementation, it allows a three-dimensional position information from range measurements, to work in any atmospheric conditions and a continuous tracking of a LEO satellite, where a precise trajectory may be reconstructed only through elaborate orbit models.

Much work was performed in the last decade to develop and evaluate different orbit determination strategies for LEOs using GPS. The approach depends on requirements like precision, latency and availability. The orbital altitudes of the satellites range between about 300 km and 2000 km, leading to different perturbation characteristics. The orbit determination strategies may be divided into two main groups: the *kinematic strategies* and the *dynamic* and *reduced-dynamic strategies*.

Kinematic POD procedures estimate the satellite position for each observation epoch based on the GPS observations only, not needing any information concerning the gravity field and other parameters of the dynamical orbit models. The orbit solution is referenced to the phase center of the on-board GPS antenna instead of the satellite's center of mass. Kinematic solutions are more sensitive to geometrical factors, such as the direction of the GPS satellites and the GPS orbit accuracy, and they require the resolution of phase ambiguities. Nowadays, the accuracy of kinematic orbit determination may reach a few millimeters [82, Svehla & Rothacher, 2001].

On the other hand, the dynamic orbit determination requires precise models of the forces acting on the satellite. This approach implies that satellite positions are computed arc-by arc rather than point-by-point. The equations of motion are solved using the technique of numerical integration. The dynamic POD has been applied to many successful satellite missions and has become the mostly used POD approach. Dynamic model errors are the limiting factor for this technique, such as the geopotential model errors and atmospheric drag model errors.

In order to compute the satellite orbit as accurate as possible, the orbit determination process is very often a compromise between a kinematic approach and a dynamic approach, resulting in a so-called reduced-dynamic orbit determination.

The GPS data processing procedures for the LEO are common to both groups. These procedures may be distinguished by their *differencing* level namely the *zero-difference* (ZD), *double-difference* (DD) or *triple-difference* (TD) level of the original observations. All strategies make direct or indirect use of the GPS ground network, the IGS network. Direct use is made if the observations of the ground stations are used together with the LEO GPS data for the processing (DD and TD). Indirect use is made if the observations of the ground stations are not used for the LEO GPS data processing (ZD), in which case the ground based observations are required to estimate GPS clock corrections. In any case ground station data are required to compute precise GPS satellite orbits.

The different procedures for the LEO GPS data processing are illustrated by Figure **??**. All procedures require GPS orbits, Earth rotation information and LEO GPS data as input for the processing. The GPS orbits and Earth rotation parameters are taken either from the IGS (or one of its analysis centers) or they may be estimated together with the LEO orbit. On the right hand side Figure **??** shows the TD and DD approaches requiring GPS data of an array of terrestrial receivers as well as the coordinates and troposphere information of these stations. The two ZD approaches on the left

hand side do not need these data, but precise GPS clock corrections at a high sampling rate (30 seconds) are required. In the two approaches in the center of the figure, the well-known ZD and the DD procedures, the ambiguities have to be estimated as real values making the procedures complex and time-consuming.

To reduce the computational complexity of orbit determination problem, its solution has been divided in two subsequent steps: first a preliminary orbit determination and then a differential correction of the orbit.

The first phase determines an approximate orbit for a minimum set of observations of the spacecraft that represent the two-body motion, i.e. only the mutual attraction of the two bodies, assumed to be point mass, is taken into account. The second-order differential vector equation which derives from gravitation law and that describes this motion is

$$\ddot{\mathbf{r}} = -\frac{GM}{r^3}\mathbf{r}, \tag{4.2.1}$$

where $\ddot{\mathbf{r}} = (\ddot{x}, \ddot{y}, \ddot{z})$ and $\mathbf{r} = (x, y, z)$ are respectively the acceleration and geocentric position vectors of the spacecraft and GM is the Earth gravitational constant. The solution of equation (4.2.1) requires six constants of integration, three velocity constants for the first integration and three position constants for the second integration. These constants are the spacecraft state vector

$$(x_{t_0}, y_{t_0}, z_{t_0}, \dot{x}_{t_0}, \dot{y}_{t_0}, \dot{z}_{t_0}) \tag{4.2.2}$$

evaluated at the same epoch t_0. The state can be represented equivalently by other sets of six parameters, including the Keplerian elements

$$(a_{t_0}, e_{t_0}, i_{t_0}, \Omega_{t_0}, \omega_{t_0} \; and \; n_{t_0}, E_{t_0} or M_{t_0}), \tag{4.2.3}$$

where

a	is the orbit semi-major axis,
e	is the eccentricity,
i	is the inclination,
Ω	is the right ascension of the ascending node,
ω	is the argument of perigee,
n	is the mean motion,
E	is the eccentric anomaly and
M	is the mean anomaly.

Many methods for preliminary orbit determination based on observations have been developed, e.g. by Gauss, Laplace, Herrick and Gibbs.

For the second phase of orbit determination a collection of more observation is utilized and those data are fitted to an orbit by some systematic mathematical means, usually by least-squares method, obtaining the corrections to the parameters of the preliminary orbit. For the definition of this problem also the perturbing acceleration is considered, thus the (4.2.1) becomes.

$$\ddot{\mathbf{r}} = -\frac{GM}{r^3}\mathbf{r} + \mathbf{P}, \tag{4.2.4}$$

where $\mathbf{P}$ is the vectorial sum of the perturbing accelerations acting on the space vehicle. The principal perturbing accelerations consist of:

- the non-sphericity of the Earth,
- the non-uniformity of the Earth's mass density,
- gravitational influences of other celestial bodies (in particular the Sun, Moon and Jupiter),
- solid earth and ocean tides,
- atmospheric drag,

- direct and indirect solar radiation pressure,
- relativistic effects and
- maneuvering thrusters.

The magnitudes of these acceleration are function of spacecraft attitude.

4.3. The state vector

Treating the case of artificial satellite orbit determination, we introduce the system state vector defined as

$$\mathbf{X}_{ssv} = \begin{pmatrix} \mathbf{r} \\ \mathbf{v} \\ \mathbf{p} \\ \mathbf{q} \end{pmatrix}, \tag{4.3.1}$$

where $\mathbf{r}$ and $\mathbf{v}$ are respectively the satellite position and velocity, $\mathbf{p}$ is the set of dynamic parameters, dependent on the dynamic model, and $\mathbf{q}$ is the set of kinematic parameters, dependent on the observation model. In the case we are considering, $\mathbf{q}$ consists of clock offsets and biases.

The dynamical state vector is defined as

$$\mathbf{X}_{dsv} = \begin{pmatrix} \mathbf{r} \\ \mathbf{v} \\ \mathbf{p} \end{pmatrix} \tag{4.3.2}$$

and the motion state vector as

$$\mathbf{X}_{msv} = \begin{pmatrix} \mathbf{r} \\ \mathbf{v} \end{pmatrix}. \tag{4.3.3}$$

In our case the vector of dynamic parameters $\mathbf{p}$ is given by

$$\mathbf{p} = \begin{pmatrix} C_r \\ C_{alb} \\ C_{if} \\ \mathbf{CD} \\ \mathbf{EA} \end{pmatrix}, \tag{4.3.4}$$

where C_r is the solar radiation pressure coefficient, C_{alb} is the albedo coefficient, C_{if} is IR radiation coefficient, $\mathbf{CD}$ is the vector containing drag coefficients and $\mathbf{EA}$ contains the empirical accelerations respectively with n_{cd} and n_{ea} components.

The state vector in the form of $\mathbf{X}_{ssv}$ is fundamental for the satellite orbit determination. The estimation algorithm, that in our case is a batch filter, uses $\mathbf{X}_{ssv}$ as a starting point to calculate the corrections $\mathbf{x}_{ssv,0} = \mathbf{X}_{ssv,0} - \mathbf{X}^*_{ssv,0}$ of the linearized problem at the initial time, where $\mathbf{X}^*_{ssv,0}$ is the nominal system state vector at the initial time. Given $\mathbf{X}^*_{ssv,0}$ and calculated the corrections $\mathbf{x}_{ssv,0}$, the estimated system state vector can be obtained from the difference $\mathbf{X}_{ssv,0} = \mathbf{X}^*_{ssv,0} + \mathbf{x}_{ssv,0}$. At next iteration $\mathbf{X}_{ssv,0}$ will be the new nominal system state vector and this procedure is repeated until it converges.

The state vector related to the process of orbit and partial derivatives numerical integration is $\mathbf{X}_{dsv}$. To determine its size it is necessary to know the dimension n_p of $\mathbf{p}$, corresponding to the number of dynamic parameters that have to be estimated. Therefore the dimension of $\mathbf{X}_{dsv}$ is $6+n_p$. The dynamic problem is not linear and satisfies the following differential equation with assigned initial conditions

$$\dot{\mathbf{X}}_{dsv}(t) = \mathbf{F}(\mathbf{X}_{dsv}, t), \qquad \mathbf{X}_{dsv}(t_0) = \mathbf{X}_{dsv,0}, \tag{4.3.5}$$

where $\mathbf{F}$ contains the acceleration and is given by

$$\mathbf{F} = \begin{pmatrix} \mathbf{v} \\ \mathbf{a} \\ \mathbf{0}_{n_p} \end{pmatrix}. \tag{4.3.6}$$

From the linearization of the dynamic problem (Tapley, 2004) it follows that the vector of corrections $\mathbf{x}_{ssv}$ satisfies the differential equation

$$\dot{\mathbf{x}}_{ssv}(t) = \mathbf{A}(t)\mathbf{x}_{ssv}(t), \tag{4.3.7}$$

where

$$\mathbf{A}(t) = \left[\frac{\partial \mathbf{F}}{\partial \mathbf{X}_{ssv}}\right]^{*}. \tag{4.3.8}$$

The general solution of the Equation (4.3.7) is

$$\mathbf{x}_{ssv}(t) = \mathbf{\Phi}(t, t_0)\mathbf{x}_{ssv,0}, \tag{4.3.9}$$

where $\mathbf{\Phi}(t, t_0)$ is the state transition matrix from the state in t_0 to the state in t.

The Equation (4.3.7) is used to determine $\mathbf{\Phi}(t, t_0)$: in fact the state transition matrix satisfies the same differential equation that applies to the vector of corrections $\mathbf{x}_{ssv}$

$$\dot{\mathbf{\Phi}}(t, t_0) = \mathbf{A}(t)\mathbf{\Phi}(t, t_0). \tag{4.3.10}$$

The state transition matrix $\mathbf{\Phi}(t, t_0)$ is obtained integrating the Equation (4.3.10) numerically, together with the equations of motion. The matrix $\mathbf{A}$, containing the partial derivatives of the force model $\mathbf{F}$ with respect to the dynamical state vector $\mathbf{X}_{dsv}$ along the nominal orbit, is analytical, therefore it is known at any time because, during the numerical integration, it is known the satellite nominal vector $\mathbf{X}^{*}_{dsv}$. In particular, $\mathbf{A}$ is defined as

$$\mathbf{A} = \begin{pmatrix} \mathbf{A_{11}} & \mathbf{A_{12}} & \mathbf{A_{13}} \\ \mathbf{A_{12}} & \mathbf{A_{22}} & \mathbf{A_{23}} \\ \mathbf{A_{13}} & \mathbf{A_{32}} & \mathbf{A_{33}} \end{pmatrix} \tag{4.3.11}$$

and explicitly as

$$\mathbf{A} = \begin{pmatrix} \frac{\partial \mathbf{v}}{\partial \mathbf{r}} & \frac{\partial \mathbf{v}}{\partial \mathbf{v}} & \frac{\partial \mathbf{v}}{\partial \mathbf{p}} \\ \frac{\partial \mathbf{a}}{\partial \mathbf{r}} & \frac{\partial \mathbf{a}}{\partial \mathbf{v}} & \frac{\partial \mathbf{a}}{\partial \mathbf{p}} \\ \mathbf{0}_{p\times 3} & \mathbf{0}_{p\times 3} & \mathbf{0}_{p\times p} \end{pmatrix}. \tag{4.3.12}$$

The partials $\frac{\partial \mathbf{v}}{\partial \mathbf{p}}$ and $\frac{\partial \mathbf{v}}{\partial \mathbf{r}}$ are zero because $\mathbf{v}$ does not depend on $\mathbf{p}$ and $\mathbf{r}$, therefore the Equation (4.3.12) becomes

$$\mathbf{A} = \begin{pmatrix} \mathbf{0}_{3\times 3} & \mathbf{I}_{3\times 3} & \mathbf{0}_{3\times p} \\ \frac{\partial \mathbf{a}}{\partial \mathbf{r}} & \frac{\partial \mathbf{a}}{\partial \mathbf{v}} & \frac{\partial \mathbf{a}}{\partial \mathbf{p}} \\ \mathbf{0}_{p\times 3} & \mathbf{0}_{p\times 3} & \mathbf{0}_{p\times p} \end{pmatrix}. \tag{4.3.13}$$

The state transition matrix can be expressed by

$$\mathbf{\Phi} = \begin{pmatrix} \mathbf{\Phi}_{11} & \mathbf{\Phi}_{12} & \mathbf{\Phi}_{13} \\ \mathbf{\Phi}_{21} & \mathbf{\Phi}_{22} & \mathbf{\Phi}_{23} \\ \mathbf{\Phi}_{21} & \mathbf{\Phi}_{22} & \mathbf{\Phi}_{33} \end{pmatrix} \tag{4.3.14}$$

and developing the multiplication between the matrices $\mathbf{A}$ and $\mathbf{\Phi}$, the differential equation for $\mathbf{\Phi}$ is given by

$$\dot{\mathbf{\Phi}} = \mathbf{A}(t)\mathbf{\Phi} = \begin{pmatrix} \mathbf{\Phi}_{21} & \mathbf{\Phi}_{22} & \mathbf{\Phi}_{23} \\ \mathbf{B}_{11} & \mathbf{B}_{12} & \mathbf{B}_{13} \\ \mathbf{0}_{p\times 3} & \mathbf{0}_{p\times 3} & \mathbf{0}_{p\times p} \end{pmatrix}, \tag{4.3.15}$$

where

$$\begin{aligned} \mathbf{B}_{11} &= \mathbf{A_{21}}\mathbf{\Phi_{11}} + \mathbf{A_{22}}\mathbf{\Phi_{21}} + \mathbf{A_{23}}\mathbf{\Phi_{31}}, \\ \mathbf{B}_{12} &= \mathbf{A_{21}}\mathbf{\Phi_{12}} + \mathbf{A_{22}}\mathbf{\Phi_{22}} + \mathbf{A_{23}}\mathbf{\Phi_{32}}, \\ \mathbf{B}_{13} &= \mathbf{A_{21}}\mathbf{\Phi_{13}} + \mathbf{A_{22}}\mathbf{\Phi_{23}} + \mathbf{A_{23}}\mathbf{\Phi_{33}}. \end{aligned} \tag{4.3.16}$$

Integrating the last raw of $\dot{\mathbf{\Phi}}$ using the Equation (4.3.15) with the initial conditions $\mathbf{\Phi}(t_0, t_0) = \mathbf{I}_{(6+p)\times(6+p)}$ produces

$$\mathbf{\Phi_{31}} = \mathbf{\Phi_{32}} = \mathbf{0}_{p\times 3}, \qquad \mathbf{\Phi_{33}} = \mathbf{I}_{p\times p}. \tag{4.3.17}$$

Therefore the set of Equations (4.3.16) is written as

$$\begin{aligned} \mathbf{B}_{11} &= \mathbf{A_{21}}\mathbf{\Phi_{11}} + \mathbf{A_{22}}\mathbf{\Phi_{21}}, \\ \mathbf{B}_{12} &= \mathbf{A_{21}}\mathbf{\Phi_{12}} + \mathbf{A_{22}}\mathbf{\Phi_{22}}, \\ \mathbf{B}_{13} &= \mathbf{A_{21}}\mathbf{\Phi_{13}} + \mathbf{A_{22}}\mathbf{\Phi_{23}} + \mathbf{A_{23}}. \end{aligned} \tag{4.3.18}$$

Finally, the equations that have to be integrated are

$$\dot{\mathbf{\Phi}}_{11} = \mathbf{\Phi_{21}}, \tag{4.3.19}$$

$$\dot{\mathbf{\Phi}}_{12} = \mathbf{\Phi_{22}}, \tag{4.3.20}$$

$$\dot{\mathbf{\Phi}}_{13} = \mathbf{\Phi_{23}} \tag{4.3.21}$$

and

$$\dot{\mathbf{\Phi}}_{21} = \mathbf{A_{21}}\mathbf{\Phi_{11}} + \mathbf{A_{22}}\mathbf{\Phi_{21}}, \tag{4.3.22}$$

$$\dot{\mathbf{\Phi}}_{22} = \mathbf{A_{21}}\mathbf{\Phi_{12}} + \mathbf{A_{22}}\mathbf{\Phi_{22}}, \tag{4.3.23}$$

$$\dot{\mathbf{\Phi}}_{23} = \mathbf{A_{21}}\mathbf{\Phi_{13}} + \mathbf{A_{22}}\mathbf{\Phi_{23}} + \mathbf{A_{23}}. \tag{4.3.24}$$

4.3.1. Considerations

From the estimation theory (Tapley, 2004) it results that the best estimate of the corrections $\hat{\mathbf{x}}_{ssv}$ to the vector $\mathbf{X}_{ssv}$ is expressed by

$$\hat{\mathbf{x}}_{ssv} = (\mathbf{H}^T\mathbf{R}^{-1}\mathbf{H})^{-1}\mathbf{H}^T\mathbf{R}^{-1}\mathbf{y}, \tag{4.3.25}$$

where R^{-1} is the weight matrix, $\mathbf{y}$ is the vector of the observation residuals and $\mathbf{H}$ is the matrix containing the partial derivatives of the observations with respect to $\mathbf{X}_{ssv}$. The matrices $\mathbf{H}^T\mathbf{R}^{-1}\mathbf{H}$ and $\mathbf{H}^T\mathbf{R}^{-1}\mathbf{y}$ have to be determined through accumulation in the following way

$$\mathbf{H}^T\mathbf{R}^{-1}\mathbf{H} = \sum_{i=1}^{l} \left[\bar{\mathbf{H}}_i\mathbf{\Phi}(t_i, t_0)\right]^T \mathbf{R}_i^{-1}\bar{\mathbf{H}}_i\mathbf{\Phi}(t_i, t_0), \tag{4.3.26}$$

$$\mathbf{H}^T\mathbf{R}^{-1}\mathbf{y} = \sum_{i=1}^{l} \left[\bar{\mathbf{H}}_i\mathbf{\Phi}(t_i, t_0)\right] \mathbf{R}_i^{-1}\mathbf{y}, \tag{4.3.27}$$

where $\bar{\mathbf{H}}_i$ is the partial derivative of the i-esim observation with respect to $\mathbf{X}_{ssv}$ and $\mathbf{\Phi}(t_i, t_0)$ is the state transition matrix obtained integrating its differential equations numerically.

The motion state vector $\mathbf{X}_{msv}$ and $\mathbf{\Phi}(t, t_0)$ have the same role and therefore they have to be possibly memorized at fixed and equidistant intervals. $\mathbf{X}_{msv}$ is necessary to reconstruct the orbit at a certain time or to produce an ephemeris every minute or hour (during this procedure $\mathbf{X}_{dsv}$ is not needed because the parameters p remain constant).

On the other hand, $\mathbf{\Phi}$ is necessary to determine $\mathbf{H}^T\mathbf{R}^{-1}\mathbf{H}$ and $\mathbf{H}^T\mathbf{R}^{-1}\mathbf{y}$ and so to calculate the partial derivative of the observation with respect to $\mathbf{X}_{ssv,0}$.

Moreover, the Equations (4.3.19) and (4.3.22) show that it not necessary to memorize the entire matrix $\mathbf{\Phi}$, because only blocks $\mathbf{\Phi_{11}}$, $\mathbf{\Phi_{12}}$, $\mathbf{\Phi_{13}}$, $\mathbf{\Phi_{21}}$, $\mathbf{\Phi_{22}}$, $\mathbf{\Phi_{23}}$ are not zero and $\mathbf{\Phi_{33}} = \mathbf{I}$.

If there are also kinematic parameters $\mathbf{q}$, the matrix $\mathbf{\Phi}$ in the block related to these parameters behaves as if in the case of dynamic parameters, therefore the raw corresponding to $\mathbf{q}$ is zero, with the exception of the diagonal block that is unitary.

4.4. The observation vector

Having p observations at each epoch t_i, $(i = 1, 2, ..., l)$, an observation vector $\mathbf{y}_i$, of dimension $m = l \times p$, can be formed. The equation

$$\mathbf{y}_i = \mathbf{G}(\mathbf{X}_i, t_i) + \boldsymbol{\varepsilon}_i \qquad i = 1, 2, ..., l \tag{4.4.1}$$

links the observations $\mathbf{y}_i$ to the measurements model $\mathbf{z} = \mathbf{G}(\mathbf{X}_i, t_i)$, and accounts also for the measurements noise $\boldsymbol{\varepsilon}_i$.

It is well known that the solution to an initial value problem like that expressed by Eq. (**??**) has the form

$$\mathbf{X}(t_i) = \boldsymbol{\Theta}(\mathbf{X}_0, t_0, t_i), \tag{4.4.2}$$

and therefore it follows that

$$\mathbf{y}_i = \mathbf{G}(\boldsymbol{\Theta}(\mathbf{X}_0, t_0, t_i), t_i) + \boldsymbol{\varepsilon}_i, \tag{4.4.3}$$

that is

$$\mathbf{y}_i = \tilde{\mathbf{G}}(\mathbf{X}_0, t_0, t_i) + \boldsymbol{\varepsilon}_i, \tag{4.4.4}$$

which is an implicit relationship. Usually an explicit relationship can not be found due to the complexity of the problem. More generally, if we define the above relationship as

$$\mathbf{y} = \tilde{\mathbf{G}}(\mathbf{X}_0, t_0) + \boldsymbol{\varepsilon}, \tag{4.4.5}$$

the following definition can be given

Definition 13 *The orbit determination process consists on the determination of the best estimate of the state (including satellite-related and other type of parameters), whose initial conditions is known with some degree of uncertainty, using the observations* $\mathbf{y}$ *(affected by measurement errors* $\boldsymbol{\varepsilon}$*) and a dynamic model that has a limited degree of precision.*

Eq. ch3:osserv is a system of $m = l \times p$ algebraic equations with n unknown state components and m measurement error components $\boldsymbol{\varepsilon}$. If $\boldsymbol{\varepsilon}_i = 0$, $(i = 1, 2, ..., l)$, any set of n equations of the type ch3:ossest could be used to determine $\mathbf{X}_0$ (and hence the state at any other time t_k) through Eq. ch3:t116. In the real case of $\boldsymbol{\varepsilon}_i \neq 0$, a best-fit technique must be employed. Usually, the selected criterion is to minimize the sum of the squares of the observation errors, i.e. the *residuals*. For reasons of unicity of the solution, a *linearization* is first performed. This step implicitly assumes that our our a-priori knowledge of the problem is already *close* to the true solution.

4.5. Linearization

If the state and the observation vector are linked by a linear relationship, the powerful techniques of the linear estimation theory can be applied. In the case at hand, this is equivalent to assuming that the true and the project (nominal) trajectories of a space vehicle are close enough. In this case, the nominal trajectory $\mathbf{X}^*$ can be expanded by Taylor series around the true trajectory $\mathbf{X}$ at every epoch. If the series is truncated at first order, then the *deviations* from the reference trajectory can be described by a linear system of equations with time-dependent coefficients. A linear relationship between the observations and the state is obtained in a similar way.

Let

$$\mathbf{x}(t) = \mathbf{X}(t) - \mathbf{X}^*(t) \qquad \mathbf{y}(t) = \mathbf{y}(t) - \mathbf{y}^*(t) \tag{4.5.1}$$

be the *deviations* or differences between the true and the nominal state. By performing a Taylor expansion of (**??**) and (4.4.1) around the nominal trajectory $\mathbf{X}^*$ we obtain

$$\begin{aligned}\dot{\mathbf{X}}(t) &= \mathbf{F}(\mathbf{X},t) = \mathbf{F}(\mathbf{X}^*,t) + \left[\frac{\partial \mathbf{F}}{\partial \mathbf{X}}\right]^* \mathbf{x} + ... \\ \mathbf{y}(t) &= \mathbf{G}(\mathbf{X}_i,t_i) + \epsilon_i = \mathrm{G}(\mathrm{X}^*,t) + \left[\frac{\partial \mathrm{G}}{\partial \mathrm{X}}\right]^* \mathrm{x}_i + ... + \epsilon_i.\end{aligned} \tag{4.5.2}$$

If the high-order terms are neglected and if the conditions

$$\dot{\mathbf{X}}^* = \mathbf{F}(\mathbf{X}^*,t) \tag{4.5.3}$$

and

$$\mathbf{y}_i^* = \mathbf{G}(\mathbf{X}_i^*,t_i) \tag{4.5.4}$$

are satisfied, the above equations can be written as follows

$$\begin{aligned}\dot{\mathbf{x}} &= \mathbf{A}(t)\mathbf{x} \\ \mathbf{y}_i &= \tilde{\mathbf{H}}_i\mathbf{x}_i + \epsilon_i \qquad i = 1,2,...,l,\end{aligned} \tag{4.5.5}$$

where

$$\mathbf{A}(t) = \frac{\partial \mathbf{F}}{\partial \mathbf{X}}(\mathbf{X}^*,t) \quad \text{e} \quad \tilde{\mathbf{H}} = \frac{\partial \mathbf{G}}{\partial \mathbf{X}}(\mathbf{X}^*,t). \tag{4.5.6}$$

Therefore the initial (non linear) problem is replaced by a more treatable, linear system of equations described by Eqs. (4.5.5). The most general solution of such a system is

$$\mathbf{x}(t) = \mathbf{\Phi}(t,t_k)\mathbf{x}_k, \tag{4.5.7}$$

where $\mathbf{x}(t)$ is the value of $\mathbf{x}$ at time t. The matrix $\mathbf{\Phi}(t,t_k)$ is called *state transition matrix* (STM) and has important properties that are shown[2] without proof

$$\begin{aligned}\mathbf{\Phi}(t_i,t_i) &= \mathbf{I} \\ \mathbf{\Phi}(t_i,t_k) &= \mathbf{\Phi}(t_i,t_j)\mathbf{\Phi}(t_j,t_k) \\ \mathbf{\Phi}(t_i,t_k) &= \mathbf{\Phi}^{-1}(t_k,t_i).\end{aligned} \tag{4.5.8}$$

It is also easy to prove that $\mathbf{\Phi}$ satisfies the following differential equation

$$\dot{\mathbf{\Phi}}(t,t_k) = \mathbf{A}(t)\mathbf{\Phi}(t,t_k) \tag{4.5.9}$$

with $\mathbf{\Phi}(t_k,t_k) = \mathbf{I}$ as initial conditions.

Using Eq. (4.5.7), the second equation of Eqs. (4.5.5) can be written in terms of the state at time t_0 as

$$\begin{aligned}\mathbf{y}_1 &= \tilde{\mathbf{H}}_1\mathbf{\Phi}(t_1,t_0)\mathbf{x}_0 + \epsilon_1 \\ \mathbf{y}_2 &= \tilde{\mathbf{H}}_2\mathbf{\Phi}(t_2,t_0)\mathbf{x}_0 + \epsilon_2 \\ &\vdots \\ \mathbf{y}_l &= \tilde{\mathbf{H}}_l\mathbf{\Phi}(t_l,t_0)\mathbf{x}_0 + \epsilon_l.\end{aligned} \tag{4.5.10}$$

Eqs. (4.5.10) contain $m = p \times l$ observations and n unknown state vector components. If the following definitions are used

[2] For the proof see Gelb, [Gelb].

$$\mathbf{y} = \begin{bmatrix} \mathbf{y}_1 \\ \vdots \\ \mathbf{y}_l \end{bmatrix} \qquad \mathbf{H} = \begin{bmatrix} \tilde{\mathbf{H}}_1 \mathbf{\Phi}(t_1, t_0) \\ \vdots \\ \tilde{\mathbf{H}}_1 \mathbf{\Phi}(t_1, t_0) \end{bmatrix} \qquad = \begin{bmatrix} 1 \\ \vdots \\ l \end{bmatrix}, \tag{4.5.11}$$

and if we neglect the underscore 0 of $\mathbf{x}_0$, Eqs. (4.5.10) can be rewritten as

$$\mathbf{y} = \mathbf{H}\mathbf{x} + \epsilon \tag{4.5.12}$$

where $\mathbf{y}$ is a vector of size $m \times 1$, $\mathbf{x}$ is a vector $n \times 1$, is a vector $m \times 1$ and $\mathbf{H}$ is an $m \times n$ matrix, m being the total number of observations. If l is large enough, the condition $m > n$ is satisfied.

4.6. Satellite Observation and the Estimation Problem

If at some time t_0 the satellite state vector X is known (X_0) and the forces acting on the satellite are known, then the satellite equation of motion can be integrated to determine the state process vector of the satellite at any future time. However, the initial state vector is never know exactly. Moreover, certain forces models require physical parameters which are know only approximately, i.e. the satellite drag coefficients in aerodynamical forces, or the coefficients of the spherical harmonics expansion representation of the terrestrial gravity field. This is also the case with geophysical parameters that affect indirectly the equation of the motion (like Earth rotation and polar motion). Consequently, to determine the position of the satellite at a future time it is necessary that observations of the satellites are taken and used to obtain a better estimate of the satellite trajectory. The observation data, which will be subjected to both systematic and random errors, will usually consist of measurement such as range, range-rate (doppler), azimuth, elevation or some other observable quantity. These measurements have to be corrected with models which are imperfect (e.g. tropospheric correction) and are usually taken from stations whose earth-fixed coordinates are not exactly known.

The problem of determining the best estimate of the satellite state vector (and optionally other parameters and geodetic quantities) is referred to as *statical orbit determination*. Sometimes the main interest is focused on the estimation of geophysical and geodetic quantities themselves: this field is called *space geodesy*. Another variation of the problem is *simulation and covariance analysis* in which orbit determination strategies for future mission are studied in terms of coverage, accuracy requirements and weighting of tracking data, orbit determination accuracy expectation, optimal arc-length...

The problem can be generalized as follow: given an initial state vector at time t_0 and the initial values of parameters to be estimated (not necessary at t_0), together with their a priori covariance matrix, and given a set of real or simulated observation (not necessary after t_0) also with their initial covariance matrix, find the "best" estimate of the state vector at a future time and of the rest of the parameters, together with an a posteriori parameter and observation covariance matrix. So in matrix notation the a priori values are

$$\mathbf{X}_0 = \begin{bmatrix} x_0 \\ y_0 \\ z_0 \\ \dot{x}_0 \\ \dot{y}_0 \\ \dot{z}_0 \\ \alpha_1 \\ \dots \\ \alpha_k \end{bmatrix}, \quad \mathbf{P}_0 = \begin{bmatrix} \sigma_{11}^2 & \sigma_{12}^2 & \dots & \sigma_{1n}^2 \\ \sigma_{21}^2 & \sigma_{22}^2 & \dots & \sigma_{2n}^2 \\ \vdots & \vdots & \ddots & \vdots \\ \sigma_{n1}^2 & \dots & \dots & \sigma_{nn}^2 \end{bmatrix}, \tag{4.6.1}$$

$$\mathbf{y} = \begin{bmatrix} y_1 \\ y_2 \\ \vdots \\ y_m \end{bmatrix}, \quad \mathbf{Q}_0 = \begin{bmatrix} \sigma_1^2 & 0 & \dots & 0 \\ 0 & \sigma_2^2 & \dots & 0 \\ \vdots & \vdots & \ddots & \vdots \\ 0 & \dots & \dots & \sigma_m^2 \end{bmatrix}, \tag{4.6.2}$$

where $\mathbf{X}_0$ is the vector of estimated parameters or *extended initial state vector* (n is the total number of estimated parameters), $\mathbf{P}_0$ is the a priori covariance matrix of the parameters in $\mathbf{X}_0$, $\mathbf{y}$ is the matrix containing the observations (m is the total number of observations, $m > n$) and $\mathbf{Q}_0$ is the observation a priori covariance matrix. We will assume here that the observations are a priori non correlated, i.e. the matrix $\mathbf{Q}_0$ is diagonal, but this is not exactly true.

$\widehat{\mathbf{X}}(t)$ is the best estimate of the extended state vector at time t. In practice the "best" estimate is to minimize the sum of the square of the *weighted residual observations errors*, that is, the square of the difference between the observations and the expected values computed from an observation model multiplied by a weight factor according to the observation importance, method called *least-square estimators*.

The observations are computed by evaluating the satellite state vector at the observation time and finding a geometric/kinematic relationship between the satellite position/velocity and the magnitude which is observed. The residual observation vector in function of $\widehat{\mathbf{X}}(t)$ is defined as:

$$\varepsilon = \begin{bmatrix} y_1 - f_1\left(\widehat{\mathbf{X}}\left(t_1\right)\right) \\ \\ \dots \\ \\ y_m - f_m\left(\widehat{\mathbf{X}}\left(t_m\right)\right) \end{bmatrix} \tag{4.6.3}$$

The quantity to be minimized is called the *loss function* and can be expressed as:

$$\mathbf{J} = \varepsilon^{+} \cdot \mathbf{Q}_0^{-1} \cdot \varepsilon, \tag{4.6.4}$$

where $\mathbf{Q}_0^{-1}$ is the *weight matrix*.

The loss function described in 4.6.4 can be modified to account for the uncertainties of the a priori values of the estimated parameters:

$$\mathbf{J} = \varepsilon^{+} \cdot \mathbf{Q}_0^{-1} \cdot \varepsilon + \mathbf{\Psi}, \tag{4.6.5}$$

where $\mathbf{\Psi}$ uses information on the covariance of the $\widehat{\mathbf{X}}$.

There are two main classes of least square estimators, *batch* and *sequential*.

A *batch* estimator updates the extended state vector $\mathbf{X}_0$ (and optionally $\mathbf{P}_0$ and $\mathbf{Q}_0$)iteratively after a high enough number of observations (which define the *estimation arc*) has been collected after the epoch t_0. Once the process has converged to a best estimate of $\mathbf{X}_0$, the satellite state vector can be propagated to any future time using as initial values the ones from $\widehat{\mathbf{X}}_0$.

In a *sequential* estimator the observations are processed as soon as they are received, and the *extended state vector* $\mathbf{X}$ and its covariance matrix $\mathbf{P}$ are propagated/updated with every new observation or small set of observations. The main application of these estimators is the operational real-time orbit determination.

4.6.1. Batch estimation

As long as the satellite state vector can be propagated to any time from the initial state vector, the computed observations are a function of $\widehat{\mathbf{X}}_0$ and the time. The residual observation matrix can then be written as

$$\varepsilon\left(\widehat{\mathbf{X}}_0\right) = \begin{bmatrix} y_1 - f_1\left(\widehat{\mathbf{X}}_0, t_1\right) \\ \\ \dots \\ \\ y_m - f_m\left(\widehat{\mathbf{X}}_0, t_m\right) \end{bmatrix}. \tag{4.6.6}$$

In this case the *loss function* is

$$J\left(\widehat{\mathbf{X}}_0\right) = \varepsilon^{+} \cdot \mathbf{Q}^{-1} \cdot \varepsilon + \Delta\mathbf{X}_0{}^{+} \cdot \mathbf{P}_0{}^{+} \cdot \Delta\mathbf{X}_0, \tag{4.6.7}$$

where $\Delta\mathbf{X}_0 = \widehat{\mathbf{X}}_0 - \mathbf{X}_0$.

An $\widehat{\mathbf{X}}_0$ has to be found which minimize the loss function $J\left(\widehat{\mathbf{X}}_0\right)$. This is achieved by differentiating the equation (4.6.7) with respect to the estimated parameters $\widehat{\mathbf{X}}_0$ and setting the resulting expression to zero. The problem has to be linearized in order to be solved. If $\Delta\mathbf{X}_0$ is small (i.e. the initial values of the estimated parameters are a good enough approximation of the optimal ones), then the computed observations can be expressed as their first order Taylor expansion around $\mathbf{X}_0$

$$\mathbf{F}_i\left(\widehat{\mathbf{X}}_0, t_i\right) = f_i\left(\mathbf{X}_0, t_i\right) + \sum_{j=1}^{n} \frac{\partial f_i}{\partial \boldsymbol{\beta}_j} \cdot \left(\widehat{\boldsymbol{\beta}}_j - \boldsymbol{\beta}_j\right), \tag{4.6.8}$$

where the betas are all the estimated parameters, i.e. the elements of the $\mathbf{X}_0$ vector. The residuals can be expressed then as

$$\boldsymbol{\varepsilon}\left(\widehat{\mathbf{X}}_0\right) = \begin{bmatrix} y_1 - f_1\left(\widehat{\mathbf{X}}_0, t_1\right) \\ \dots \\ y_m - f_m\left(\widehat{\mathbf{X}}_0, t_m\right) \end{bmatrix} - \mathbf{F} \cdot \left(\widehat{\mathbf{X}}_0 - \mathbf{X}_0\right). \tag{4.6.9}$$

$\mathbf{F}$ is the *matrix of observation equation coefficients*, which contains the partial derivatives of the computed observation with respect to the estimated parameters

$$\mathbf{F} = \begin{bmatrix} \frac{\partial f_1}{\partial x_0} & \frac{\partial f_1}{\partial y_0} & \frac{\partial f_1}{\partial z_0} & \frac{\partial f_1}{\partial \dot{x}_0} & \frac{\partial f_1}{\partial \dot{y}_0} & \frac{\partial f_1}{\partial \dot{z}_0} & \frac{\partial f_1}{\partial \alpha_1} & \cdots & \frac{\partial f_1}{\partial \alpha_k} \\ \frac{\partial f_2}{\partial x_0} & \frac{\partial f_2}{\partial y_0} & \frac{\partial f_2}{\partial z_0} & \frac{\partial f_2}{\partial \dot{x}_0} & \frac{\partial f_2}{\partial \dot{y}_0} & \frac{\partial f_2}{\partial \dot{z}_0} & \frac{\partial f_2}{\partial \alpha_1} & \cdots & \frac{\partial f_2}{\partial \alpha_k} \\ \vdots & \vdots & \vdots & \vdots & \vdots & \vdots & \vdots & \ddots & \vdots \\ \frac{\partial f_m}{\partial x_0} & \frac{\partial f_m}{\partial y_0} & \frac{\partial f_m}{\partial z_0} & \frac{\partial f_m}{\partial \dot{x}_0} & \frac{\partial f_m}{\partial \dot{y}_0} & \frac{\partial f_m}{\partial \dot{z}_0} & \frac{\partial f_m}{\partial \alpha_1} & \cdots & \frac{\partial f_m}{\partial \alpha_k} \end{bmatrix}. \tag{4.6.10}$$

Substituting equation (4.6.9) in 4.6.7 and differentiating respect to $\widehat{\mathbf{X}}_0$ leads to the iterative *normal equation*

$$\widehat{\mathbf{X}}_0^{k+1} = \widehat{\mathbf{X}}_0^{k} + \left(\mathbf{P}_0^{-1} + \mathbf{F}^{+} \cdot \mathbf{Q}_0^{-1} \cdot \mathbf{F}\right)^{-1} \cdot \left(\mathbf{F}^{+} \cdot \mathbf{Q}_0^{-1} + \Delta\mathbf{y}^{k} + \mathbf{P}_0^{-1} \cdot \left(\mathbf{X}_0 - \widehat{\mathbf{X}}_0^{k}\right)\right), \tag{4.6.11}$$

where $\widehat{\mathbf{X}}_0^{k}$ is the estimation of $\widehat{\mathbf{X}}_0$ on iteration k ($\widehat{\mathbf{X}}_0^{0} = \mathbf{X}_0$) and $\Delta\mathbf{y}^{k}$ is the residual observation matrix calculated propagating $\widehat{\mathbf{X}}_0^{k}$

$$\boldsymbol{\Delta}\mathbf{y}^{\boldsymbol{k}} = \begin{bmatrix} y_1 - f_1\left(\widehat{\mathbf{X}}_0^{k}, t_1\right) \\ \dots \\ y_m - f_m\left(\widehat{\mathbf{X}}_0^{k}, t_m\right) \end{bmatrix}. \tag{4.6.12}$$

The following matrix

$$\mathbf{N} = \mathbf{P}_0^{-1} + \mathbf{F}^{+} \cdot \mathbf{Q}_0^{-1} \cdot \mathbf{F} \tag{4.6.13}$$

is called *normal matrix*. It can be shown that the inverse of the normal matrix $\mathbf{N}$ is the best estimation of the covariance matrix of the estimated parameters, that is

$$\widehat{\mathbf{P}} = \mathbf{N}^{-1} = \left(\mathbf{P}_0^{-1} + \mathbf{F}^{+} \cdot \mathbf{Q}_0^{-1} \cdot \mathbf{F}\right)^{-1} \tag{4.6.14}$$

and it is called the *covariance matrix*. It is usual to use the following expression

$$\widehat{\mathbf{P}} = \frac{\mathbf{J}}{m}\mathbf{N}^{-1} = \frac{\mathbf{J}}{m}\left(\mathbf{P}_0^{-1} + \mathbf{F}^{+} \cdot \mathbf{Q}_0^{-1} \cdot \mathbf{F}\right)^{-1}, \tag{4.6.15}$$

where $\mathbf{J}$ is the value of the loss function and m is the number of observations.

4.6.2. Observation equation coefficients and variational parts

The calculation method of the differential partial derivatives in $\mathbf{F}$ depends highly on the nature of the variable with respect to which the derivative has to be calculated. Some of them are zero because the observation does not depend on the parameter. Other calculation are straightforward; for example, if the observation is a one-way range from a ground station and the parameter in question is the one of the station coordinates, then the computed observation would be:

$$R = \sqrt{(x - X_s)^2 + (y - Y_s)^2 + (z - Z_s)^2}, \tag{4.6.16}$$

where (x, y, z) is the position of the satellite at the time of observation and (X_s, y_s, Z_s) are the station coordinates. The partial derivative of R with respect to the parameter X_s would be:

$$\frac{\partial R}{\partial X_s} = \frac{X_s - x}{R}. \tag{4.6.17}$$

A special set of parameters are the *dynamic parameters*, which are the satellites initial state vector $(x_0, y_0, z_0, \dot{x}_0, \dot{y}_0, \dot{z}_0)$ and the force model unknowns. The partial derivatives of an observation with respect to a dynamic parameter can be expressed as:

$$\frac{\partial f}{\partial \boldsymbol{\beta}} = \begin{bmatrix} \frac{\partial f}{\partial x} & \frac{\partial f}{\partial y} & \frac{\partial f}{\partial z} & \frac{\partial f}{\partial \dot{x}} & \frac{\partial f}{\partial \dot{y}} & \frac{\partial f}{\partial \dot{z}} \end{bmatrix} \cdot \begin{bmatrix} \frac{\partial x}{\partial \boldsymbol{\beta}} \\ \frac{\partial y}{\partial \boldsymbol{\beta}} \\ \frac{\partial z}{\partial \boldsymbol{\beta}} \\ \frac{\partial \dot{x}}{\partial \boldsymbol{\beta}} \\ \frac{\partial \dot{y}}{\partial \boldsymbol{\beta}} \\ \frac{\partial \dot{z}}{\partial \boldsymbol{\beta}} \end{bmatrix}. \tag{4.6.18}$$

The coefficients of the file matrix in the right-hand side of equation (4.6.18) are the partial derivatives of the computed observation with respect to the satellite position and velocity at the time of observation, and can be easily evaluated for any kind of observation. These coefficients have to be obtained by numerical integration of the *variational equations*. The column matrices for all the dynamic parameters to be estimated from the matrix of *position partials*

$$\mathbf{X}_m = \begin{bmatrix} \frac{\partial x}{\partial x_0} & \frac{\partial x}{\partial y_0} & \frac{\partial x}{\partial z_0} & \frac{\partial x}{\partial \dot{x}_0} & \frac{\partial x}{\partial \dot{y}_0} & \frac{\partial x}{\partial \dot{z}_0} & \frac{\partial x}{\partial \alpha_1} & \cdots & \frac{\partial x}{\partial \alpha_l} \\ \frac{\partial y}{\partial x_0} & \frac{\partial y}{\partial y_0} & \frac{\partial y}{\partial z_0} & \frac{\partial y}{\partial \dot{x}_0} & \frac{\partial y}{\partial \dot{y}_0} & \frac{\partial y}{\partial \dot{z}_0} & \frac{\partial y}{\partial \alpha_1} & \cdots & \frac{\partial y}{\partial \alpha_l} \\ \frac{\partial z}{\partial x_0} & \frac{\partial z}{\partial y_0} & \frac{\partial z}{\partial z_0} & \frac{\partial z}{\partial \dot{x}_0} & \frac{\partial z}{\partial \dot{y}_0} & \frac{\partial z}{\partial \dot{z}_0} & \frac{\partial z}{\partial \alpha_1} & \cdots & \frac{\partial z}{\partial \alpha_l} \end{bmatrix}, \tag{4.6.19}$$

where $h = 6 + l$ is the number of dynamic parameters. Matrix $\mathbf{X}_m$ is evaluated by integrating the following equation of matrices called *variational equations*

$$\ddot{\mathbf{X}}_m = D_1 \cdot \mathbf{X}_m + D_2 \dot{\mathbf{X}}_m + A_f, \tag{4.6.20}$$

being

$$\ddot{\mathbf{X}}_m = \begin{bmatrix} \frac{\partial \ddot{x}}{\partial x_0} & \frac{\partial \ddot{x}}{\partial y_0} & \frac{\partial \ddot{x}}{\partial z_0} & \frac{\partial \ddot{x}}{\partial \dot{x}_0} & \frac{\partial \ddot{x}}{\partial \dot{y}_0} & \frac{\partial \ddot{x}}{\partial \dot{z}_0} & \frac{\partial \ddot{x}}{\partial \alpha_1} & \cdots & \frac{\partial \ddot{x}}{\partial \alpha_l} \\ \frac{\partial \ddot{y}}{\partial x_0} & \frac{\partial \ddot{y}}{\partial y_0} & \frac{\partial \ddot{y}}{\partial z_0} & \frac{\partial \ddot{y}}{\partial \dot{x}_0} & \frac{\partial \ddot{y}}{\partial \dot{y}_0} & \frac{\partial \ddot{y}}{\partial \dot{z}_0} & \frac{\partial \ddot{y}}{\partial \alpha_1} & \cdots & \frac{\partial \ddot{y}}{\partial \alpha_l} \\ \frac{\partial \ddot{z}}{\partial x_0} & \frac{\partial \ddot{z}}{\partial y_0} & \frac{\partial \ddot{z}}{\partial z_0} & \frac{\partial \ddot{z}}{\partial \dot{x}_0} & \frac{\partial \ddot{z}}{\partial \dot{y}_0} & \frac{\partial \ddot{z}}{\partial \dot{z}_0} & \frac{\partial \ddot{z}}{\partial \alpha_1} & \cdots & \frac{\partial \ddot{z}}{\partial \alpha_l} \end{bmatrix}, \tag{4.6.21}$$

and

$$\dot{\mathbf{X}}_m = \begin{bmatrix} \frac{\partial \dot{x}}{\partial x_0} & \frac{\partial \dot{x}}{\partial y_0} & \frac{\partial \dot{x}}{\partial z_0} & \frac{\partial \dot{x}}{\partial \dot{x}_0} & \frac{\partial \dot{x}}{\partial \dot{y}_0} & \frac{\partial \dot{x}}{\partial \dot{z}_0} & \frac{\partial \dot{x}}{\partial \alpha_1} & \cdots & \frac{\partial \dot{x}}{\partial \alpha_l} \\ \frac{\partial \dot{y}}{\partial x_0} & \frac{\partial \dot{y}}{\partial y_0} & \frac{\partial \dot{y}}{\partial z_0} & \frac{\partial \dot{y}}{\partial \dot{x}_0} & \frac{\partial \dot{y}}{\partial \dot{y}_0} & \frac{\partial \dot{y}}{\partial \dot{z}_0} & \frac{\partial \dot{y}}{\partial \alpha_1} & \cdots & \frac{\partial \dot{y}}{\partial \alpha_l} \\ \frac{\partial \dot{z}}{\partial x_0} & \frac{\partial \dot{z}}{\partial y_0} & \frac{\partial \dot{z}}{\partial z_0} & \frac{\partial \dot{z}}{\partial \dot{x}_0} & \frac{\partial \dot{z}}{\partial \dot{y}_0} & \frac{\partial \dot{z}}{\partial \dot{z}_0} & \frac{\partial \dot{z}}{\partial \alpha_1} & \cdots & \frac{\partial \dot{z}}{\partial \alpha_l} \end{bmatrix} \tag{4.6.22}$$

respectively the matrices of *acceleration partials* and *velocity partials*. The coefficients of A_f are the direct derivatives of the acting accelerations with respect to the force parameters.

$$A_f = \begin{bmatrix} 0 & 0 & 0 & 0 & 0 & 0 & \frac{\partial a_x}{\partial \alpha_1} & \cdots & \frac{\partial a_x}{\partial \alpha_l} \\ 0 & 0 & 0 & 0 & 0 & 0 & \frac{\partial a_y}{\partial \alpha_1} & \cdots & \frac{\partial a_y}{\partial \alpha_l} \\ 0 & 0 & 0 & 0 & 0 & 0 & \frac{\partial a_z}{\partial \alpha_1} & \cdots & \frac{\partial a_z}{\partial \alpha_l} \end{bmatrix}. \tag{4.6.23}$$

D_1 and D_2 are given by

$$D_1 = \begin{bmatrix} \frac{\partial a_x}{\partial x} & \frac{\partial a_x}{\partial y} & \frac{\partial a_x}{\partial z} \\ \frac{\partial a_y}{\partial x} & \frac{\partial a_y}{\partial y} & \frac{\partial a_y}{\partial z} \\ \frac{\partial a_z}{\partial x} & \frac{\partial a_z}{\partial y} & \frac{\partial a_z}{\partial z} \end{bmatrix}, \; D_2 = \begin{bmatrix} \frac{\partial a_x}{\partial \dot{x}} & \frac{\partial a_x}{\partial \dot{y}} & \frac{\partial a_x}{\partial \dot{z}} \\ \frac{\partial a_y}{\partial \dot{x}} & \frac{\partial a_y}{\partial \dot{y}} & \frac{\partial a_y}{\partial \dot{z}} \\ \frac{\partial a_z}{\partial \dot{x}} & \frac{\partial a_z}{\partial \dot{y}} & \frac{\partial a_z}{\partial \dot{z}} \end{bmatrix}, \tag{4.6.24}$$

and they are respectively the derivatives of the acting accelerations w.r.t. the satellite position and velocity.

Equation (4.6.20) is a system of second order differential equations with initial conditions

$$\mathbf{X}_m^0 = \begin{bmatrix} 1 & 0 & 0 & 0 & 0 & 0 & 0 & \dots & 0 \\ 0 & 1 & 0 & 0 & 0 & 0 & 0 & \dots & 0 \\ 0 & 0 & 1 & 0 & 0 & 0 & 0 & \dots & 0 \end{bmatrix}, \; \mathbf{V}_m^0 = \begin{bmatrix} 0 & 0 & 0 & 1 & 0 & 0 & 0 & \dots & 0 \\ 0 & 0 & 0 & 0 & 1 & 0 & 0 & \dots & 0 \\ 0 & 0 & 0 & 0 & 0 & 1 & 0 & \dots & 0 \end{bmatrix} \tag{4.6.25}$$

of dimensions $(3 \times h)$.

Chapter 5

Radio Occultation with LEO Satellites

"¡Citation¿."

¡Author¿, *'¡Title¿'*

5.1. Introduction

In this chapter... TBW

5.2. Excess Phase Computation

The excess phase is defined as the difference between the phase observable measured by a GNSS receiver on board a LEO satellite received from a GPS satellite which is not in the line of sight because of the Earth interposition, corrected for the LEO and GPS satellite clock errors and the geometric distance between the two satellites involved (note that the ionospheric delay is not corrected).

In this section the algorithm developed for the excess phase computation will be described in detail.

Remember that (*see* sction 2.3.2) the terms with the subscript φ are expressed in units of cycles while the terms with the subscript P (referring to pseudorange) and F (for carrier phase) are expressed in units of length. The relation between phase terms expressed in unit of length and in unit of cycles is $\delta X^o_{l,L_i,F}(t) = \lambda_i \delta X^o_{l,L_i,\varphi}(t)$ (e.g $\delta I^o_{l,L_i,F}(t) = \lambda_i \delta I^o_{l,L_i,\varphi}(t)$ for the ionospheric delay or $N^o_{l,L_i,F} t = \lambda_i N^o_{l,L_i,\varphi} t$ for the ambiguities). The tropospheric delay is convert to cycles using the factor f_i/c. The ionospheric term has a *negative value* because the ionosphere advances the carrier phase, that is

$$\delta I^o_{l,L_i,P}(t) = -\delta I^o_{l,L_i,F}(t) = -\frac{f_i}{c}\delta I^o_{l,L_i,\varphi}(t) \quad \text{and} \tag{5.2.1}$$

$$\delta I^o_{l,L_i,P}(t) = \frac{40.30}{f_i^2}\text{TEC}. \tag{5.2.2}$$

Moreover

$$\delta I^o_{l,L_2,\{P,F\}}(t) = \frac{f_1^2}{f_2^2}\delta I^o_{l,L_1,\{P,F\}}(t) \quad \text{and} \tag{5.2.3}$$

$$\delta I^o_{l,L_2,\varphi}(t) = \frac{f_1}{f_2}\delta I^o_{l,L_1,\varphi}(t). \tag{5.2.4}$$

5.2.1. Excess Phase in Units of Cycles

The carrier phase observable has been already expressed by equation 2.3.36, but for the sake of convenience it is here referred again and simplified in equation 5.2.5.

$$\begin{aligned}\varphi^{o}_{l,L_i}(t_k) = \frac{f_i}{c}\rho^{o}_{l}(t_k) - f_i dt_l + f_i\, dt^o + N^{o}_{l,L_i,\varphi} + \delta I^{o}_{l,L_i,\varphi}(t_k) \\ + \frac{f_i}{c}\delta T^{o}_{l}(t_k) + \delta^{o}_{l,L_i,\varphi}(t_k) + \epsilon^{o}_{l,L_i,\varphi}(t_k),\end{aligned} \tag{5.2.5}$$

where

- $\delta^{o}_{l,L_i,\varphi}(t_k) = \delta E_{l,L_i,\varphi}(t_k) + \delta E^{o}_{L_i,\varphi}(t_k) + \delta M^{o}_{l,L_i,\varphi}(t_k)$ and
- dt_l is the LEO receiver clock bias,
- dt^o is the occultef GPS satellite clock bias,
- $\delta I^{o}_{l,L_i,\varphi}(t_k)$ is the delay due to the ionosphere (always positive) between the LEO receiver and the occulted GPS satellite for the carrier frequency L_i, $i = 1, 2$,
- $\delta T^{o}_{l}(t_k)$ is the delay due to the troposphere (always positive) between the LEO receiver and the occulted GPS satellite,
- $\delta E_{l,L_i,\varphi}(t_k)$ is the LEO receiver hardware phase delay,
- $\delta E^{o}_{L_i,\varphi}(t_k)$ is the occulted GPS satellite hardware phase delay,
- $\delta M^{o}_{l,L_i,\varphi}(t_k)$ is the multipath delay between the LEO receiver and the occulted GPS satellite,
- $\epsilon^{o}_{l,L_i,\varphi}(t_k)$ is the unmodeled error,
- $\rho^{o}_{l}(t_{r,k})$ is the distance traveled by the signal between the instants of signal emission and reception, or *topocentric distance*.

To remove the LEO clock error the phase single difference is computed: the phase observable of a second link, called "reference" link, is subtracted to the phase observable of the LEO occulted GPS link, the "occultation" link. The main feature of the reference link is that, if the reference satellite is chosen sufficiently high, it is not affected by tropospheric delay, since the reference GPS satellite is higher than LEO. The basic phase observable equation for the reference link is:

$$\varphi^{r}_{l,L_i}(t_k) = \frac{f_i}{c}\rho^{r}_{l}(t_k) - f_i dt_l + f_i\, dt^r + N^{r}_{l,L_i,\varphi} + \delta I^{r}_{l,L_i,\varphi}(t_k) + \delta^{r}_{l,L_i,\varphi}(t_k) + \epsilon^{r}_{l,L_i,\varphi}(t_k) \tag{5.2.6}$$

The phase observable single difference equation is

$$\begin{aligned}\varphi^{o-r}_{l,L_i}(t_k) &\equiv \varphi^{o}_{l,L_i}(t_k) - \varphi^{r}_{l,L_i}(t_k) \\ &= \frac{f_i}{c}\left[\rho^{o}_{l}(t_k) - \rho^{r}_{l}(t_k)\right] + f_i\,(dt^o - dt^r) + N^{o}_{l,L_i,\varphi} - N^{o}_{l,L_i,\varphi} + \delta I^{o}_{l,L_i,\varphi}(t_k) - \delta I^{r}_{l,L_i,\varphi}(t_k) \\ &\quad + \frac{f_i}{c}\delta T^{o}_{l}(t_k) + \delta^{o-r}_{l,L_i,\varphi}(t_k) + \epsilon^{o-r}_{l,L_i,\varphi}(t_k) \\ &= \frac{f_i}{c}\rho^{o-r}_{l}(t_k) + f_i dt^{o-r} + N^{o-r}_{l,L_i,\varphi} + \delta I^{o}_{l,L_i,\varphi}(t_k) - \delta I^{r}_{l,L_i,\varphi}(t_k) \\ &\quad + \frac{f_i}{c}\delta T^{o}_{l}(t_k) + \delta^{o-r}_{l,L_i,\varphi}(t_k) + \epsilon^{o-r}_{l,L_i,\varphi}(t_k),\end{aligned} \tag{5.2.7}$$

where

$$\rho^{o-r}_{l}(t_k) = \rho^{o}_{l}(t_k) - \rho^{r}_{l}(t_k) \tag{5.2.8}$$

$$N^{o-r}_{l,L_i,\varphi} = N^{o}_{l,L_i,\varphi} - N^{r}_{l,L_i,\varphi} \tag{5.2.9}$$

$$\delta I^{o-r}_{l,L_i,\varphi}(t_k) = \delta I^{o}_{l,L_i,\varphi}(t_k) - \delta I^{r}_{l,L_i,\varphi}(t_k) \tag{5.2.10}$$

$$\delta^{o-r}_{l,L_i,\varphi}(t_k) = \delta^{o}_{l,L_i,\varphi}(t_k) - \delta^{r}_{l,L_i,\varphi}(t_k) \tag{5.2.11}$$

$$\epsilon^{o-r}_{l,L_i,\varphi}(t_k) = \epsilon^{o}_{l,L_i,\varphi}(t_k) - \epsilon^{r}_{l,L_i,\varphi}(t_k). \tag{5.2.12}$$

The excess phase $E_{L_i,\varphi}$ is then computed as

$$E_{L_i,\varphi} = \varphi^{o-r}_{l,L_i}(t_k) - \frac{f_i}{c}\rho^{o-r}_l(t_k) - f_i dt^{o-r} + \delta I^r_{l,L_i,\varphi}(t_k) \tag{5.2.13}$$

The ionospheric delay of the reference link in equation 5.2.13 is removed by using the geometry free φ_4 combination, since the geometry terms are removed, as the clock error terms and the tropospheric delay. The φ_4 combination is defined in Equation (2.5.45) and reported again in Equation (5.2.14) for convenience

$$\begin{aligned}
\varphi^r_{l,L_4}(t_k) &= \varphi^r_{l,L_1}(t_k) - \frac{f_1}{f_2}\varphi^r_{l,L_2}(t_k) \\
&= \frac{f_1}{c}\rho^r_l(t_k) - f_1 dt_l + f_1\, dt^r + \delta I^r_{l,L_1,\varphi}(t_k) + N^r_{l,L_1,\varphi} + \delta^r_{l,L_1,\varphi}(t_k) + \epsilon^r_{l,L_1,\varphi}(t_k) \\
&\quad - \frac{f_1}{f_2}\left(\frac{f_2}{c}\rho^r_l(t_k) - f_2 dt_l + f_2\, dt^r + \delta I^r_{l,L_2,\varphi}(t_k) + N^r_{l,L_2,\varphi} + \delta^r_{l,L_2,\varphi}(t_k) + \epsilon^r_{l,L_2,\varphi}(t_k)\right) \\
&= \delta I^r_{l,L_1,\varphi}(t_k) - \frac{f_1}{f_2}\delta I^r_{l,L_2,\varphi}(t_k) + N^r_{l,L_1,\varphi} - \frac{f_1}{f_2}N^r_{l,L_2,\varphi} + \delta^r_{l,L_4,\varphi}(t_k) + \epsilon^r_{l,L_4,\varphi}(t_k) \\
&= \delta I^r_{l,L_1,\varphi}(t_k) - \frac{f_1^2}{f_2^2}\delta I^r_{l,L_1,\varphi}(t_k) + N^r_{l,L_1,\varphi} - \frac{f_1}{f_2}N^r_{l,L_2,\varphi} + \delta^r_{l,L_4,\varphi}(t_k) + \epsilon^r_{l,L_4,\varphi}(t_k) \\
&= \left(1 - \frac{f_1^2}{f_2^2}\right)\delta I^r_{l,L_1,\varphi}(t_k) + N^r_{l,L_4,\varphi} + \delta^r_{l,L_4,\varphi}(t_k) + \epsilon^r_{l,L_4,\varphi}(t_k),
\end{aligned} \tag{5.2.14}$$

where

$$N^p_{k,L_4,\varphi} = N^p_{k,L_1,\varphi} - \frac{f_1}{f_2}N^p_{k,L_2,\varphi}, \tag{5.2.15}$$

$$\delta^p_{k,L_4,\varphi}(t_k) = \delta^p_{k,L_1,\varphi}(t_k) - \frac{f_1}{f_2}\delta^p_{k,L_2,\varphi}(t_k), \tag{5.2.16}$$

$$\epsilon^p_{k,L_4,\varphi}(t_k) = \epsilon^p_{k,L_1,\varphi}(t_k) - \frac{f_1}{f_2}\epsilon^p_{k,L_2,\varphi}(t_k). \tag{5.2.17}$$

Hence, the ionospheric delay affecting the reference link can be computed as

$$\delta I^r_{l,L_1,\varphi}(t_k) = \frac{\varphi^r_{l,L_4}(t_k) - N^r_{l,L_4,\varphi} - \delta^r_{l,L_4,\varphi}(t_k) - \epsilon^r_{l,L_4,\varphi}(t_k)}{\left(1 - \frac{f_1^2}{f_2^2}\right)}, \tag{5.2.18}$$

$$\delta I^r_{l,L_2,\varphi}(t_k) = \frac{f_1}{f_2}\delta I^r_{l,L_1,\varphi}(t_k) = \frac{f_1}{f_2}\frac{\varphi^r_{l,L_4}(t_k) - N^r_{l,L_4,\varphi} - \delta^r_{l,L_4,\varphi}(t_k) - \epsilon^r_{l,L_4,\varphi}(t_k)}{\left(1 - \frac{f_1^2}{f_2^2}\right)}, \tag{5.2.19}$$

and the *ionospheric function* $I^r_{l,L_i,\varphi}(t_k)$ is expressed as

$$I^r_{l,L_1,\varphi}(t_k) = \frac{\varphi^r_{l,L_4}(t_k)}{\left(1 - \frac{f_1^2}{f_2^2}\right)} = \delta I^r_{l,L_1,\varphi}(t_k) + \frac{N^r_{l,L_4,\varphi} + \delta^r_{l,L_4,\varphi}(t_k) + \epsilon^r_{l,L_4,\varphi}(t_k)}{\left(1 - \frac{f_1^2}{f_2^2}\right)} \tag{5.2.20}$$

$$\begin{aligned}
I^r_{l,L_2,\varphi}(t_k) &= \frac{f_1}{f_2}I^r_{l,L_1,\varphi}(t_k) = \frac{f_1}{f_2}\frac{\varphi^r_{l,L_4}(t_k)}{\left(1 - \frac{f_1^2}{f_2^2}\right)} \\
&= \frac{f_1}{f_2}\delta I^r_{l,L_1,\varphi}(t_k) + \frac{f_1}{f_2}\frac{N^r_{l,L_4,\varphi} + \delta^r_{l,L_4,\varphi}(t_k) + \epsilon^r_{l,L_4,\varphi}(t_k)}{\left(1 - \frac{f_1^2}{f_2^2}\right)} \\
&= \delta I^r_{l,L_2,\varphi}(t_k) + \frac{f_1}{f_2}\frac{N^r_{l,L_4,\varphi} + \delta^r_{l,L_4,\varphi}(t_k) + \epsilon^r_{l,L_4,\varphi}(t_k)}{\left(1 - \frac{f_1^2}{f_2^2}\right)}
\end{aligned} \tag{5.2.21}$$

The excess phase is finally expressed as

$$\begin{aligned} E_{L_1,\varphi} = {} & \frac{f_1}{c}\delta T_l^o(t_k) + \delta I_{l,L_1,\varphi}^o(t_k) + N_{l,L_1,\varphi}^{o-r} + \delta_{l,L_1,\varphi}^{o-r}(t_k) + \epsilon_{l,L_1,\varphi}^{o-r}(t_k) \\ & + \frac{N_{l,L_4,\varphi}^r + \delta_{l,L_4,\varphi}^r(t_k) + \epsilon_{l,L_4,\varphi}^r(t_k)}{\left(1 - \frac{f_1^2}{f_2^2}\right)}. \end{aligned} \tag{5.2.22}$$

$$\begin{aligned} E_{L_2,\varphi} = {} & \frac{f_2}{c}\delta T_l^o(t_k) + \delta I_{l,L_2,\varphi}^o(t_k) + N_{l,L_2,\varphi}^{o-r} + \delta_{l,L_2,\varphi}^{o-r}(t_k) + \epsilon_{l,L_2,\varphi}^{o-r}(t_k) \\ & + \frac{f_1}{f_2}\frac{N_{l,L_4,\varphi}^r + \delta_{l,L_4,\varphi}^r(t_k) + \epsilon_{l,L_4,\varphi}^r(t_k)}{\left(1 - \frac{f_1^2}{f_2^2}\right)}. \end{aligned} \tag{5.2.23}$$

Besides the tropospheric and ionospheric delays of the occulted link, the excess phase contains also the ambiguities and the multipath delays. Since the excess phase is used only to obtain its time derivative, the excess doppler, the ambiguities contained in equation **??** will be eliminated by differencing while the other terms are considered quite small and therefore negligible.

5.2.2. Excess Phase in Units of Length

The excess phase can be computed also with the carrier phase observable expressed in meters. Then, carrier phase observable equation becomes

$$\begin{aligned} F_{l,L_i}^o(t_k) &= \rho_l^o(t_k) - cdt_l + f_i\, dt^o + N_{l,L_i,F}^o + \delta I_{l,L_i,F}^o(t_k) + \delta T_l^o(t_k) + \delta_{l,L_i,F}^o(t_k) + \epsilon_{l,L_i,F}^o(t_k) \\ &= \rho_l^o(t_k) - cdt_l + f_i\, dt^o + N_{l,L_i,P}^o - \delta I_{l,L_i,P}^o(t_k) + \delta T_l^o(t_k) + \delta_{l,L_i,P}^o(t_k) + \epsilon_{l,L_i,P}^o(t_k), \end{aligned} \tag{5.2.24}$$

while for the reference link it becomes

$$\begin{aligned} F_{l,L_i}^r(t_k) &= \rho_l^r(t_k) - cdt_l + f_i\, dt^r + N_{l,L_i,F}^r + \delta I_{l,L_i,F}^r(t_k) + \delta_{l,L_i,F}^r(t_k) + \epsilon_{l,L_i,F}^r(t_k) \\ &= \rho_l^r(t_k) - cdt_l + f_i\, dt^r + N_{l,L_i,P}^r - \delta I_{l,L_i,P}^r(t_k) + \delta_{l,L_i,P}^r(t_k) + \epsilon_{l,L_i,P}^o(t_k). \end{aligned} \tag{5.2.25}$$

The phase observable single difference equation becomes

$$\begin{aligned} F_{l,L_i}^{o-r}(t_k) &\equiv F_{l,L_i}^o(t_k) - F_{l,L_i}^r(t_k) \\ &= \rho_l^o(t_k) - \rho_l^r(t_k) + c\,(dt^o - dt^r) + N_{l,L_i,F}^o - N_{l,L_i,F}^r + \delta I_{l,L_i,F}^o(t_k) - \delta I_{l,L_i,F}^r(t_k) \\ &\quad + \delta T_l^o(t_k) + \delta_{l,L_i,F}^{o-r}(t_k) + \epsilon_{l,L_i,F}^{o-r}(t_k) \\ &= \rho_l^o(t_k) - \rho_l^r(t_k) + c\,(dt^o - dt^r) + N_{l,L_i,P}^o - N_{l,L_i,P}^r - \delta I_{l,L_i,P}^o(t_k) + \delta I_{l,L_i,P}^r(t_k) \\ &\quad + \delta T_l^o(t_k) + \delta_{l,L_i,P}^{o-r}(t_k) + \epsilon_{l,L_i,P}^{o-r}(t_k) \\ &= \rho_l^{o-r}(t_k) + cdt^{o-r} + N_{l,L_i,F}^{o-r} + \delta I_{l,L_i,F}^o(t_k) - \delta I_{l,L_i,F}^r(t_k) + \delta T_l^o(t_k) \\ &\quad + \delta_{l,L_i,F}^{o-r}(t_k) + \epsilon_{l,L_i,F}^{o-r}(t_k) \\ &= \rho_l^{o-r}(t_k) + cdt^{o-r} + N_{l,L_i,P}^{o-r} - \delta I_{l,L_i,P}^o(t_k) + \delta I_{l,L_i,P}^r(t_k) + \delta T_l^o(t_k) \\ &\quad + \delta_{l,L_i,P}^{o-r}(t_k) + \epsilon_{l,L_i,P}^{o-r}(t_k), \end{aligned} \tag{5.2.26}$$

and then the excess phase computation becomes

$$\begin{aligned} E_{L_i,P} &= F_{l,L_i}^{o-r}(t_k) - \rho_l^{o-c}(t_k) - c\, dt^{o-r} + \delta I_{l,L_i,F}^r(t_k) \\ &= F_{l,L_i}^{o-r}(t_k) - \rho_l^{o-c}(t_k) - c\, dt^{o-r} - \delta I_{l,L_i,P}^r(t_k), \end{aligned} \tag{5.2.27}$$

where

$$F_{l,L_i}^{o-r}(t_k) = \lambda_i \varphi_{l,L_i}^{o-r}(t_k). \tag{5.2.28}$$

The ionospheric delay of the reference link in equation 5.2.27 is removed by using the geometry free combination $F^r_{l,L_4}(t_k)$, defined in Equation (2.5.34) and reported again in Equation (5.2.30)

$$\begin{aligned} F^r_{l,L_4}(t_k) &= F^r_{l,L_1}(t_k) - F^r_{l,L_2}(t_k) \\ &= \rho^r_l(t_k) - cdt_l + c\,dt^r + \delta I^r_{l,L_1,F}(t_k) + N^r_{l,L_1,F} + \delta^r_{l,L_1,F}(t_k) + \epsilon^r_{l,L_1,F}(t_k) \\ &\quad - \rho^r_l(t_k) + cdt_l - c\,dt^r - \delta I^r_{l,L_2,F}(t_k) - N^r_{l,L_2,F} - \delta^r_{l,L_2,F}(t_k) - \epsilon^r_{l,L_2,F}(t_k) \\ &= \rho^r_l(t_k) - cdt_l + c\,dt^r - \delta I^r_{l,L_1,P}(t_k) + N^r_{l,L_1,P} + \delta^r_{l,L_1,P}(t_k) + \epsilon^r_{l,L_1,P}(t_k) \\ &\quad - \rho^r_l(t_k) + cdt_l - c\,dt^r + \delta I^r_{l,L_2,P}(t_k) - N^r_{l,L_2,P} - \delta^r_{l,L_2,P}(t_k) - \epsilon^r_{l,L_2,P}(t_k), \end{aligned} \tag{5.2.29}$$

that simplifying the equal terms becomes

$$\begin{aligned} F^r_{l,L_4}(t_k) &= \delta I^r_{l,L_1,F}(t_k) - \delta I^r_{l,L_2,F}(t_k) + N^r_{l,L_1,F} - N^r_{l,L_2,F} + \delta^r_{l,L_4,F}(t_k) + \epsilon^r_{l,L_4,F}(t_k) \\ &= \delta I^r_{l,L_2,P}(t_k) - \delta I^r_{l,L_1,P}(t_k) + N^r_{l,L_1,P} - N^r_{l,L_2,P} + \delta^r_{l,L_4,P}(t_k) + \epsilon^r_{l,L_4,P}(t_k) \\ &= \delta I^r_{l,L_1,F}(t_k) - \frac{f_1^2}{f_2^2}\delta I^r_{l,L_1,F}(t_k) + N^r_{l,L_1,F} - N^r_{l,L_2,F} + \delta^r_{l,L_4,F}(t_k) + \epsilon^r_{l,L_4,F}(t_k) \\ &= \frac{f_1^2}{f_2^2}\delta I^r_{l,L_1,P}(t_k) - \delta I^r_{l,L_1,P}(t_k) + N^r_{l,L_1,P} - N^r_{l,L_2,P} + \delta^r_{l,L_4,P}(t_k) + \epsilon^r_{l,L_4,P}(t_k) \\ &= \left(1 - \frac{f_1^2}{f_2^2}\right)\delta I^r_{l,L_1,F}(t_k) + N^r_{l,L_4,F} + \delta^r_{l,L_4,F}(t_k) + \epsilon^r_{l,L_4,F}(t_k) \\ &= \left(\frac{f_1^2}{f_2^2} - 1\right)\delta I^r_{l,L_1,P}(t_k) + N^r_{l,L_4,P} + \delta^r_{l,L_4,P}(t_k) + \epsilon^r_{l,L_4,P}(t_k). \end{aligned} \tag{5.2.30}$$

where

$$N^p_{k,L_4,P} = N^p_{k,L_1,P} - N^p_{k,L_2,P}, \tag{5.2.31}$$

$$\delta^p_{k,L_4,P}(t_k) = \delta^p_{k,L_1,P}(t_k) - \delta^p_{k,L_2,P}(t_k), \tag{5.2.32}$$

$$\epsilon^p_{k,L_4,P}(t_k) = \epsilon^p_{k,L_1,P}(t_k) - \epsilon^p_{k,L_2,P}(t_k). \tag{5.2.33}$$

In this case, the ionospheric delay affecting the reference link can be computed as

$$\delta I^r_{l,L_1,P}(t_k) = \frac{F^r_{l,L_4}(t_k) - N^r_{l,L_4,P} - \delta^r_{l,L_4,P}(t_k) - \epsilon^r_{l,L_4,P}(t_k)}{\left(\frac{f_1^2}{f_2^2} - 1\right)}, \tag{5.2.34}$$

$$\delta I^r_{l,L_1,F}(t_k) = \frac{F^r_{l,L_4}(t_k) - N^r_{l,L_4,F} - \delta^r_{l,L_4,F}(t_k) - \epsilon^r_{l,L_4,F}(t_k)}{\left(1 - \frac{f_1^2}{f_2^2}\right)}, \tag{5.2.35}$$

$$\delta I^r_{l,L_2,P}(t_k) = \frac{f_1^2}{f_2^2}\delta I^r_{l,L_1,P}(t_k) = \frac{f_1^2}{f_2^2}\frac{F^r_{l,L_4}(t_k) - N^r_{l,L_4,P} - \delta^r_{l,L_4,P}(t_k) - \epsilon^r_{l,L_4,P}(t_k)}{\left(\frac{f_1^2}{f_2^2} - 1\right)}, \tag{5.2.36}$$

$$\delta I^r_{l,L_2,F}(t_k) = \frac{f_1^2}{f_2^2}\delta I^r_{l,L_1,F}(t_k) = \frac{f_1^2}{f_2^2}\frac{F^r_{l,L_4}(t_k) - N^r_{l,L_4,F} - \delta^r_{l,L_4,F}(t_k) - \epsilon^r_{l,L_4,F}(t_k)}{\left(1 - \frac{f_1^2}{f_2^2}\right)}, \tag{5.2.37}$$

and the *ionospheric function* $I^r_{l,L_i,P}(t_k)$ is expressed as

$$I^r_{l,L_1,P}(t_k) = \frac{F^r_{l,L_4}(t_k)}{\left(\frac{f_1^2}{f_2^2}-1\right)} = \delta I^r_{l,L_1,P}(t_k) + \frac{N^r_{l,L_4,P} + \delta^r_{l,L_4,P}(t_k) + \epsilon^r_{l,L_4,P}(t_k)}{\left(\frac{f_1^2}{f_2^2}-1\right)} \tag{5.2.38}$$

$$I^r_{l,L_1,F}(t_k) = \frac{F^r_{l,L_4}(t_k)}{\left(1-\frac{f_1^2}{f_2^2}\right)} = \delta I^r_{l,L_1,F}(t_k) + \frac{N^r_{l,L_4,F} + \delta^r_{l,L_4,F}(t_k) + \epsilon^r_{l,L_4,F}(t_k)}{\left(1-\frac{f_1^2}{f_2^2}\right)} \tag{5.2.39}$$

$$\begin{aligned} I^r_{l,L_2,P}(t_k) &= \frac{f_1^2}{f_2^2} I^r_{l,L_1,P}(t_k) = \frac{f_1^2}{f_2^2}\frac{F^r_{l,L_4}(t_k)}{\left(\frac{f_1^2}{f_2^2}-1\right)} \\ &= \frac{f_1^2}{f_2^2}\delta I^r_{l,L_1,P}(t_k) + \frac{f_1^2}{f_2^2}\frac{N^r_{l,L_4,P} + \delta^r_{l,L_4,P}(t_k) + \epsilon^r_{l,L_4,P}(t_k)}{\left(\frac{f_1^2}{f_2^2}-1\right)} \\ &= \delta I^r_{l,L_2,P}(t_k) + \frac{f_1^2}{f_2^2}\frac{N^r_{l,L_4,P} + \delta^r_{l,L_4,P}(t_k) + \epsilon^r_{l,L_4,P}(t_k)}{\left(\frac{f_1^2}{f_2^2}-1\right)} \end{aligned} \tag{5.2.40}$$

$$\begin{aligned} I^r_{l,L_2,F}(t_k) &= \frac{f_1^2}{f_2^2} I^r_{l,L_1,F}(t_k) = \frac{f_1^2}{f_2^2}\frac{F^r_{l,L_4}(t_k)}{\left(1-\frac{f_1^2}{f_2^2}\right)} \\ &= \frac{f_1^2}{f_2^2}\delta I^r_{l,L_1,F}(t_k) + \frac{f_1^2}{f_2^2}\frac{N^r_{l,L_4,F} + \delta^r_{l,L_4,F}(t_k) + \epsilon^r_{l,L_4,F}(t_k)}{\left(1-\frac{f_1^2}{f_2^2}\right)} \\ &= \delta I^r_{l,L_2,F}(t_k) + \frac{f_1^2}{f_2^2}\frac{N^r_{l,L_4,F} + \delta^r_{l,L_4,F}(t_k) + \epsilon^r_{l,L_4,F}(t_k)}{\left(1-\frac{f_1^2}{f_2^2}\right)} \end{aligned} \tag{5.2.41}$$

and the excess phase is finally expressed as

$$\begin{aligned} E_{L_1,P} = {} & \delta T^o_l(t_k) - \delta I^o_{l,L_1,P}(t_k) + N^{o-r}_{l,L_1,P} + \delta^{o-r}_{l,L_1,P}(t_k) + \epsilon^{o-r}_{l,L_1,P}(t_k) \\ & - \frac{N^r_{l,L_4,P} + \delta^r_{l,L_4,P}(t_k) + \epsilon^r_{l,L_4,P}(t_k)}{\left(\frac{f_1^2}{f_2^2}-1\right)}, \end{aligned} \tag{5.2.42}$$

$$\begin{aligned} E_{L_1,F} = {} & \delta T^o_l(t_k) + \delta I^o_{l,L_1,F}(t_k) + N^{o-r}_{l,L_1,F} + \delta^{o-r}_{l,L_1,F}(t_k) + \epsilon^{o-r}_{l,L_1,F}(t_k) \\ & - \frac{N^r_{l,L_4,F} + \delta^r_{l,L_4,F}(t_k) + \epsilon^r_{l,L_4,F}(t_k)}{\left(\frac{f_1^2}{f_2^2}-1\right)}, \end{aligned} \tag{5.2.43}$$

$$\begin{aligned} E_{L_2,P} = {} & \delta T^o_l(t_k) - \delta I^o_{l,L_2,P}(t_k) + N^{o-r}_{l,L_2,P} + \delta^{o-r}_{l,L_2,P}(t_k) + \epsilon^{o-r}_{l,L_2,P}(t_k) \\ & - \frac{f_1^2}{f_2^2}\frac{N^r_{l,L_4,P} + \delta^r_{l,L_4,P}(t_k) + \epsilon^r_{l,L_4,P}(t_k)}{\left(\frac{f_1^2}{f_2^2}-1\right)}, \end{aligned} \tag{5.2.44}$$

$$\begin{aligned} E_{L_2,F} = {} & \delta T^o_l(t_k) + \delta I^o_{l,L_2,F}(t_k) + N^{o-r}_{l,L_2,F} + \delta^{o-r}_{l,L_2,F}(t_k) + \epsilon^{o-r}_{l,L_2,F}(t_k) \\ & - \frac{f_1^2}{f_2^2}\frac{N^r_{l,L_4,F} + \delta^r_{l,L_4,F}(t_k) + \epsilon^r_{l,L_4,F}(t_k)}{\left(\frac{f_1^2}{f_2^2}-1\right)}, \end{aligned} \tag{5.2.45}$$

Also in Equation (5.2.42), (5.2.43), (5.2.44), (5.2.45), besides the tropospheric and ionospheric delays of the occulted link, the excess phase contains the ambiguities and the multipath delays, that also in this case will be respectively eliminated and ignored.

5.2.3. L_1 and L_2 Excess Phase Differentiation w.r.t. the Geometry Free Combination

The calculation of the L_1 and L_2 excess phase difference is realized to verify the goodness of the excess phase computation formula obtained in section (5.2.2). This difference is expressed as

$$\begin{aligned}
E_{L_4,P} &= E_{L_1,P} - E_{L_2,P} \\
&= F^{o-r}_{l,L_1}(t_k) - \rho^{o-c}_l(t_k) - c\,dt^{o-r} - I^r_{l,L_1,P}(t_k) \\
&\quad - F^{o-r}_{l,L_2}(t_k) + \rho^{o-c}_l(t_k) + c\,dt^{o-r} + I^r_{l,L_2}(t_k) \\
&= \rho^{o-r}_l(t_k) + cdt^{o-r} + N^{o-r}_{l,L_1,P} - \delta I^o_{l,L_1,P}(t_k) \\
&\quad + \delta T^o_l(t_k) + \delta^{o-r}_{l,L_1,P}(t_k) + \epsilon^{o-r}_{l,L_1,P}(t_k) \\
&\quad - \rho^{o-r}_l(t_k) - cdt^{o-r} - N^{o-r}_{l,L_2,P} + \delta I^o_{l,L_2,P}(t_k) \\
&\quad - \delta T^o_l(t_k) - \delta^{o-r}_{l,L_2,P}(t_k) - \epsilon^{o-r}_{l,L_2,P}(t_k) \\
&= N^{o-r}_{l,L_1,P} - N^{o-r}_{l,L_2,P} - \delta I^o_{l,L_1,P}(t_k) + \delta I^o_{l,L_2,P}(t_k) \\
&\quad + \delta^{o-r}_{l,L_1,P}(t_k) - \delta^{o-r}_{l,L_2,P}(t_k) + \epsilon^{o-r}_{l,L_1,P}(t_k) - \epsilon^{o-r}_{l,L_2,P}(t_k) \\
&= \left(\frac{f_1^2}{f_2^2} - 1\right) \delta I^o_{l,L_1,P}(t_k) + N^{o-r}_{l,L_1,P} - N^{o-r}_{l,L_2,P} \\
&\quad + \delta^{o-r}_{l,L_1,P}(t_k) - \delta^{o-r}_{l,L_2,P}(t_k) + \epsilon^{o-r}_{l,L_1,P}(t_k) - \epsilon^{o-r}_{l,L_2,P}(t_k) \\
&= \left(\frac{f_1^2}{f_2^2} - 1\right) \delta I^o_{l,L_1,P}(t_k) + N^{o-r}_{l,L_1,P} - N^{o-r}_{l,L_2,P} \\
&\quad + \delta^o_{l,L_4,P}(t_k) - \delta^r_{l,L_4,P}(t_k) + \epsilon^o_{l,L_4,P}(t_k) - \epsilon^r_{l,L_4,P}(t_k).
\end{aligned} \tag{5.2.46}$$

The geometry-free combination instead gives, as already obtained in Equation (5.2.30),

$$F^o_{l,L_4}(t_k) = F^o_{l,L_1}(t_k) - F^o_{l,L_2}(t_k) = \left(\frac{f_1^2}{f_2^2} - 1\right) \delta I^o_{l,L_1,P}(t_k) + N^o_{l,L_4,P} + \delta^o_{l,L_4,P}(t_k) + \epsilon^o_{l,L_4,P}(t_k). \tag{5.2.47}$$

Then, we obtain that

$$\frac{dE_{L_4,P}}{dt} \simeq \frac{dF^o_{l,L_4}(t_k)}{dt}, \tag{5.2.48}$$

unless of high values for minor effects (multipath, transmitter and receiver electronic delays) and residuals effects on the reference link.

5.3. Table of RO events

TBW

Chapter 6

SWOrD Algorithm Descriptions And Results

"¡Citation¿."

¡Author¿, *'¡Title¿'*

6.1. Introduction

In what follows the algorithms and the strategies implemented in SWOrDwill be illustrated, together with some preliminary results related to the validation activity carried out on the release of SWOrDfor the "Base" Version (see section 1.5) of the ROSA-ROSSA processing chain. The tests have been performed using three days of CHAMP data, from 20 July 2004 to 22 July 2004, which are part of the ROSA ROSSA validation dataset, and one day of GRAS data, 13 October 2007, made available by EUMETSAT. The three days CHAMP data has been used to test the *chain functionality*. The validation using the the results about the tests with GRAS data regards overall the observation pre-processing without any a priori knowledge of the reference orbit. In the end, SWOrDhas been used to process a small set of about seven hours (four orbits) of preliminary (pre-commissioning) ROSA data made available by TAS-I.

6.2. Formation of Zero Difference Observation Arcs

Currently, the POD process is based on ionosphere-free combinations of phase double differences. However, future developments will include the use of ionosphere-free zero difference observables. In this perspective, the software has been developed so that while reading the RINEX files and the observations are inserted into the *Observations* multi-index database by the *Observation_Insertion* class, which at the same time keeps track of satellites that are observed continuously, as explained in section 3.4.2. At every epoch *Observation_Insertion* computes the geometry free, the ionosphere free, the wide lane and the Melborne-Wübbena combinations. It also compute the difference of the geometry free and the Melborne-Wübbena combinations with the same quantities of the previous epoch, if available. If the time differences are higher then a user-defined value (usually one L_1 cycle) then the tracking of the corresponding arc is interrupted. Even if at same epoch a GPS satellite is not present anymore the arc is interrupted. When an arc is interrupted its time length is evaluated w.r.t. a user-defined value (usually 600 seconds) to decide whether to keep the arc or discard it because too short. Figure 6.1, Figure 6.2 and Figure 6.3 show the time differences analysis results for data taken respectively from CHAMP, MetOp/GRAS and Oceansat-2/ROSA missions. From Figure 6.2 it is evident that GRAS data is of very good quality because time differences are always below one L_1

cycle. No comment can be made about ROSA data because this analysis has been performed using a small set of data.

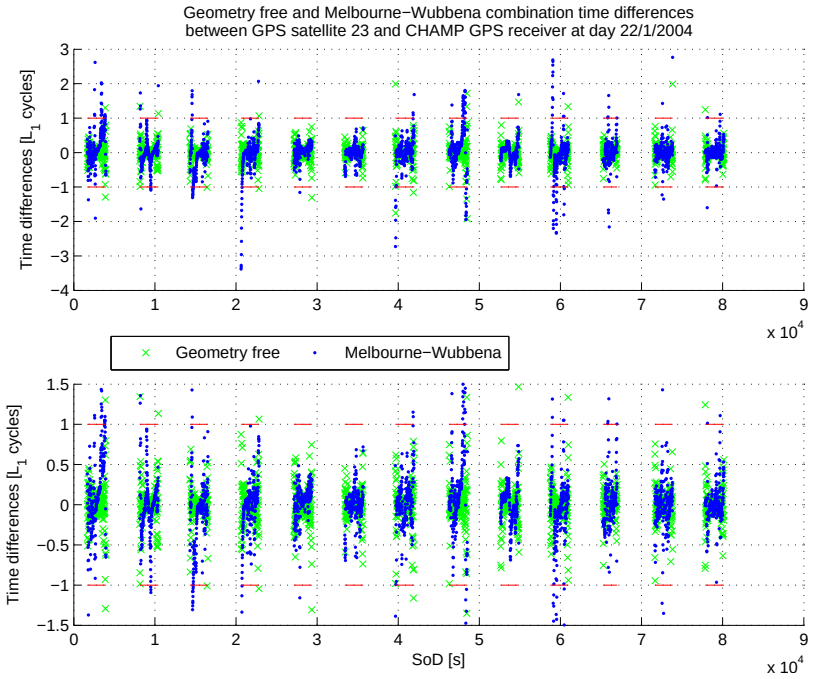

(a) A good link.

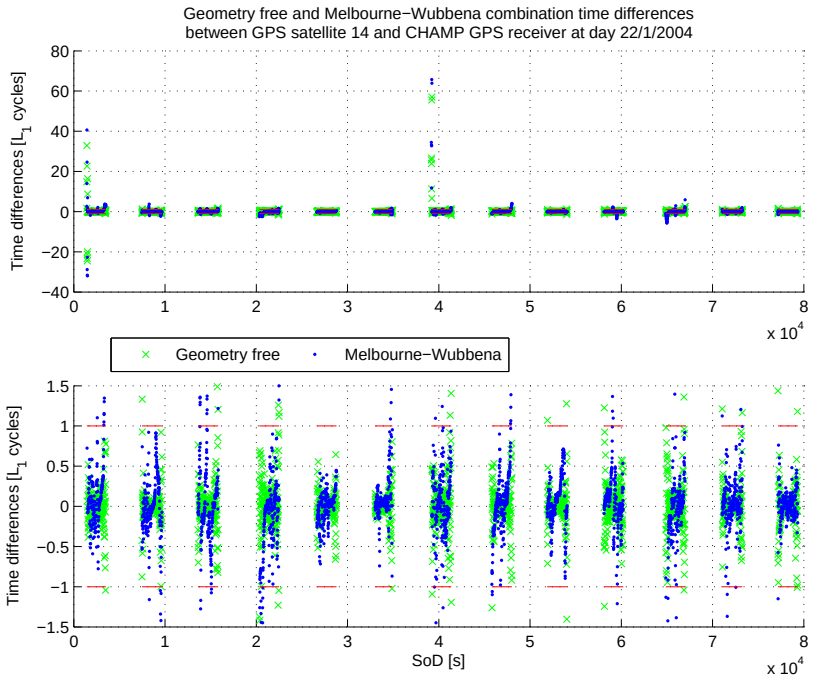

(b) A bad link.

Figure 6.1. Time differences analysis with CHAMP data. The bottom graph of each sub-figure is a zoom around the time difference limit chosen (1 L_1 cycles).

There are a lot of sub-options which allow for the *corrections* of observables for some effects and make a quality check. Observations from both ground stations and orbiting receivers can be corrected for the following effects:

- ionosphere delay,
- receiver clock bias and drift

- transmitter clock bias and drift,
- GPS antenna orientation and center of mass correction,
- orbiting receiver center of mass (knowing the attitude law of the orbiting receiver),
- Ambiguity fixing (obtained without any a priori knowledge of the reference orbit),
- cycle-slips detection.

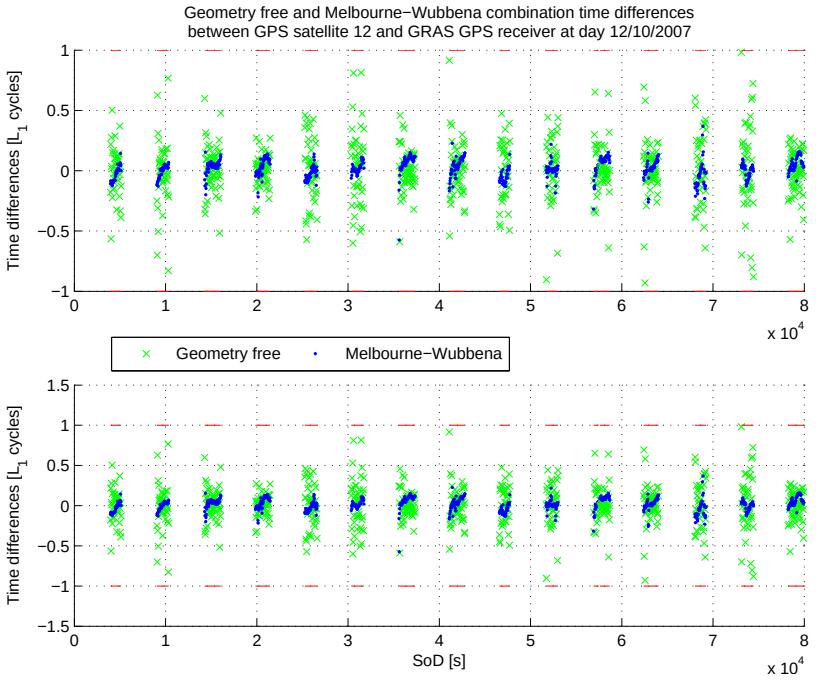

(a) A good link.

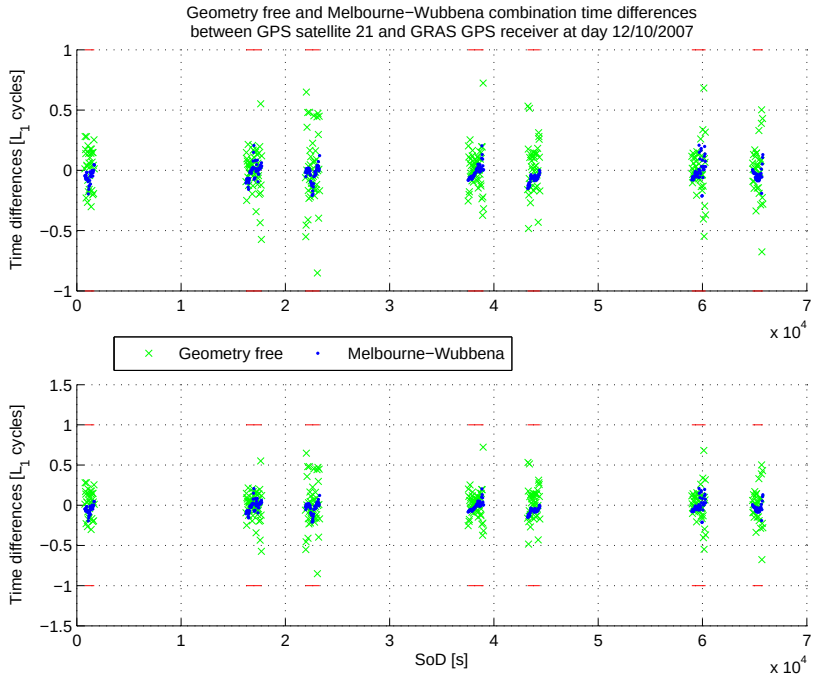

(b) A bad link.

Figure 6.2. Time differences analysis with GRAS data. The bottom graph of each sub-figure is a zoom around the time difference limit chosen (1 L_1 cycles). In this case data have a very good quality and time differences are always below 1 L_1 cycles.

Every time an arc of undifferenced observations is formed adopting the logic described above, it is inserted into the *Zero_Difference_Arcs* multi-index database class, that keeps the information about the pass (its length, which is the receiver, which is the transmitter, iterators to the first and last observation in the database, number of observation contained into the arc and so on). Figure 6.4, 6.5 and 6.6 show a representation of the visibility matrix for the whole day of reference respectively for CHAMP, GRASS and ROSA data.

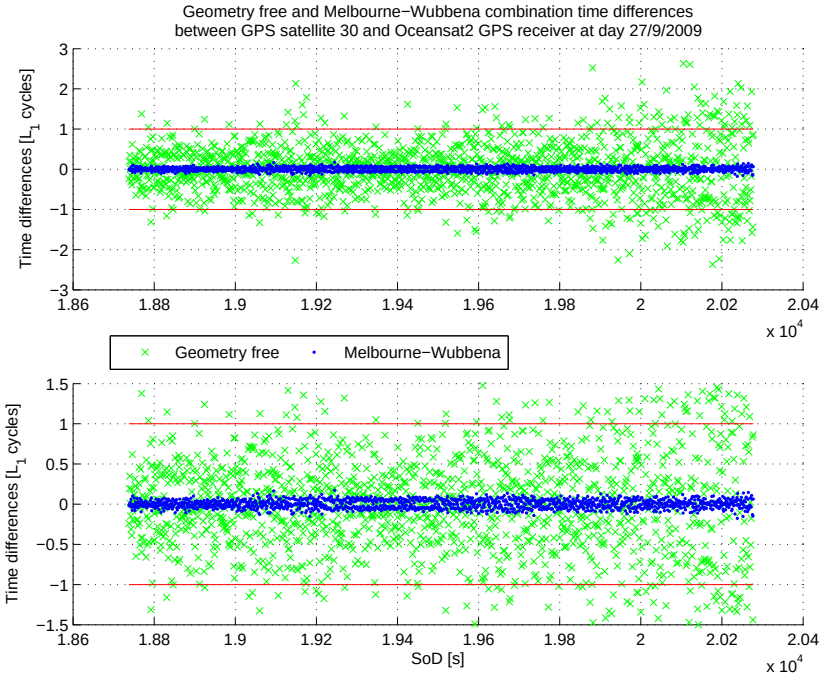

(a) A good link.

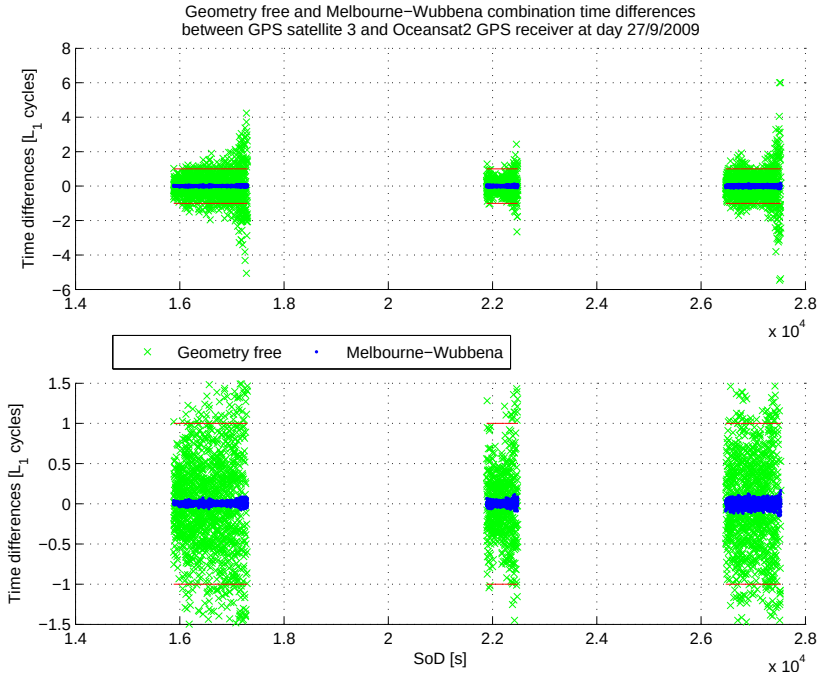

(b) A bad link.

Figure 6.3. Time differences analysis with ROSA data. The bottom graph of each sub-figure is a zoom around the time difference limit chosen (1 L_1 cycles).

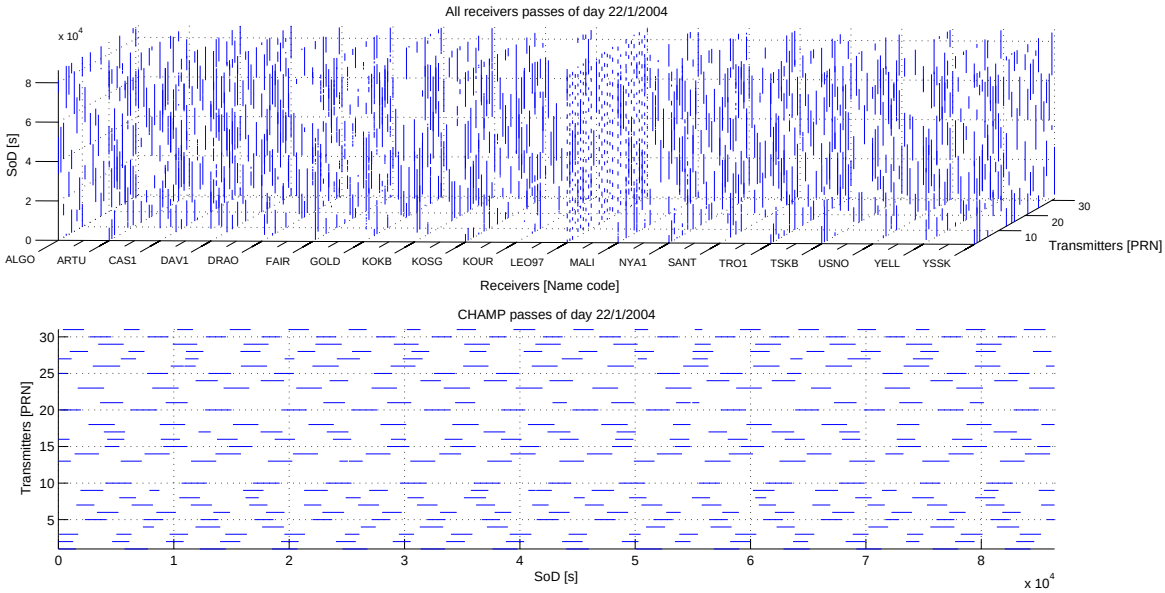

Figure 6.4. Top: Visibility matrix for all the receivers and transmitters involved in the CHAMP data analysis for 22 January 2004. LEO97 is the code name given to the CHAMP GPS receiver. Bottom: visibility plot for the CHAMP receiver.

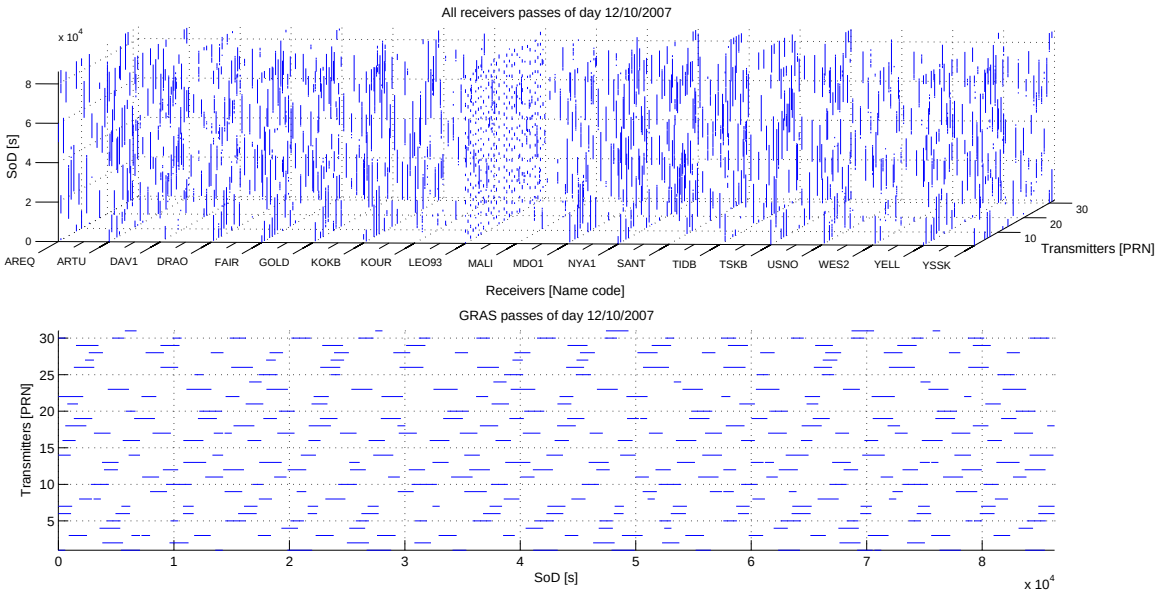

Figure 6.5. Top: Visibility matrix for all the receivers and transmitters involved into the GRAS data analysis for the whole 13 July 2007. LEO93 is the code name given to the GRAS GPS receiver. Bottom: visibility plot for the GRAS receiver.

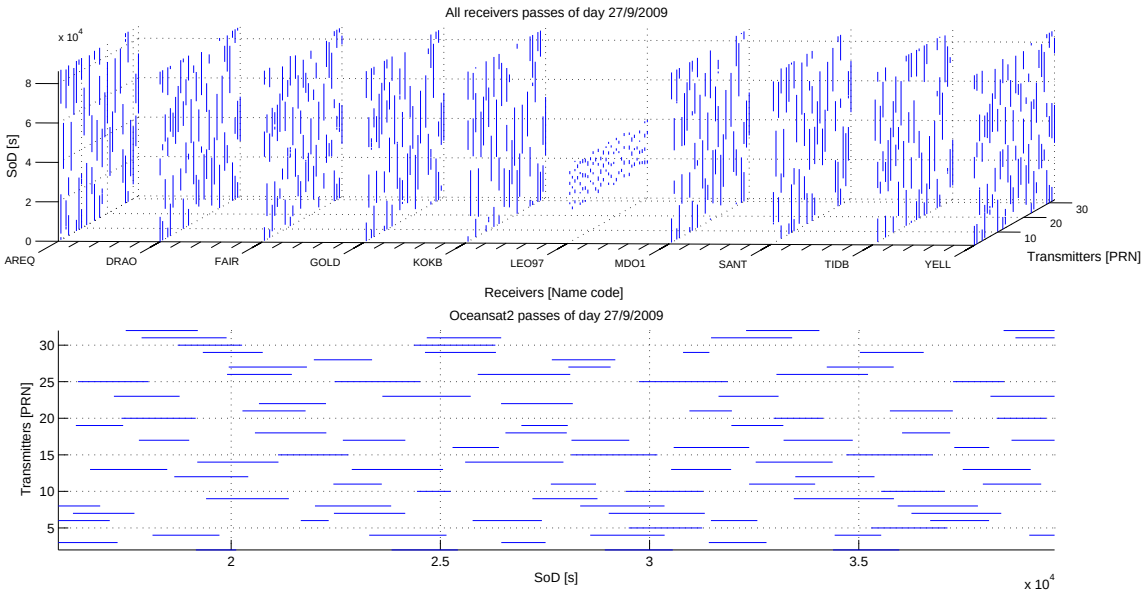

Figure 6.6. Top: Visibility matrix for all the receivers and transmitters involved into the ROSA data analysis for the whole 27 October 2009. LEO97 is the code name given to the ROSA GPS receiver. Bottom: visibility plot for the ROSA receiver. The top figure shows clearly that ROSA data do not cover the whole day so that the statistic refereed to those arcs is not directly comparable with the statistic done for CHAMP and GRAS observations, that instead cover the whole 24 hours of the respective data day.

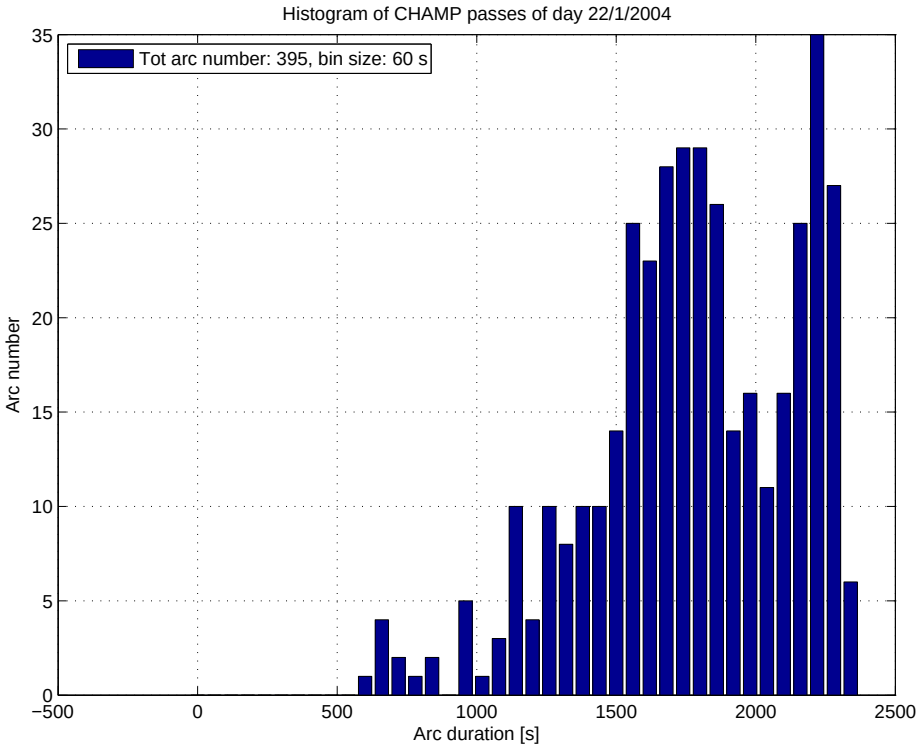

Figure 6.7. Histogram of the undifferenced arc lengths for CHAMP data.

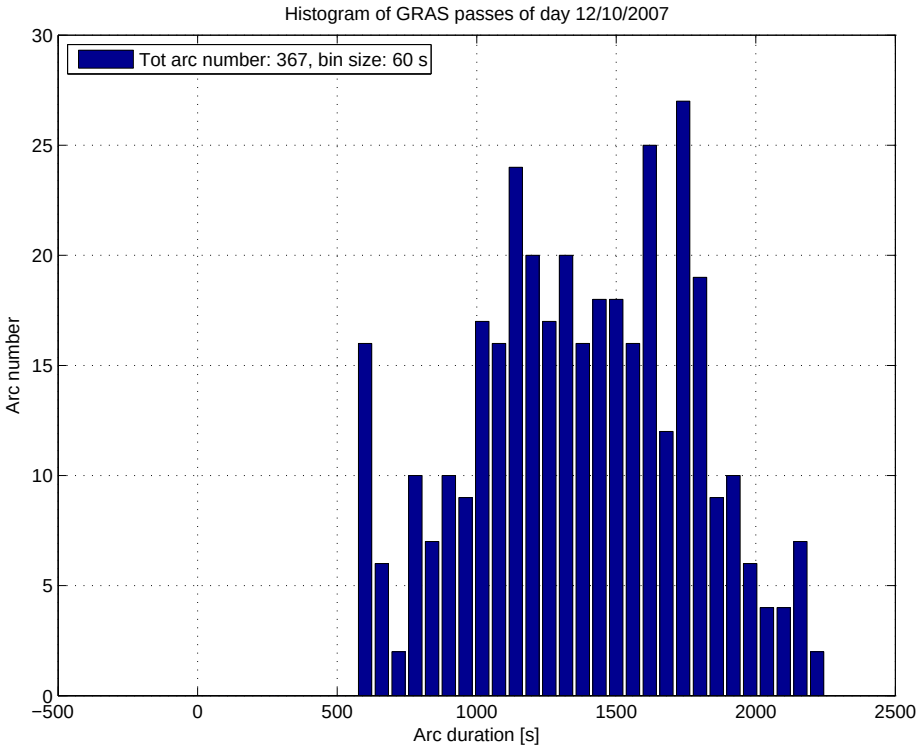

Figure 6.8. Histogram of the undifferenced arc lengths for GRAS data.

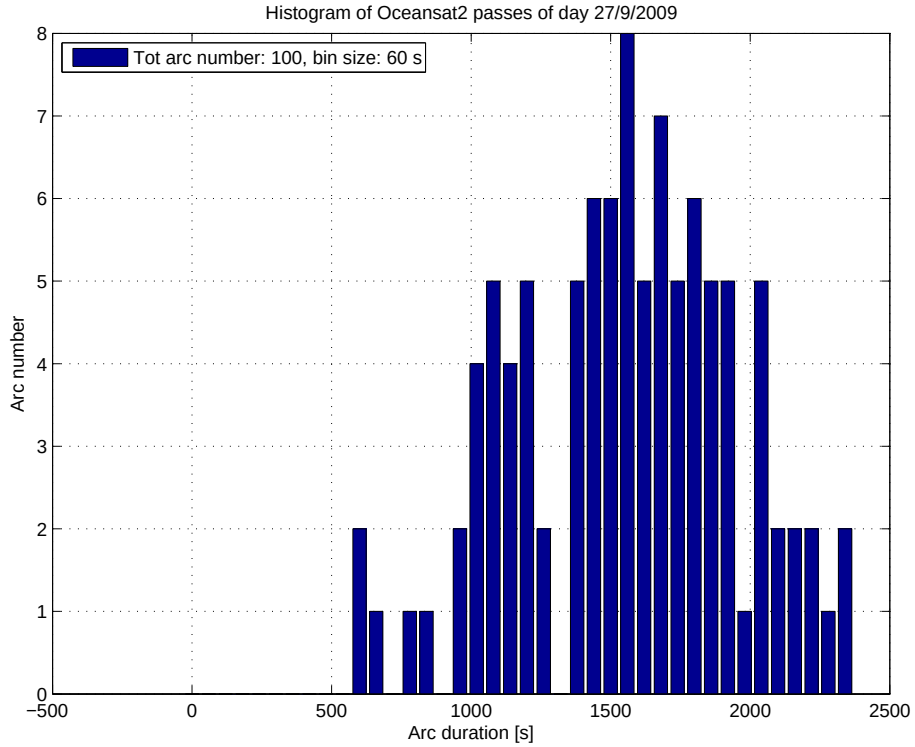

Figure 6.9. Histogram of the undifferenced arc lengths for Oceansat-2 data.

6.3. Formation of Double Difference Observation Arcs

Every time an undifferenced arc is inserted into the multi-index database, this link is the starting point for a search of double differences among the other arcs already inserted. Then, all the arcs that overlap with the starting instant of the arc just inserted are traversed to find out a *double difference path* (see Figure 6.10 for an example of double difference arc).

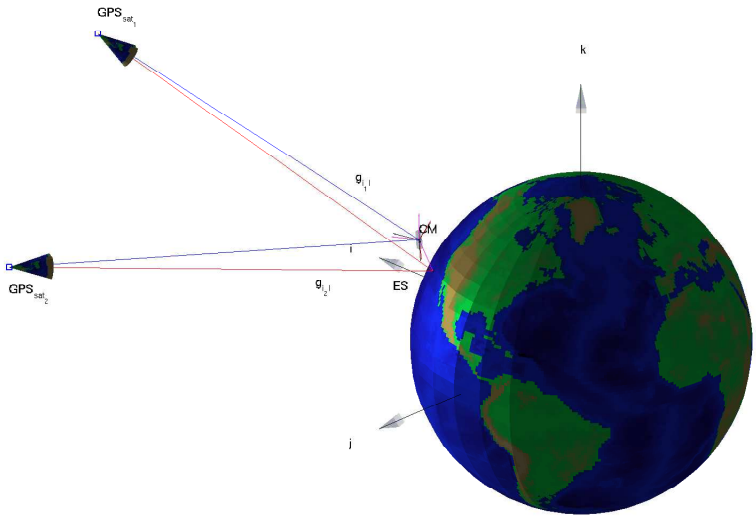

Figure 6.10. Example of typical situation for double difference formation.

If at a given instant a double difference is found, then this arc is maintained for the successive instant up to one of the four undifferenced links that forms the double difference ends. The double difference arc so built is then checked for its time length and inserted, if longer than a user defined parameter, into the *Double_Difference_Arcs* multi-index database class.

Algorithm 1 Linearly Independent Max Length Double Difference Arcs Selection

Starting from a list of zero differenced arcs ordered according to their norm (length) in a red list of red links to be processed and a list of zero differenced arcs ordered according to their norm (length) in an initially empty green list of processed green links
while red list contains at least one red link **do**
  Select the longest red link, as the current green link
  Accept current green link into the green list
  for all the remaining links in the ordered red list **do**
    if current red link overlaps current green link **then**
      Update overlapping list associated with current current green link to contain red link
      Check for independence of red link w.r.t. all overlapping links
      if independent **then**
        do nothing (which means keep the red link in the red list)
      else
        eliminate the red link
      end if
    end if
    Consider the next red link
  end for
end while

See [99, Zin 2001] for details about the algorithm to check the linear independence of overlapping double difference arcs.

Once all the undifferenced and double difference arcs has been found, a linearly independent set of double difference arcs must be kept. This task is done by considering all the double difference arcs found in every instant of the run interval and then, after having ordered them from the longer to the shorter, they are checked using the Algorithm 1.

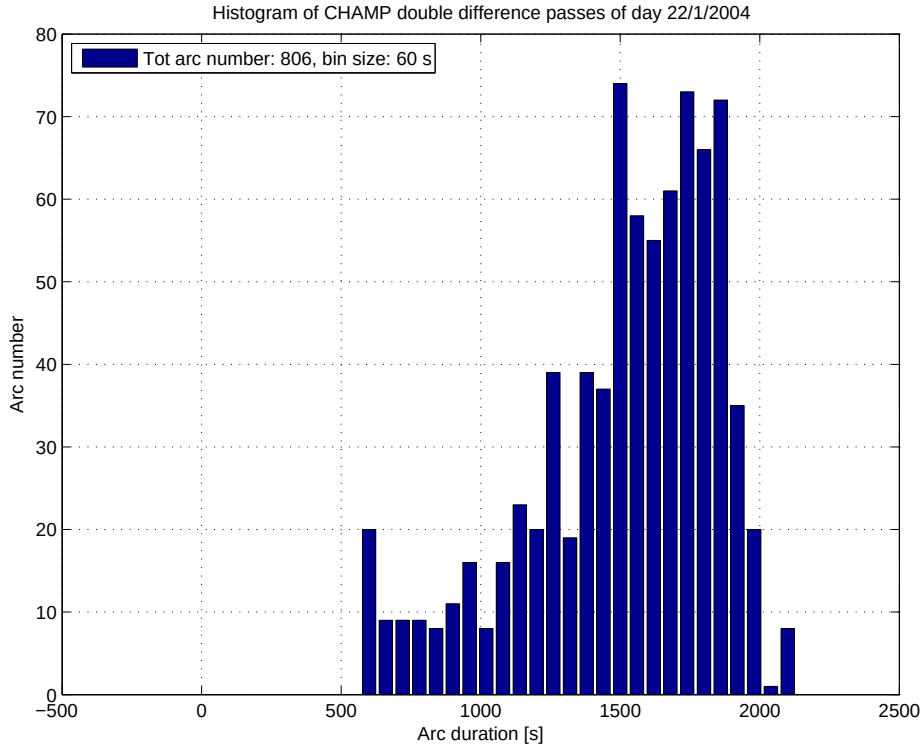

Figure 6.11. Histogram of double difference passes obtained from CHAMP data of day 22 January 2004.

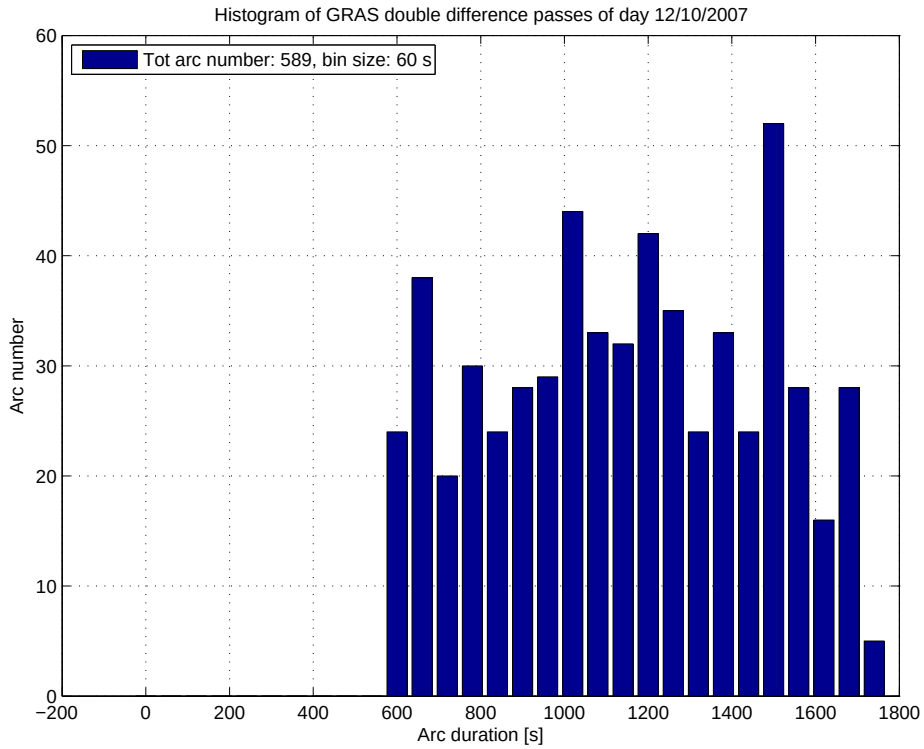

Figure 6.12. Histogram of double difference passes obtained from GRAS data of day 13 October 2007.

Figure 6.11, 6.12 and 6.13 shows the histogram of double difference arc lengths, respectively com-

puted using CHAMP, GRAS and ROSA data.

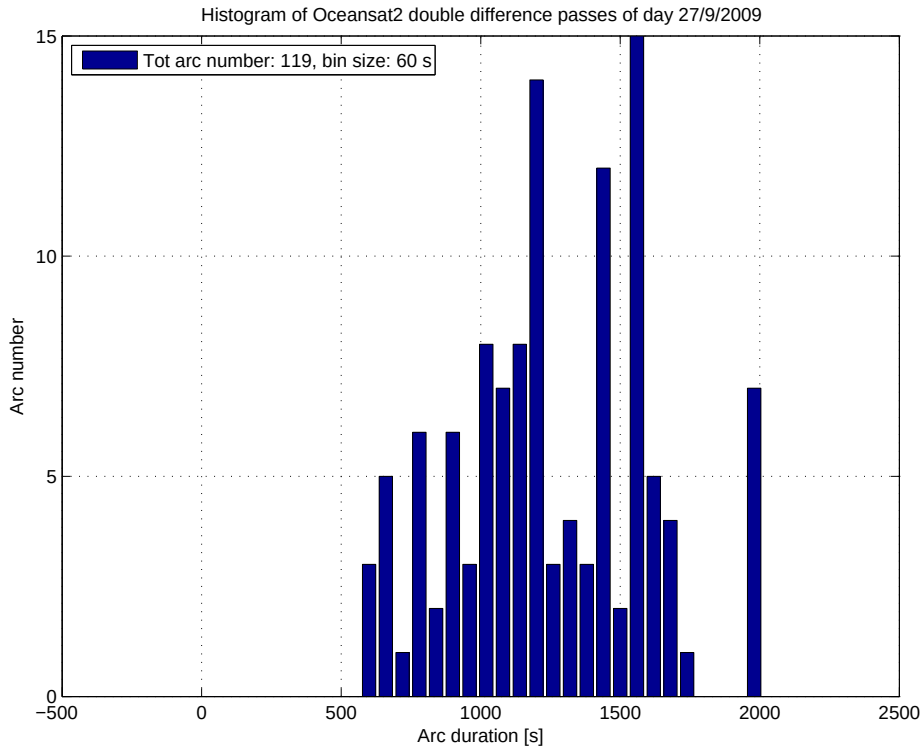

Figure 6.13. Histogram of double difference passes obtained from ROSA data of day 27 September 2009.

6.4. Software Validation with CHAMP Data

In order to test the algorithms implemented in SWOrD, CHAMP data has been fed into the ROSA ROSSA processing chain to be processed by SWOrD. The SWOrDoutput has then been compared with the original equivalent CDAAC DATA.

6.4.1. Orbit Validation

Since the generation of excess phase is one one of the primary goals of SWOrD, it has been compared the range and its range rate computation between the orbiting receiver and a GSP satellite, during the occultation events, with the equivalent level two data available from the CDAAC on-line database. The result of this comparison is shown in Figure 6.14. The medians of the range and the range rate errors are 0.34 m and 0.28 mm/s but must be kept in mind that

- the Rx clock error is disciplined, not corrected,

- SWOrDfor the base version uses the IGS rapid or final GPS orbits (depending on which is the best orbit available at the moment of the run).

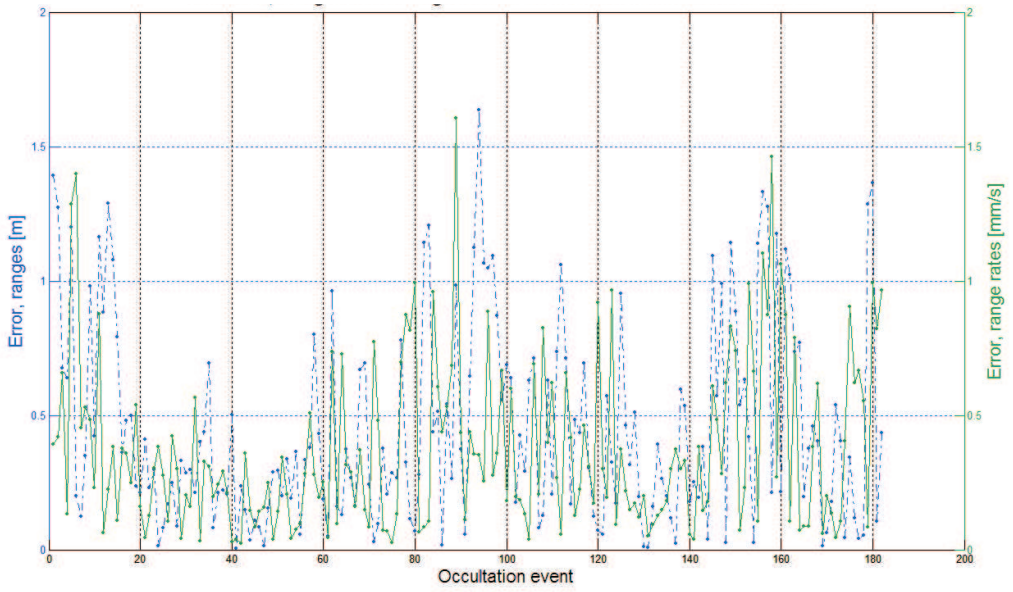

Figure 6.14. Comparison w.r.t. official CHAMP data of the ranges and range rates between the LEO and the GPS satellites during RO events of day 22 January 2004.

6.4.2. Excess phase Validation

The phase excess is the final datum that SWOrDproduces starting from RO GPS measurements and its own LEO precise orbit determination(Figure 6.16 shown an example of a profile for a RO event). The subsequent data generators of the ROSA ROSSA chain extract Doppler excess from the phase excess to accomplish their climatological and meteorological analyses.

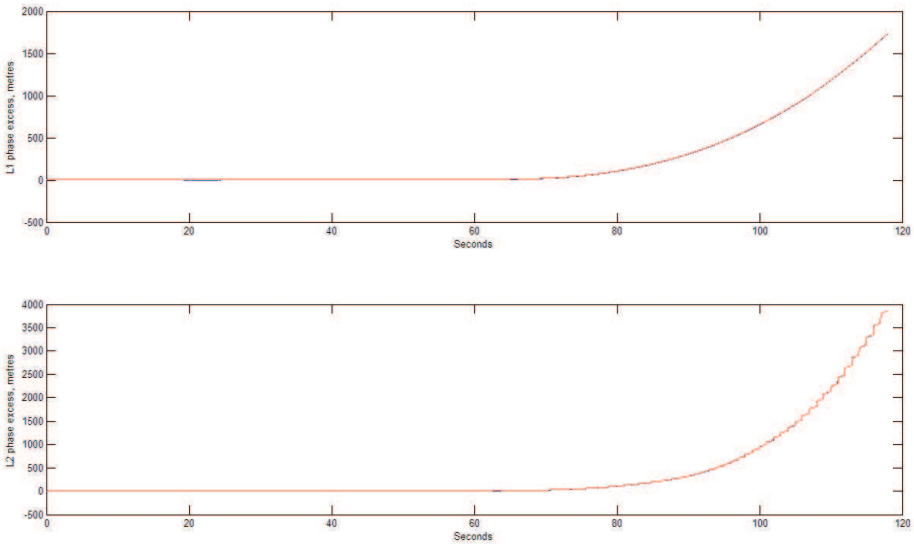

Figure 6.15. An example of CHAMP excess phase profile.

A comparison for the excess phase computation has been performed with CHAMP data,, that is shown in Figure 6.16, while the values of the mean, median, and standard deviation (STD) are shown in Table 6.1.

Band	Mean [m]	Median [m]	STD [m]
L_1	0.464	0.375	0.324
L_1	0.547	0.483	0.346

Table 6.1. Mean median and standard deviation for excess phase of RO events over one day of CHAMP data

.

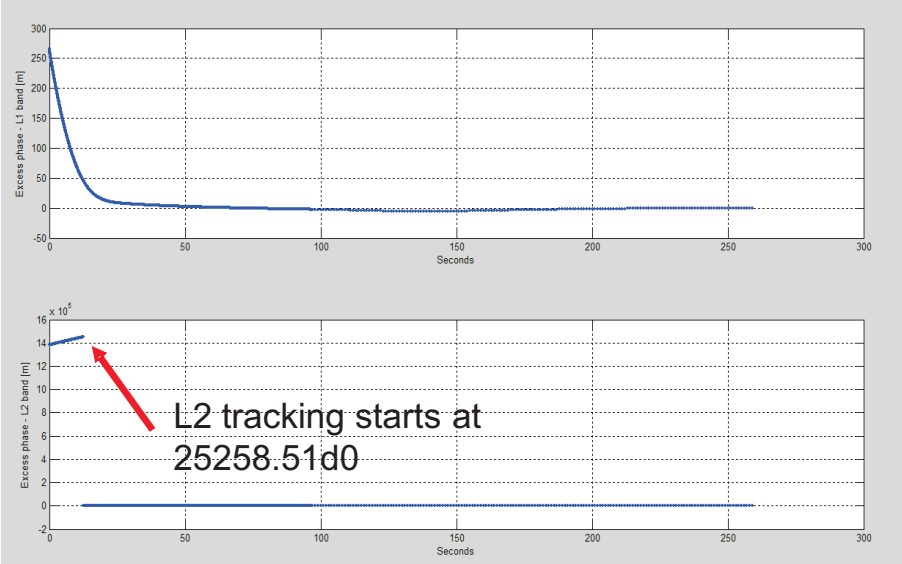

Figure 6.16. RMS of L_1 phase excess differences between SWOrD- and CDAAC-generated values for CHAMP. RMS values of L_2 phase excess differences are very similar to L_1 RMS values.

6.5. Orbit Validation with GRAS Data

Radio occultation observations, as well as precise orbits and receiver clock errors, were provided by EUMETSAT.

6.5.1. Orbit Validation

The geometry of the MetOp/GRAS orbit is more similar to that of Oceansat-2 than to CHAMP's, so that an official GRAS orbit has been used to check the dynamical model fit in SWOrDand the results are shown in Figure 6.17, 6.18 and 6.19.

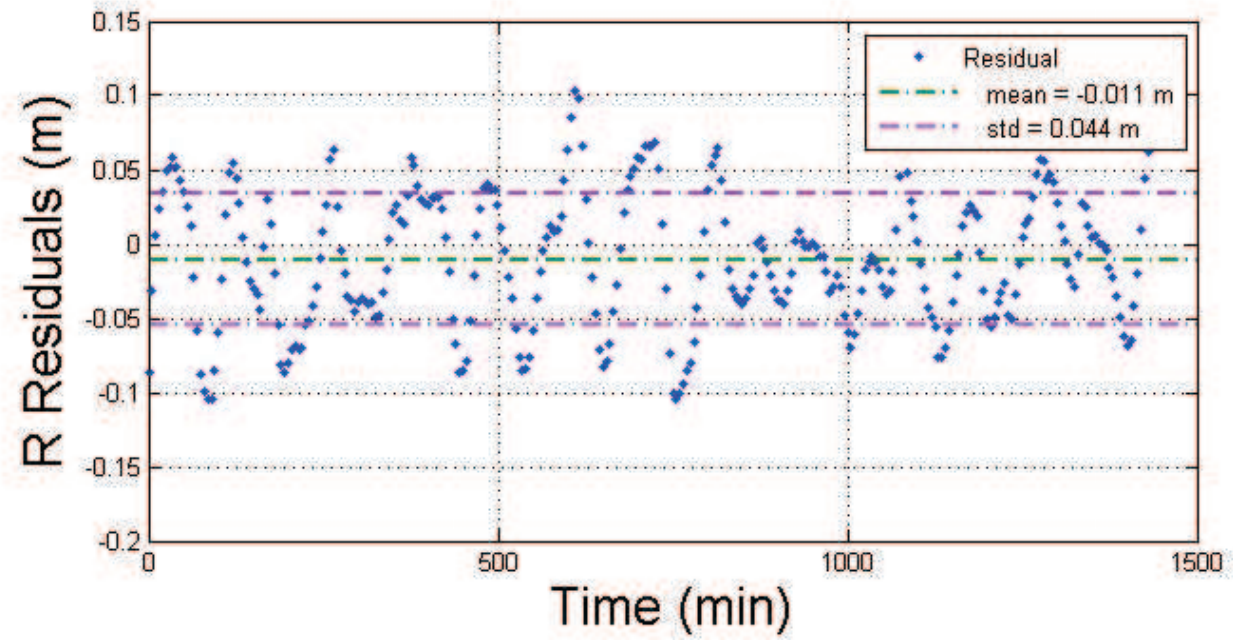

Figure 6.17. Residuals in the radial direction of the dynamic fit of the official GRAS orbit.

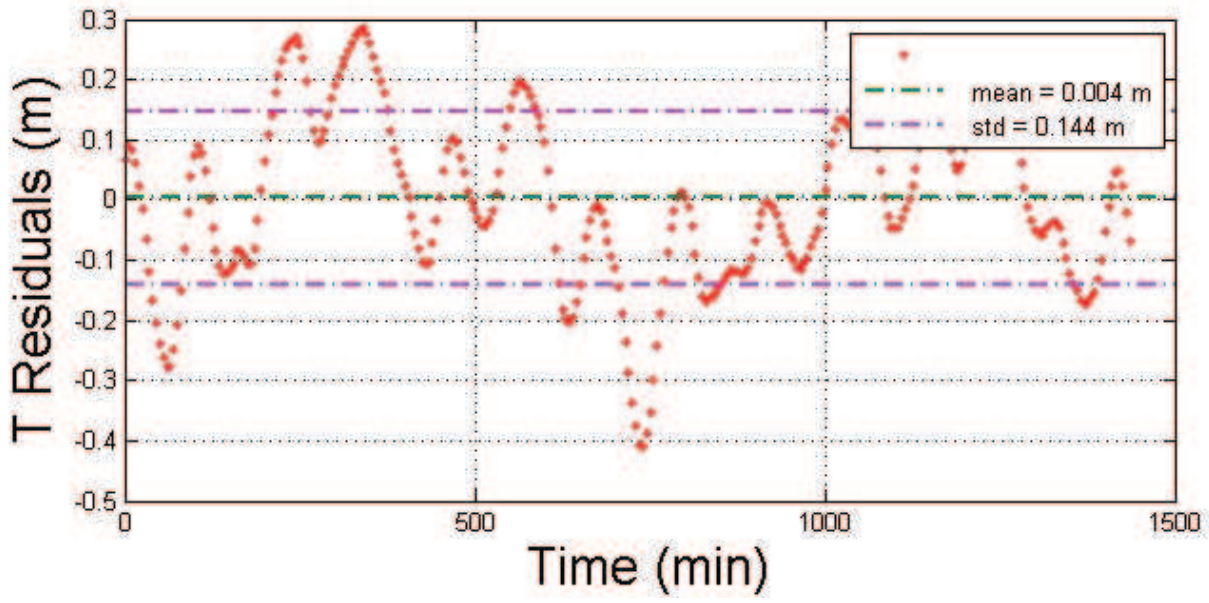

Figure 6.18. Residuals in the along track direction of the dynamic fit of the official GRAS orbit.

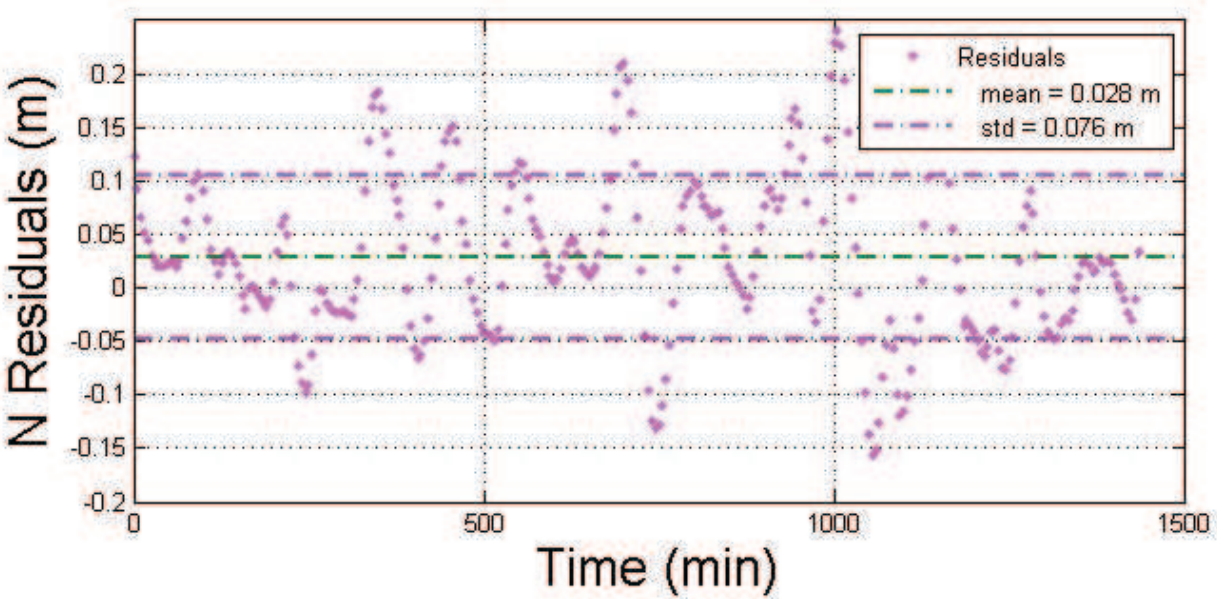

Figure 6.19. Residuals in the normal direction of the dynamic fit of the official GRAS orbit.

6.5.2. Excess phase Validation

We compared the excess phase values with analogous EUMETSAT excess phase values, as already done for CHAMP, and results are shown in Figure 6.20. This time the excess phase were obtained starting directly from the officials GRAS orbit to test only the quality the algorithm for the computation of the excess phase.

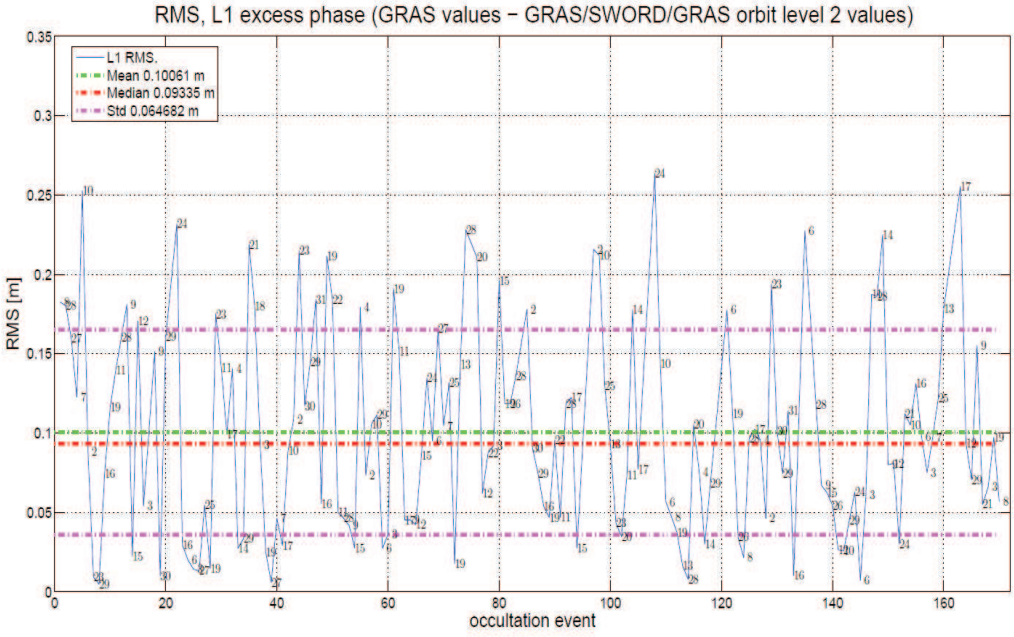

Figure 6.20. RMS of L_1 phase excess differences between SWOrD- and EUMETSAT-generated values for GRAS. RMS values of L_2 phase excess differences are very similar to L_1 RMS values.

6.6. Preliminary Analysis of ROSA Data

ROSA data for 27 September 2009 were made available as a quick-look dataset. As such, it has not been possible to fully analyze the phase data complement to provide a precise orbit. For this reason

only a phase smoothed point positioning solution has been determined. These positions ere later fitted to a dynamical orbit by SWOrD. In Figure 6.21 it is shown the ROSA orbit in the ECEF reference frame. From Figure 6.22(a) to Figure 6.22(c) the residual of the fit of the PPP done to obtain the reference orbit are shown in the RTN system.

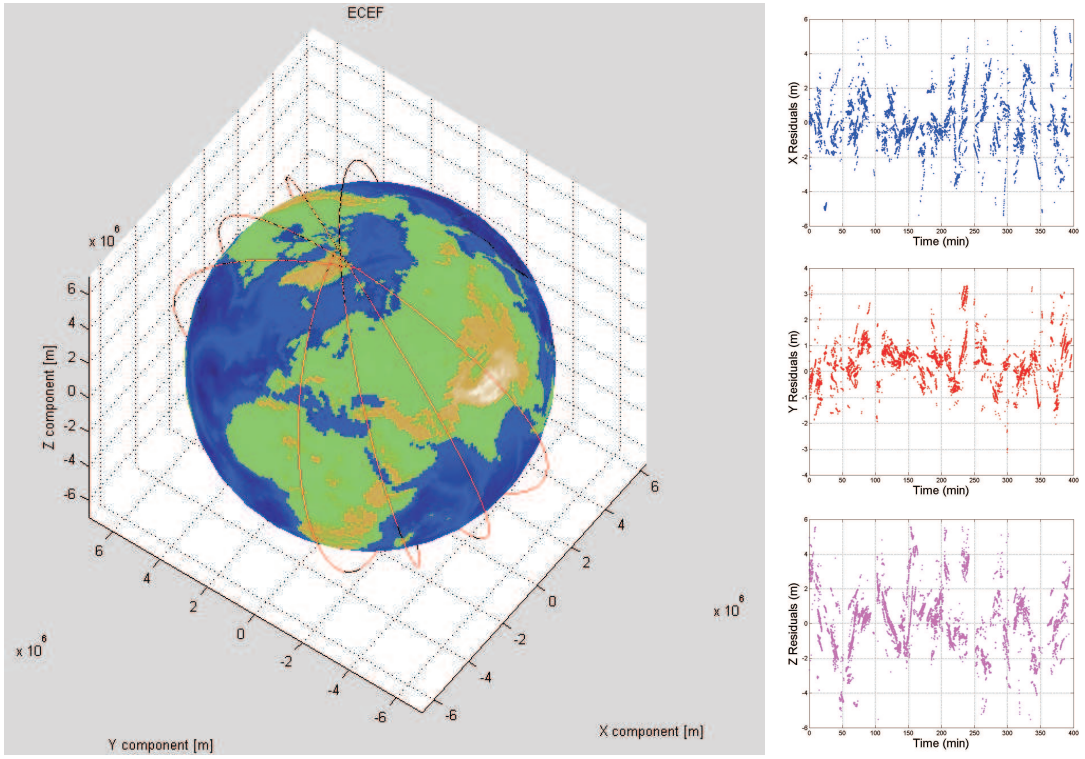

Figure 6.21. Oceansat-2 orbit visualization for the 7 hours data of 27 September 2009 and the residuals of the dynamic fit of the Oceansat-2 PPP (ITRF reference system).

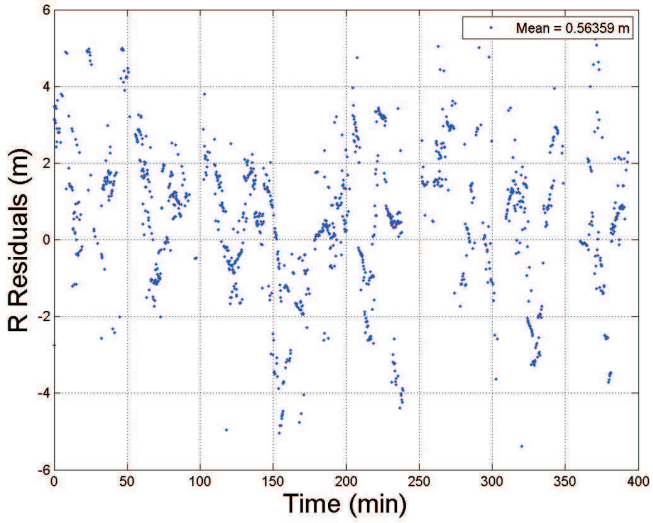

(a) R

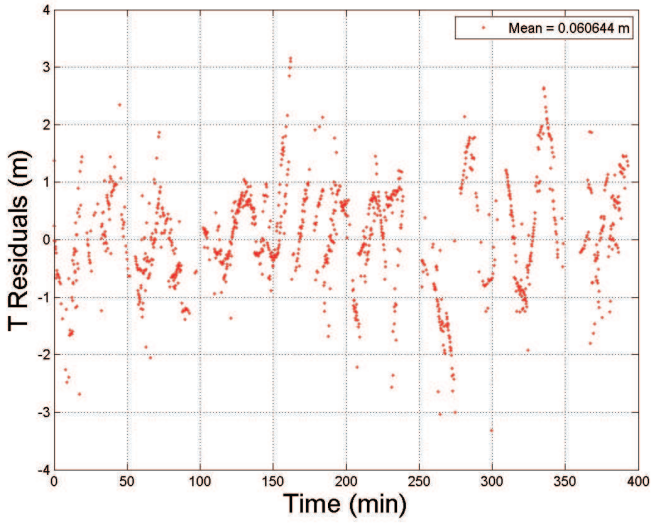

(b) T

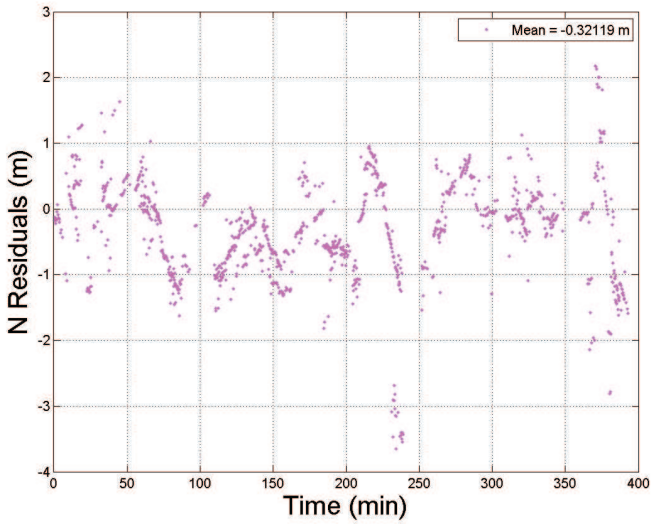

(c) N

Figure 6.22. Residuals of the dynamic fit of the Oceansat-2 PPP (RTN reference system).

Chapter 7

Conclusions and Future Developments

The research led for this dissertation deals with the assessment of precise orbits for LEO satellites bringing on board GNSS receivers. The main goal was to developed a new innovative software that fully supports the orbit determination, orbit prediction and phase excess data generation activities connected with the operations of the Italian GNSS receiver ROSA during the ISRO mission OCEANSAT-2. The new software system SWOrD is under development for precise orbit determination and radio occultation excess phase computation within the ASI ROSA ROSSA project. SWOrD is characterized by a software architecture relying on object oriented programming and C++/Fortran interoperability. An in-core database-driven technology has been implemented in order to improve computational performance. Preliminary results show that SWOrD compares favorably with official radio occultation phase excess results from the CHAMP and Metop/GRAS missions. In particular the level of agreement with the CHAMP excess phase results for a 24-hour data set is about 0.34 m. The dynamical fit of the official GRAS orbit computed by SWOrDagrees within 15 cm per component, which confirms the goodness of the dynamical model, while the level of agreement with the GRAS phase excess results for a 24-hour data set is about 12 cm. The better agreement with GRAS data can be explained with the better quality of GRAS data (CHAMP has a problem on the L_2 observable due to spikes generated by it reference clock) and also to the higher agreement with the orbit geometry of GRAS than with CHAMP's.

7.1. Future Developments

The future developments of SWOrDwill provide the capability of multi satellite orbit determination, to include the GPS satellite POD, the investigation for faster algorithms of GPS observables correction for satellite attitude, for the implementation of the the POD task using zero difference observables and for the realization of a better stochastic clock model for kinematic POD.

Appendix A

Coordinate systems

In Space mission analysis it is necessary and convenient to represent the position of an object, such as a spacecraft, in several different coordinate system. Each coordinate system corresponds to a particular way of expressing the position of an object with respect to a coordinate frame. The two most important reference frames are the celestial reference frame (linked to the fixed stars) and the terrestrial reference frame (dependent on the Earth's rotation).

A.1. International Celestial Reference System (ICRF)

The International Astronomical Union recommends that the origin of the International Celestial Reference System (ICRS) is to be at the barycenter of the Solar System and the directions of the axes should be fixed with respect to quasars. The principal plane of the celestial reference system should be as close as possible to the mean equator at J2000.0 and that the origin of the plane should be as close as possible to the dynamical equinox at J2000.0. The ICRS is materialized by the International Celestial Reference Frame (ICRF).

A.2. International Terrestrial Reference System (ITRF)

A Terrestrial Reference System (TRS) is a spatial reference system corotating with the Earth. The Conventional Terrestrial Reference System (CTRS) monitored by IERS is the International Terrestrial Reference System (ITRS). Realizations of the ITRS are produced by IERS under the name of International Terrestrial Reference Frame (ITRF), which consist of list of coordinates and velocities for a selection of IERS site (see IERS conventions).

Appendix B

Time systems

Time is the independent variable used in SWOrD. Time appears in the dynamical theories of the motion of all celestial bodies and in all computations concerned with them. Time also appears in the tagging of all observations to be processed by SWOrD. Time is also fundamental in all GNSS observations proper.

Time is measured in several *time systems*, or *timescales*. SWORD is concerned with and makes use of several of these timescales owing to its special processing needs. In particular, the timescales used in SWORD are

- *UTC*, or Universal Time Coordinated;
- *UT1*, or Universal Time 1;
- *TT*, or Terrestrial Time;
- *TAI*, or Temps Atomique International;
- *GPS Time*.

Time systems can be classified into three main categories: atomic time, universal time and dynamical time. We will briefly describe each of them and introduce for each the different realizations that are available.

In general, the choice of the timescale for the description of a particular event or phenomenon depends on the nature of the event itself and on the accuracy required.

In each timescale a specific event may be described in different formats. We will address the most common time formats in Section 3.1.4.

B.1. Atomic Time: TAI and GPS Time

Atomic Time (AT) is generated and maintained by an international network of atomic clocks run by different agencies. It is based on the oscillation frequency of the cesium atom (the ^{133}Cs nuclide) at mean sea level. The duration of the SI (International System) second is 9,192,631,770 oscillations of a particular transition.

The realizations of AT of interest for SWORD are TAI and GPS Time. GPS Time is behind TAI by 19 SI seconds, so that

$$GPST = TAI - 19\ s. \tag{B.1.1}$$

B.2. Universal Time: UTC and UT1

Universal time (UT) is based on the rotation of the Earth. As such, it is more akin to an angle than a time as generally perceived. There are different realizations of UT. The fundamental one is UT0 and is computed from measurements of stellar transits (or meridian passages) which determine local sidereal time. UT1 is UT0 corrected for polar motion. UTC is the basis for all civil timekeeping. In the past it was known as Greenwich Mean Time (GMT). In space applications it is also known as Zulu time (Z).

The UTC time unit is the SI second. UTC is a piecewise uniform timescale which is kept close to UT1 such that $|UTC - UT1| \leq 0.9$s by the occasional introduction or removal of one SI second in the UTC timescale. The UTC and the UT1 timescales are related by

$$UT1 = UTC + \Delta UT1. \tag{B.2.1}$$

The quantity $\Delta UT1$ is provided by the IERS as a function of UTC. UTC is related to TAI by

$$TAI = UTC + \Delta AT, \tag{B.2.2}$$

where the quantity ΔAT is known as the number of *leap seconds* and has been provided by the IERS as a function of UTC since 1972. As of January 2009, the number of leap seconds is $\Delta AT = 33$s.

B.3. Dynamical Time: TT, TDB and TCB

Dynamical time is the independent variable in the mathematical theories of the motion of celestial bodies and of the ensuing ephemerides. Several realizations exist of dynamical time, depending on the spatial reference frame adopted to develop the theory. The several flavors of dynamical time are Terrestrial Time (TT), Barycentric Dynamical Time (TDB), Barycentric Coordinate Time (TCB). TDB is the independent variable in theories of the motion based on the barycenter of the Solar System, and is also the coordinate time adopted in General Relativity. TT is the independent variable in theories of the motion based on the center of mass of the Earth (and Moon). TT is also the proper time of General Relativity. TT is related to TAI by a fixed lag

$$TT = TAI + 32.184\ s. \tag{B.3.1}$$

An approximate relation between TT and TDB is

$$TDB \approx TT + 0.001658 \sin M_E + 0.00001385 \sin 2M_E, \tag{B.3.2}$$

where M_E is the mean anomaly of the Earth in its heliocentric orbit and the coefficients are given in units of seconds. Note that the Earth's mean anomaly may be approximated as

$$M_E = 357.5277233^\circ + 35,999.05034^\circ/\text{cy}\ T_{TT}, \tag{B.3.3}$$

where T_{TT} is time in Julian centuries (cy) computed as

$$T_{TT} = \frac{JD_{TT} - 2,451,545.0}{36,525}, \tag{B.3.4}$$

with JD_{TT} the Julian date corresponding to T_{TT}.

The Solar System ephemerides provided by the Jet Propulsion Laboratory (JPL) are given with respect to TDB.

B.4. Time formats: JD, MJD and GD

Events are physical occurrences and can be tagged in different time scales. The time tag associated with an event can be given in several ways, or formats. The two formats of widespread use are the better known Gregorian date format (GD) and the Julian date format (JD), mostly known in the astronomical and, more recently, in the astrodynamic community.

B.4.1. Julian Date (JD) and Modified Julian Date (MJD)

JD is given as a real number. It is formed by the sum of the number of Julian days elapsed at Greenwich noon of the current or previous day since noon of January 1 of year –4713 of the Julian proleptic calendar and the fractional part of the day since the preceding Greenwich noon.

The astronomical and the astrodynamic communities have adopted as a standard epoch what is known as J2000.0, or less accurately, the J2000 epoch. J2000.0 is defined as epoch GD 01 Jan 2000, 12:00:00.000 in the TT time system. J2000.0 is expressed as JD 2451545.0 TT.

The Modified Julian Date format (MJD) is also used, together with several other variants. MJD is defined as

$$MJD = JD - 2450000.5 \tag{B.4.1}$$

and clearly refers to the midnight as the beginning of the MJD day, rather than to noon, as is the case with JD.
The JD format for the epoch J2000.0 is

- 2451545.0 TT
- 2451544.9996274998411 TAI
- 2451544.9992571294708 UTC
- 2451544.9999999990686 TDB

in the various timescales indicated.

B.4.2. Gregorian Date (GD)

GD is given by specifying the usual sequence of day, month, year, hour, minute, second from an initial epoch known as the beginning of the Christian era.

The GD format for the epoch J2000.0 is

- 01 Jan 2000 12:00:00.000 TT
- 01 Jan 2000 12:59:27.815986276 TAI
- 01 Jan 2000 12:59:55.815986276 UTC
- 01 Jan 2000 12:59:59.999919534 TDB

Appendix C

Transformation between Celestial and Terrestrial Reference Systems

The transformation from ICRS to ITRS at the epoch t is the following

$$[ITRS] = W(t)R(t)N(t)P(t)[ICRS] \tag{C.0.1}$$

where $N(t)$ $P(t)$ is the transformation arising from the motion of the Celestial Ephemeris Pole (CEP) in the CRS, $R(t)$ is the transformation arising from the rotation of the Earth around the axis of CEP and finally $W(t)$ is the polar motion matrix.

C.1. Precession

Both the ecliptic, that is the plane of the Earth's orbit, and the plane of the Earth's equator are not fixed with respect to stars. The motion of the ecliptic is due to the gravitational attraction of the planets on the Earth's orbit and it is known as planetary precession. The motion of the equator is due to the torque of the Sun, Moon and planets on the dynamical figure of the Earth. It is separated into two parts: the lunisolar precession, the smooth and long period motion of the mean pole of the equator about the pole of the ecliptic, and nutation, the short period motion of the true pole around the mean pole. The combination of lunisolar and planetary precession is called general precession.

The precession matrix $\mathbf{P}(t)$ transforms equatorial rectangular coordinates from an arbitrary mean equator and equinox of a fixed epoch ε_F usually (J2000.0) to a mean equator and equinox of date ε_D

$$\mathbf{P}[\varepsilon_F, \varepsilon_D] = \mathbf{R}_3(-z)\mathbf{R}_2(\theta)\mathbf{R}_3(-\zeta) \tag{C.1.1}$$

where $\mathbf{R}_3$ and $\mathbf{R}_2$ are rotation matrix and standard values for z, θ and ζ are part of the 1976 IAU Theory of Precession and are given as a series of function of two time parameters t and T both expressed in TDB time scale. The parameter T represents Julian centuries from J2000.0 to an arbitrary epoch. When the arbitrary epoch is chosen to be J2000.0, the precession quantities z, θ and ζ have the values

$$\zeta = 2306''.2181t + 0''.30188t^2 + 0''.017998t^3, \tag{C.1.2}$$

$$\theta = 2004''.3109t - 0''.42665t^2 - 0''.041833t^3, \tag{C.1.3}$$

$$z = 2306''.2181t + 1''.09468t^2 + 0''.018203t^3. \tag{C.1.4}$$

C.2. Nutation

The short period motion of the Earth's rotation axis with respect to a fixed coordinate system is called nutation. Nutation is strictly connected with polar motion, the movement of the rotation axis of the Earth's with respect to an Earth's fixed coordinate system. Both for nutation and polar motion the reference pole is the Celestial Ephemeris Pole (CEP). The 1980 IAU Theory of Nutation describes

the motion of the true pole with respect to the mean pole and may be resolved into two components: these component the nutation in longitude $\Delta\Psi$ and the nutation in obliquity $\Delta\varepsilon$. The nutation matrix transforms equatorial coordinates referred to the mean equator and equinox of date to the true equator and equinox of date and is given by

$$\mathbf{N} = \mathbf{R}(-\varepsilon)\mathbf{R}(-\Delta\Psi)\mathbf{R}(\varepsilon_0), \tag{C.2.1}$$

where ε_0 is the mean obliquity of ecliptic and $\varepsilon = \varepsilon_0 + \Delta\varepsilon$. The value of the mean obliquity of ecliptic ε_0 is given by

$$\varepsilon_0 = 84381''.448 - 46''.8150t - 0''.00059t^2 + 0''.001813t^3. \tag{C.2.2}$$

The values of the nutation in longitude $\Delta\Psi$ and of the nutation in obliquity $\Delta\varepsilon$ are

$$\Delta\Psi_{180} = \sum_{i=1}^{106}(A_i + B_i(t))\sin a_p, \tag{C.2.3}$$

$$\Delta\varepsilon_{180} = \sum_{i=1}^{106}(C_i + D_i(t))\cos a_p, \tag{C.2.4}$$

where A_i, B_i, C_i and D_i are the constants of the IAU 1980 Theory of Nutation and

$$a_p = a_1 l + a_2 l' + a_3 F + a_4 D + a_5\Omega. \tag{C.2.5}$$

The quantity a_i $(i = 1, ..., 5)$ are the integers multiplying the fundamental argument of the nutation theory, that is the mean anomaly of the Moon l, the mean anomaly of the Sun l', the mean argument of latitude of the Moon F, the difference between the mean longitude of the Sun and Moon D and the mean longitude of the ascending node of the Moon's orbit Ω, whose values are

$$l = 134.96340251 + 1717915923''.2178t + 31''.8792t^2 + 0''.051635t^3 - 0''.00024470t^4, \tag{C.2.6}$$

$$l' = 357.52910918 + 129596581''.0481t - 0''.5532t^2 + 0''.000136t^3 - 0.00001149t^4, \tag{C.2.7}$$

$$F = 93.27209062 + 1739527262''.8478t - 12''.7512t^2 - 0''.001037t^3 + 0.00000417t^4, \tag{C.2.8}$$

$$D = 297.85019547 + 1602961601''.2090t - 6''.3706t^2 + 0''.006593t^3 - 0''.00003169t^4, \tag{C.2.9}$$

$$\Omega = 125.04455501 - 6962890''.2665t + 7''.4722t^2 + 0''.007702t^3 - 0''.00005939t^4. \tag{C.2.10}$$

Using the observed offsets $\delta\Delta\Psi$ and $\delta\Delta\varepsilon$ published in the IERS Bulletins the corrected nutation is given by

$$\Delta\Psi = \Delta\Psi_{180} + \delta\Delta\Psi, \tag{C.2.11}$$

$$\Delta\varepsilon = \Delta\varepsilon_{180} + \delta\Delta\varepsilon. \tag{C.2.12}$$

C.3. Apparent Sidereal Time (GAST)

The position of the terrestrial reference frame with respect to the true equator and equinox of date is defined by successive rotations through two small angle x_p and y_p and the Greenwich apparent sidereal time θ_{GAST}. The rotation matrix involving θ_{GAST} is defined as

$$\mathbf{R} = \mathbf{R}_3\theta_{GAST}. \tag{C.3.1}$$

The Greenwich apparent sidereal time θ_{GAST} is computed by

$$\theta_{GAST} = \theta_{GMST} + EE, \tag{C.3.2}$$

where EE is the equation of equinox computed as

$$EE = \Delta\Psi \cos\varepsilon + 0''.00264 \sin\Omega + 0''.000063 \sin 2\Omega \tag{C.3.3}$$

and

$$\theta_{GMST} = 1''.00965822615 \cdot 10^6 + 4''.746600277219299 \cdot 10^{10} T_{UT1} + 1''.396560 T_{UT1}^2 + 9.3 \cdot 10^{-5} T_{UT1}^3. \tag{C.3.4}$$

C.4. Polar Motion

The position of the terrestrial reference frame with respect to the true equator and equinox of date is defined by successive rotations through two small angle x_p and y_p and the Greenwich apparent sidereal time θ_{GAST} (see previous section). The angles x_p and y_p correspond to the coordinates of the CEP with respect to the terrestrial pole measured along the meridians at longitude 0° and 270°. Time series for polar motion can be retrieved from the IERS Bulletin B. The polar motion matrix $\mathbf{W}$ is expressed as

$$\mathbf{W} = \mathbf{R}_2(-x_p)\mathbf{R}_1(-y_p). \tag{C.4.1}$$

Bibliography

[1] Barbieri, C., Naletto, G. P., Occhipinti, T., Facchinetti, C., Verroi, E., Di Paola, A., Billotta, S., Zoccarato, P., Bolli, P., Tamburini, F., Bonanno, G., D'Onofrio, M., Marchi, S., Anzolin, G., Capraro, I., Messina, F., Belluso, M., Pernechele, C., Zaccariotto, M., Zampieri, L., Da Deppo, V., Fornasier, S. (2008): AquEYE, a single photon counting photometer for astronomy, *Journal Of Modern Optics*, **56**(2), 261-272, doi: 10.1080/09500340802450565.

[2] Bertiger, W. I., Bar-Sever, Y. E., Christensen, E. J., Davis, E. S., Guinn, J. R., Haines, B. J., Ibanez-Meier, R. W., Lee, J. R., Lichten, S. M., Melbourne, W. G., Muellerschoen, R. J., Munson, T. N., Vigue, Y., Wu, S. C., Yunck, T. P., Schutz, B. E., Abusali, P. A. M., Rim, H. J., Watkins, M. M., Willis, P. (1994): GPS precise tracking of TOPEX/POSEIDON: Results and implications, *Journal of Geophysical Research*, **99**(C12), 24449-24464.

[3] Bertiger, W. I., Wu, S. (1996): Single Frequency GPS Orbit Determination For Low Earth Orbiters, *Proceedings of the National Technical Meeting (ION): Technology and Operations: Partnerships for Success in Navigation*, 463-473, JPL/Caltech.

[4] Beutler, G., Gurtner, W., Bauersima, I., Rothacher, M. (1986): Efficient computation of the inverse of the covariance matrix of simultaneous GPS carrier phase difference observations *Manuscripta Geodetica*, **11**, 249-255.

[5] Beutler, G. (2005): *Methods of Celestial Mechanics*, Volumes I & II, Springer, Heidelberg.

[6] Bisnath, S. B., Langley, R. B. (2001): High-Precision Platform Positioning with a Single GPS Receiver, Paper presented at *ION GPS* 2001, 11-14 September, Salt Lake City, Utah, USA.

[7] Blewitt, G. (1989): Carrier phase ambiguity resolution for the Global Positioning System applied to geodetic baselines up to 2000 km, *Journal of Geophysical Research*, **94**(B8), 10,187-10,203.

[8] Bock, Y., Gourevitch, S. A., Counselman, C. C. III, King, R. W., Abbot, R. I. (1986) Interferometric analysis of GPS phase observations, *Manuscripta Geodetica*, **11**, 282-288.

[9] Bock, H., Beutler, G., Hugentobler, U. (2001): Kinematic Orbit Determination for Low Earth Orbiters (LEOs), *IAG Scientific Assembly*, 2-7 September, Budapest, Hungary.

[10] Bock, H. (2003): *Efficient methods for determining precise orbits for Low Earth Orbiters using the Global Positioning System*, PhD Thesis, Vol. 65 of Geodätisch-geophysikalische Arbeiten in der Schweiz, Schweizerische Geodätische Kommission, Zürich, Switzerland, ISBN: 3-908440-08-4.

[11] Bock, H., Jäggi, A., Svehla, D., Beutler, G., Hugentobler, U., Visser, P. (2007): Precise orbit determination for the GOCE satellite using GPS, *Advances in Space Research*, **39**, 1638-1647.

[12] Bock, H., Dach, R., Jäggi, A., Beutler, G. (2009): High-rate GPS clock corrections from CODE: support of 1 Hz applications, *Journal of Geodesy*, **83**, 1083-1094, doi: 10.1007/s00190-009-0326-1.

[13] Boost Multi-index Containers library: http://www.boost.org/libs/multi_index

[14] Boost Units library: http://www.boost.org

[15] Byun, S.H. (1998): *Satellite orbit determination using GPS carrier phase in pure kinematic mode*, PhD Thesis, University of Texas, Austin.

[16] Byun, S.H. (2003): Satellite orbit determination using triple-differenced GPS carrier phase in pure kinematic mode, *Journal of Geodesy*, **76**, 569-585.

[17] Capraro, I., Occhipinti, T., Zoccarato, P., Bonato, C., Tamburini, F., Barbieri, C., Villoresi, P. (2007): The utilization of the GALILEO timing signals for Quantum Communications, *1st Colloquium: Scientific and Fundamental Aspects of the Galileo Programme*, 1-4 October, Toulouse, France.

[18] Cariolaro, G. (1996): *La teoria unificata dei segnali*, Nuova Edizione, UTET Libreria, Torino.

[19] Casotto, S., Dow, J. M., Martin-Mur, T. (1995): TOPEX/Poseidon precise orbit determination using GPS double difference phase observables, *Advances in Space Research*, **16**(12), 63-66, doi: 10.1016/0273-1177(95)98782-J.

[20] Casotto, S., Zoccarato, P., Nardo, A., Bardella, M. (2009): SWORD - An Orbit Determination Software System for Application to ROSA-ROSSA GNSS Radio Occultation, *2nd International Colloquium: Scientific and Fundamental Aspects of the Galileo Programme - COSPAR Colloquium*, 14-16 October, Padua, Italy.

[21] Casotto, S. (2006-2007): *Introduzione alla Meccanica Celeste*, Course of Celestial Mechanics.

[22] CHAMP Data Access: http://cosmic-io.cosmic.ucar.edu/pub_pp/champ/

[23] CHAMP: http://op.gfz-potsdam.de/champ

[24] CodeSynthesis XSD: http://www.codesynthesis.com/products/xsd/

[25] Colombo O. L., Hernández-Pajares, M., Juan, M. J., Sanz, J., Talaya, J. (1999): Resolving carrier-phase ambiguities on the fly, at more than 100 km from nearest reference site, with the help of ionospheric tomography, *ION GPS 1999: 12th International Technical Meeting of the Satellite Division of US Institute of Navigation*, 14-17 September, Nashville, Tennessee, 1635-1642.

[26] De Jonge, P., Tiberius, C. C. J. M. (1996): The LAMBDA method for integer ambiguity estimation: implementation aspects, *Technical report LGR Series*, No. 12, Delft Geodetic Computing Centre, Delft University of Technology, The Netherlands.

[27] Deleflie, F. J., Exertier, P., Valk, S., Guzzo, M., Portmann, C. (2007): Stability of the Galileo Constellation, and Long Term Evolution of Disposal Orbits, *1st Colloquium: Scientific and Fundamental Aspects of the Galileo Programme*, 1-4 October, Toulouse, France.

[28] Delporte, J., Mercier, F., Laurichesse, D., Galy, O. (2007): Fixing integer ambiguities for GPS carrier phase time transfer, *Frequency Control Symposium, 2007 Joint with the 21st European Frequency and Time Forum. IEEE International*, 29 May - 1 June, Geneve, Switzerland, 927-932.

[29] Doxygen: http://www.stack.nl/ dimitri/doxygen/

[30] Ellis, T. M. R., Philips, I. R., Lahey, T. M. (1994): *Fortran 90 Programming*, International Computer Science Series, Addison-Wesley, ISBN 0-201-54446-6.

[31] Fantino, E., Casotto, S. (2009): Methods of harmonic synthesis for global geopotential models and their first-, second- and third-order gradients, *Journal of Geodynamics*, **83**, 595-619, doi:10.1007/s00190-008-0275-0.

[32] Fu, L., Christensen, E. J., Yamarone, C. A., Lefebvre, M., M'enard, Y., Dorrer, M., Escudier, P. (1994): TOPEX/POSEIDON mission overview, *Journal of Geophysical Research*, **99**(C12), 24369-24381.

[33] Gao, Y., Li, Z. (1999): Cycle slip detection and ambiguity resolution algorithms for dual-frequency GPS data processing, *Marine Geodesy*, **22**(4), 169-181.

[34] GFO: http://gfo.wff.nasa.gov/

[35] Goad, C. C. (1985): Precise relative position determination using global positioning system carrier phase measurements in a nondifference mode, *Proceedings of First International Symposium on Precise Positioning with GPS*, Rockville, Maryland, 347-356.

[36] Goad, C. C., Mueller, A. (1988): An automated procedure for generating an optimum set of independent double difference observables using Global Positioning System carrier phase measurements, *Manuscripta Geodetica*, **13**, 365-369.

[37] Goad, C. C. (1990): Optimal filtering of pseudoranges and phases from single-frequency GPS receivers, *Journal of the Institute of Navigation*, **37**(3), 191-204.

[38] GOCE: http://www.esa.int/SPECIALS/GOCE/index.html

[39] GPSTk Library: http://www.gpstk.org/

[40] GPSTk Doxygen documentation: http://www.gpstk.org/doxygen/

[41] GRACE: http://www.csr.utexas.edu/grace

[42] Grejner-Brzezinska, D. A., Ge, S., Kwon, J., Shum, C. K., Zhao, C. Y. (2002): GPS/LEO Rapid Orbit Determination in Support of GPS Meteorology: Status and Future Plans, Presented at the *First CHAMP Science Meeting*, 22-25 January, GFZ Potsdam, Germany.

[43] Grunwaldt, L., Meehan, T. K. (2003): *CHAMP Orbit and Gravity Instrument Status*, First CHAMP Mission Results for Gravity, Magnetic and Atmospheric Studies, edited by C. Reigber et al., 3-10, Springer, Berlin, ISBN 3-540-00206-5.

[44] Habrich, H., Beutler, G., Gurtner, W., Rothacher, M. (1999): Double difference ambiguity resolution for GLONASS/GPS carrier phase, *GPS ION 1999: 12th International Technical Meeting of the Satellite Division of the U.S. Institute of Navigation*, 14-17 September, Nashville, Tennessee, 1609-1618.

[45] Hernández, C., Catalán, C., Curiel, A. M., Sardón, E. (2207): Advanced Real-Time Synchronisation for Networks of Sensor Stations with High Accuracy and Integrity, *1st Colloquium: Scientific and Fundamental Aspects of the Galileo Programme*, 1-4 October, Toulouse, France.

[Heuberger, 1984] Heuberger, H. (1984): Performance of the GPS Package on LANDSAT5, *IEEE Position Location and Navigation Symposium.*

[46] Hofmann-Wellenhof, B., Lichtenegger, H., Collins, J. (2001): *GPS: Theory and Practice*, Fifth revised Edition, Springer-Verlag Wien New York, ISBN 3-211-83534-2.

[47] Hugentobler, U., Dach, R., Fridez, P., Meindl, M. (2006): *Bernese GPS software, Version 5.0*, Astronomical Institute, University of Berne.

[48] ICESat: http://icesat.gsfc.nasa.gov

[49] IGS: http://igscb.jpl.nasa.gov/

[50] Intel compiler manual: http://www.intel.com/software/products/compilers/docs/flin/main_for/me

[51] JPL - Solar System Dynamics: http://ssd.jpl.nasa.gov/

[52] Kaplan, E. D. (1996): *Understanding GPS: Principles and Applications*, Artech House Inc., Norwood, Massachusetts.

[53] Kursinski, E. R. (1997): *The GPS radio occultation concept: theoretical performance and initial results*, PhD Thesis, California Institute of Technology, Pasadena, California, USA.

[54] De Lacy, M. C., Gil, A. J., Moreno, B., Reguzzoni, M., Rodríguez, G., Sansò, F., Venuti, G. (2007): A method for cycle-slip detection of multifrequency GNSS data, *1st Colloquium: Scientific and Fundamental Aspects of the Galileo Programme*, 1-4 October, Toulouse, France.

[55] Leick, A. (1995): *GPS satellite surveying*, Second Edition, John Wiley & Sons, Inc, USA.

[56] JASON-1: http://sealevel.jpl.nasa.gov/mission/jason-1.html

[57] Martin, C., Lewis, H., Walker, R. (2001): Studying the MEO & GEO Space Debris Environments with the Integrated Debris Evolution Suite (IDES) Model, *Proceedings of the Third European Conference on Space Debris*, ESOC, Darmstadt, Germany, 351-354.

[58] Maybeck, P. S. (1982): *Stochastic models, estimation, and control*, Mathematics in Science and Engineering, Vol. 141-1,2,3, Academic Press.

[59] McCarthy, D. D., Petit, G. (2003): *IERS Conventions (2003), Technical Note 32*, Verlag des Bundesamts für Kartographie und Geodäsie, Frankfurt, Germany, ISBN 3-89888-884-3.

[60] Melbourne, W. G., Davis, E. S., Duncan, C. B., Hajj, G. A., Hardy, K. R., Kursinski, E. R., Meehan, T. K., Young, L. E., Yunck, T. P. (1994): *The Application of Spaceborne GPS to Atmospheric Limb Sounding and Global Change Monitoring*, JPL Publication 94-18, Jet Propulsion Laboratory, California Institute of Technology, Pasadena, California, USA.

[61] Montenbruck, O., Gill, E. (2000): *Satellite Orbits*, Springer-Verlag Berlin Heidelberg.

[62] Naletto, G., Barbieri, C., Occhipinti, T., Capraro, I., Di Paola, A., Facchinetti, C., Verroi, E., Zoccarato, P., Anzolin, G., Belluso, M., Billotta, S., Bolli, P., Bonanno, G., Da Deppo, V., Fornasier, S., Germanà, C., Giro, E., Marchi, S., Messina, F., Pernechele, C., Tamburini, F., Zaccariotto, M., Zampieri, L. (2009): Iqueye, a single photon counting photometer applied to the ESO New Technology Telescope, *Astronomy and Astrophysics*, **508**(1), 531-539, doi: 10.1051/0004-6361/200912862.

[63] National Geophysical Data Centre (NGDC): http://www.ngdc.noaa.gov/ngdc.html

[64] Occhipinti, T., Zoccarato, P., Capraro, I., Bolli, P., Messina, F., Naletto, G., Villoresi, P., Barbieri, C. (2007): The Importance of Time and Frequency Reference in Quantum Astronomy and Quantum Communications, *39th Annual Precise Time and Time Interval (PTTI) Meeting*, 26-29 November, Long Beach, California, USA.

[65] OCEANSAT-2: http://space.skyrocket.de

[66] Ørsted: http://web.dmi.dk/projects/oersted

[67] Padovan, B. (2007): *Precise Orbit Determination for missions CHAMP and Eneide using GPS measurements, in preparation for mission GOCE*, PhD Thesis, University of Padua, Italy.

[68] Parkinson, B.W., Spilker, J., Axelrad, P., Enge, P. (1996): *Global Positioning System: Theory & Applications*, volumes I & II, Progress in Astronautics and Aeronautics, American Institute of Aeronautics and Astronautics, Inc., 370 L'Enfant Promenade, SW, Washington D.C., USA.

[69] Perona, G., F., Notarpietro, R., Molinaro, M., Casotto, S., Zoccarato, Cucca, M., Petitta, M., Sutera, A., Tartaglione, N., Speranza, A., Nava, B., Radicella, S., Gallipoli, A., Vespe, F. (2009): The Italian software for GPS radio occultation: validation using COSMIC and CHAMP data, *EGU General Assembly*, April, Wien, Austria.

[70] Perona, G., Vespe, F., Notarpietro, R., Molinaro, M., Paolella, S., Cucca, M., Casotto, S., Zoccarato, P., Nardo, A., Bordi, I., Sutera, A., Petitta, M., Tartaglione, N., Speranza, A., Nava, B., Radicella, S., Gallipoli, A. (2009): The GPS Radio Occultation ROSA-ROSSA Software: preliminary results, *2nd International Colloquium: Scientific and Fundamental Aspects of the Galileo Programme - COSPAR Colloquium*, 14-16 October, Padua, Italy.

[71] Picci, G. (2007): *Filtraggio statistico (Wiener, Levinson, Kalman) e applicazioni*, Edizioni Libreria Progetto Padova.

[72] Quarteroni, A., Sacco, R., Saleri, F. (2000): *Numerical Mathematics*, Springer Verlag, New York.

[73] Reigber C., Lühr H., Schwintzer P. (1998): *Status of the CHAMP Mission - Towards an Integrated Global Geodetic Observing System (IGGOS)*, IAG Symposium No. 120, edited by Rummel, R., Drewes, H., Bosch, W. et al., pp. 63-65, Springer, Berlin, ISBN 3-540-67079-3.

[74] Reigber C., Lühr H., Schwintzer P., Wickert, J. (2005): *Earth Observation with CHAMP: Results from Three Years in Orbit*, Springer-Verlag Berlin Heidelberg, ISBN: 978-3-540-22804-2.

[75] Saalfeld, A. (1999): Generating basis sets of double differences, *Journal of Geodesy*, **73**, 291-297.

[76] SAC-C: http://www.gsfc.nasa.gov/gsfc/service/gallery/fact_sheets/spacesci/sac-c.htm

[77] Schaer, S. (1999): *Mapping and Predicting the Earth's Ionosphere Using the Global Positioning System*, Vol. 59, Geodätisch-geophysikalische Arbeiten in der Schweiz, Schweizerische Geodätische Kommission.

[78] Schutz, B. E., Tapley, B. D., Abusali, P. A. M., Rim, H. J. (1994): Dynamic orbit determination using GPS measurements from TOPEX/POSEIDON, *Geophysical Research Letters*, **21**(19), 2179-2182.

[79] Sjöberg, L. E. (1999): Unbiased vs biased estimation of GPS phase ambiguities from dual-frequency code and phase observables, *Journal of Geodesy*, **73**, 118-124.

[80] Springer, T. A. (2000): *Modeling and Validating Orbits and Clocks Using the Global Positioning System*, PhD Thesis, University of Berne, Switzerland.

[81] Sunsat: http://ilrs.gsfc.nasa.gov/satellite_missions/list_of_satellites/suns_general.html

[82] Svehla, D., Rothacher, M. (2001): Kinematic Orbit Determination of LEOs based on zero or double-difference algorithms using simulated and real SST GPS data, *IAG Scientific Assembly*, 2-7 September, Budapest, Hungary.

[83] Swift, E. R., Gouldman, M. W. (1989): Preliminary evaluation of GPS orbit/clock determination accuracy, *Manuscripta Geodetica*, **14**, 125-132.

[84] Tapley, B. D., Schutz, B. E., Born, G. H. (2004): *Statistical Orbit Determination*, Elsevier Academic Press, Boston.

[85] Tavella, P., Zucca, C., (2005): The clock model and its relationship with the Allan and related variances, *IEEE transactions on ultrasonics, ferroelectrics, and frequency control*, **52**(2).

[86] Tiberius, C. C. J. M., De Jong, K. (2002): Developments in Global Navigation Satellite Systems, *The Hydrographic Journal*, **104**.

[87] Vallado, D. A. (2007): *Fundamentals of Astrodynamics and Applications*, Third Edition, Space Technology Library.

[88] Verhagen, S., Teunissen, P. J. G. (2006): New global navigation satellite system ambiguity resolution method compared to existing approaches, *Journal of Guidance, Control and Dynamics*, **29**(4), 981-991.

[89] Visser, P. N. A. M., van den IJssel, J. (2000): GPS-based precise orbit determination of the very low Earth-orbiting gravity mission GOCE, *Journal of Geodesy*, **74**, 590-602.

[90] Yunck, T. P. (1995): GPS data, acquisition, environmental effects, *Reviews of Geophysics*, **33**(S1), 349-352.

[91] Wertz, J. R. (1978): *Spacecraft attitude determination and control*, Astrophysics and Space Science Library, Kluver Academic Publishers, The Netherlands.

[92] Wickert, J. (2002): *Das CHAMP-Radiookkultationsexperiment : Algorithmen, Prozessierungssystem und erste Ergebnisse*, PhD Thesis, GeoForschungsZentrum Publications, Potsdam, Germany.

[93] Wu, J. T. (1994): Processing mixed pseudorange and carrier phase GPS data, *Manuscripta Geodetica*, **20**, 27-33.

[94] XML Schema: http://www.w3.org/XML/Schema

[95] Xu, G. (2003): *GPS: Theory, Algorithms and Applications*, Springer-Verlag Berlin Heidelberg, ISBN 3-540-67812-3.

[96] Zampieri, L., Germanà, C., Barbieri, C., Naletto, G., Cadez, A., Capraro, I., Di Paola, A., Facchinetti, C., Occhipinti, T., Verroi, E., Zoccarato, P. (2009): The Crab pulsar seen from Asiago-Cima Ekar Observatory, *2nd International Colloquium: Scientific and Fundamental Aspects of the Galileo Programme - COSPAR Colloquium*, 14-16 October, Padua, Italy.

[97] Zhang, J., Zhang, K., Grenfell, R., Deakin, R. (2006): Short Note: On the relativistic Doppler effect for precise velocity determination using GPS, *Journal of Geodesy*, **80**, 104-110, doi: 10.1007/s00190-006-0038-8.

[98] Zilli, G. (2003): *Lezioni di Calcolo Numerico*, Edizioni Libreria Progetto Padova.

[99] Zin, A. (2001): *Precise orbit determination of Low-Earth Orbiting satellites using the Global Navigation Satellite System (GNSS)*, PhD Thesis, University of Padua, Italy.

[100] Zoccarato, P., Occhipinti, T., Facchinetti, C., Bolli, P., Messina, F., Capraro, I., Tamburini, F., Dalla Torre, A., Zanello, R., Cadez, A., Barbieri, C. (2007): The utilization of the GALILEO timing signals for advanced astronomical applications, *1st Colloquium: Scientific and Fundamental Aspects of the Galileo Programme*, 1-4 October, Toulouse, France.

[101] Zoccarato, P., Barbieri, C., Occhipinti, T., Cadez, A., Ponikvar, D., Naletto, G., Capraro, I., Cantelmo, C. (2009): The importance of accurate timing of astronomical photons, *2nd International Colloquium: Scientific and Fundamental Aspects of the Galileo Programme - COSPAR Colloquium*, 14-16 October, Padua, Italy.